Stability of rock on mild slopes

Msc Thesis

J.F.S. van Wijland
August 2020

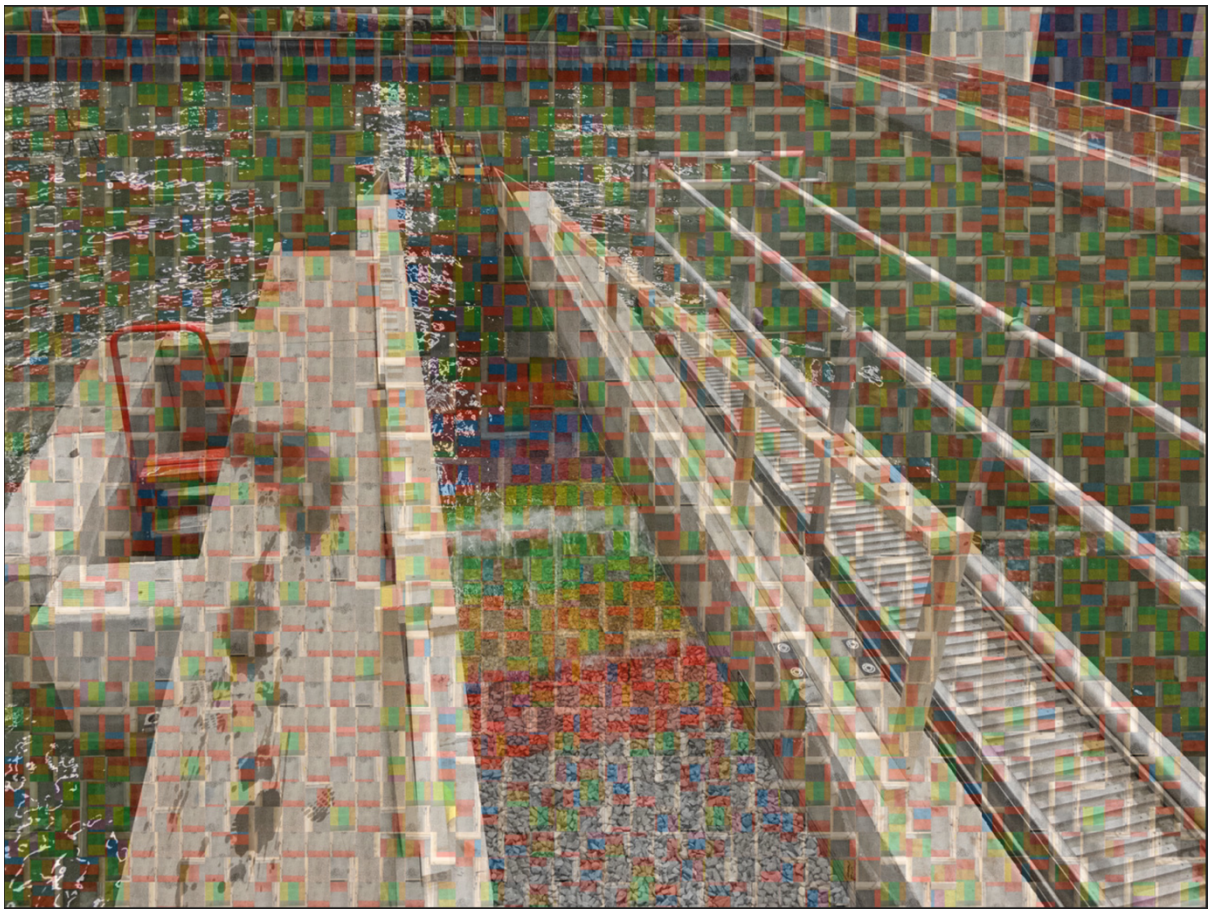

de Vries & van de Wiel
Dredging & Environmental Solutions

TU Delft

Deltares
Enabling Delta Life

Stability of rock on mild slopes

by

J.F.S. van Wijland

To obtain the degree of Master of Science
at the Delft University of Technology,
to be defended on Thursday August 20, 2020 at 10:00 AM

Master of Science program
Hydraulic Engineering

Student number:	4151593	
Project duration:	October 15, 2019 – August 20, 2020	
Thesis committee:	Dr.ir. B. Hofland,	Delft University of Technology, chair
	Ing. C. Kuiper,	Delft University of Technology
	Dr. R.C. Lindenbergh,	Delft University of Technology
	Dr.ir. M.R.A. van Gent,	Deltares
	Ir. H.D. Jumelet,	de Vries & van de Wiel
	Ir. E.A.F. Wendt,	de Vries & van de Wiel

Preface

This MSc thesis is part of my study to fulfil my Master of Science degree Hydraulic Engineering at the TU Delft, under supervision of Bas Hofland. The project has been a collaboration between the Technical University of Delft, Deltares and de Vries & van de Wiel.

The project was only possible with the support and guidance of the graduation committee. First of all, I would like to thank Bas Hofland, Coen Kuiper and Roderik Lindenbergh of the TU Delft for the all advice and feedback during the project. Secondly, I appreciate all support and guidance given by Marcel van Gent on the planning, execution and analysis of the results for the physical model tests carried out at Deltares. At last, I would thank Daan Jumelet and Emiel Wendt for supportiveness, supervision and the amazing experience at the De Vries & van de Wiel and the possibility to carry out physical model tests. I would also like to express my gratitude towards all laboratory technicians and especially to Wesley Stet for the guidance during the physical model tests. A last I would like to thank my familiy for the moral support during the process.

Looking back, I consider this research project a fruitful experience and I have gained a lot of new knowledge.

Sebastiaan van Wijland
Delft, August 2020

Acknowledgement

The financial contribution by the TKI project "Dynamica van waterbouwkundige constructies, fase 2", for facilitating the physical model tests at Deltares and the supervision by participants, is acknowledged.

Abstract

Until now, an extensive design method for mild slopes has not been available. The aim of this thesis is to understand the stability of rock on mild slopes under wave attack for impermeable cores in order to optimize designs. Physical model tests have been executed to study this stability for a 1:8 slope. Mossinkoff (2019) executed physical model tests for a 1:10 slope and a re-analysis of these tests is included in this thesis as well. Damage caused by entrained rocks is quantified by damage parameters using stereophotogrammetry and coloured rocks in strips. In this study, the influence of several hydraulic and structural parameters on damage parameters has been investigated for mild slopes. A positive correlation has been found between the significant wave height and the damage parameters. Besides this, based on the analysis it can be concluded that the wave steepness and damage parameters are negatively correlated. An increase in layer thickness of the rocks does not seem to increase the stability of rock on mild slopes. However, the slope angle does have an effect on the stability as a milder slope is associated with less damage. Another conclusion is that more damage continues to be observed even after 15 000 waves. Based on the results of the physical model tests, a design formula is developed for mild slopes to be able to increase efficiency in designs of coastal structures for these mild slopes. This study also provides evidence that rocks on mild slopes have different characteristics of damage and damage development compared to steep slopes. The largest share of entrained rocks transport in upward direction and rocks on mild slopes seem to be more mobile compared to steep slopes. This suggested that it might be more efficient to study the moment when the filter layer or the core becomes visible instead of the static stability of rock within the armour layer itself.

Extended summary

The aim of this thesis is to understand the static stability of rock on mild slopes under wave attack for impermeable cores. Physical model tests have been executed to study this stability for a 1:8 slope. Mossinkoff (2019) has executed physical model test for a 1:10 slope and a re-analysis of these tests is included in this thesis. Stereophotogrammetry, wave gauges, coloured rocks and cameras were used to measure damage, transportation of rocks and the incoming waves. An improved method has been applied for the stereophotogrammetry. This improved method entails additional Ground Control Points (GCPs) at the upper part and bottom part of the slope. These additional GCPs are added to avoid bias problems. Absence of these outer GCPs results in a bias curve affecting the outcomes for the entire part of the slope.

Damage have been quantified using stereophotogrammetry and the studied profile based damage parameters are S, S_{all}, E_{2D}, $E_{3D,1}$, $E_{3D,3}$ and $E_{3D,5}$. In this thesis, the $E_{3D,3}$ is considered to be the most suitable profile based damage parameter for mild slopes. This conclusion is based on the concept of the damage parameters, the damage domain, the measuring accuracy and the variability of the damage parameters.

In this study, the influence of several hydraulic and structural parameters on damage parameters have been investigated. A positive correlation was found between the significant wave height H_s and the damage parameters. The wave steepness $s_{o,p}$ is negatively correlated with the damage parameters. Evidence is provided that the 1:8 slope incurs more damage compared to the 1:10 slope for a similar significant wave height H_s and wave steepness $s_{o,p}$. An increase in the layer thickness T from 2.5 d_{n50} to 5.0 d_{n50} did not seem to increase the stability of the structure. A linear relationship is found between the number of waves N and the 2D damage parameters. Evidence is provided that even after 15000 waves damage still increased. A similar linear relationship was found between the number of waves N and the 3D damage parameters, but with an initial jump/offset.

The distribution between the plunging and spilling waves was determined for each Iribarren number ξ_p on a 1:8 slope. The outcomes were compared to the results for a 1:10 slope analysed by Mossinkoff (2019). According to the results, the Iribarren number ξ_p is able to describe the distribution between plunging and spilling waves on mild slopes.

The transportation direction of entrained and deposited rocks is determined for the 1:8 and 1:10 slope using coloured rocks in strips for all wave steepnesses $s_{o,p}$. For a wave steepness $s_{o,p}$ of 0.01, on average 92 percent of the rocks deposited upslope for the 1:10 slope. This number decreased to 82 percent for a wave steepness $s_{o,p}$ of 0.05. The 1:8 slope showed lower results. 82 percentage of the rocks deposited upslope for a wave steepness $s_{o,p}$ of 0.01 and this reduced to 60 percent for a wave steepness $s_{o,p}$ of 0.05. The mobility parameter MP is the gross number of transported coloured rocks divided by the net number of transported coloured rocks. The medians of this parameter are 3.0 for the 1:8 slope and 2.9 for the 1:10 slope. This indicates that approximately three rocks are transported where only one rocks is causing erosion. This number probably underestimates the actual mobility parameter, because the coloured rocks also move within a coloured strip of rocks of 0.5 meters itself.

The probability graphs for the deposited location of entrained coloured rocks are determined for the 1:8 and 1:10 slope. Downward entrained rocks only deposit one strip down the slope, where one strip has a width of 0.5 m. This is different for the upward entrained rocks. A majority of the upward entrained rocks are deposited only one strip upslope. However, when the significant wave height H_s increases the fraction of rocks that travel two or three strips upslope increases for all wave steepnesses $s_{o,p}$.

Based on the analysis of this thesis, a design formula has been established and the formula is depicted below. The coefficients are determined based on the root mean squared error (RMSE) for damage parameter $E_{3D,3}$. To find the best curve fitting design formula, the RMSE is minimised. The minimal RMSE is equal to 0.20. The formula is valid for a layer thickness of 2.5 d_{n50} on an impermeable core and are validated for Iribarren numbers ξ_p between 0.45 and 1.25 for 1:8 and 1:10 slopes. The design formula can probably be used for lower Iribarren numbers ξ_p, because the number of spilling waves will increase and which leads to lower damage levels. The damage limits values for the damage parameter $E_{3D,3}$ are 0.3 for initial damage, 0.6 for intermediate damage and 1.5 for failure of the structure. The failure limit has been decreased from 2.0 to a more conservative value of 1.5 to deal with observed temporary failures during testing. This decrease of 0.5 is still an initial number and needs further justification. This design formula allows higher stability numbers before failure of the structure compared to an extrapolation of the Van der Meer (1988) formula.

$$\frac{H_s}{\Delta d_{n50}} = 7.55 * E_{3D,3}^{0.62} * \xi_p^{-1.10} * N^{-0.13}$$

Evidence provided in this thesis suggests that rock on mild slopes seems to have its own character of damage. Mild slopes also have a different behaviour compared to steep slopes regarding the transportation direction and the mobility of the rocks. Indications for this are the recorded mobility parameter *MP* of approximately three, temporary failures and a restorative effect during testing and the presence of some longshore transport during testing caused by an observed boundary effect. Static stability is associated with a steep profile with rather large rocks. In such a design, the rocks transport in downslope direction and every movement is considered as damage meaning that the entrained rocks do not remain in the area of wave attack. Dynamic stability relates to mild slopes with rather small rocks where rocks transport in both upslope and downslope direction and the structure is starting to deform towards an equilibrium profile. The physical model tests performed for this thesis seems to be somewhere between statically stable and dynamically stable structures. An equilibrium profile can never be reached within the executed physical model tests due to limited number of rocks within the layer thickness of 2.5 d_{n50}. The relative thin layer thickness of 2.5 d_{n50} is therefore limits the research to a statically stable approach, where a limited number of displaced rocks within the structure is allowed. During the observed temporary failures and the restorative effect, the core or filter layers of a structure becomes visible. This can be considered as failure of the structure because the the filter layer and core erosion will quickly erode affecting the entire stability of the structure. Another stability approach can be that a structure will fail when the filter layers or core becomes visible. From this perspective, the structure is not failing as long as the filter layer is protected. This is especially interesting for mild slopes where the nominal diameter d_{n50} of the rock is rather small and where these rocks seem to have different behaviour. Based on all mentioned reasons, it might be more efficient to study the moment when the filter layer or core becomes visible instead of focussing on the static stability of rock within the armour layer itself.

Table of Contents

Preface ..... ***iv***

Acknowledgement ..... ***iv***

Abstract ..... ***vi***

Extended summary ..... ***viii***

1 Introduction ***1***

1.1 Background **1**

1.2 Problem analysis **1**

1.3 Research objective and sub-research questions **3**

1.4 Scope **3**

1.5 Outline of report **4**

2 Literature review ***5***

2.1 Governing parameters **5**

2.1.1 Hydraulic parameters 5

2.1.2 Structural parameters 7

2.2 Damage parameters and damage profiles **9**

2.2.1 2D damage parameter, S 9

2.2.2 2D damage parameter, E_{2D} 10

2.2.3 3D damage parameter, $E_{3D,m}$ 10

2.2.4 Damage parameter, N_{od} 11

2.2.5 Discussion of the profile based damage parameters 11

2.2.6 Damage profiles 12

2.3 Research on the stability of rock under wave attack **12**

2.3.1 Stability of rock in breaking waves on steep slopes 12

2.3.2 Stability of rock under wave attack on mild slopes 15

3 Methodology ***21***

3.1 Physical model tests for 1:8 slope **21**

3.1.1 Test set-up 21

3.1.2 Measuring techniques 24

3.1.3 Test Procedure 26

3.1.4 Test plan 27

3.2 Re-analysis of the physical model tests for 1:10 slope performed by Mossinkoff (2019) **27**

3.2.1 Test set-up 28

3.2.2 Measuring techniques 28

3.2.3 Test plan 30

3.3 Processing the stereophotogrammetry and determining the damage parameters **30**

3.3.1 Processing the stereophotogrammetry 30

3.3.2 Determining 2D damage parameters 32

3.3.3 Determining 3D damage parameters 34

3.3.4 Effect of measuring inaccuracy on damage parameters 35

3.3.5 Damage domain and location 37

3.4 Analysing the video material to determine wave breaking type **37**

3.5 Processing the entrained and deposited coloured rocks **40**

4 Results *42*
4.1 Visual observations **42**
4.2 Profile based damage parameters **43**
4.2.1 Influence of wave height, wave steepness and slope angle 43
4.2.2 Influence of layer thickness 46
4.2.3 Influence of the number of waves 48
4.2.4 Variability of damage parameters 49
4.2.5 Influence of boundary effect on profile based damage parameters 51
4.3 Damage domain and location **52**
4.4 Wave breaking types **53**
4.5 Entrained and deposited individual coloured rocks **55**
4.5.1 The damage parameters N_{od} and S_{od} 55
4.5.2 The mobility parameter *MP* and nominal diameter of entrained rocks 57
4.5.3 The transport direction of entrained and deposited coloured rocks 58
4.5.4 The transport length of entrained and deposited coloured stones 59
4.6 Design formula for mild slopes **60**
4.6.1 Damage limits 60
4.6.2 Design formula 61
4.6.3 Comparison to an extrapolation of the Van der Meer (1988) formula 62
4.7 Discussion of results **63**
5 Conclusion *67*
6 Recommendations *71*
References *72*
List of Figures *75*
List of Tables *77*
List of Symbols *79*
Appendix A: Additional literature review *81*
Appendix B: Impressions of test set-up 1:8 slope *84*
Appendix C: Distribution of significant wave heights during the tests *88*
Appendix D: Complete test plan *98*
Appendix E: Software settings *100*
Appendix F: Average profile change graphs *101*
Appendix G: 3D profile change graphs *104*
Appendix H: Profile based damage parameters *142*
Appendix I: Damage domain and damage location *146*
Appendix J: Results of entrained and deposited coloured rocks *148*
Appendix K: Determining the design formula *154*
Appendix L: Probability graphs of entrained rocks *155*
Appendix M: Simplified approach to determine $E_{3D,3}$ *157*

1 Introduction

Improving knowledge on coastal protections is still ongoing and relatively little research is done on the stability of rock on mild slopes. In this study, mild slopes are defined as slopes which are more gentle than 1:6. This chapter starts with the background of the project in section 1.1, followed by a problem analysis in section 1.2. Section 1.3 presents the research objective and research questions. Section 1.4 describes the scope of this thesis and the outline of the report is specified in section 1.5.

1.1 Background

Extensive studies have been executed on the stability of rock on slopes under wave attack. These studies mainly concentrated on steep slopes and design methods for this kind of slopes have been developed by for example by Hudson (1959) and Van der Meer (1988). However, there are situations where mild slopes need to be constructed. Mild slopes are mainly present at pipeline landings at beaches and foreshore protections at sea defences, lakes and estuaries. At this moment an extensive design method, such as the Van der Meer Formula for steep slopes, does not exists for mild slopes.

De Vries & van de Wiel is a Dutch contractor specialised in many fields within hydraulic engineering. One of these fields is coastal protections. Rock protection works with milder slopes than 1:6 are often designed using an extrapolation of the Van der Meer (1998) formula. It is arguable that such an approach leads to conservative rock sizes and inefficient designs. The Van der Meer (1988) formula is only validated for slopes between 1:1.5 and 1:6. De Vries & van de Wiel suspects that the designs for rock protection works on mild slopes can be improved. For this reason, de Vries & van de Wiel and TU Delft have started to research the stability of rock protection designs on mild slopes in cooperation with MSc students. In 2018, the Department of Coastal Structures and Waves of Deltares also joined the research when more physical model tests were performed by Mossinkoff (2019).

1.2 Problem analysis

For mild slopes, two breaker types of waves are important: plunging and spilling waves. Plunging waves have a higher impact on a coastal protection compared to spilling waves. This is because wave energy dissipation is absorbed over a smaller area of the slope and plunging waves create a plunging jet with more impact directly on the slope. Which breaker type will develop depends mainly on two parameters: the slope angle and wave steepness. These parameters can be expressed by the Iribarren number. A gradual transition zone was observed between the plunging and spilling waves for mild slopes (Mossinkoff, 2019). Mossinkoff (2019) investigated the distribution of the plunging and spilling waves for Iribarren numbers between 0.45 and 1.00 for a 1:10 slope. A 50/50 distribution was observed for an Iribarren number of 0.45. The amount of pluning waves increases to 100 percent when the Iribarren number equals 1.00 (Mossinkoff, 2019).

As already mentioned, the Van der Meer (1988) formula is derived from physical model tests for 1:6 slopes and steeper. The number of spilling waves (low impact on the slope) are very limited in the physical model tests of Van der Meer (1988) based on the observations of Mossinkoff (2019). Designing mild slope revetments based on an extrapolation of the Van der Meer (1988) formula for plunging waves would indeed lead to conservative rock dimensions. Schiereck et al. (1994) and Schiereck & Fontijn (1996) have already concluded this based on the physical model tests for 1:10 and 1:25 slopes performed by Sistermans (1993) and Ye (1996).

Besides the conservative rock dimensions, also the character of damage changes for mild slopes as displaced rocks are not moved out of the area of wave attack as quickly. Kramer (2016) observed this

changing character based on damage profiles during physical model testing. A berm damage profile is noticed for a mild 1:10 slope and a bar damage profile was seen for a steep 1:5 slope (Figure 5). Mossinkoff (2019) concluded that the rock transport for a 1:10 slope is 90 percent upslope directed which affirms the changing character of damage.

Since 2015, five master students have already fulfilled their thesis project on the stability of rock on mild slopes. Wit (2015), Postma (2016) and Wendt (2017) studied the potential of the process-based numerical model XBeach-G to design a statically stable rock protection on mild slopes (XBeach-G is a numerical model to research reshaping gravel beaches). The approach did not lead to satisfactory results, because the model could not determine the acceleration and velocity of flow near the bed accurately enough. Wendt (2017) concluded that the XBeach-G model is not suitable to describe the static stability of stones on mild slopes. Mossinkoff (2019) examined if other numerical models than the XBeach-G model are capable of determining the static stability of rock on mild slopes. Her conclusion is that, up to now, no reliable numerical model is available to describe the static stability of rock/gravel on mild slopes for statically stable structures. Mossinkoff (2019) also concluded that physical model tests are the preferred approach to describe the stability of rock on mild slopes and to develop a design formula.

Kramer (2016) performed physical model tests using regular waves to determine the hydrodynamic forces and the initiation of rock motion by using Bubble Image Velocimetry (BIV). The data of these tests were analysed by Wendt (2017) with the intention to develop a design method to describe the static stability of rocks on mild slopes under wave attack. A design method based on flow velocities induced by waves is very complex and will include many uncertainties if the level of damage has to be estimated. A design method for the static stability of rock on mild slopes based on a damage parameter derived from empirical tests is preferred and can be used as a baseline for more process-based models.

Kramer (2016) also executed a limited number of physical model tests with irregular waves for 1:5, 1:10 and 1:15 slopes to determine the static stability of rock on mild slopes. Kramer (2016) concluded that the damage depth parameter $E_{3D,3}$ describes damage better than the damage level parameter S used by Van der Meer (1988). A positive correlation was found between increasing significant wave height and increased damage depth $E_{3D,3}$. If the slope angle is increased this positive correlation becomes stronger. Mossinkoff (2019) executed physical model tests for a constant 1:10 slope and an unchanged nominal stone diameter. The significant wave height, the wave steepness, the layer thickness and the number of waves are varied one-by-one to understand underlying correlations with damage. Mossinkoff (2019) proposed a design formula for mild slopes. The validity region is now between Iribarren numbers of 0.45 and 1.00 for a constant slope of 1:10 and a layer thickness of 2.5 d_{n50} on an impermeable core.

The previous studies discussed above have given much insight in the rock behaviour on gentle slopes, but the design methods to describe the stability of rocks on mild slopes under wave attack are limited to a 1:10 slope only. Kramer (2016) and Mossinkoff (2019) both concluded that the damage depth $E_{3D,3}$ is the preferred damage parameter. Before these thesis projects were executed no datasets were available which included this damage depth parameter $E_{3D,3}$ for mild slopes. A limited dataset is gathered by Kramer (limited) (2016) and Mossinkoff (2019) including this damage depth $E_{3D,3}$ but both suffered from experimental imperfections. The slopes analysed until now are 1:5, 1:10 and 1:15 but gaps are still present. The gap between 1:5 and 1:10 is especially interesting, because it covers the gap between the studies of Van der Meer (1988), Mossinkoff (2019) and Kramer (2016). A slope between the range of 1:5 and 1:10 might also give insight into the transition between a bar (1:5 slope) and berm (1:10 slope) damage profile. This thesis will elaborate further on the previous work and will try

to create new scientific knowledge to develop more effective and competitive designs for coastal protections of rock on mild slopes.

1.3 Research objective and sub-research questions

This master thesis uses the results described in section 1.2 and will focus in more detail on the stability of rock on mild slopes. The research objective of this thesis is comparable to the previous theses and states:

''Describe the stability of rock on mild slopes under wave attack for impermeable cores.''

This research objective will be addressed using sub-research questions. These sub-research questions are based on the literature review are as follows:

1. *What are the influences of the hydraulic parameters significant wave height, wave steepness, Iribarren number and number of waves and the structural parameters slope angle and layer thickness on damage on mild slopes?*
2. *Which damage parameter is most suitable to describe the damage on mild slopes?*
3. *What is the distribution of plunging and spilling waves for mild slopes and can this be described by the Iribarren number?*
4. *What is the main direction of the entrained and deposited rocks on mild slopes in the range of 1:8 and 1:10 and what is the transportation length?*
5. *What design formula can be established for rock on mild slopes resulting in more efficient designs?*

1.4 Scope

The scope of this study consisted of physical model tests for a 1:8 slope and a re-analysis of the physical model tests for a 1:10 slope performed by Mossinkoff (2019). A 1:8 slope was selected to fill the knowledge gap between the research of Van der Meer (1988), Mossinkoff (2019) and Kramer (2016) as described in the section 1.2.

Mossinkoff (2019) and Kramer (2016) investigated the damage level, the erosion depth and the damage depth and have suggested that damage depth is the most suitable profile based damage parameter. This thesis added value by verifying these profile based damage parameters and extended the research for a 1:8 slope which is steeper than previously investigated by Mossinkoff (2019) and in between the results of the limited data set from Kramer (2016). The statistical standard deviation and variation of each damage parameter have been investigated for this 1:8 mild slope as well by repeating tests under the same test conditions. Furthermore, the correlations between damage parameters and hydraulic and structural parameters have been investigated by varying the significant wave height, the wave steepness, the number of waves, the slope angle and the layer thickness.

As described in section 1.2, spilling and plunging waves have different impact on rock displacements and the correlation with the stability of rock on mild slopes has hardly been examined. Mossinkoff (2019) investigated the distribution of plunging and spilling waves for Iribarren numbers between 0.45 and 1.00 for a 1:10 slope. My study has extended this distribution for a 1:8 slope to study if the Iribarren number can describe this distribution for irregular waves.

Strips of coloured rocks were also used to research the character of damage. Studying the entrained and deposited coloured rocks gave insight on the mobility of rocks and the transportation direction

and length. The damage parameter N_{od} is also determined based on these entrained and deposited coloured rocks.

As discussed in section 1.2, Mossinkoff (2019) proposed a design formula for mild slopes. The validity region is now between Iribarren numbers 0.45 and 1.00 for a constant slope of 1:10 and layer thickness of $2.5d_{n50}$ on an impermeable core. My study focussed on the extension of this formula for steeper 1:8 slopes.

1.5 Outline of report

This thesis report starts in chapter 2 with a literature review based on the previous thesis projects and other relevant literature on this topic. Chapter 3 describes the research methodology and illustrates how to achieve results that can be used to answer the research objective and sub-research questions. The method consists of another set of physical model tests for a 1:8 slope. A re-analysis of the physical model test performed by Mossinkoff (2019) for a 1:10 slope is executed as well to be certain that damage parameters are determined in a similar manner. Chapter 3 also documents the approach of processing and determination of the damage parameters. This chapter concludes the method to determine the distribution of plunging and spilling waves and the main direction and transportation length of the rocks. The results are presented and interpreted in chapter 4. The conclusions are drawn in chapter 5 followed by the recommendations for future research in chapter 6.

2 Literature review

The stability of coastal rock protection structures under wave attack is complex and many mechanisms play a role. Section 2.1 describes the governing parameters for the stability of mild slopes divided in hydraulic and structural parameters. Hydraulic parameters give information about the loads initiated by the waves. The structural parameters provide insight on the strength and resistance of the structure. Section 2.2 discusses how to define damage to coastal rock protection structures by different damage parameters and corresponding damage profiles. Section 2.3 reviews the research on the stability of rock on slopes under wave attack. Additional literature on the forces acting on an individual rock and the stability of rock on a horizontal bed is added in Appendix A.

2.1 Governing parameters

This section presents the governing parameters in this study. The hydraulic and structural properties considered in this research are listed in Table 1. Section 2.1.1 elaborates on the hydraulic parameters and is followed by the structural parameters in section 2.1.2. Thorough descriptions and visualisations of the hydraulic and structural parameters are presented in CIRIA et al. (2007).

Table 1: *The hydraulic and structural parameters in this research.*

	Parameter	Description	unit
Hydraulic parameters	H_s	Significant wave height	m
	T_p	Peak wave period	s
	h	Water depth	m
	$s_{o,p}$ (=$H_s/(1.56T_p^2)$)	Wave steepness	-
	ξ_p (= tan $\alpha/\sqrt{s_{o,p}}$)	Irribaren number	-
Structural parameters	α	Slope angle	°
	P	Notional permeability	-
	d_{n50} (= $\sqrt[3]{M_{50}/\rho_s}$)	Nominal rock diameter	m
	Δ (=$(\rho_s - \rho_w)/\rho_w$)	Relative density	-
	N_s (=$H_s/(\Delta\, d_{n50})$)	Stability number	-

2.1.1 Hydraulic parameters

Wave spectrum, wave period and significant wave height
Waves in oceans and seas are irregular and are described by a wave spectrum. A Joint North Sea Wave Project (Jonswap) spectrum is used to be able to make a good comparison between the results obtained from the physical model test for a 1:8 slope in this study to the results of Mossinkoff (2019) for a 1:10 slope. The Jonswap spectrum is representative for the wave spectrum at the Dutch coastline (Holthuijsen, 2007). Van der Meer (1988) used a Pierson-Moskowitz (PM) spectrum for most of his physical model tests. This makes a comparison between his results and analysis in this report less accurate.

The wave period *T* of a wave spectrum can be expressed in the peak period T_p, the mean period T_m or the mean energy period $T_{m-1,0}$. Van der Meer (1988) used T_m in his analysis for rocks on steep slopes, without any basic motivation for this choice (Van der Meer, 1998). Van Gent et al. (2003) showed that the mean energy period $T_{m-1,0}$ is the optimal wave period in the stability relation for rock slopes with shallow foreshores. Mossinkoff (2019) used the peak period T_p in her analysis for mild slopes. The peak period T_p will mainly be used in this report in order to compare the results with Mossinkoff (2019).

The wave height *H* of a wave spectrum is generally expressed by the significant wave height H_s. This significant wave height H_s can be defined as either $H_{1/3}$ or H_{m0}. $H_{1/3}$ is the average of the highest one-

third waves in the time domain and H_{m0} is based on the spectral analysis. Mossinkoff (2019) and van der Meer (1988) both measured the wave height in from of the structure and used $H_{1/3}$ as the significant wave height H_s. To be able to compare the results, the significant wave height H_s in this study is also based on the highest one-third waves.

Wave steepness

The wave steepness $s_{o,p}$ is determined by the significant wave height H_s and the wave length $L_0 (= \frac{gT_p{}^2}{2\pi} = 1.56T_p{}^2)$ in deep water. Eq. 2.1 depicts this relationship. The wave steepness $s_{o,p}$ for irregular waves has a maximum of approximately 0.05 representing wind waves. The wave steepness $s_{o,p}$ for swell waves is approximately 0.01. Mossinkoff (2019) showed that the wave steepness $s_{o,p}$ (via the wave height and wave period) influences the damage and is for that reason an important hydraulic parameter in this study on mild slopes.

$$s_{o,p} = \frac{H_s}{L_0} = \frac{2\pi H_s}{g\,T_p^2} = \frac{H_s}{1.56\,T_p^2} \qquad \text{Eq. 2.1}$$

Iribarren number

The wave characteristics and their activity on a slope can be expressed by the Iribarren number ξ which is defined in the research of Battjes (1974). This parameter ξ is depicted in Eq. 2.2.

$$\xi = \frac{\tan\alpha}{\sqrt{s_o}} \qquad \text{Eq. 2.2}$$

The Iribarren number ξ expresses the ratio between α, the slope angle of the structure, and the wave steepness s_o (Battjes, 1974). This dimensionless parameter is used to define the following breaker types: surging, collapsing, plunging and spilling waves. These types of waves and corresponding Iribarren number are visually illustrated in Figure 1. The experiments performed by Battjes (1974) were executed on smooth slopes with regular waves.

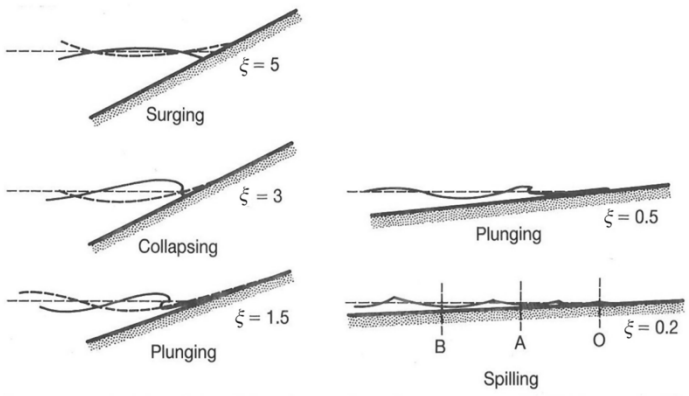

Figure 1: *The different types of wave breaking based on the Iribarren number on smooth slopes and regular waves (Battjes, 1974) & (CIRIA et al., 2007).*

In this research, the Iribarren number is based on the peak period T_p and H_s and is defined as ξ_p in Eq. 2.3. In this report, ξ_m is also mentioned and similarly defined as ξ_p, but is based on the mean period T_m instead of the peak period T_p.

$$\xi_p = \frac{\tan\alpha}{\sqrt{s_{o,p}}} \qquad \text{Eq. 2.3}$$

The different impact of plunging and spilling waves is important for the stability of rock on mild slopes. The wave crest of plunging waves is very asymmetrical and this causes the wave to curve. Air gets confined and the crest eventually bumps into the slope as depicted in Figure 2. This plunging crest creates a plunging water jet attacking the slope and entrains air which generates turbulence (Battjes, 1974). The result is that this plunging jet harms the slope very locally which corresponds with a lot of wave energy dissipation on a short section of the slope profile. On milder slopes waves start to break like spilling breakers. The spilling breaker has a wave crest that is less asymmetric and the plunging water jet is not present. A roller is formed and water separates this roller from the bed limiting the impact on the slope. The wave energy dissipation of spilling wave is stretched over a longer distance on the slope profile as depicted in Figure 2.

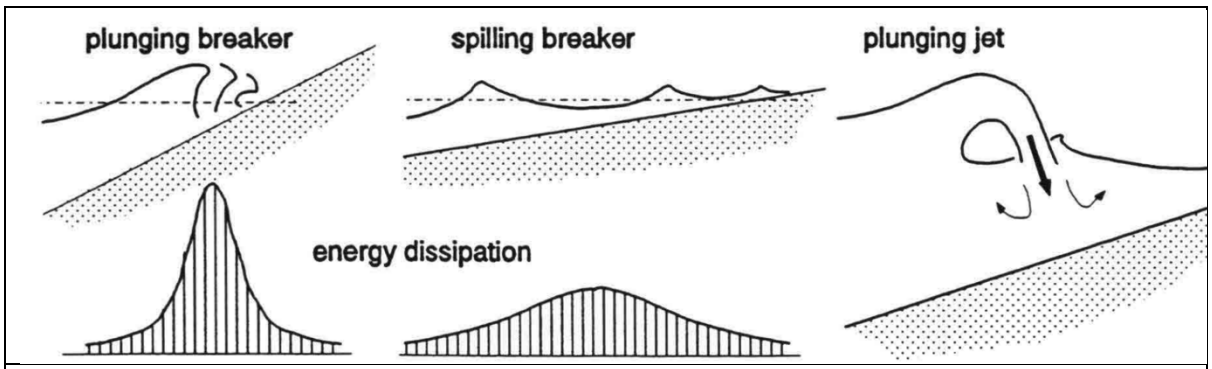

Figure 2: *The different types of energy dissipation for spilling and plunging breakers and the plunging jet (Schriereck and Fontijn 1995 & 1996).*

Battjes (1974) has also stated that the transition between the different breaker types are gradual even for regular waves. After a wave plunged on the slope, shoreward a formed roller travels further and carries the wave energy that is left (Battjes, 1974). When a slope becomes milder or wave steepness increases, the size of the plunging jet decreases until it is not noticeable anymore. The moment where this plunging jet is not noticeable anymore the wave becomes a spilling breaker (Battjes, 1974).

Mossinkoff (2019) has analysed the distribution of spilling waves and plunging waves for Iribarren numbers ξ_p between 0.45 and 1.00 for a constant slope of 1:10. Her findings are presented in Table 2. In the results of Mossinkoff (2019) it is shown that the transition zone between plunging and spilling waves for irregular waves (on a rough slope) is already present for Iribarren numbers ξ_p of 0.71 or less. In this study, this distribution of plunging and spilling waves is further researched for a 1:8 slope.

Table 2: *The distribution of plunging and spilling waves for different Iribarren numbers ξ_p under a constant slope of 1:10 (Mossinkoff, 2019).*

Slope angle [Cot α]	Wave steepness [$s_{o,p}$]	Iribarren number, [ε_p]	Percentage plunging [%]	Percentage spilling [%]
10	0.01	1.00	100	0
10	0.02	0.71	94	6
10	0.03	0.58	73	27
10	0.04	0.50	64	36
10	0.05	0.45	51	49

2.1.2 Structural parameters

Stability number

The most important parameter for rock stability on slopes under wave attack is the stability number N_s which is depicted in Eq. 2.4 (CIRIA et al., 2007).

$$N_s = \frac{H}{\Delta d} \qquad \text{Eq. 2.4}$$

In this study, *d* is defined as the nominal rock diameter d_{n50} which is based on the weight of rocks used and is depicted in Eq. 2.5.

$$d_{n50} = \sqrt[3]{\frac{M_{50}}{\rho_s}} \qquad \text{Eq. 2.5}$$

M_{50} represents the median weight where 50 percent of the particles is lighter and 50 percent is heavier than this median weight. ρ_s is the density of the rock. Relative density Δ is the weight of the particles under water (the submerged density) and is expressed in Eq. 2.6.

$$\Delta = \frac{\rho_s - \rho_w}{\rho_w} \qquad \text{Eq. 2.6}$$

Using the significant wave height H_s, the nominal diameter d_{n50} and the relative density Δ, the stability number N_s is defined in Eq. 2.7.

$$N_s = \frac{H_s}{\Delta d_{n50}} \qquad \text{Eq. 2.7}$$

Notional Permeability

Van de Meer (1988) researched the effect of the permeability of a structure on the stability of rock and introduced the notional permeability coefficient *P*. This coefficient simply quantifies the permeability of different structures but has no physical context (Van der Meer, 1988). In the study of Van der Meer (1988), a notional permeability coefficient *P* of 0.1 is determined for a structure with an impermeable core. Eldrup et al. (2019) studied the notional permeability *P* of six structures with an impermeable core as shown in Figure 3. Their research showed that the notional permeability *P* varies between 0.1 and 0.38 for different thicknesses of the armour layer and underlayers on an impermeable core. An empirical relation has been developed by Eldrup et al. (2019) to determine the notional permeability *P* of a structure. The description and steps to determine the notional permeability *P* are explained in Eldrup et al. (2019). This method is used to determine the notional permeability *P* of the structures used in the physical model tests in this study. This approach is also used to determine the notional permeability *P* of the physical model tests of Mossinkoff (2019) and Kramer (2019).

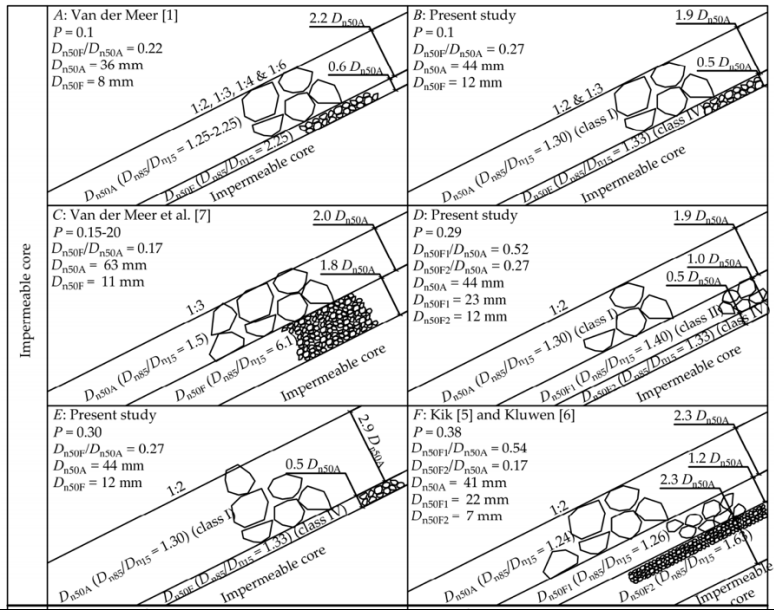

Figure 3: *The notional permeability coefficient of various structures (Eldrup et al., 2019).*

2.2 Damage parameters and damage profiles

In order to fulfil the condition of static stability, no or little displacements of the rocks of the coastal structure are allowed (Van der Meer, 1988). These displacements can be characterized by the damage parameters. These damage parameters are discussed in this section. Damage is visible when rocks are displaced from their initial position (Van der Meer, 1988). Multiple damage parameters are presented in literature. Damage to a coastal protection structure is hard to quantify due to the random character of turbulent flows and the position of stones (Hofland, 2005). In this section, an insight is given into the damage parameters and the damage profiles of rock on slopes under wave attack. Profile based damage parameters can be divided into 2D and 3D damage parameters. 2D damage parameters are averaged over the width of the flume along the slope. 3D damage parameters are based on a spatial moving average covering the entire slope. Both are described in this section. Besides this, attention will be given to the damage parameter N_{od} based on the number of eroded rocks. All damage parameter concepts are assessed in this study.

2.2.1 2D damage parameter, *S*

Van der Meer (1988) used the profile based damage parameter S as shown in Eq. 2.8 which was first introduced by Broderick & Ahrens (1982). It is a dimensionless parameter described by the erosion area A_e averaged over the characterization width w divided by the square of the nominal rock diameter d_{n50}. The d_{n50} has already been introduced in Eq. 2.5.

$$S = \frac{A_{\langle e \rangle w}}{{d_{n50}}^2} \qquad \text{Eq. 2.8}$$

The erosion area A_e is depicted in Figure 4 (a) and is defined as the cross-sectional area which is eroded from the armour layer in a coastal protection averaged over the characterization width w (De Almeida et al., 2019). The characterization width w is the width of the structure in a physical model test as depicted in Figure 4 (b). Van der Meer (1988) has tested slopes between 1:1.5 and 1:6 with a layer thickness of the armour layer of 2 d_{n50}. Damage starts to occur when the damage parameter S takes a value between 2 and 3, depending on the slope (Van der Meer, 1988). If the damage parameter S has a value between 8 and 17 the parameter is associated with failure of the structure. Again this exact value depends on the slope angle (1:1.5-6) (Van der Meer, 1988). The values for initial damage level S and failure damage level S are summarized in Table 3. Damage limits of S for a 1:8 and 1:10 slope are not present in literature (based on physical model tests). A first estimate for these slopes can be made for the start of damage using a method proposed by Wit (2015) as shown in Eq. 2.9. This method assumes that the erosion depth d_e does not vary for different slopes.

$$S(\alpha) = S_{start} * \frac{\sin(\alpha_{start})}{\sin(\alpha)} \qquad \text{Eq. 2.9}$$

Using the method of Wit (2015) start of damage for a 1:8 slope occurs for S values equal to 4. This value increase to 5 for a 1:10 slope. The larger S value can be explained by the increase in erosion length L_e for milder slopes.

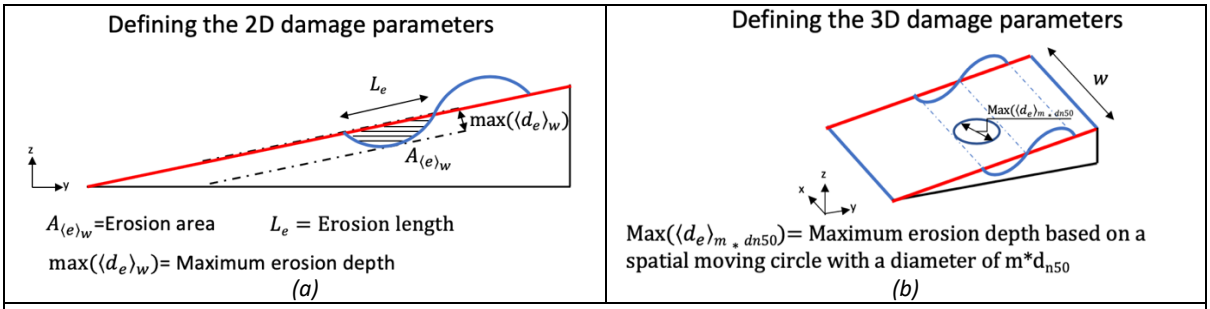

Figure 4: *(a) A schematization to define the 2D damage parameter S and E_{2D}. (b) A schematization to define the 3D damage parameter $E_{3D,m}$.*

2.2.2 2D damage parameter, E_{2D}

Erosion depth d_e is the difference between an initial profile and a damaged profile. The erosion depth d_e is measured perpendicular to the initial slope profile and is depicted in in Figure 4 (a). The E_{2D} parameter is the maximum erosion depth d_e averaged over the characterization width w as depicted in Figure 4 (a) (De Almeida et al., 2019). This damage concept is a development of Hofland et al. (2011), which was based on the research of Melby & Kobayashi (1998). The 2D damage parameters E_{2D} is depicted in Eq. 2.10. The damage limits are investigated by Almeida et al. (2019) and the results are shown in Table 3.

$$E_{2D} = \frac{\max(\langle d_e \rangle_w)}{d_{n50}} \qquad \text{Eq. 2.10}$$

2.2.3 3D damage parameter, $E_{3D,m}$

The damage parameters E_{2D} and $E_{3D,m}$ are both based on erosion depth d_e, where E_{2D} was defined in section 2.2.2. The damage parameter $E_{3D,m}$ is the maximum erosion depth d_e averaged for a moving circle with a diameter of m d_{n50} given a characterization width w, as depicted in Figure 4 (b) (De Almeida et al., 2019). This damage parameter $E_{3D,m}$ is also a development of Hofland et al. (2011), which was again based on the research of Melby & Kobayashi (1998). $E_{3D,m}$ is depicted in Eq. 2.11. Initial, intermediate and failure damage values are presented in literature and are also summarized in Table 3. Different values for m in the $E_{3D,m}$ parameter are used by Hofland et al. (2011), De Almeida et al. (2019) and Mossinkoff (2019). A higher m value leads to an increase of the spatial moving circle and a lower acceptable value for initial, intermediate and failure damage.

$$E_{3D,m} = \frac{\max(\langle d_e \rangle_{m*dn50})_w}{d_{n50}} \qquad \text{Eq. 2.11}$$

The damage depth $E_{3D,3}$ limits for initial, intermediate and failure damage presented by Hofland et al. (2011) are valid for a 2 d_{n50} layer thickness. For larger layer thicknesses Hofland et al. (2011) proposes to correct the failure damage values by adding the actual layer thickness minus the layer thickness 2 d_{n50} used by Hofland et al. (2011).

Table 3: *The initial damage, intermediate damage and failure damage limits for the damage level S, damage depth E_{2D} and $E_{3D,m}$ in different researches.*

	S (Van der Meer, 1988)	**E_{2D} (De Almeida et al., 2019)**	**$E_{3D,1}$ (De Almeida et al., 2019**	**$E_{3D,5}$ (De Almeida et al., 2019)**	**$E_{3D,3}$ (Hofland et al., 2011)**	**$E_{3D,3}$ (Mossinkoff, 2019)**
Layer thickness, T	2 d_{n50}	2 d_{n50}	2 d_{n50}	2 d_{n50}	2 d_{n50}	2.5 d_{n50}
Slope angle	1:1.5-1:6	1:3	1:3	1:3	1:2-1:3	1:10
Initial damage	2-3	0.2	1.0	0.3	0.2-0.3	0.5
Intermediate damage		0.5	1.5	0.7	0.5-0.6	1.2
Failure damage	8-17	0.9	2.0	1.1	1.5-1.6	2.3

2.2.4 Damage parameter, N_{od}

The previous described damage parameters are all profile based. Another damage parameter that could be analysed is N_{od}, which is based on the number of displaced rock units from the armour layer (CIRIA et al., 2007). The damage parameter N_{od} is depicted in Eq. 2.12 and is equal to the total visible number of displaced stones n_{tot} multiplied with the nominal rock diameter d_{n50} divided by the width of the flume (characterization width) w (CIRIA et al., 2007). T

$$N_{od} = \frac{n_{tot} d_{n50}}{w} \qquad \text{Eq. 2.12}$$

Sistermans (1993) and Ye (1996) used coloured rocks within 0.25 m strips for 1:10 and 1:25 slopes and counted the number of displaced stones after a test (Schriereck & Fontijn, 1996). In this research coloured strips with a length of 0.5 m are used to determine the total number of transported n_{tot} and eroded rocks. The damage parameter N_{od} requires formally that all individual measured rock displacements are including. This method using coloured rocks within strips has a disadvantage. The rock displacements within a coloured strip are not recorded. These unobserved rock movements within a strip are considered to be a measuring error.

2.2.5 Discussion of the profile based damage parameters

The shape of the erosion area A_e is not taken into account for the determination of the damage parameter S. An erosion area which is shallow and has a long erosion length L_e can result in a high damage parameter S value but without exposure of the filter layer. It can also be vice versa. In this case, the erosion area A_e can be deep with a short erosion length L_e resulting in a low damage level S value, but an exposed filter layer. That is why damage levels S for the initial damage and failure damage of a structure varies for different slope angles. This can be regarded as a disadvantage of using S as a damage parameter. Especially when assessing mild slopes, which tend to have a long erosion length, this disadvantage becomes even more prominent.

The damage parameters S and E_{2D} are both width average parameters and $E_{3D,m}$ is based on a spatial moving average (De Almeida et al., 2019). A large disadvantage of the width averaging damage parameters S and E_{2D} is the bias in damage characterization. If the characterization width w of a test is increased, the observed width averaged damage will decrease due to the reduced influence of the magnitude of maxima (De Almeida et al., 2019). The damage parameter $E_{3D,m}$ measures the maximum erosion depth based a spatial moving average of m d_{n50} within the characterization width w and is robust against this specific bias problem.

Almeida et al. (2019) analysed $E_{3D,m}$ with an m value of 5. According to this study, advantages of the damage parameter $E_{3D,5}$ are a lower random error for lower damage values, better ability to distinguish damage levels and applicability to all kind of structures and all slopes (De Almeida et al., 2019). This extensive applicability is especially interesting for mild slopes.

Another advantage of the damage parameter $E_{3D,m}$ is the applicability of extreme value analyses using a Gumbel distribution to deal with the length effect (Van Gent et al., 2019). This length effect is defined as an increasing chance that damage exceeds a specified damage limit somewhere along the structure when the width of this structure increases (van Gent et al., 2019). This extreme value analysis is possible, because the damage parameter $E_{3D,m}$ is based on maximum values instead of average values. Kramer (2016) and Mossinkoff (2019) both conclude that the damage depth $E_{3D,3}$ is the most suitable damage parameter for mild slopes.

2.2.6 Damage profiles

The initial profile of a coastal protection structure changes due to damage caused by loads. The final damage profile has areas of accretion and erosion deviating from the initial profile. An interesting distinction is observed in the damage profiles for mild slopes compared to steeper slopes studied by Kramer (2016). A bar damage profile is found on steeper slopes and a berm damage profile on milder slopes as depicted in Figure 5 (a) and (b) for a 1:5 slope and a 1:10 slope (Kramer, 2016). A bar profile is formed due to a net downward-slope rock transportation. A berm profile is formed due to a net upward-slope transport of stones. This distinction is also concluded by Wit (2015) using an XBeach-G model for 1:5, 1:10 and 1:25 slopes. Mossinkoff (2019) has performed physical model tests for a 1:10 slope and berm profiles are observed in these tests. The behaviour of damaged profiles for coastal structures containing a slope between 1:8 slope is still unknown and is determined in this research. A combination of a berm and a bar profile might be a plausible result.

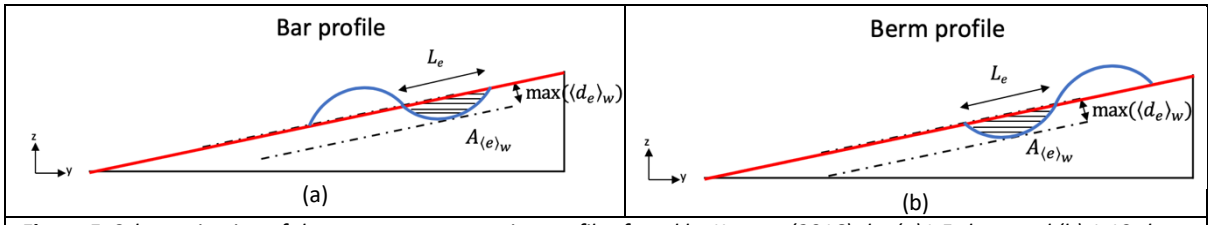

Figure 5: *Schematization of the average cross-section profiles found by Kramer (2016) the (a)1:5 slope and (b) 1:10 slope.*

2.3 Research on the stability of rock under wave attack

This section presents an overview of the research on the stability of rocks. Section 2.3.1 reviews literature on the stability of rock under wave attack on steep slopes. Section 2.3.2 documents the research on stability of rock on mild slopes and gives insight in the accomplishments and results achieved by previous students on this research topic.

2.3.1 Stability of rock in breaking waves on steep slopes

Iribarren (1938) and Hudson (1952)
Iribarren (1938) and Hudson (1952) both based their design formula on the stability in flow as depicted in Eq. 2.13. The first term is the drag force, the second term is the resisting force and the last term is the slope correction.

$$\overset{\text{"drag" force}}{\rho_w g H d_{50}{}^2} \propto \overset{\text{"resisting" force}}{(\rho_s - \rho_w) g d_{50}^3} * \overset{\text{slope correction}}{(\tan\phi \cos\alpha \pm \sin\alpha)} \qquad \text{Eq. 2.13}$$

Iribarren (1938) proposes the formula as shown in Eq. 2.14 where $M \propto \rho_s d^3$ is the mass of stones.

$$M \propto \frac{\rho_s H^3}{\Delta^3 (\tan\phi \cos\alpha \pm \sin\alpha)^3} \qquad \text{Eq. 2.14}$$

Hudson (1952) has presented the formula as depicted in Eq. 2.15 after many tests. The slope correction is simplified to $\cot\alpha$. $H_{sc}/\Delta d_{n50}$ is the dimensionless stability parameter N_s. The Hudson formula is valid for a slope between 1:1.5 and 1:4. K_D is a "dustbin factor" that depends on the material used for the tests (Schiereck & Verhagen, 2016). This dustbin factor for natural rock is between three and four. The formula is relatively simple and does for example not include the

Iribarren number. Other parameters left out of the formula are the permeability, number of waves and damage level. All these factors influence the stability and are researched by Van der Meer (1988).

$$M = \frac{\rho_s {H_{sc}}^3}{K_D \Delta^3 \cos\alpha} \quad or \quad \frac{H_{sc}}{\Delta d_{n50}} = \sqrt[3]{K_D \cot\alpha} \qquad \text{Eq. 2.15}$$

Van der Meer (1988)
Van der Meer (1988) has proposed two design formulas for surging and plunging waves after performing extensive series of physical model tests. More parameters are included in the formula compared to the Hudson (1952) formula in Eq. 2.15. The static stability for plunging waves is depicted in Eq. 2.16 and for surging waves in Eq. 2.17.

$$\frac{H_{sc}}{\Delta d_{n50}} = 6.2 * P^{0.18} * \left(\frac{S}{\sqrt{N}}\right)^{0.2} * \xi_m^{-0.5} \qquad \text{Eq. 2.16}$$

$$\frac{H_{sc}}{\Delta d_{n50}} = 1.0 * P^{-0.13} * \left(\frac{S}{\sqrt{N}}\right)^{0.2} * \xi_m^{P} * \sqrt{\cot\alpha} \qquad \text{Eq. 2.17}$$

In these equations, $H_{sc}/\Delta d_{n50}$ is the dimensionless stability parameter N_s consisting of the critical significant wave height H_{sc}, the nominal diameter d_{n50}, and the relative density Δ. The permeability is described by the permeability coefficient P as mentioned in section 2.1.2 and varies between 0.1 and 0.6. The surging waves formula also includes the slope angle α. The damage level S is the damage parameter as discussed in section 2.2.1, N is the number of waves is and ξ_m is the dimensionless Iribarren number.

Van der Meer (1988) has performed physical model tests on slopes between 1:1.5 and 1:6 as stated in section 1.1. The formula of Van der Meer (1988) for plunging waves as depicted in Eq. 2.16 is extrapolated for Iribarren numbers ξ_m smaller than 1. The extrapolation is illustrated by a dashed line in Figure 8. It is interesting to investigate which physical model tests have been performed by Van der Meer (1988) for the slope 1:6, because this slope most resembles the 1:8 and 1:10 slopes analysed in this study. All physical model tests are shown in Table 4. The test parameters for this 1:6 slope can be found in the top line.

Table 4: *Physical model tests performed by van der Meer (1988), PM is Pierson-Moskowitz spectrum.*

Slope angle cot α	Grading d_{85}/d_{15}	Wave Spectrum	Core permeability	Notional Permeability	Relative mass density	Number of tests	Number of waves	Range $H_s/\Delta d_{n50}$	Range s_m	Range ξ_m
6	2.25	PM	Impermeable	0.1	1.63	26	1000-3000	1.2-4.4	0.004-0.063	0.67-2.66
4	2.25	PM	Impermeable	0.1	1.63	21	1000-3000	1.2-3.3	0.005-0.059	1.05-3.61
4	1.25	PM	Impermeable	0.1	1.62	20	1000-3000	1.2-3.4	0.005-0.059	1.05-3.61
3	2.25	PM	Impermeable	0.1	1.63	20	1000-3000	1.2-2.3	0.006-0.024	2.23-4.47
3	1.25	PM	Impermeable	0.1	1.62	21	1000-3000	1.4-2.9	0.006-0.038	1.78-4.47
3	2.25	Narrow	Impermeable	0.1	1.63	19	1000-3000	1.0-2.8	0.004-0.054	1.49-5.47
3	2.25	Wide	Impermeable	0.1	1.63	20	1000-3000	1.0-2.4	0.004-0.043	1.67-5.47
3	1.25	PM	Permeable	0.5	1.62	19	1000-3000	1.6-3.2	0.008-0.060	1.41-3.87
2	2.25	PM	Impermeable	0.1	1.63	19	1000-3000	0.8-1.6	0.005-0.016	4.32-7.73
2	1.25	PM	Permeable	0.5	1.62	20	1000-3000	1.5-2.8	0.007-0.056	2.31-6.53
2	1.25	PM	Homogeneous	0.6	1.62	16	1000-3000	1.8-3.2	0.008-0.059	2.25-6.11
2	1.25	PM	Permeable	0.5	0.95	10	1000-3000	1.7-2.7	0.016-0.037	2.84-4.32
2	1.25	PM	Permeable	0.5	2.05	10	1000-3000	1.6-2.5	0.014-0.032	3.05-4.62
2	1.25	PM	Permeable	0.5	1.62	16	1000-3000	1.6-2.5	0.014-0.031	3.10-4.62
2	1.25	PM	Permeable	0.5	1.62	31	1000-3000	1.4-5.9	0.010-0.046	2.55-5.46
1.5	1.25	PM	Permeable	0.5	1.62	21	1000-3000	1.5-2.6	0.008-0.050	3.52-8.80

Van der Meer (1988) tested three structure types: homogeneous structure, a structure with a permeable core and a structure with an impermeable core. An impermeable core is used by Van der

Meer (1988) for the 1:6 slope tests. An impermeable and permeable core are tested for a 1:3 slope. All three structure are tested for a 1:2 slope and these results are depicted in Figure 6. The impermeable core structure is the most unstable structure, followed by the permeable core structure and the homogeneous structure as shown in Figure 6. The physics behind the different results is that during the wave impact energy can dissipate into the rock layer. This reduces the forces on the outer stones of the armour layer. Another relevant factor influencing the stability is occurring during the run-down of the flow. When the core is impermeable, the run-down flow can only go through the armour layer, which increases the force on the outer rocks. When a permeable or homogeneous core is present, the flow can also dissipate into the core reducing the forces of the run-down flow on the outer stones of the armour layer. Van der Meer (1988) introduces the coefficient P to take into account these permeability differences which is also described in section 2.1.2. For a structure with an impermeable core this coefficient P is defined as 0.1. For an armour layer with a permeable core and a homogeneous structure this coefficient P is respectively 0.5 and 0.6.

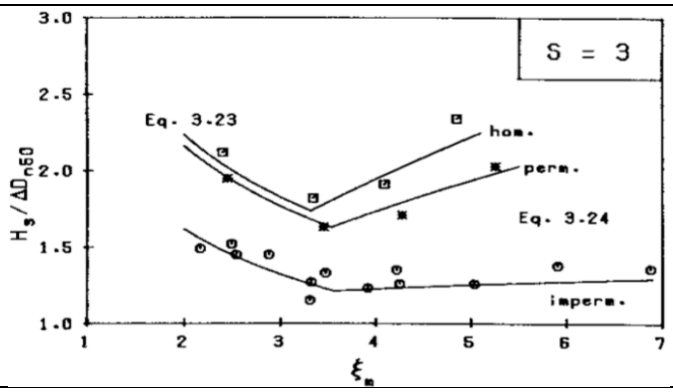

Figure 6: *The stability of a homogeneous, permeable and impermeable structure researched by Van der Meer (1988) for a 1:2 slope and damage level S of 3.*

A minimum stability is visible in Figure 6 corresponding with an Iribarren number in the range of 3.5. This represents the transition between surging and plunging waves. In this case, a possible explanation is that both the plunging jet force and the roller surface turbulence act directly on the slope (Schiereck & Verhagen, 2016).

Thompson and Shultter (1975) have performed physical model tests varying the number of waves N. In their preliminary tests the number of waves are extended up to 20 000 waves for a slope of 1:3. Their main tests are up to 5000 waves and the slopes used varied between 1:2 and 1:6. For these main tests Thompson and Shultter (1975) have concluded that the erosion N_Δ, expressed in stones removed over a width of nine stones, increases rapidly at the start of the test and limited extra erosion is seen between 4000 and 5000 waves. If the significant wave height H_s is not large enough to lead to failure of the structure, meaning exposure of the filter layer, the erosion N_Δ eventually becomes stable for higher number of waves. Van der Meer (1988) has re-analysed the data of Thompson and Shultter (1975) and the results are visualized in Figure 7 (a). The damage parameter S is the damage level as defined in section 2.2.1. A linear relation is present between the damage level S and the first 500 waves. This relationship changes into a squared root relation, $S \sim \sqrt{N}$, after 500 waves until approximately 8500 waves. The waves thereafter is estimated to be 1.3S(5000) where S(5000) is the damage level after 5000 waves. Marginal damage is negligible after 15 000 waves as is illustrated in Figure 7 (a).

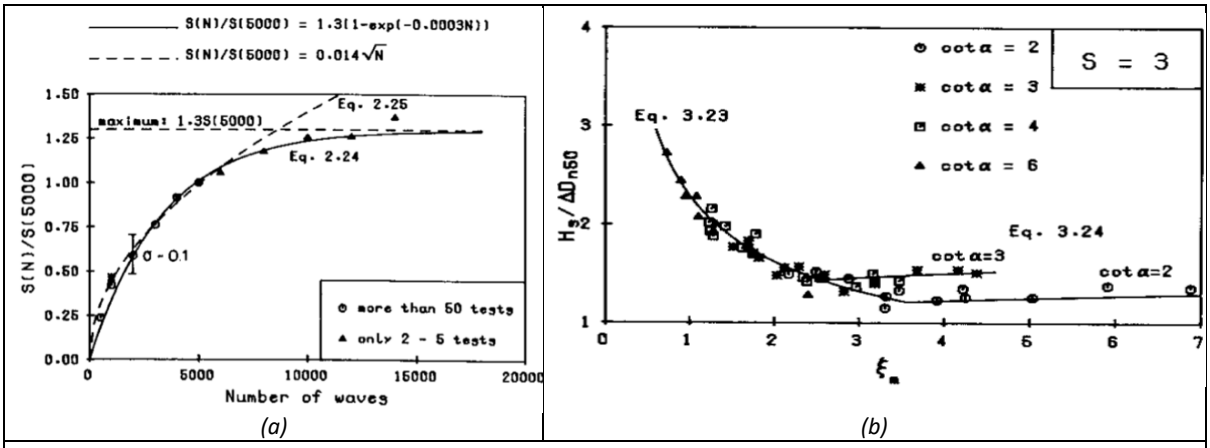

Figure 7: *(a)The influence of the number of waves N on the damage level S (Van der Meer, 1988). (b) The influence of the slope angle on the stability parameter Hs/Δd_{n50} for slope angles between 1:2 and 1:6 for a damage level S of 3 (Van der Meer, 1988)*

Van der Meer (1988) has researched the influence of the slope angle α on the stability of rocks and the results are summarized in Figure 7 (b). The Iribarren number ξ_m is on the horizontal axis. The stability number N_s $(= H_s/\Delta d_{n50})$ is shown on the vertical axis. The slope angle α has an influence on the Iribarren number ξ_m as stated in section 2.1.1. A milder slope will reduce the Iribarren number ξ_m and the a lower Iribarren number ξ_m is associated with a higher stability number N_s $(= H_s/\Delta d_{n50})$.

2.3.2 Stability of rock under wave attack on mild slopes

Sistermans (1993) and Ye (1996)

Sistermans (1993) has performed physical model tests for a 1:25 slope on an impermeable core for both regular and irregular waves with a Jonswap spectrum. The results state that an increase of the Iribarren number ξ leads to a decrease of the stability number N_s.

Ye (1996) has performed physical model tests for 1:10 and 1:25 slopes and an overview of the tests is given in Table 5. Test results show that a lower wave steepness $s_{o,p}$ is unfavourable for the stability of stones (Ye, 1996). Ye (1996) recommends that an increase of relative stone density Δ is more efficient to increase stability compared to an increase of the nominal stone diameter d_{n50} for mild slopes. A plausible explanation for this efficiency difference is that for steeper slopes the slope parallel component of the gravity forces are more dominant compared to mild slopes. One of the damage parameters that has been used is N_{od} as described in Eq. 2.12 (section 2.2.4).

The results of Ye (1996) are compared with the extrapolated Van der Meer (1988) formula shown by the dashed line in Figure 8. The results of the physical model tests confirm that the Van der Meer (1988) formula is conservative. A higher value for the stability number N_s $(= H_s/\Delta d_{n50})$ is allowed compared to the extrapolated Van der Meer (1988) formula as illustrated in Figure 8. However, it was unclear which damage limits were used and when the structure failed.

Table 5: *Physical scale tests performed by Ye (1996).*

Slope angle cot α	Grading D_{85}/D_{15}	Wave Spectrum	Core permeability	Relative mass density	Number of tests	Number of waves	Range $H_s/\Delta D_{n50}$	Range S_p	Range ξ_p
10	1.5	Jonswap	None	1.55/1.85	33	2000	2.37-7.48	0.01-0.04	0.47-0.91
25	1.5	Jonswap	None	1.55/1.85	16	2000	4.95-14.06	0.01-0.05	0.18-0.40

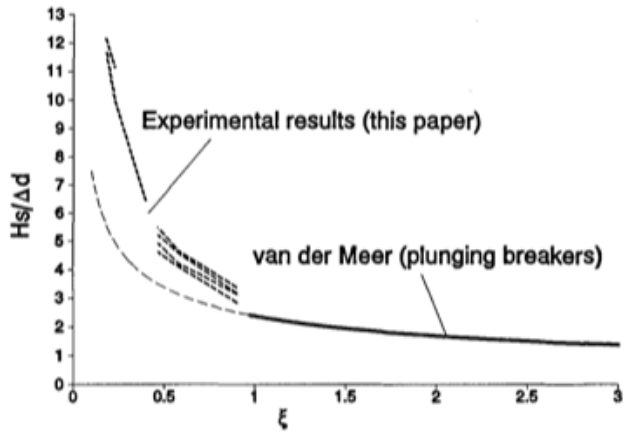

Figure 8: *Results of Ye (1996) depicted in a (ξ, $H_s/\Delta d_{n50}$) diagram (Schiereck & Fontijn, 1996).*

Wit (2015)

Wit (2015) studied the potential use of the process-based numerical model XBeach-G to design a rock protection on mild slopes. Simulation calculations for homogeneous structures showed that the acceptable damage level can be higher for milder slopes than for steeper slopes. The explanation given by Wit (2015) that for mild slope more stones need to move to reach the same damage level compared to steeper slopes. Wit (2015) also proposed to use erosion depth as a damage parameter. Differences were found between the XBeach-G simulations from Wit (2015) and the extrapolated Van der Meer (1988) formula. Two reasons are mentioned by Wit (2015). The first reason is that homogeneous slope structures were only tested for 1:2 slopes by Van der Meer (1988) and were therefore only applicable for steeper slopes. The second reason is that calibration factors used in the model were very sensitive leading to different results.

Postma (2016)

Postma (2016) studied the verification of XBeach-G model as a design tool. Some of the experiments of Van der Meer (1988) were reproduced. The results were compared with sediment transport formulas from Nielsen (2006) and Van Rijn (2007). Postma (2016) concluded that both formulas of Nielsen (2006) and Van Rijn (2007) are not able to forecast the damage levels satisfactorily. Nielsen (2006) gave underestimating results for steeper slopes and Van Rijn (2007) gave unexpected high damage levels for mild slopes. Postma (2016) also advised to be careful using the calibration factors of Nielsen (2006) because their impact on the resulting erosion is significant.

Wendt (2017)

Using Bubble Image Velocimetry (BIV), Wendt (2017) studied the initial motion of a stone and the hydrodynamic forces that initiate the motion using the physical model test results of Kramer (2016). Wendt (2017) focused on the development of a design method to describe the static stability of stones on mild slopes under wave attack based on these findings. He also researched if the test results can be reproduced numerically with the XBeach-G model. Wendt (2017) concluded that the XBeach-G model was not capable enough to describe the static stability of stones on mild slopes, because the acceleration and velocity near the bed cannot be determined by the model.

Wendt (2017) analysed the camera material of the physical model tests performed by Kramer (2016) for a 1:5, 1:10 and 1:15 slope. Several mobility stages can be defined for movements of stones (Hofland, 2005). Rocking is defined as a stone that is moving, but remains at the same location. The initial motion is described by three modes: rolling, sliding and lifting (Hofland, 2005). Rolling occurs when the individual stone start to rotate but stays in contact with the bed. Sliding occurs when the individual particles start to move without rotation. Lifting happens when the particle no longer has contact with the bed. More movements were observed by Wendt (2017) on the 1:5 and 1:10 slopes

with a lot of rocking and some displacements of rock. For the milder slope 1:15 limited rocking was spotted and the displacement occurred sometimes. A distinction between run-up and run-down is also observed by Wendt (2017). Rocking and displacement occurred more often during run-up compared to the run-down.

Kramer (2016) and Mossinkoff (2019)

Kramer (2016) and Mossinkoff (2019) both have executed physical model tests to determine the stability of rock on mild slopes. Both have used irregular waves containing a Jonswap spectrum because this spectrum is representative for the Dutch North Sea coastline. Kramer (2016) has also performed other physical model tests using regular waves to determine the initiation of individual rock motion by using Bubble Image Velocimetry (BIV) analyses. Three different slopes are tested by Kramer (2016): 1:5, 1:10 and 1:15. These tests are summarized in Table 6. The physical model tests executed by Mossinkoff (2019) are summarized in Table 7. The slope angle α of the structure, the nominal stone diameter d_{n50}, the grading and the relative density Δ are kept constant. The significant wave height H_s, the wave steepness $s_{o,p}$, the layer thickness T, and the number of waves N are changed one-by-one to understand underlying correlations and their influence on damage.

Table 6: *Physical model tests performed by Kramer (2016).*

Slope angle cot α	Grading D_{85}/D_{15}	Wave Spectrum	Core permeability	Notional permeability P via method Eldrup et a. (2019)	Relative mass density	Number of tests	Number of waves	Range $H_s/\Delta D_{n50}$	Range S_p	Range ξ_p
5	?	Jonswap	impermeable	0.1	1.69	2	3000	2.08/2.26	0.04	1.0
10	?	Jonswap	impermeable	0.1	1.69	2	3000	3.25/4.93	0.04	0.5
15	?	Jonswap	impermeable	0.1	1.69	2	3000	4.86/7.31	0.04	0.33

Table 7: *Physical model tests performed by Mossinkoff (2019).*

Slope angle cot α	Grading D_{85}/D_{15}	Wave Spectrum	Core permeability	Notional permeability P via method Eldrup et a. (2019)	Relative mass density	Number of tests	Number of waves	Range $H_s/\Delta D_{n50}$	Range S_p	Range ξ_p
10	1.4	Jonswap	impermeable	0.12 and 0.48 (2.5 d_{n50} - 5 d_{n50})	1.94	47	300-11000	2.44-7.66	0.009-0.0.052	0.44-1.06

Kramer (2016) and Mossinkoff (2019) both concluded that damage depth parameter $E_{3D,3}$ is describing damage better compared to the damage level parameter S, which was used by van der Meer (1988). Therefore they used the $E_{3D,3}$ to research the effect of hydraulic and structural parameters on this damage parameter. Mossinkoff (2019) and Kramer (2016) have investigated the effect of the significant wave height H_s on the damage parameter $E_{3D,3}$. They both have found a positive correlation, meaning a higher significant wave height H_s corresponds to more damage. The results of Kramer (2016) are shown in Figure 9 and the results of Mossinkoff (2019) are depicted in Figure 10. A larger significant wave height H_s increases the wave energy by the power of two ($E_{wave} \sim H_s^2$) (Holthuijsen, 2007). This energy will dissipate and is absorbed by the armour layer of the coastal structure.

Kramer (2016) has researched the influence of the slope angle α on the relation between the significant wave height H_s and the damage parameter $E_{3D,3}$. The results are depicted in Figure 9 for the 1:5, 1:10 and 1:15 slopes. As discussed earlier, a higher significant wave height H_s is associated with higher values for the damage parameter $E_{3D,3}$. The slope angle α influences the magnitude of this correlation. A milder slope reduces the effect of the significant wave height H_s on the damage would

$E_{3D,3}$. The explanation given by Kramer (2016) is that the changing Iribarren number ξ_m causes the wave energy to dissipate over a longer distance on the slope.

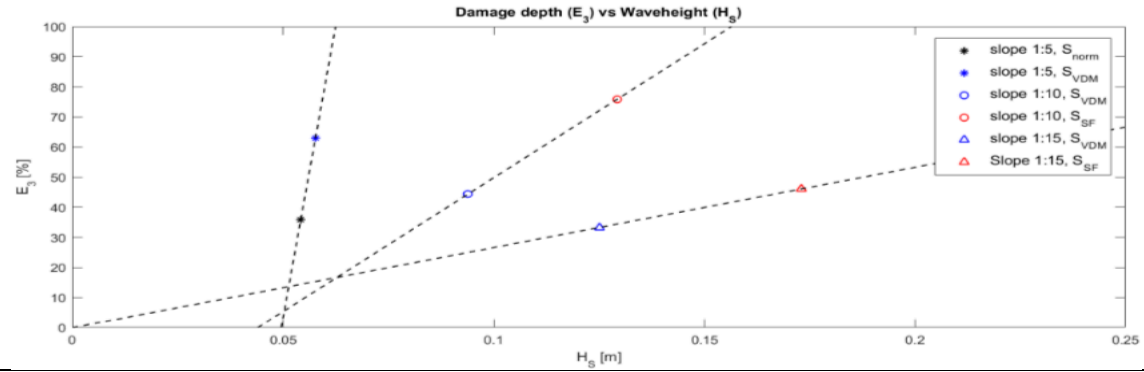

Figure 9: *The influence of slope angle on the relation between the significant wave height Hs and the damage parameter $E_{3D,3}$ (Kramer, 2016). Estimates of for tolerable damage are used to determine the conditions for the tests. S_{VDM} is based on the work of Wit (2015) using an extrapolation of van der Meer (1998) compensation mild slopes. S_{norm} is based on van der Meer(1988) and S_{sf} is based on a extrapolation of Van der Meer (1998).*

Mossinkoff (2019) has investigated the effect of wave steepness $s_{o,p}$ on the relationship between the significant wave height H_s and the damage parameter $E_{3D,3}$. The effect of the significant wave height H_s on the damage parameter $E_{3D,3}$ increases with lower wave steepness $s_{o,p}$ as depicted in Figure 10. A lower wave steepness $s_{o,p}$ corresponds with a higher Iribarren number ξ_m resulting in relatively more plunging waves and a higher damage parameter $E_{3D,3}$.

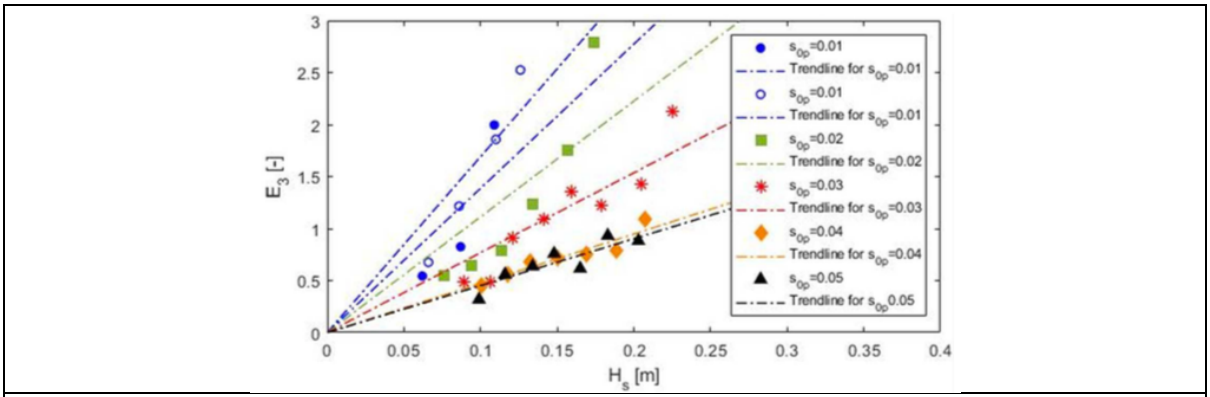

Figure 10: *The effect of the wave steepness s_0p on the relationship between the significant wave height H_s and the damage parameter $E_{3D,3}$ (Mossinkoff, 2019).*

Mossinkoff (2019) tested the relation between the number of waves *N* and the damage parameter $E_{3D,m}$. for a 1:10 slope. The results are depicted in Figure 11 (a). Mossinkoff (2019) has concluded the presence of a linear relationship between the number of waves *N* and the damage parameter $E_{3D,m}$. After 11,000 waves, Mosinkoff (2019) found that the increase of damage parameter $E_{3D,m}$ remained constant. This is contrary to the observations of Van der Meer (1988). Mosinkoff (2019) states that this contradiction is related to the difference in damage profile development between mild slopes and steep slopes. For the steeper slopes, researched by Van der Meer (1988), a bar damage profile is formed resulting in a milder slope where damage develops. Mossinkoff (2019) argues that such a milder slope is not formed for 1:10 slope during the test, due to berm damage profile development. Therefore, extra damage will continue to emerge even after 11,000 waves. According to Mossinkoff (2019), one peculiar data point is observed after the 1,135th wave measuring point. At 2,236 waves the damage depth$E_{3D,m}$ reduced compared to the damage level after 1,135 waves. Mossinkoff (2019) has concluded that this test is not completely reliable and more physical model tests should be performed.

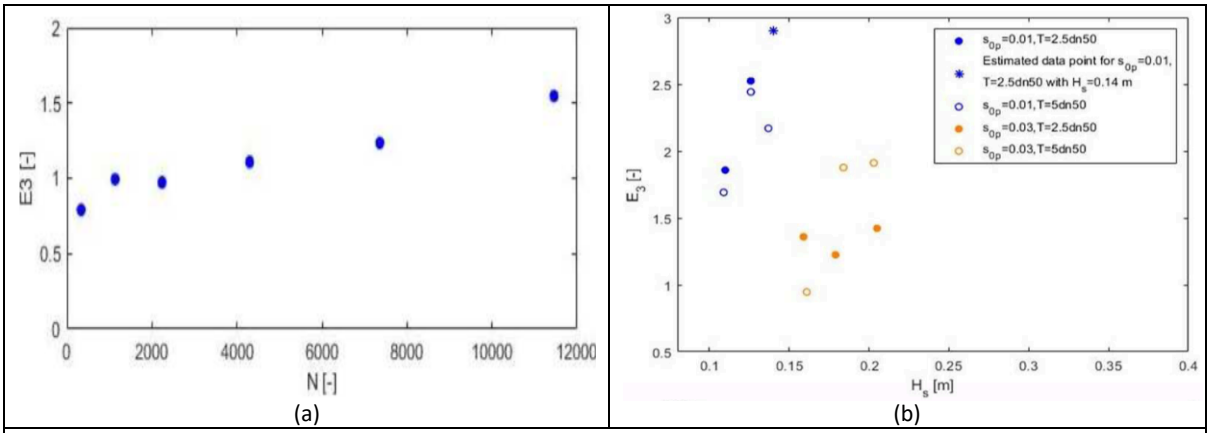

Figure 11: *(a) The influence of the number of waves N on the damage depth, E3D,3 for a slope of 1:10 of the structure with a layer thickness of 2.5 dn50 (Mossinkoff, 2019). (b) The influence of the wave steepness, the layer thickness and wave height on the damage depth (Mossinkoff, 2019).*

Mossinkoff (2019) researched whether the layer thickness T has effect on the damage parameter $E_{3D,3}$. Layer thicknesses of 2.5 d_{n50} and 5.0 d_{n50} have been investigated. Most physical model tests were performed with a layer thickness of 2.5 d_{n50} with an impermeable core. This was done to replicate an armour layer of 2.0 d_{n50} with a filter layer of 0.5 d_{n50} on an impermeable core, which was analysed by Van der Meer (1988). This should have resulted in a comparable notional permeability *P* equal to 0.1 similar to Van der Meer (1988) (Mossinkoff, 2019). It was expected that a thicker armour layer on an impermeable core would increase the stability of the outer stones. More voids are present and the water flow can dissipate more easily into the thicker layer. Also during the run-down of the water within the armour layer a larger area is available reducing the forces on the outer stones.

The results of Mossinkoff (2019) for layer thicknesses of 2.5 d_{n50} and 5.0 d_{n50} are depicted in Figure 11 (b). For a wave steepness of 0.01, the damage parameter $E_{3D,3}$ seems to be lower for the thicker armour layer. However, for a wave steepness of 0.03 a different result is shown in Figure 11 (b). An increase of the layer thickness resulted into a higher damage depth $E_{3D,3}$ for two out of the three tests. Mossinkoff (2019) stated that it is plausible that tests with a high wave steepness, waves reach the core of the layer thickness of 2.5 d_{n50} and do not for the thicker layer of 5.0 d_{n50}.

Mossinkoff (2019) also reviewed the effect of the layer thickness on the damage parameter S. For this damage parameter S, the increase in layer thickness results into a lower damage level. An explanation given by Mossinkoff (2019) was the difference of focus of the damage. The damage level S does not give insight whether the damage is shallow and wide or deep and centred at a specific spot on the slope. Another interesting phenomenon is that an increase of the significant wave height H_s does not necessarily lead to more damage as depicted Figure 11 (b). The bed was not repaired when a higher significant wave height is used for further testing and it is possible that a self-healing effect occurred.

An initial design formula has been developed by Mossinkoff (2019) and is depicted in Eq. 2.18. The design formula is only valid for Iribarren numbers ξ_p between 0.45 and 1 for a 1:10 slope and a layer thickness T of 2.5 d_{n50}. The damage depth parameter $E_{3D,3}$ indicates the magnitude of the damage. Mossinkoff (2019) indicates that Initial damage occurs at a value of 0.5 for the damage parameter $E_{3D,3}$. Intermediate damage starts at 1.2 and failure damage is reached at a value 2.3.

$$\frac{H_s}{\Delta \mathrm{d}_{n50}} = 6.1 * E_{3D,3}^{0.6} * {\xi_p}^{-1.31} * N^{-0.12} \qquad \text{Eq. 2.18}$$

The design formula of Mossinkoff (2019) and the Van der Meer (1988) formula for plunging waves (Eq. 2.16) are depicted in Figure 12. Currently, these two formulas are not connected and a small

discontinuity is visible in the figure for an Iribarren number ξ_p of 1.0. The steeper 1:8 slope, analysed in my study, enables to close the gap between the research of Mossinkoff (2019) and Van der Meer (1988). The studied Iribarren numbers ξ_p are between 0.56 and 1.25 in my research.

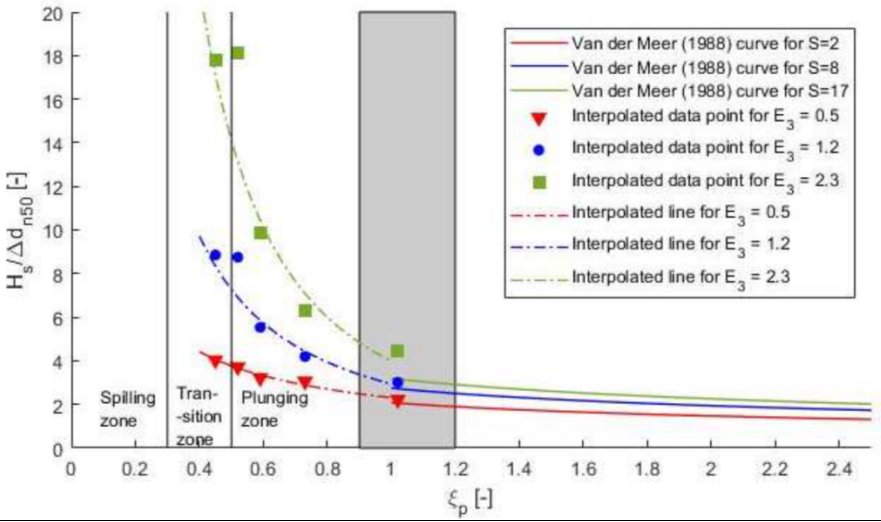

Figure 12: *The Van der Meer (1988) formula and the proposed design formula of Mossinkoff (2019) for 1000 waves and a layer thickness of 2.5 dn50 (Mossinkoff,2019).*

Mossinkoff (2019) has researched the displacements of coloured rocks within strip containing a width of 0.5 m. She showed that a berm damage profile, as discussed in section 2.2.6, develops for 1:10 slope. Mossinkoff (2019) concluded that 90 percent of the rock transport is directed upwards. The erosion is maximum for the strip 1.0 m to 1.5 m below still water level (SWL) and the deposition is maximum between 0 m to 0.5 m below SWL. Other conclusions from Mossinkoff (2019) were that an increase of the Iribarren number, the wave height and the number of waves increases the number of entrained rocks. A thicker armour layer resulted in less stone transport (Mossinkoff, 2019).

3 Methodology

This chapter elaborates on the methodology used in this study to answer the research objective and sub-research questions. The approach consists of a new set of physical model tests for a 1:8 slope and the re-analysis of the physical model tests for a 1:10 slope performed by Mossinkoff (2019). The test set-up, the measuring techniques, the test procedure and the executed tests for the 1:8 slope are presented in section 3.1. Section 3.2 briefly discusses the same items for the physical model tests for the 1:10 slope performed by Mossinkoff (2019). The data obtained from the physical model tests. The applied processing methods for the stereophotogrammetry are debated in section 3.3. A camera is used to record the waves and subsequently determine the wave breaking types. Section 3.4 explains this approach further. Coloured rocks in strips are used to get insight in the transport of rocks. Section 3.5 describes this technique in more detail.

3.1 Physical model tests for 1:8 slope

3.1.1 Test set-up

The physical model tests (both 1:8 and 1:10 slope) have been performed in the Pacific Basin at the laboratory of Deltares in Delft. An impression of the test set-up is presented in Figure 13. The dimensions of the basin are 28 m by 14 m. The height of the basin is 1.25 m where the water height can vary between 0.25 and 1.0 m. The basin contains two wave generators each with a length of 7 m, which can generate long-crested irregular waves. The wave paddles have no reflection compensation, but to minimize re-reflections from the basin walls, wave dampening slopes are present. A flume has been built in the basin and the side walls consist of large concrete blocks. The flume contains a 1:8 slope and has a width of 1 m. The slope is made of steel plates to model an impermeable core. At the bottom part of the slope concrete has been applied to smoothen the conversion from the steel plates to the bottom of the basin. Wooden triangle shaped structures have been placed at the lower end of the flume to reduce the reflection effect of the rectangular blocks (Figure 14). The reflected waves within the flume are assumed to disperse over the full width of the basin and are eventually absorbed by the wave dampening slopes. Figure 14 shows all dimensions concerning the test set-up. Table 8 depicts the main characteristics of the model. Appendix B shows more photos to give a more detailed impression of the test set-up.

Figure 13: *The Pacific basin facility at Deltares during a test. The flume with the mild slope can be seen in the middle.*

Table 8: *Main characteristics of the physical model tests for a 1:8 slope deduced from Mossinkoff (2019) to create similar circumstances to be able to make a comparison between the 1:8 and 1:10 slope.*

Main characteristics	Value
Slope angle, α	1:8
Wave spectrum	Jonswap
Nominal diameter of rocks, d_{n50} (Mossinkoff, 2019)	14.8 mm
d_{85}/d_{15} (Mossinkoff, 2019)	1.4
Rock density, ρ_s (Mossinkoff, 2019)	2944 kg/m^3
Water density, ρ_s *(assumption)*	1000 kg/m^3
Relative density, Δ	1.94
Water depth, h	0.75 m
Strip width of coloured stones, W_{strip}	0.5 m

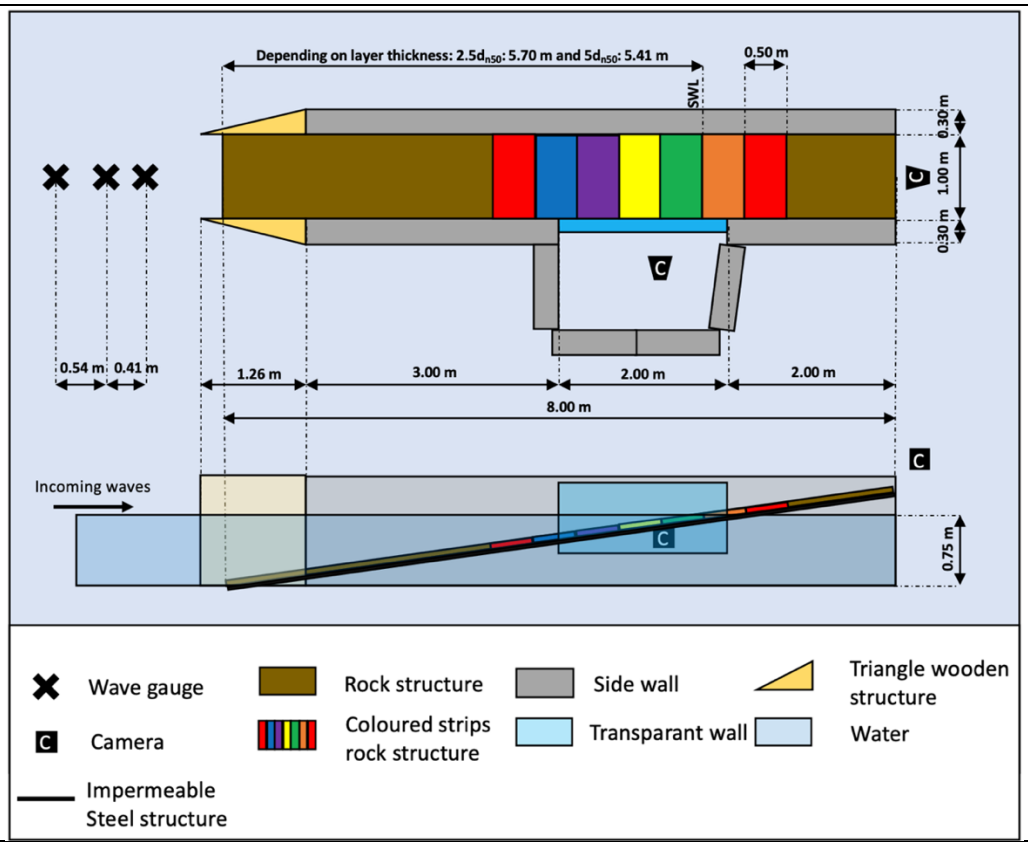

Figure 14: *Sketch of test set-up of the flume for the 1:8 slope in the Pacific Basin.*

Slope angle

The aim of this research is to study the stability of rocks on mild slopes. Mild slopes ensure that a share of the breaking waves can be denoted as spilling breakers. Mossinkoff (2019) selected a 1:10 slope. For my study I selected a 1:8 slope. Using a steeper slope 18 enabled the opportunity to investigate the knowledge gap between the physical model tests of Mossinkoff (2019) and the physical model tests of Van der Meer (1988). Van der Meer (1988) researched slopes up to a 1:6 slope, for which most of the breaking types can be denoted as plunging/collapsing waves. A steeper slope than 1:8 reduces the number of spilling waves such that the transition zone between spilling and plunging waves might not be present anymore. A milder slope, close to the 1:10 slope researched by Mossinkoff (2019), is considered to add limited value.

Types of waves

Irregular waves containing the Jonswap spectrum have been used to ensure that the physical model tests comply with the wave spectrum used by Mossinkoff (2019) and Kramer (2016) in their physical model tests. A Jonswap spectrum also represents the real-life situation for the Dutch North Sea coastlineclosely compared to other available wave spectrums.

Characteristics of rock

The same rock material has been used as Mossinkoff (2019). This material consists of a gravel batch between 15/25 mm. Mossinkoff (2019) researched the nominal diameter d_{n50}, the grading of the gravel and density of the rocks. The nominal diameter d_{n50} for these rocks is 14.8 mm and the d_{85}/d_{15} is 1.4 which is a narrow grading (Mossinkoff, 2019). According to the NEN-EN-ISO 14688, these rocks are considered to be gravel. The density of stones ρ_s is 2944 kg/m^3 resulting in a relative density Δ of 1.94 (Mossinkoff, 2019). Based on the density of rocks, the material is most likely to be basalt. Figure 16 gives an impression of the rocks. The rocks are crushed material and has irregular shapes without rounded edges. Keeping the rock characteristics constant will ensure that the influence from slope angle can been investigated properly and for that reason this gravel batch is optimal for this research. As stated in section 2.3.2, Ye (1996) concluded that an increase in relative density Δ improves the stability of rock more compared to an increase of the nominal diameter d_{n50}. The relative density Δ in these tests is relatively high. For that reason, it might have influenced the results of this study and the outcomes might deviate to similar rock sizes with lower relative densities.

For these physical model tests, the Reynolds number is equal or larger than 7000 and does not meet the lower limit of $3*10^4$ to avoid scale effects, as stated by Dai and Kamel (1969). Juul Jensen and Klinting (1983) concluded that the Reynolds number must be 6000 or larger in order to properly scale the armour layer. It can therefore be concluded that this limit is met in this study. In rubble mound structures, the scale effects are first seen in the core and underlayers resulting in less permeability (Hughes, 1993). This may cause relative larger pressures from inside the structure. Another consequence can be differences in reflection compared to the prototype scale (Hughes, 1993). In the current test set-up an impermeable core is simulated using steel plates. For that reason, no significant scale effects are expected since underlayers and a core are absent.

Water depth

The water depth during the tests has been kept equal to the water depth during the tests of Mossinkoff (2019) to be able to compare her results with my outcomes. The water depth has been selected to represent deep water conditions and to minimise the duration time for filling and emptying the basin between the tests. Mossinkoff (2019) analysed the wave conditions for a 1:10 slope and concluded that a water depth of 0.75 m was the optimum for a 1:10 slope. The ratio h/L_0 for the 1:8 slope and water depth of 0.75 m is between 0.07 and 0.62. This is partly in the intermediate water depth regime and partly in the deep water regime. Frostick, McLelland, & Mercer (2011) considered that the deep water section should meet a h/H_s ratio larger than 3 for every physical model test to simulate a deep water regime. The largest significant wave height used is 0.20 m which results in a h/H_s ratio of at least 3.75 for all tests. For that reason, a water depth of 0.75 m is considered to have a negligible influence on the waves representing deep water conditions in front of the structure. Distribution plots of the recorded wave heights H are added to Appendix C to give insight into the number of breaking waves during the tests.

Strip width

The strip width is the width of the sections with coloured rocks as depicted in Figure 14. Section 2.2 explained that a steeper slope will reduce the erosion length. Mossinkoff (2019) used a strip width of 0.5 m for a 1:10 slope. She found significant rock displacements outside the six coloured strips. Mossinkoff (2019) also showed that the damage domain is mainly between $-1.5H_s$ and $-0.2H_s$. My study used a significant wave height H_s between 0.02 and 0.20 m. It is assumed that the damage domain found by Mossinkoff (2019) does not change from a 1:10 slope to a 1:8 slope. The bottom boundary of the damage domain for a 1:8 slope should vary between 0.03 and 0.30 m below SWL. The top part of the damage domain should be between 0.00 and 0.06 m below SWL. To ensure that most entrained rocks are captured within the coloured rocks strips a similar strip width of 0.5 m is chosen

for the 1:8 slope. 5 strips are below SWL and 1 is above. In this case the lowest boundary would be at 0.31 m below SWL and the top at 0.06 meter above SWL. This should cover the damage domain for the highest waves and should minimise the probability that coloured rocks will be displaced outside the coloured strips and that none coloured rocks will end up inside the coloured strips. After the first test series it was observed that some rocks were deposited outside the coloured strips upslope. Therefore, an additional strip was added at the top part of the slope.

3.1.2 Measuring techniques

1. Wave gauges to determine the wave characteristics
The incoming wave characteristics were measured in front of the flume by means of three wave gauges (Figure 14). The three wave gauges have been used to separate the incoming and reflected waves, which originated from the wave generator. The distances between the three wave gauges depends on the local wave length. For the tests in this study the optimum distances between the gauges were 0.54 and 0.41 m.

2. Cameras to determine the breaking wave type
A camera was used as a measuring tool to determine the distribution between spilling and plunging breaking waves. The position of the camera is upslope pointing towards the incoming breaking waves. This location is shown in Figure 14.

3. Coloured strips to research the entrained and deposited rocks
Entrainment and deposition of rocks have been measured by counting coloured stones in strips of 0.5 m. A camera was positioned directly above the flume at a height of approximately 15 m. Photos have been taken from a fixed position before and after a test. This made it possible to compare the initial and the damaged slopes. The number of displaced rocks and the transportation length were determined based on these photos. The coloured strips are presented in the schematization in Figure 14. Another camera is positioned under water at the side of the glass walled flume which indicated whether stones were starting to move (rocking, entrainment etc.). This is also depicted in the schematization in Figure 14.

4. Stereophotogrammetry to determine the profile based damage parameters
Photogrammetry is the science of obtaining reliable information about the properties of surfaces and objects without physical contact with the objects, and of measuring and interpreting this information (Schenk, 2005). Stereophotography is the technique where two or more photos from different locations are used to retrieve height information (Rees, 2013). Stereophotogrammetry is the procedure to determine the geometric information (Rees, 2013). The initial and damaged profile were measured using stereophotogrammetry to obtain 3D models of the slopes. These models are used to determine the profile based damage parameters.

Hofland et al. (2011) researched the verification of stereophotogrammetry. A structure was measured by a mechanical profiler and using stereophotogrammetry. It was concluded that the stereophotogrammetry measurements are more accurate for the determination of the mean profiles and the damage as higher resolution data was obtained.

An iPhone Xr (12 megapixels) has been applied to photograph the slope. The app ‘’Camera+2’’ has been used to save pictures as TIFF-files to ensure properties of pictures were not deformed. Saving the photos as TIFF-files is highly recommended by the guide manual of the photogrammetric processing software Agisoft Metashape. 63 photos were taken perpendicular to the slope at a height of approximately 1.25 m to be certain that all damage is encountered on the slope. In horizontal direction 3 photos were made and 21 photos were taken along the slope, as depicted in Figure 16.

The distance between these 63 camera position is 0.25 m. The number of photos and the distance between them are required to be certain that there is enough overlap between the pictures to obtain the geometric information over the entire slope where damage occurs. A frame is built to make sure that the 63 photos are taken on the same location after each test.

Ground Control Points (GCPs) were used to identify locations on photos where the XYZ coordinates are known. 12 coloured disks containing a diameter of 8 mm are made and attached to the side wall of the flume as shown on the photo and in the sketch of Figure 16. This differs to the approach of Mossinkoff (2019) who attached GCPs to the side wall as shown in Figure 18. These GCPs are poorly visible on some photos since they are placed vertically on the side walls. Therefore, I changed the type of GCPs in this study. Extra GCPs 1, 7, 6 and 12 are also added at the upper and bottom part of the slope compared to Mossinkoff (2019) and these extra GCPs are depicted in Figure 16. This improvement ensures that a bias curve is not formed as illustrated in Figure 15. In the graph, al lines are profile changes from two tests containing the same undamaged profile. These profile changes should be zero along the entire slope. The original GCP plan did not contain the extra outer GCPs 1, 7, 6 and 12 and showed a bias curve. The extra outer GCPs 1, 7, 6 and 12 were included in the extended GCP plan test 1 and 2 as depicted in Figure 15. The bias curve disappeared. This is discussed in more detail in section 3.2.2 for the re-analysis of the 1:10 slope. The exact XYZ coordinates of the centre point of the GCPs are determined using a total station (Leica TCRA1202). These coordinates are displayed in Table 9 for the layer thicknesses 2.5 d_{n50} and 5 d_{n50}. The processing of the photos in order to obtain the 3D models is discussed in more detail in section 3.3.

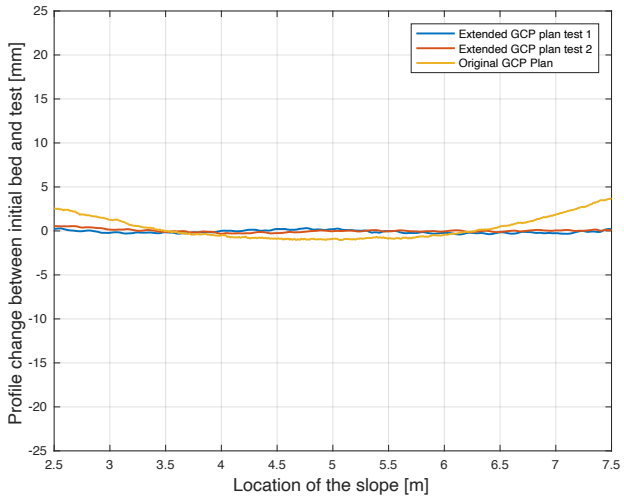

Figure 15: *Average profile plots from an undamaged profile where two tests contained the extra outer GCPs and one test were without the extra outer GCPs.*

Table 9: *The XYZ coordinates of Ground Control Points for the two-layer thickness tested (2.5 d_{n50} and 5.0 d_{n50}) for the 1:8 slope.*

	Layer thickness of 2.5 d_{n50}			Layer thickness of 5.0 d_{n50}		
	X [m]	**Y [m]**	**Z [m]**	**X [m]**	**Y [m]**	**Z [m]**
GCP 1	0.024	1.849	0.296	0.027	2.030	0.363
GCP 2	0.029	3.092	0.441	0.026	3.084	0.492
GCP 3	0.032	4.334	0.600	0.026	4.321	0.650
GCP 4	0.031	5.577	0.751	0.026	4.565	0.797
GCP 5	0.030	6.818	0.904	0.028	6.810	0.954
GCP 6	0.028	7.767	1.031	0.030	7.747	1.077
GCP 7	0.969	1.842	0.292	0.964	2.018	0.360
GCP 8	0.967	3.083	0.431	0.964	3.066	0.483
GCP 9	0.964	4.321	0.587	0.962	4.311	0.645
GCP 10	0.969	5.564	0.745	0.967	5.552	0.798
GCP 11	0.975	6.808	0.903	0.968	6.801	0.947
GCP 12	0.984	7.802	1.034	0.967	7.793	1.080

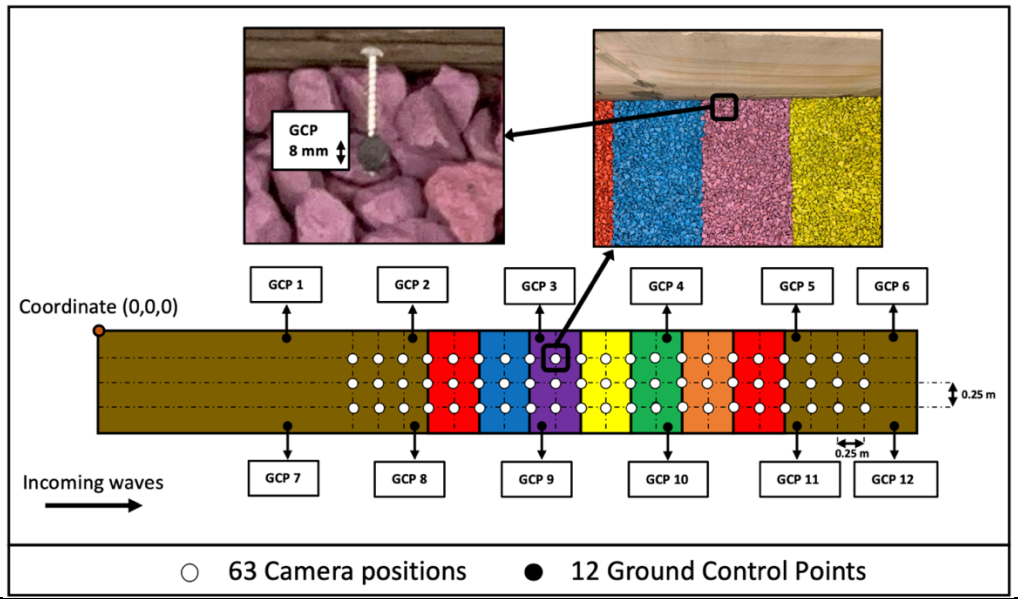

Figure 16: *Sketch of the camera positions and the locations of the Ground Control Points including an example of a photo for the 1:8 slope tests.*

3.1.3 Test Procedure

The test procedure is enumerated below and consists of three parts: preparation of a test series, starting a test and after a test. The rock slope was not rebuilt within a test series when the significant wave height H_s was increased or the number of waves N was increased. This was done to be able to record cumulative damage. This is similar to the approach of Mossinkoff (2019). The underlying hypothesis is that cumulative damage tests have limited effect on the damage parameters compared to non-cumulative damage tests. De Almeida (2017) studied the tests using cumulative and non-cumulative damage tests for 1:2 and 1:3 slopes for rubble mound structures. He then compared the results of the different tests. According to the results of De Almeida (2017) variations in cumulative and non-cumulative damage tests are small and both present similar values for the damage parameters S and $E_{3D,5}$. To save time the cumulative damage concept is used in this research.

Preparation of a test series:

1. (Re)build the slope to the desired layer thickness and place the coloured rocks in the correct positions.
2. Check visually whether GCPs are damaged or not.
3. Fill and empty the basin to ensure that the bed is wet to reduce measurement errors.
4. Take the 63 pictures of the undamaged slope using the frame.
5. Take the picture from 15 m height of the undamaged slope.

Starting a test:

1. Create the steering file for the wave generators with the desired wave characteristics.
2. Fill the basin until the still water level is at 0.75 m.
3. Check the steering file, still water level and measuring equipment (battery, availability memory, etc.).
4. Start the video cameras from the side and in front of the flume.
5. Start the wave generator and activate the wave gauges after 30 seconds (wave generator needs some time to build up waves).
6. Check whether wave gauges and cameras are recording during the test.

After a test:

1. Empty the basin until a level is reached, so that measurement of the damaged slope is not disturbed.
2. Take the 63 pictures of the damaged slope using the frame.
3. Take the picture from 15 m height from the damaged slope.
4. Repeat the steps from ''Starting a test'' until failure is reached. In case of finalization of a test series start again at ''Preparation of a test series'' (This is not applicable for test series 9 studying non-cumulative damage).

3.1.4 Test plan

The test plan consisted of ten test series. Several parameters have been varied to study the stability of the mild slope. The test plan is summarized in Table 10. An extended version of the executed tests is added in Appendix D.

Test series 1 until 5 research the effect of an ascending significant wave height H_s for a specific wave steepness $s_{o,p}$ on the damage parameters. Test series 6 investigated the influence of the number of waves on the damage parameters and to research whether the correlation differs compared to steep slopes. The layer thickness of 2.5 d_{n50} is used for these test series to simulate the permeability coefficient *P* equal to 0.1 as highlighted in section 2.3 (van der Meer, 1988). In the research of Van der Meer (1988), the permeability coefficient *P* equal to 0.1 contains an armour layer of 2 d_{n50}, a filter layer 0.5 d_{n50} and an impermeable core. Both d_{n50}*'s* are equal to the nominal rock diameter of the armour layer. A thicker layer of 5 d_{n50} is researched to investigate the effect of the layer thickness on the stability of rock on the slope. This thicker layer of 5 d_{n50} is also researched by Mossinkoff (2019). The notional permeability *P* is determined based on the empirical method of Eldrup et al. (2019). Using this method, the notional permeability *P* is 0.12 for a layer thickness of 2.5 d_{n50} and 0.48 for the thicker 5 d_{n50} armour layer. The effect of this increase in layer thickness *T* on damage is examined in test series 7 and 8. All test series 1 till 8 are based on the cumulative damage concept meaning that the slope is not rebuilt within the test series. Test series 9 is based on the non-cumulative damage concept and investigated the variability of damage parameters. The concept of cumulative damage is also verified in this test series. The last test series 10 is very similar to test series 9. Only a measurement is added within the test series after 20 waves to check the damage after a limited number of waves.

Table 10: *The executed test plan for the 1:8 slope.*

Test series	$s_{o,p}$	ξ_p	H_s [m]	N	P	T	Number of tests	Researched effect on damage parameters
1	0.01	1.25	0.02-0.09	1000	0.12	2.5 d_{n50}	8	sig. wave height (and Iribarren number)
2	0.02	0.88	0.03-0.11	1000	0.12	2.5 d_{n50}	8 (+1 fail)	sig. wave height (and Iribarren number)
3	0.03	0.72	0.05-0.15	1000	0.12	2.5 d_{n50}	14	sig. wave height (and Iribarren number)
4	0.04	0.63	0.05-0.17	1000	0.12	2.5 d_{n50}	8	sig. wave height (and Iribarren number)
5	0.05	0.56	0.06-0.19	1000	0.12	2.5 d_{n50}	9	sig. wave height (and Iribarren number)
6	0.03	0.72	0.12	250-14000	0.12	2.5 d_{n50}	8	Number of waves
7	0.03	0.72	0.06-0.20	1000	0.48	5.0 d_{n50}	12	Layer thickness
8	0.01	0.56	0.03-0.12	1000	0.48	5.0 d_{n50}	11	Layer thickness
9	0.03	0.72	0.12	1000	0.12	2.5 d_{n50}	5	Variability
10	0.03	0.72	0.12	1000	0.12	2.5 d_{n50}	1	Variability and noise of small stones
							84 tests total	

3.2 Re-analysis of the physical model tests for 1:10 slope performed by Mossinkoff (2019)

The stereophotogrammetry part of the study of Mossinkoff (2019) has been re-analysed in this study. In this manner, it is guaranteed that the processing and the determination of the damage parameters of the 1:8 and 1:10 slope are identical. Processing of the data is described in section 3.3. Photos of the

coloured strips of tests 3F and 3G were not yet analysed for the 1:10 slope by Mossinkoff (2019) and were also examined in this study. The test set-up, measuring techniques and executed test-plan are briefly discussed in this section. For a more detailed elaboration on these items reference is made to Mossinkoff (2019).

3.2.1 Test set-up

The physical model tests of Mossinkoff (2019) are also performed in the Pacific Basin at Deltares which is already discussed in more detail in section 3.1.1. A slope of 1:10 is researched and a sketch of the test set-up is shown in Figure 17. The main characteristics are depicted in Table 11. The main characteristics of the 1:8 slope have been deduced from the study of Mossinkoff (2019) and are for that reason similar except for the slope angle. A comparable approach ensures that a good comparison between the results of the two slopes can be made.

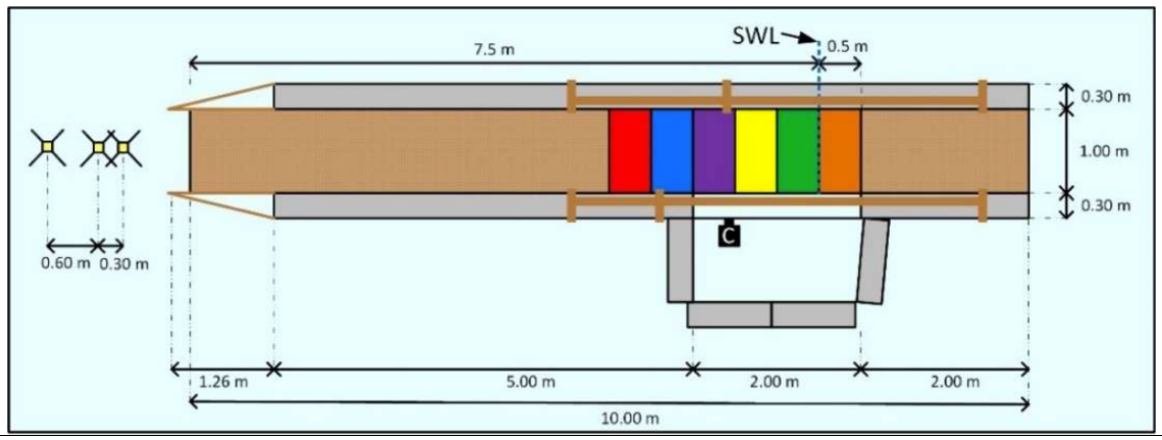

Figure 17: *Sketch of the test set-up of the flume for the 1:10 slope in the Pacific Basin (Mossinkoff, 2019)*

Table 11: *Main characteristics of the physical model tests for a 1:10 slope performed by Mossinkoff (2019).*

Main characteristics	Value
Slope angle, α	1:10
Wave spectrum	Jonswap
Nominal diameter of rocks, d_{n50}	14.8 mm
d_{85}/d_{15}	1.4
Rock density, ρ_s	2944 kg/m^3
Water density, ρ_s (assumption)	1000 kg/m^3
Relative density, Δ	1.94
Water depth, h	0.75 m
Strip width of coloured stones, W_{strip}	0.5 m

3.2.2 Measuring techniques

The measuring techniques used by Mossinkoff (2019) are comparable to the physical model tests for the 1:8 slope as discussed in section 3.1.2. The stereophotogrammetry data of Mossinkoff (2019) is re-processed in this research to ensure that the damage parameters are determined in a similar way. For that reason, this item and procedure is discussed more extensively in this section. An iPhone was likewise applied as the camera and 66 photos were taken perpendicular to the slope. In horizontal direction 3 photos were made and 22 photos were taken along the slope as depicted in Figure 18. The distance between the locations of the camera for each photo is 0.25 m.

When analysing the data of Mossinkoff (2019), I observed bias during the determination of the damage parameters. It seemed that the stereophotogrammetry procedure did not to work properly. The bias was visible at the upper and bottom part of the slope and effected also the middle part of

the slope. The data presented an undesirable curve along the slope similar to the bias curve depicted in Figure 15. After a trial and error process I found a plausible cause. The outer photos, highlighted as red dots in Figure 18, were taken on a part of the slope where GCPs were insufficiently present. GCPs are used to identify locations on photos where the XYZ coordinates are known. The partly absence of these GCPs could lead to a lack of direction on these photos. This might have resulted in the curves which were observed. After removing the outer 9 photos at the upper and bottom part the observed ''curve'' disappeared. Every test has been analysed using only 48 pictures which are presented as white dots in Figure 18. The largest damage occurs within the area that is measured by these 48 photos. However, a part of the damage will not be measured for the tests containing the most severe condition as damage in the outer regions of the slope will not be recorded. It is assumed that this influence is limited on the final outcome of the damage parameters.

Mossinkoff (2019) attached double GCPs to the side of the wall of the flume for the 1:10 slope as depicted in Figure 18. The corresponding coordinates are displayed in Table 12 for the layer thicknesses 2.5 d_{n50} and 5 d_{n50}. After observing the bias in the data of Mossinkoff (2019), I tried to improve the measuring techniques when studying the 1:8 slope. Several possible solutions were tried. In the end, I concluded that best improvement was to place extra GCPs at the outer regions of the slope. The type of GCPs is changed as well for the 1:8 slope to improve the visibility of these GCPs. The processing of the photos in order to obtain the 3D models are discussed in more detail in section 3.3.

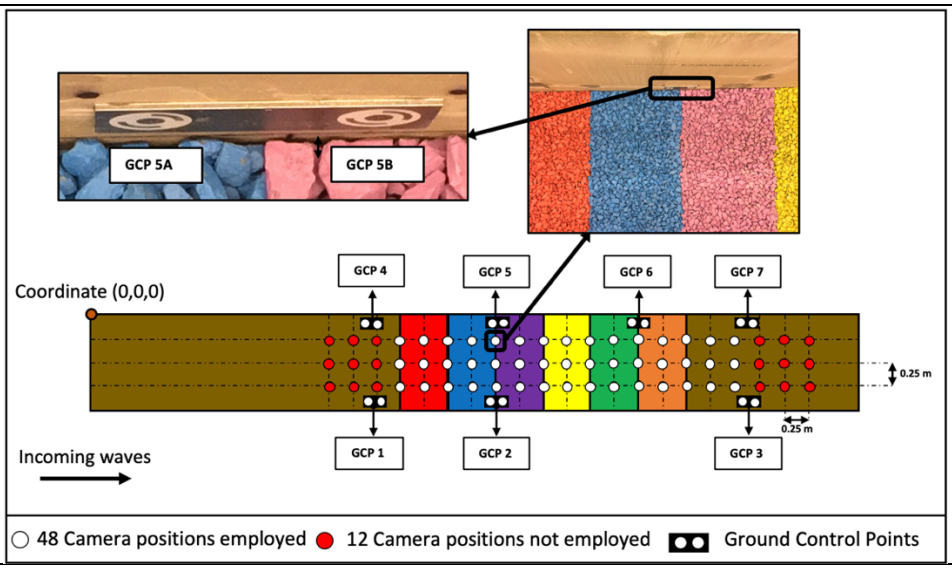

Figure 18: *Sketch of the camera positions and the locations of the Ground Control Points including an example of a photo for the 1:10 slope tests performed by Mossinkoff (2019).*

Table 12: *The XYZ coordinates of Ground Control Points for the two-layer thickness tested (2.5 d_{n50} and 5.0 d_{n50}) for the 1:10 slope performed by Mossinkoff (2019).*

	Layer thickness of 2.5 d_{n50}			Layer thickness of 5.0 d_{n50}		
	X [m]	Y [m]	Z [m]	X [m]	Y [m]	Z [m]
GCP 1A	0.997	4.393	0.500	0.997	4.394	0.514
GCP 1B	0.997	4.504	0.512	0.997	4.503	0.524
GCP 2A	0.997	5.899	0.636	0.997	5.900	0.677
GCP 2B	0.997	6.009	0.645	0.997	6.009	0.684
GCP 3A	0.997	8.881	0.930	0.997	8.878	0.965
GCP 3B	0.997	8.990	0.941	0.997	8.989	0.979
GCP 4A	0.003	4.402	0.493	0.003	4.396	0.526
GCP 4B	0.003	4.513	0.499	0.003	4.506	0.535
GCP 5A	0.003	5.877	0.646	0.003	5.876	0.669
GCP 5B	0.003	5.987	0.655	0.003	5.985	0.679
GCP 6A	0.003	7.379	0.789	0.003	7.374	0.814
GCP 6B	0.003	7.489	0.797	0.003	7.485	0.824
GCP 7A	0.003	8.884	0.921	0.003	8.885	0.965
GCP 7B	0.003	8.995	0.939	0.003	8.995	0.978

3.2.3 Test plan

The executed test plan performed by Mossinkoff (2019) is summarized in Table 13 and an extended version of test plan can be found in her study. Mossinkoff (2019) also used the cumulative damage concept already explained in section 3.1.3. All her test series are based on this concept. Test series 1 until 5 and 11 investigated the effect of an ascending significant wave height H_s for a specific wave steepness $s_{o,p}$ on the damage parameters. Test series 6 investigated the influence of the number of waves on the damage parameters for the 1:10 slope. Test series 7 and 8 studied the correlations between the layer thickness and the damage parameters.

Table 13: *The executed test plan for the 1:10 slope performed by Mossinkoff (2019) .*

Test series	$S_{o,p}$	ξ_p	H_s [m]	N	P	T	Number of tests	Researched effect on damage parameters
1	0.01	1.00	0.07-0.11	1000	0.12	2.5 d_{n50}	3	sig. wave height (and Iribarren number)
11	0.01	1.00	0.07-0.13	1000	0.12	2.5 d_{n50}	4	sig. wave height (and Iribarren number)
2	0.03	0.58	0.09-0.23	1000	0.12	2.5 d_{n50}	8	sig. wave height (and Iribarren number)
3	0.05	0.45	0.10-0.22	1000	0.12	2.5 d_{n50}	7	sig. wave height (and Iribarren number)
4	0.02	0.71	0.08-0.18	1000	0.12	2.5 d_{n50}	6	sig. wave height (and Iribarren number)
5	0.04	0.50	0.10-0.22	1000	0.12	2.5 d_{n50}	7	sig. wave height (and Iribarren number)
6	0.03	0.58	0.15	300-11000	0.12	2.5 d_{n50}	6	Number of waves
7	0.01	1.00	0.11-0.15	1000	0.48	5.0 d_{n50}	3	Layer thickness
8	0.03	0.58	0.17-0.21	1000	0.48	5.0 d_{n50}	3	Layer thickness
							47 tests total	

3.3 Processing the stereophotogrammetry and determining the damage parameters

3.3.1 Processing the stereophotogrammetry

In sections 3.1.2 and 3.2.2, the stereophotogrammetry measuring technique was explained. The 3D models are obtained from 63 photos for each test for the 1:8 slope and 48 photos per test for the 1:10 slope. These photos need to be processed to retrieve geometric information. Agisoft Metashape software is used to convert the photos into 3D point clouds. The most import settings in the software are summarized in Appendix E. The point clouds contain approximately 1.8 million data points resulting in 53 xyz points per cm^2. An impression of the resulting point clouds is shown in Figure 19.

Before determining the damage parameters, I measured the accuracy of the stereophotogrammetry procedure. This gives insight into possible deviations within the damage parameters which are not related to actual damage. To determine the accuracy, two samples of 63 photos were taken from an undamaged profile with a 1:8 slope. Both samples are processed by Agisoft Metashape. The generated point clouds are placed on top of each other using the software CloudCompare. The average distance and standard deviation between the two point clouds are estimated by the software based on a random sample chosen by CloudCompare. In this report, this procedure is called a check test and was performed two times. The two check tests are depicted in Figure 20 (a) and (b). The first check test showed some bias at the top part of the slope and the second check test indicated some bias at the bottom part. An explanation could be that the outer GCPs are only two or three times seized on photos, which is less compared to the middle GCPs as they appear more than 10 times on pictures. This might result in a less accurate alignment of these outer GCPs leading to some bias at the bottom and upper part of the slope.

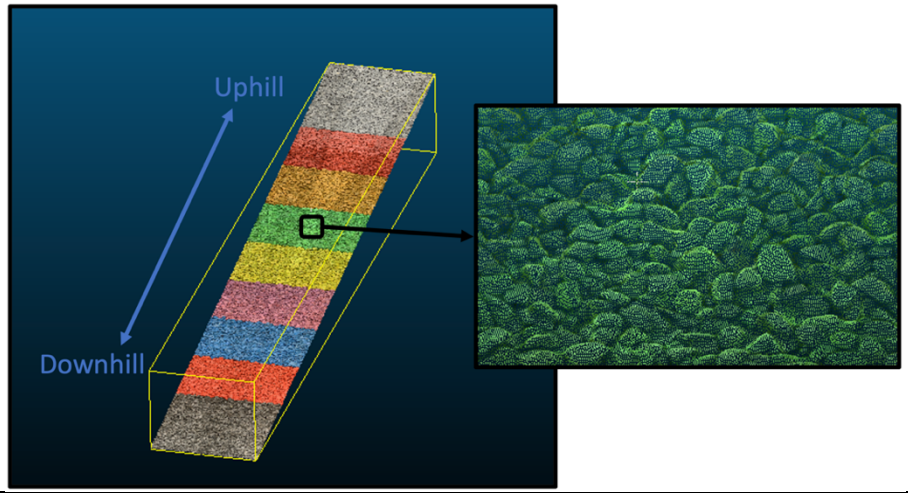

Figure 19: *Impressions of the resulting Point cloud containing approximately*

A tool in CloudCompare is used to align the point clouds such that the bias at the edges disappears. This tool is the Iterative Closest Point (ICP) algorithm and registers two entities. Two main requirements need to be fulfilled to be able to use this algorithm (CloudCompare manual, 2020):

- Both point clouds should already be registered.
- Both point clouds should represent the same object or partly have an overlap.

The point clouds are already registered by Agisoft Metashape fulfilling the first requirement. A large section of the slope is captured by the stereophotogrammetry procedure resulting in undamaged overlapping parts on the upper and bottom parts of the slope even when much damage on the slope is present. The result is that the second requirement is also met and the IPC algorithm is allowed to be used. The results after applying the IPC algorithm are shown in Figure 20 (c) and (d). The bias observed in Figure 20 (a) and (b) disappeared and a ‘’pepper and salt’’ distribution is visible. This means that deviations vary on the slope, but relatively larger deviations do not concentrate on a specific location. The settings of the IPC tool are added in Appendix E. The points clouds are now ready to be analysed and suitable to determine the 2D and 3D damage parameters for each test. This next step is explained in the section 3.3.2 and 3.3.3.

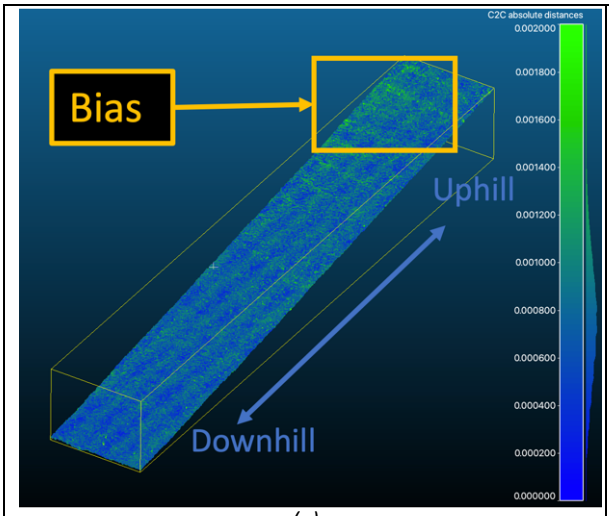

(a)
Mean distance: 0.760 mm
Standard deviation: 0.304 mm
Check test 1

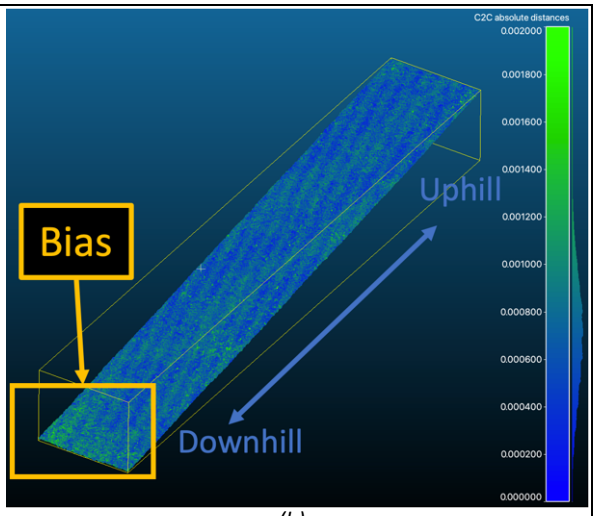

(b)
Mean distance: 0.716 mm
Standard deviation: 0.263 mm
Check test 2

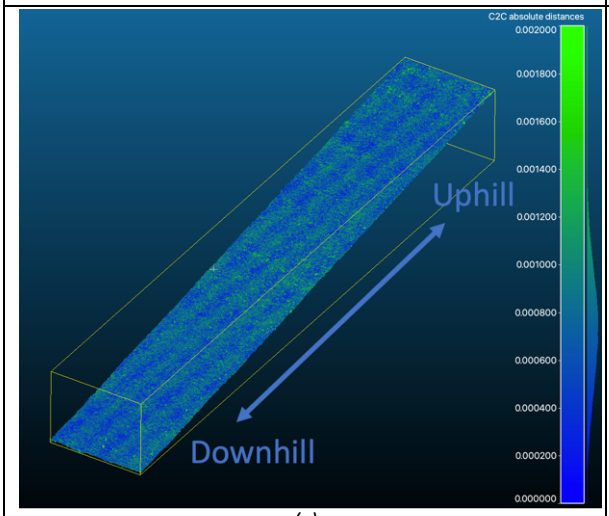

(c)
Mean distance: 0.740 mm
Standard deviation: 0.271 mm
Check test 1 after IPC

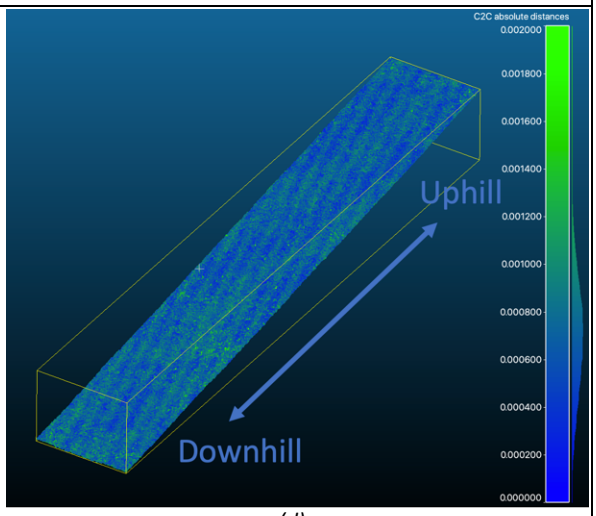

(d)
Mean distance: 0.704 mm
Standard deviation: 0.256 mm
Check test 2 after IPC

Figure 20: *Comparing two point clouds of the same profile before and after using the ICP tool.*

3.3.2 Determining 2D damage parameters

The point clouds have been further analysed using the software program Matlab. The process to determine the 2D damage parameters is schematised in Figure 21. The point cloud of the initial undamaged profile and the point cloud of a damaged profile after a test are averaged over the width of the rock slope in order to determine the 2D damage parameter E_{2D} and S. Width averaging is applied in sections of 0.5 cm where each section contains approximately 2000 points of the point cloud. A moving average of 3 d_{n50} is applied as a smoothening method to reduce noise effects. This smoothening method was also applied by Hofland et al. (2011). All information within the moving average of 3 d_{n50} is equally valued and no (normal) distribution is applied in this smoothening process. The averaged profiles of the initial undamaged slope and the damaged profiles are merged resulting in width average profile changes as also done by Van der Meer (1988). The results show regions of erosion and accretion. The profile change graphs of test series 5 are shown as an example in Figure 21. All average profile changes graphs are attached in Appendix F.

The damage parameter *S* was introduced in chapter 2. In this study, this damage parameter is determined in two manners *S* and S_{all}. These equations are depicted in Eq. 3.1 and 3.2.

$$S = \frac{A_{1\langle e\rangle w}}{{d_{n50}}^2} \quad \text{Eq 3.1}$$

$$S_{all} = \frac{A_{1\langle e\rangle w} + A_{2\langle e\rangle w} + \ldots + A_{n\langle e\rangle w}}{{d_{n50}}^2} \quad \text{Eq 3.2}$$

In the damage parameter *S* as defined in Eq 3.1, only the largest erosion area measured is used. This largest erosion area lays within the measuring area of the stereophotogrammetry which is around still water level. This is an approach to simulate the parameter *S* of Van der Meer (1988). The difference with Van der Meer (1988) is that he used a surface profiler to determine the erosion area A_e and this study applied stereophotogrammetry.

I have chosen to only consider an erosion area A_e which has a minimum erosion depth d_e of 0.5 mm or more when determining the damage parameters *S*. This choice is based on the check tests because there a maximum deviation of 0.46 mm was observed which gives insight on the measuring accuracy. This 0.5 mm threshold ensures that measuring inaccuracy will not disturb the calculation of *S* and limits the effect of noise created by the voids between the stones.

The damage parameter S_{all}, as depicted in Eq. 3.2, is using the cumulative damage of all erosion areas within the measuring area of the stereophotogrammetry. Again, a threshold for the erosion depth d_e of 0.5 mm is applied. Mild slopes show multiple locations of erosion. As an example, this can be observed for test series 5 in Figure 21. The consequence of considering only the largest erosion area A_e is that some damage will remain unobserved. For that reason, it is plausible that the damage parameter S_{all} is preferred over the damage parameter *S* for mild slopes.

The damage parameter E_{2D} was introduced in chapter 2 and is deocited in Eq. 3.3. The determination procedure of E_{2D} is similar to *S* and S_{all} and this process is shown in Figure 21.

$$E_{2D} = \frac{\max(\langle d_e\rangle_w)}{d_{n50}} \quad \text{Eq. 3.3}$$

The 2D damage parameters are determined for the entire characterization width *w* (54 d_{n50}) and two separate sections (2*27 d_{n50}). Almeida et al. (2019) studied the influence of the characterization width *w* and concluded that a characterization width *w* of approximately 25 d_{n50} is optimal for studying damage. The results of both the entire characterization width *w* (54 d_{n50}) and two separate sections (2*27 d_{n50}) presented in Appendix H.

Measuring inaccuracy can have an influence on the calculation of the 2D damage parameters. The average and maximum influence on the damage parameters *S*, S_{all} and E_{2D} are depicted in Table 14. These values are based on the results of the check tests 1 and 2 and will be discussed further in section 3.3.4.

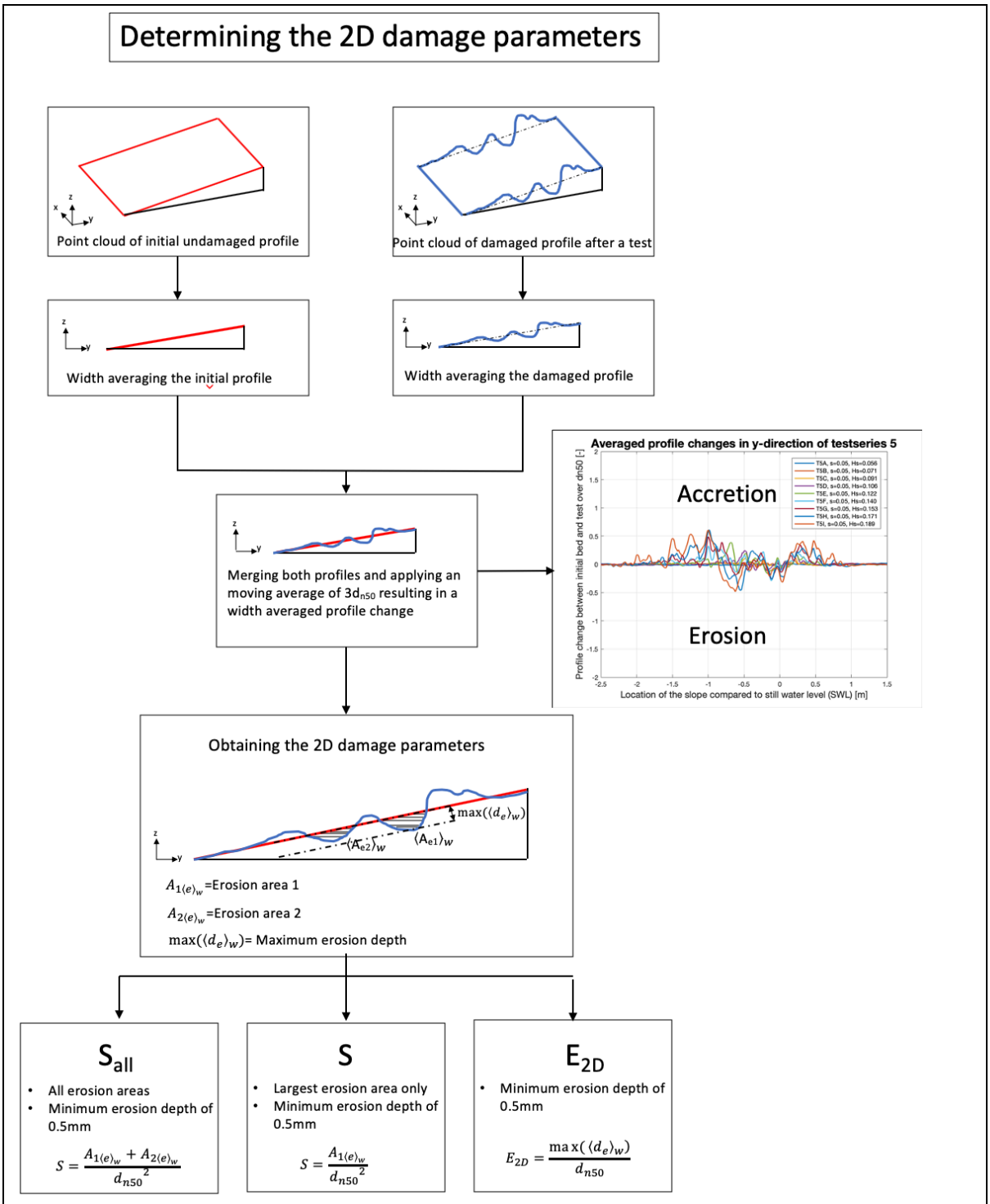

Figure 21: *Process of obtaining the 2D damage parameters*

3.3.3 Determining 3D damage parameters

For determining the 3D damage parameters, the point clouds are again analysed using the software Matlab. This Process is schematised in Figure 22. The damage parameter $E_{3D,m}$ is the 3D damage parameter that is studied and was already introduced in chapter 2. The damage parameter $E_{3D,m}$ is depicted in Eq. 3.4.

$$E_{3D,m} = \frac{\max\left(\langle d_e \rangle_{m*dn50}\right)_w}{d_{n50}} \qquad \text{Eq. 3.4}$$

The $E_{3D,m}$ is the maximum erosion depth d_e averaged over a moving circle with a diameter of m d_{n50} within the characterization width w. The point cloud of the initial undamaged profile is compared to the point cloud of a damaged profile after a test. A grid field is used with a grid size of 0.005 m by 0.005 m where 0.005 m is approximately one third of the nominal diameter of the rocks d_{n50} (0.0148 m). The result is a grid field consisting of 800 by 160 grid cells. Each grid cell contains approximately 13 xyz points (0.25 cm^2). The damage parameters $E_{3D,1}$, $E_{3D,3}$ and $E_{3D,5}$ are determined based on this grid field. The determination of these parameters is shown in Figure 22. Each grid cell uses its surrounding grid cells to simulate the spatial moving average containing a circle with a diameter of m d_{n50}. This was already discussed in section 2.1.2. In this analysis m is equal to 1, 3 or 5. A larger value of m increases the area of the spatial moving average. Depending on the value of m, the circle is a better representation of a circle using the grid size mentioned. As the value m increases the simulation of the circle improves as depicted in Figure 22.

The next step is to combine and merge the initial and damaged profile to obtain the profile change in a similar grid field of 800 by 160 grid cells. Three examples of these profile changes are depicted in Figure 22, where the approach to obtain the damage parameters $E_{3D,1}$, $E_{3D,3}$ and $E_{3D,5}$ is given as well. The grid cell which contains the lowest negative value is used to determine these damage parameters. This is also depicted in Figure 22 and in Eq. 3.4. The 3D plots for the damage parameter $E_{3D,1}$ are added in Appendix G. Measuring inaccuracy can influence the 3D damage parameters. The mean deviation and maximum deviation of the damage parameters $E_{3D,1}$, $E_{3D,3}$ and $E_{3D,5}$ are determined and depicted in Table 14. These values are based on the results of the check tests 1 and 2 which were discussed in section 3.3.1. This influence will be further discussed in the next section.

The 3D damage parameters are determined for the entire characterization width (54 d_{n50}) and 2 separate sections (2*27 d_{n50}). This is similar to the approach regarding the 2D damage parameters and is based on the research of Almeida et al. (2019). As already mentioned, he concluded that a characterization width of approximately 25 d_{n50} is optimal. The results for both characterization widths are added to Appendix H.

3.3.4 Effect of measuring inaccuracy on damage parameters

The effect of the measuring inaccuracy is analysed based on the check tests 1 and 2 which were discussed in section 3.3.1. A check test consists of two different samples of the same undamaged profile. The difference will examine the measuring inaccuracy of the stereophotogrammetry procedure. The mean deviation and maximum deviation between the two different samples are determined for each check test and are depicted in Table 14. These deviations are measured for the 1:8 slope only. The procedure for the 1:10 slope is very similar compared to the 1:8 slope procedure. For that reason, it is assumed that the inaccuracy measured for the 1:8 slope is comparable to the inaccuracy for the 1:10 slope. This measuring inaccuracy can be used to argue whether the use of a damage parameter is preferred or not. Concluding remarks on the damage parameters will be discussed in more detail in section 5.1.4.

***Table 14**: The effect of measuring accuracy on the damage parameters.*

		S/S_{all} [per mm erosion length]	E_{2D}	$E_{3D,1}$	$E_{3D,3}$	$E_{3D,5}$
Check test 1	Mean deviation	0.00046	0.007	0.006	0.006	0.006
	Max deviation	0.00192	0.028	0.203	0.099	0.063
Check test 2	Mean deviation	0.00027	0.004	0.003	0.003	0.003
	Max deviation	0.00160	0.023	0.170	0.082	0.052

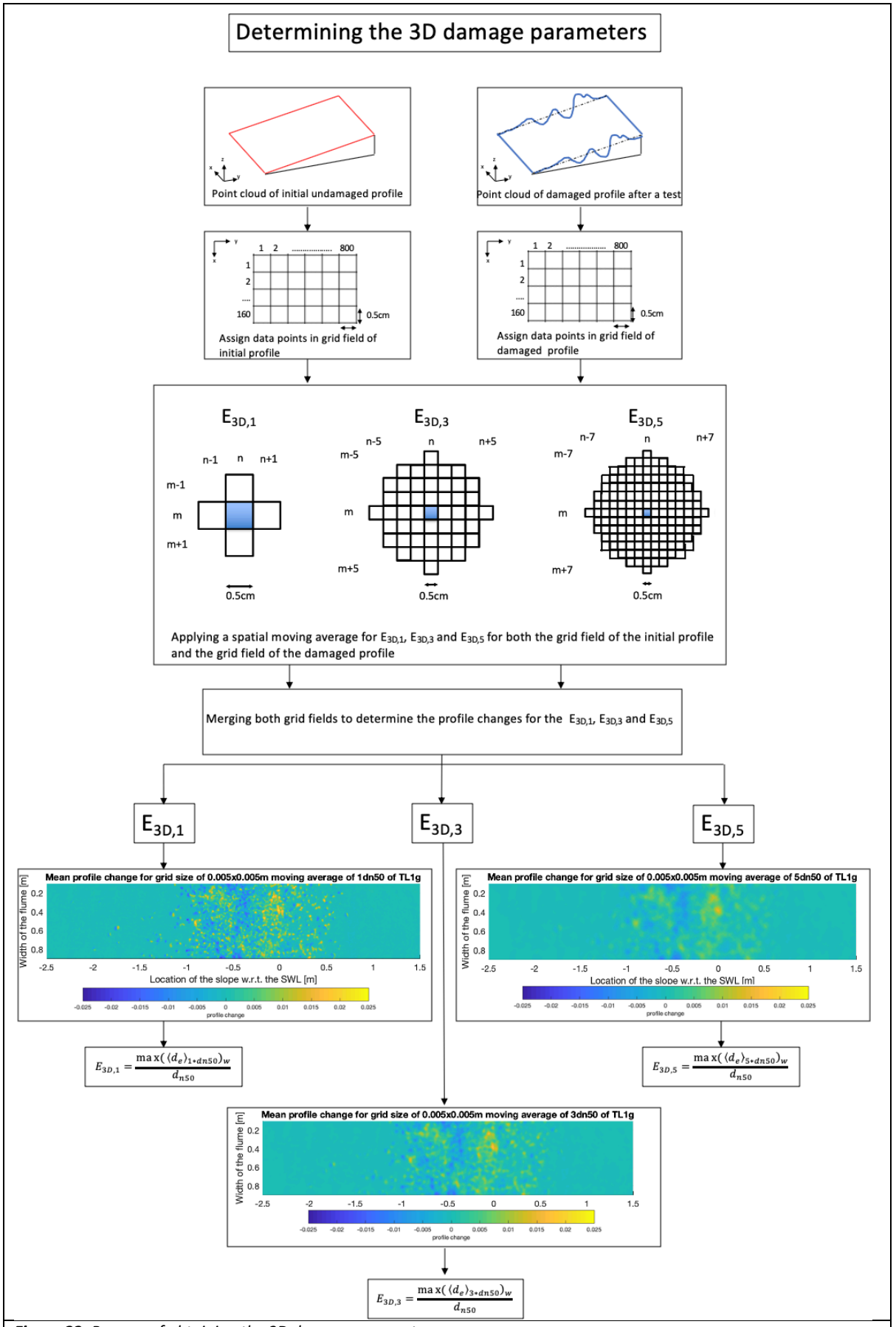

Figure 22: *Process of obtaining the 3D damage parameters.*

3.3.5 Damage domain and location

The damage domain indicates where erosion is present after a test. The software CloudCompare was used to understand the range of damage along the slope. After each test, five damage locations are defined on the slope designated to indicate the damage domains Low, Mid-Low, Low-Area, Mid-High and High. Low is the location of the damage domain where erosion of one individual rock occurred at the lowest part of the slope. Mid-Low is the lowest location where erosion of two rocks occurred at the same section of the slope. Mid-High and High are similar to the locations Low and Mid-Low, but for the top part of the slope. Low-Area is defined as the downslope location where randomness of entrained rocks is not present anymore. All five locations are depicted in Figure 23. The y-coordinate of each location is used to determine the vertical distance compared to SWL (distance in z direction). This vertical distance is expressed in the significant wave height H_s. The results are discussed in section 4.3 and are presented in detail in appendix I. For the 1:10 slope a smaller area is measured along the slope due to reasons described in section 3.2. The result is that especially the Low location of the damage domain could not be determined for each test. Appendix I indicates which tests are included in the analysis for each location.

The location of maximum damage along the slope is based on the results of the 2D and 3D damage parameters as discussed in sections 3.3.2 and 3.3.3. The Profile change plots shown in Figure 21 illustrates the location of the maximum damage for the 2D damage parameters. The location where most damage is incurred according to the 3D damage parameters is also determined. For the 3D damage parameters, the maximum damage location can be ascertained using the 3D profile change plots in Figure 22. The results for the damage domain and the location of maximum damage are discussed in section 4.3.

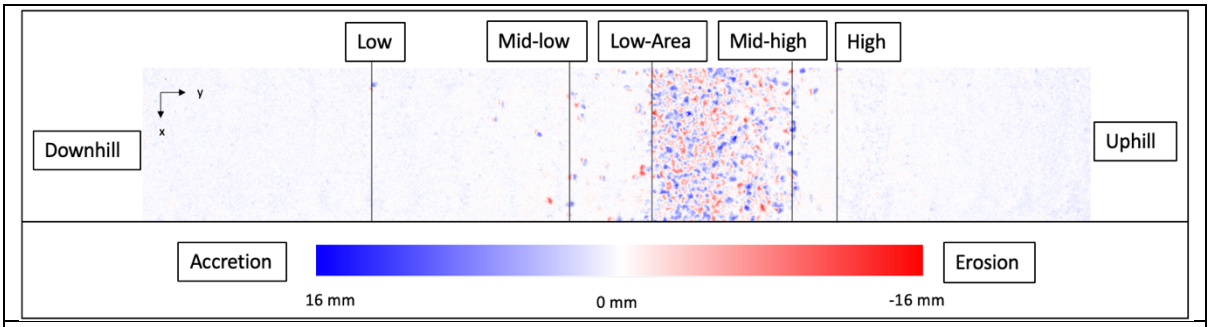

Figure 23: *A top view of the profile change of the slope after test to determine the locations: Low, Mid-Low, Mid-High and High of the damage domain.*

3.4 Analysing the video material to determine wave breaking type

The videos of the tests from the front view of the basin were analysed to determine the distribution between plunging and spilling waves. Reviewing the breaking type for every single wave for the complete test is time consuming and will have only a limited added value. For that reason, the first 100 waves of each test were analyzed. This approach is similar to the analysis conducted by Mossinkoff (2019). The influence of the slope on the distribution of breaking wave types will be analysed for the 1:8 slope. The outcomes will be compared with the results of Mossinkoff (2019) for the 1:10 slope.

Each test was recorded from the front side of the flume as illustrated in the schematisation of Figure 14. The first ten waves of the recordings are not used in the analysis, since the wave generators need some time to produce the desired waves. This means that hundred waves are analysed starting from wave eleven. How plunging waves and spilling waves are distinguished from each other is visualised in Figure 24. Spilling waves are recognised by a roller starting to form on the top part of the wave as indicated in Figure 24. This roller continues to grow on top of a water layer as the wave progresses

and advances until all wave energy has been dissipated. A plunging wave is recognised by the curling shape of the wave and breaks onto the slope defined as the plunging jet. After this plunging jet has reached the slope, a clear bouncing effect is visible by entrained air and splashing of water.

Test 3G of Mossinkoff (2019) has been analysed to check the subjectivity of this measuring method to determine the wave breaking type. Mossinkoff (2019) has counted 49 spilling waves and 51 plunging waves for this test 3G. I have reanalysed this test and counted 51 spilling waves and 49 plunging waves. This means a difference of two percent in the distribution. Some waves are difficult to quantify as a spilling or plunging wave, because both wave characteristics are present. These waves are sensitive for subjectivity, but nevertheless lead only to two percent deviation. This means that this measuring method can be used as an indication for the distribution of spilling and plunging waves. The results of the distribution between plunging and spilling waves are discussed in section 4.4.

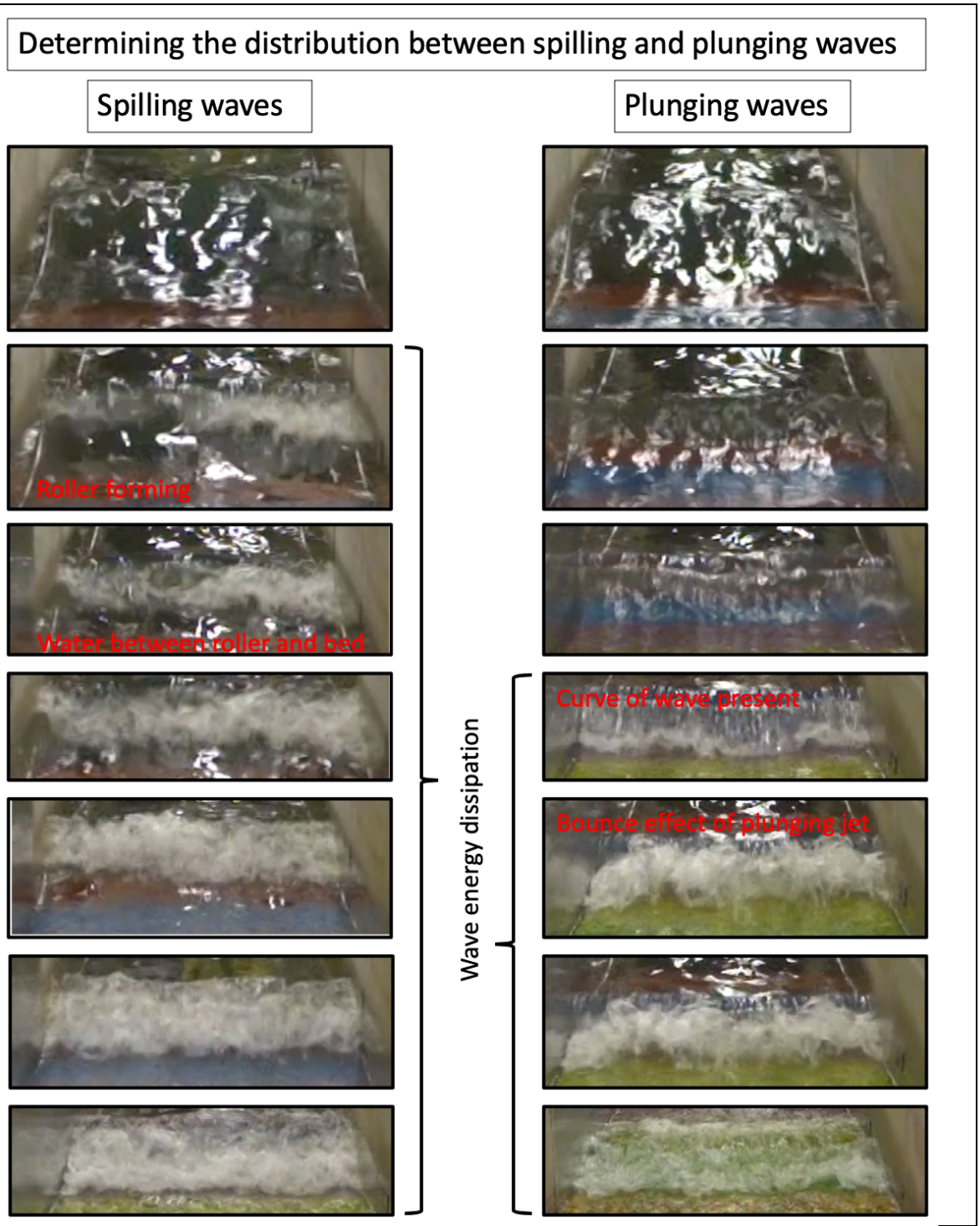

Figure 24: *Determination of the distribution between plunging and spilling waves using the camera with the front view on the flume. The photos have irregular time steps and demonstrate the important steps during wave breaking.*

3.5 Processing the entrained and deposited coloured rocks

Pictures are taken from a height of approximately 15 m above the flume section and are used to establish movements of the individual coloured rock during a test. The photos of the initial profile and the damaged profile are compared and an example is shown for test series 5G in Figure 25. The insight on transport of rocks has been extracted from these pictures. Each rock that has been displaced from one strip to another is counted. Two distinctions are made during counting. The first distinction is whether the rock deposited in an upward or downward coloured strip. The second distinction is in which specific coloured strip the entrained rock deposited. This means that for example that the number of rocks are known that eroded from the yellow strip and deposited into the orange strip as depicted in Figure 25 (Y→O).

The results for test 5.G of the 1:8 slope are illustrated in Figure 25. Based on these results two numbers are determined: The gross number of transported rocks n_{gross} and the net number of eroded rocks n_{net}. The gross number of transported rocks n_{gross} is the sum of all rocks that have been transported from one coloured strip to another. The net number of eroded coloured rocks n_{net} is the sum of all net eroded rocks that have been displaced out of every coloured strip. n_{net} is used to determine the damage parameter N_{od} which was described in section 2.4. The definition of N_{od} is repeated in Eq. 3.5.

$$N_{od} = \frac{n_{net} d_{n50}}{w} \qquad \text{Eq. 3.5}$$

N_{od} is the net number of eroded rocks n_{net} times the nominal rock diameter d_{n50} divided by the width of the test w. The damage parameter N_{od} requires formally that all individual measured rock displacements are including. This method using coloured rocks within strips has a disadvantage. The rock displacements within a coloured strip are not recorded. These unobserved rock movements within a strip are considered to be a measuring error.

This damage parameter N_{od} is transformed to S_{od} using the porosity. S_{od} is depicted in Eq. 3.6. The porosity is assumed to be equal to 0.4. S_{od} can be compared to the profile based damage parameters S and S_{all} which both were described in section 3.3.

$$S_{od} = \frac{N_{od}}{1 - porosity} \qquad \text{Eq. 3.6}$$

Besides these damage parameters the mobility parameter is determined in Eq. 3.7. This mobility parameter entails the gross number of transported rocks n_{gross} divided by the net number of eroded rocks n_{net} as depicted in Figure 25. This mobility parameter gives a good indication of the mobility of the bed. However, this number is an underestimation due to the fact that rocks also transport within a coloured strip itself. All results concerning the entrained and deposited rocks are discussed in section 4.5 and all data is presented in Appendix J.

$$MP = \frac{n_{gross}}{n_{net}} \qquad \text{Eq. 3.7}$$

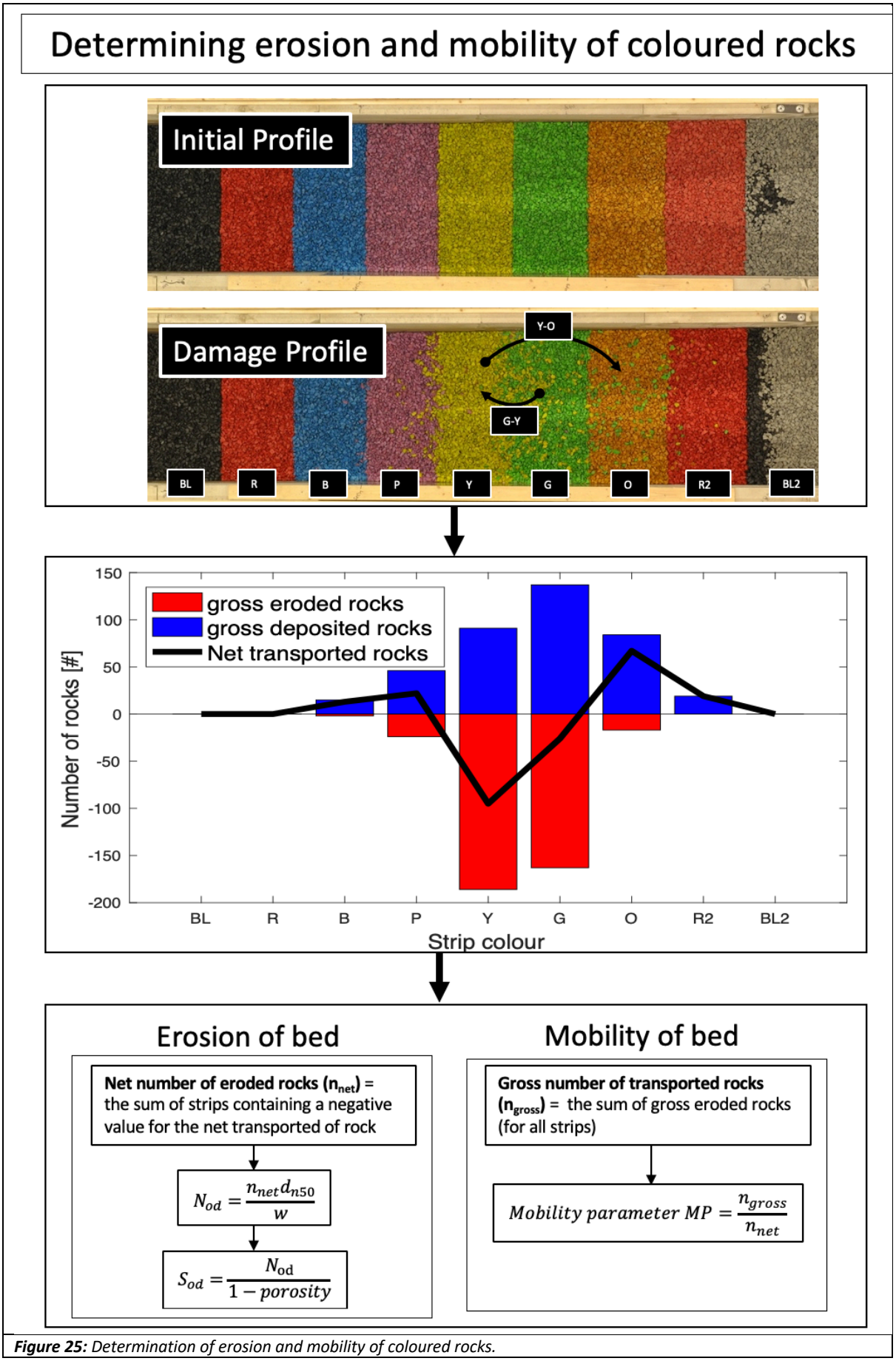

Figure 25: *Determination of erosion and mobility of coloured rocks.*

4 Results

Chapter 4 presents and discusses the results of this thesis. The results are derived from the physical model tests conducted using a 1:8 slope and the re-analysis of the physical model tests for a 1:10 slope performed by Mossinkoff (2019) as described in chapter 3. Section 4.1 discusses two visual observations which are made during testing. Section 4.2 debates the profile based damage parameters and the connection with several hydraulic and structural parameters. The variability of the profile based damage parameters is also examined. The damage domain and the maximum damage location are described in section 4.3. The distribution between plunging and spilling waves for different wave steepnesses are discussed in section 4.4. The results of the entrained and deposited coloured rocks are analysed in section 4.5. The damage parameter N_{od} and the mobility parameter *MP* of the bed are presented. The transport direction and the transportation length are derived from the coloured rocks and are also debated in section 4.5. A design formula is developed for rocks on mild slopes with an impermeable core in section 4.6. Eventually, a discussion of the results is presented in section 4.7 debating the damage parameters, the stability of the bed and the implementation in real-life situations.

4.1 Visual observations

Two main observations are made during the physical model tests and are debated in this section. The first observation is a boundary effect. During a test, this effect occurred near the side walls of the flume as depicted in Figure 26. Near the side walls more damage was observed compared to the middle part of the flume. This boundary effect was considered to be an undesirable and a wrong representation of the damage as such an outcome would not occur in a real-life situation. Measured damage parameter values will be influenced by this effect. For that reason, the outer 0.10 m near the side walls were not taken into account for the determination of the damage parameters. This approach reduces the impact of the boundary effect. A plausible cause for the boundary effect could be that the trapped air in the breaking wave or in armour layer can escape less easy and (limited) energy of the turbulent water movements perpendicular to the flume get deflected in streamwise direction, where in the middle of the flume this is gradual since water can move in every direction. This could result in larger forces acting on the rocks close to the side walls which cause more damage.

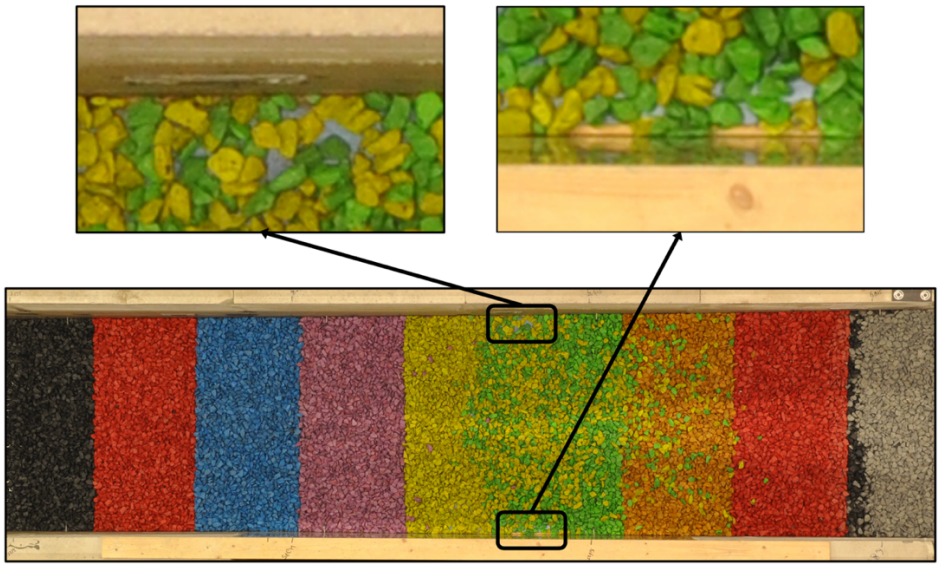

Figure 26: *The boundary effect visible close to the side walls. Example is test 1H of the 1:8 slope.*

The second observation made during the physical model tests is a restorative effect. This phenomenon is captured on photos and a video during different tests. Small parts of the bottom of the slope are visible during a test and disappear again when the test proceeds. The tests where this restorative effect is observed are Tests 2H, 2I, 3NI and 4G. The pictures of the test 4G are shown in Figure 27. This restorative effect is not directly visible in the damage parameters and should be taken into account defining the damage limits in section 4.7.

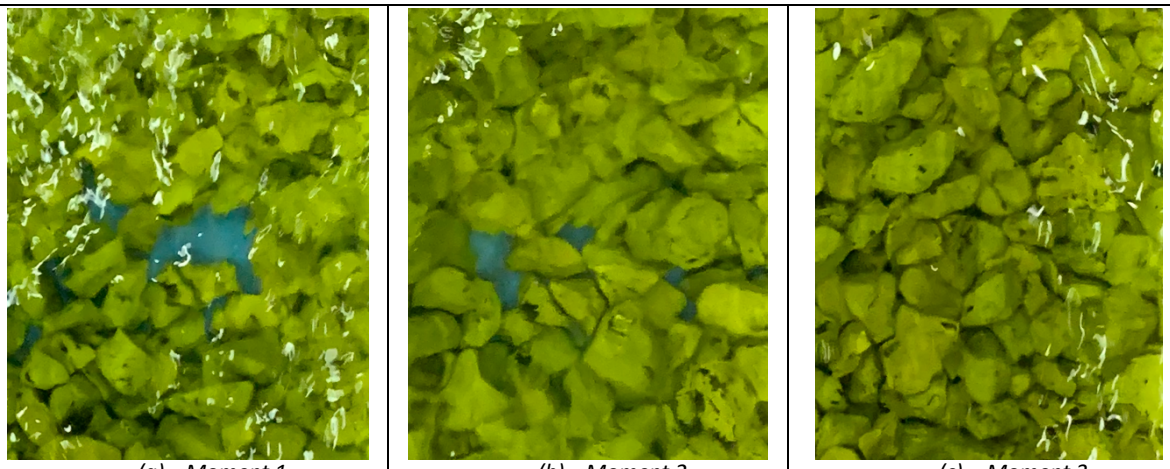

(a) Moment 1 *(b) Moment 2* *(c) Moment 3*

Figure 27: *Restorative effect captured during test 4G for the 1:8 slope.*

4.2 Profile based damage parameters

This section presents the results of the determined profile based damage parameters S, S_{all}, E_{2D}, $E_{3D,1}$, $E_{3D,3}$ *and* $E_{3D,5}$. In total 84 tests are analysed for a 1:8 slope and 47 tests for the 1:10 slope. Stereophotogrammetry is used to determine damage on the slope. Sections 3.1 and 3.2 showed the methodology for the 1:8 and 1:10 slope. Section 3.3 described the procedure to determine all profile based damage parameters. The profile based damage parameters are determined for a characterization width of 54 d_{n50} and a characterization width of 27 d_{n50} (splitting the flume into two sections of 27 d_{n50}). The outcomes for both characterization widths are shown in Appendix H.

4.2.1 Influence of wave height, wave steepness and slope angle

Figure 28 shows six graphs for the profile based damage parameters for a characterization width of 54 d_{n50}: S, S_{all}, E_{2D}, $E_{3D,1}$, $E_{3D,3}$ *and* $E_{3D,5}$. Each graph illustrates one of the damage parameters after 1000 waves against the significant wave height H_s for all wave steepnesses $s_{o,p}$ and both slopes angles. The correlations between the damage parameters and the significant wave height, wave steepness and the slope angle can be derived from the results and are discussed below.

Influence of significant wave height H_s

Upward trends are observed between a higher significant wave height H_s and every damage parameter as is shown in Figure 28. This outcome is in line with the results found by Mossinkoff (2019). This is an expected result because an increase in the significant wave height H_s has a positive quadratic relationship with wave energy. More wave energy will enlarge the impact on the structure and will increase damage parameters. The trend is increasing, but within a test series there are some specific cases where the damage parameter decreases for an increasing significant wave height H_s. Plausible explanations could be:

- The observed restorative effect (section 4.1)
- Measuring inaccuracy (section 3.3.4)
- Variability of the damage parameters (section 4.2.4)

- Longshore transport of rocks which might be caused by the boundary effect (section 4.2.5)

Influence of wave steepness $s_{o,p}$

The impact of a higher significant wave height H_s on the damage parameters is different when the wave steepness $s_{o,p}$ changes as depicted in Figure 28. In general, if the wave steepness $s_{o,p}$ is larger, the positive correlation between the significant wave height H_s and the damage parameters decreases. Mild slopes are in the transition zone between plunging and spilling waves. When the wave steepness $s_{o,p}$ increases, the Iribarren number ξ_p decreases resulting is less plunging waves and more spilling waves. Spilling waves dissipate energy over a larger area of a structure compared to plunging waves which also contains the plunging jet. This is a plausible cause for the result that an increase in the wave steepness $s_{o,p}$ reduces the impact of an increasing significant wave height H_s on the damage parameters. The correlations are visible in Figure 28, especially for large adjustments of the wave steepness $s_{o,p}$. However, if wave steepness $s_{o,p}$ is only changed slightly, it can be hard to distinguish the effect of this change. An example is the adjustment of the wave steepness $s_{o,p}$ from 0.04 to 0.05. Reasons for this could be measuring inaccuracy or the variability of the damage parameters.

Influence of the slope angle α

Figure 28 shows the influence of the 1:8 and 1:10 slopes on the damage parameters. The steeper 1:8 slope increases the impact of the significant wave height H_s on the damage parameters compared to the 1:10 slope. This has also been concluded by Kramer (2016) for 1:5, 1:10 and 1:15 slopes. The slope angle α is part of the Iribarren number ξ_p. For that reason, a steeper slope increases the Iribarren number ξ_p resulting in less spilling waves. The larger number of plunging waves results in higher values of the damage parameter values in Figure 28. Another plausible reason why steeper slopes are correlated with more damage could be the transport direction of individual stones which is documented in section 4.5. The 1:10 slope shows relatively more eroded rocks deposited upslope compared to the 1:8 slope. Consequently, it is conceivable that the slope parallel component of the gravity force on individual rocks becomes more important if the slope is steeper. This larger impact of the gravity component shall proportionally increase damage parameter for a similar significant wave height H_s.

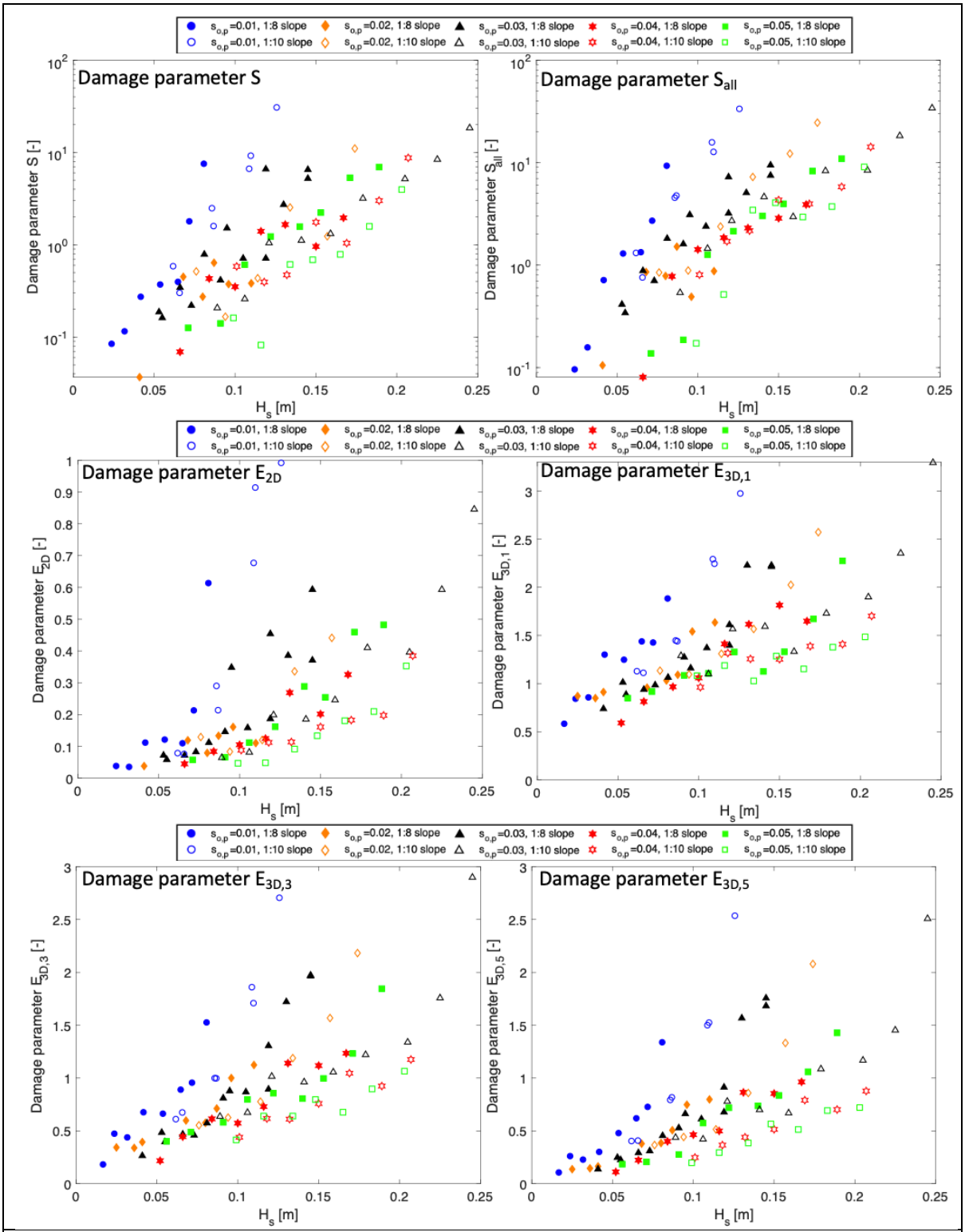

Figure 28: *The damage parameters S, S_{all}, E_{2D}, $E_{3D,1}$, $E_{3D,3}$ and $E_{3D,5}$ related to the significant wave height H_s to investigate the influence of the significant wave height H_s, wave steepness $s_{o,p}$ and slope angle on damage for mild slopes after 1000 waves.*

4.2.2 Influence of layer thickness

Two different layer thicknesses T of the armour layer are applied in the physical model tests. These armour layers had a thickness of 2.5 d_{n50} and 5.0 d_{n50}. The core of the structure was impermeable. The wave steepnesses $s_{o,p}$ equal to 0.01 and 0.03 have been researched. Figure 29 depicts the results of the influence of the layer thicknesses T on the damage parameters for the 1:8 and 1:10 slope. After examining the results, an increase in the armour layer thickness T from 2.5 d_{n50} to 5.0 d_{n50} does not seem to have impact on the stability of the rocks for both 1:8 and 1:10 slope.

According to the method of Eldrup et al. (2019), the notional permeability P of the 2.5 d_{n50} layer is equal to 0.12 and increases to 0.48 for the thicker 5.0 d_{n50} layer. The theory discussed in section 2.3.2 states that it is expected that a thicker armour layer on an impermeable core increases the stability of the outer stones. More voids are present and water flow can dissipate more easily into the thicker layer reducing destabilizing forces. Also during the run-down of the water within the armour layer a larger area is available reducing the forces on the outer rocks of this armour layer. However, the results of the physical model tests show no evidence that an increase of the layer thickness T of the armour layer from 2.5 d_{n50} to 5.0 d_{n50} increases the stability of the structure. A plausible explanation could be that the reflection forces introduced by the impermeable core overrule the dissipating effect of doubling the layer thickness.

The number of plunging waves is still much larger than the spilling waves for the researched 1:8 and 1:10 slopes as shown in section 2.1.2 and section 4.4. Forces from plunging waves act more perpendicular to the structure due to the plunging jet and impact the rocks more directly, as they are less shielded by a water layer. Water of this jet enters the structure and bumps via the shortest route onto the impermeable core and reflects. For milder slopes (e.g. 1:20) with dominant spilling waves, more horizontal velocities are present. The consequence might be that the dominant influence of the core on the structure stability reduces. The result might be that an increase of the layer thickness of the armour layer will positively influence the stability for these very mild slopes.

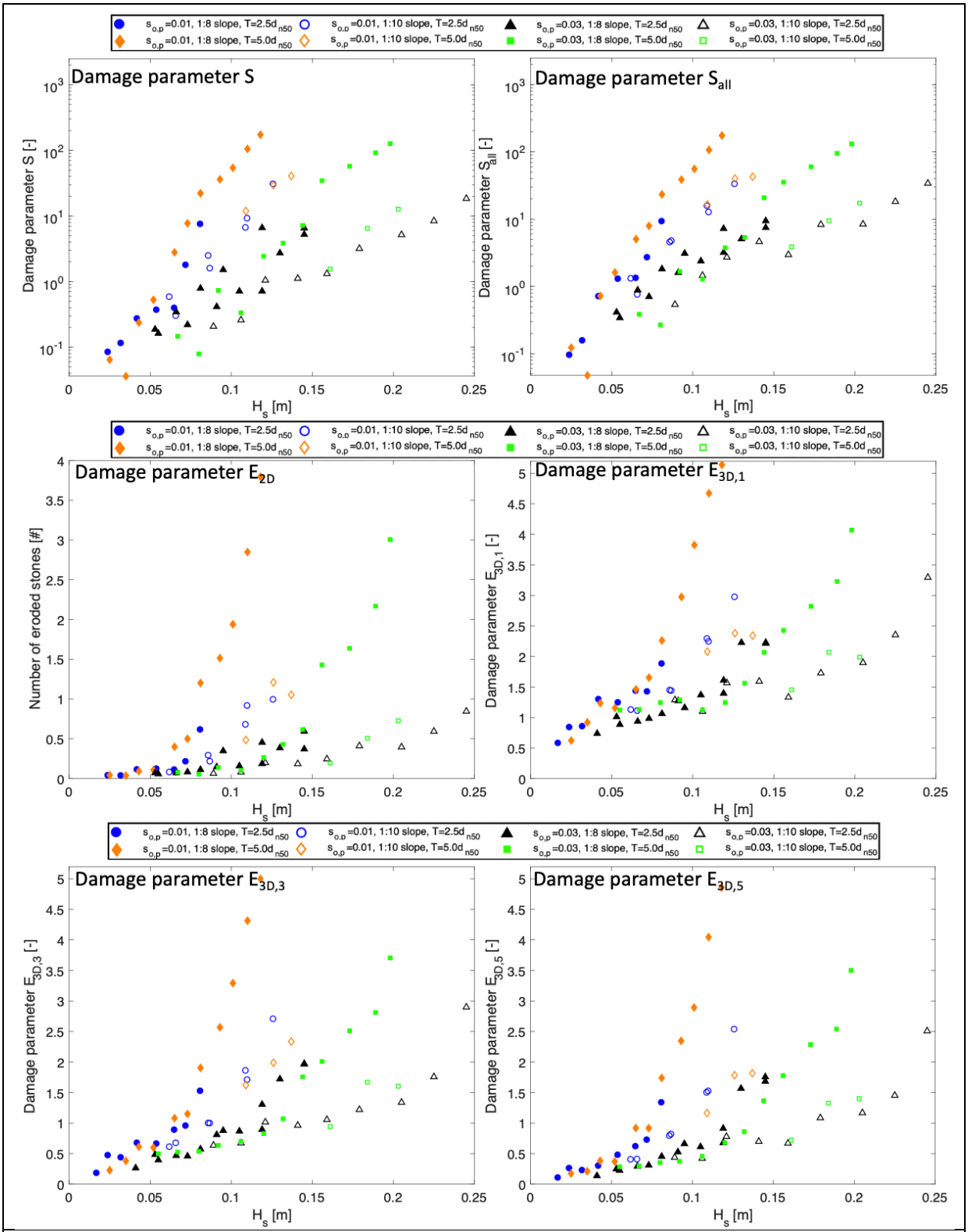

Figure 29: *The damage parameters S, S_{all}, E_{2D}, $E_{3D,1}$, $E_{3D,3}$ and $E_{3D,5}$ related to the significant wave height H_s to investigate the influence of layer thickness on damage for mild slopes after 1000 waves.*

4.2.3 Influence of the number of waves

Figure 31 depicts the number of waves against every damage parameter for the 1:8 and 1:10 slope. A clear linear trend is visible for the 2D damage parameters S, S_{all} and E_{2D}. Even after 15 603 waves the trend is still a linear increase. This correlation differs from the re-analysis by Van der Meer (1988) on the physical model tests of Thompson and Shulter (1975). Van der Meer (1988) derived for steeper slopes a square root relationship between the damage parameter S and the number of waves N ($S \sim \sqrt{N}$) and includes an upper limit. According to this re-analysis a new equilibrium will be formed after approximately 15 000 waves and no additional damage will occur. The results of the physical model tests for the mild 1:8 slope of this research show that additional damage occurs with a constant rate, even after 15 000 waves. The correlation between the number of waves and damage might be different for mild slopes compared to steep slopes.

The results for the 3D damage parameters also show a linear upward trend, but with an offset. This offset can be explained by the fact that 3D damage parameters are not an average value over the width of the flume. This means that when one rock somewhere is displaced somewhere along the slope, a substantial damage is immediately measured. The smaller the circle of the spatial moving average is within the damage parameter $E_{3D,m}$, the higher is the offset.

One outlier in the results is observed in test 6.E for the 1:8 slope after 4435 waves. A plausible cause for this outlier is found after examining the test in more detail. The boundary effect at the side walls was discussed in section 4.1 which is the reason why the outer 10 cm of the flume are not used in the determination of the damage parameters. However, it seems that 10 cm is not enough for test 6.E as depicted in Figure 30. This is because the boundary effect seems to be present beyond the 10 cm of the side walls as shown in Figure 30 (a). Test 6.F is displayed in Figure 30 (b) and shows that the boundary effect is smaller than within test 6.E. Test 6.E is for that reason considered to be an outlier. The boundary effect can have significantly more impact on the 3D damage parameter compared to the 2D damage parameters. As the damage parameters S and E_{2D} are both width-average parameters and $E_{3D,m}$ is based on a spatial moving average (De Almeida et al., 2019). For that reason, the boundary effect is not observed measuring the 2D damage parameters.

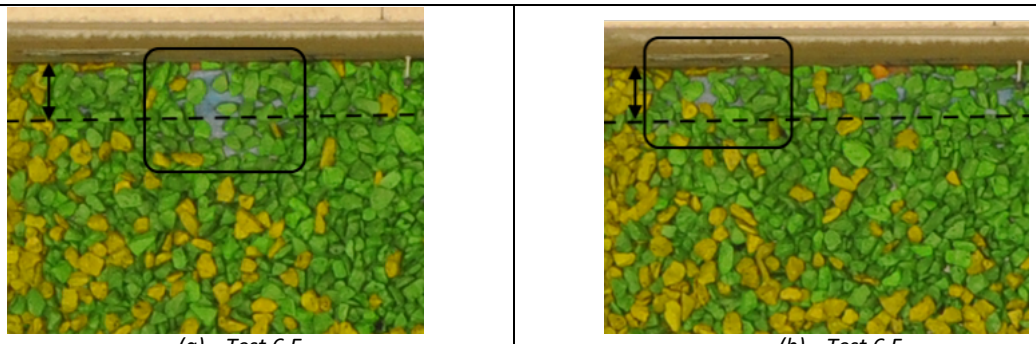

(a) Test 6.E *(b) Test 6.F*

Figure 30: *Illustration of the size of the boundary effect for test 6.E compared to test 6.F which can cause the outlier for test 6.E.*

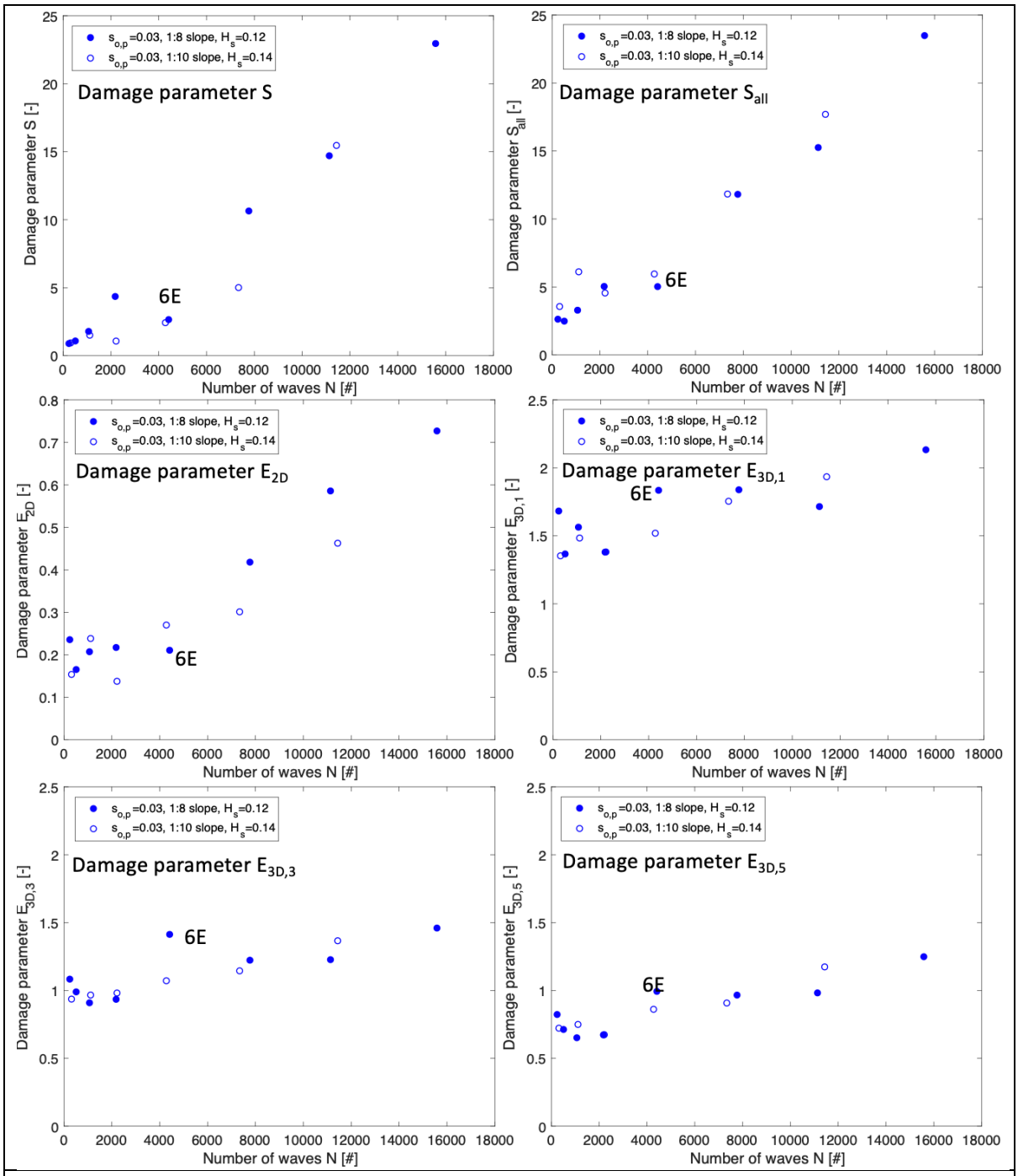

Figure 31: *The damage parameters S, S_{all}, E_{2D}, $E_{3D,1}$, $E_{3D,3}$ and $E_{3D,5}$ related to the significant wave height H_s to investigate the influence of number of waves on damage for mild slopes.*

4.2.4 Variability of damage parameters

Test series 9 for the 1:8 slope provides insight on the standard deviation and variability of the damage parameters for identical test conditions as described in section 3.1. This test series contains five tests where the significant wave height H_s is equal to 0.12 m and the wave steepness $s_{o,p}$ is equal to 0.03. After each test the bed is completely rebuilt. In this manner, the variability of the damage parameter can be determined and the cumulative damage concept as described in section 3.1 can be verified for mild slopes.

The characterization width *w* of the test flume is 54 d_{n50}. Dividing the test flume into two separate sections gives the opportunity to determine a 90 percent confidence interval of ten values for each damage parameter, in order to increase preciseness of this confidence interval. The results of all damage parameters for test series 9 for the characterization width of 27 d_{n50} are depicted in Table 25, which can be found in Appendix H. Table 15 shows the mean, standard deviations and the 90 percent confidence intervals for each damage parameter based on the results of test series 9. A t-distribution is used to determine the 90 percent confidence intervals (90 % CI =$\mu \pm 1.833\ \sigma/\sqrt{10}$).

The results in Table 15 for damage parameter *S* show that the boundary of the 90 percent confidence interval becomes negative which indicates that the distribution is skewed. This means that the assumption of uniformly distributed damage is invalidated. *S* is based on the largest erosion area as described in section 3.3.2. *S* has the largest standard deviation (1.45) and variation (0.57) compared to the other damage parameters. This might be caused by the large erosion length of the 1:8 slope where multiple erosion areas are formed. If some of these erosion areas are merged together during a test, larges values of S may occur. If these erosion areas do not connect the value of *S* can remain small. The result is a large standard deviation and variation in *S*. The damage parameter S_{all} takes every erosion area into account for the determination of its value. This could explain the smaller standard deviation (1.09) and variation (0.28) of S_{all} compared to the parameter *S,* since it does not matter whether erosion areas are connected or not when determining S_{all}.

The damage parameters E_{2D}, $E_{3D,1}$, $E_{3D,3}$ and $E_{3D,5}$ based on erosion depth d_e show lower standard deviations (0.05-0.12) and variations (0.09-0.19) compared to the damage parameters *S* and S_{all} which are based on erosion area(s) A_e. As already discussed, an explanation can be that the inclusion of the erosion length causes larger standard deviations and variations. The study of Van Gent et al. (2019) shows results of repetition tests for a 1:3 slope rubble mound revetment. The standard deviations of the 2D damage parameters *S* and E_{2D} seem to be higher for the 1:8 slope compared to this steeper 1:3 slope. The standard deviations of the 3D damage parameters $E_{3D,1}$ and $E_{3D,5}$ are in the same range.

Cumulative and non-cumulative damage results are compared to investigate whether there is a difference. Test 3NG has similar conditions as the repetition tests in test series 9, meaning a significant wave height H_s of 0.12 m and wave steepness $s_{o,p}$ of 0.03. However, the difference is that Test 3NG is part of test series 3N which is based on cumulative damage. This means that the slope is not rebuilt for an ascending significant wave heights H_s within a test series. Test series 9 is based on non-cumulative damage meaning that the slope is rebuilt after each test. The damage parameters of test 3N.G are compared to the confidence interval of the damage parameters of test series 9 to study whether cumulative and non-cumulative damage give similar results. The results are depicted in Table 15 and show that all damage parameters are within the 90% confidence intervals. This provides evidence that cumulative damage and non-cumulative damage parameters are similar and that the cumulative damage concept is valid for mild slopes.

Table 15: *The mean, standard deviation and lower and upper boundary of a 90 percent confidence interval of test series 9 (non-cumulative damage). Results of Section 1 and 2 of Test 3N.G (cumulative damage) are also depicted to compare cumulative and non-cumulative damage results.*

Damage parameter	Mean μ	Standard deviation σ	Variation σ/μ	Lower boundary 90 percent CI	Upper boundary 90 percent CI	Test 3NG section 1	Test 3NG section 2
S	2.54	1.45	0.57	-0.113	5.191	1.79	0.58
S_{all}	3.95	1.10	0.28	1.936	5.966	5.78	3.12
E_{2D}	0.27	0.05	0.19	0.177	0.362	0.26	0.19
$E_{3D,1}$	1.26	0.12	0.09	1.041	1.478	1.40	1.38
$E_{3D,3}$	0.77	0.08	0.10	0.634	0.916	0.89	0.85
$E_{3D,5}$	0.57	0.07	0.12	0.443	0.701	0.68	0.50

4.2.5 Influence of boundary effect on profile based damage parameters

As discussed in section 4.1, 80 cm of the middle part of the flume is used in the determination of all profile based damage parameters. Test series 2 gave some contradictory results. The 2D damage parameters showed a decreasing or stabilizing value at some point, where the 3D damage parameters remained increasing. Figure 32 (a) and (b) illustrate this observation for E_{2D} and $E_{3D,3}$. The orange datapoints, which are highlighted with large blue circles, indicate the results of test series 2 for the damage parameter E_{2D} and $E_{3D,3}$.

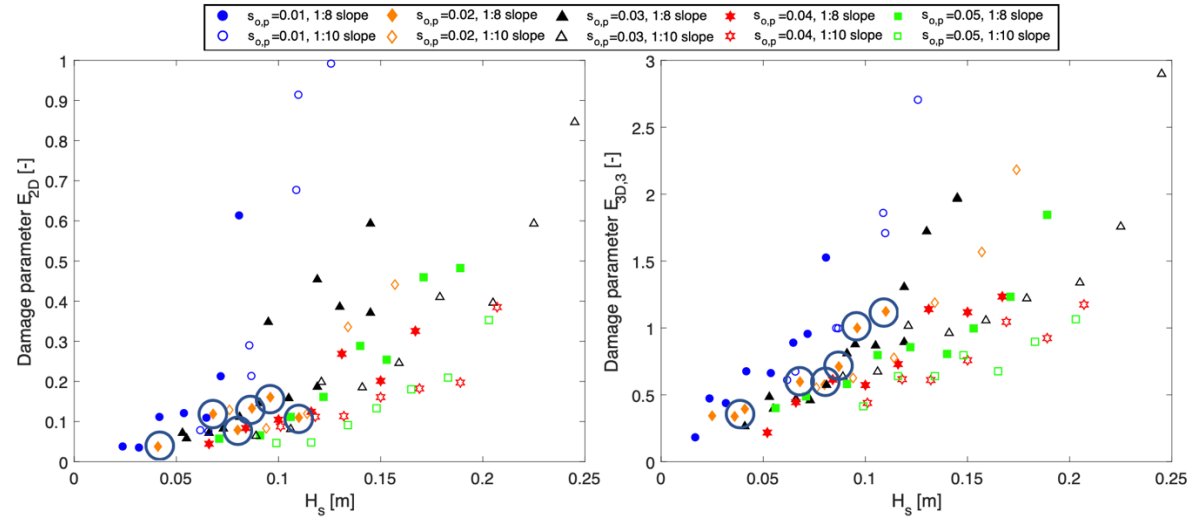

(a) Damage parameter E_{2D} *(b) Damage parameter $E_{3D,3}$*

Figure 32: *The observation that 2D damage parameters stagnated and 3D damage parameter still increased for tests series 2 of the 1:8 slope which are indicated by blue large circles.*

The profile change plots for all test series are added in the appendix F and G. These plots show relative more accretion compared to erosion. Bias does not seem to be the cause for this observation. Two reasons might explain the relatively extensive accretion. Longshore transport of rock might cause that rock from the excluded outer 10 cm is transported within the measured section of 80 cm. Another explanation might be that the voids between the rocks increased in size due to movements of rocks resulting in relative more accretion.

The effect of the exclusion of the outer 10 cm of the flume is studied for the 2D damage parameters. To investigate the longshore transport of rocks the tests of 2G, 2H, 2I and 3NG, 3NH and 3NI of the 1:8 slope are determined for a width of 95 cm of the flume and excludes only 2.5 cm of the locations close to the side walls. The results for a measuring width of 95 cm are shown in Table 16. The values for the damage parameters increased in size. This provides evidence that some longshore transport of rock is present probably caused by the observed boundary effect. This clarifies why the 2D damage parameters of test series 2 stagnated or decreased for an increasing significant wave height H_s.

Table 16: *The determination of the 2D damage parameters S_{all}, S and E_{2D} for a width of 80 cm and 95 cm of the flume.*

Test	S_{all} - 95 cm	S_{all} - 80 cm	S - 95 cm	S - 80 cm	E_{2D} - 95 cm	E_{2D} - 80 cm
2G	1.78	1.51	0.88	0.64	0.15	0.13
2H	1.67	0.49	0.71	0.38	0.22	0.16
2I	5.27	0.87	2.85	0.38	0.25	0.11
3NG	4.70	3.20	1.72	0.71	0.20	0.19
3NH	8.11	5.08	4.43	2.72	0.53	0.39
3NI	12.50	7.49	10.34	6.52	0.72	0.59

4.3 Damage domain and location

This section describes the analysis of the results for the damage domain and the maximum damage location. An increase in the insight into the damage domain and maximum damage location can be used to improve designs of coastal protection works for mild slopes. Figure 33 (a) and (b) show the box-plots of the results for the damage domain locations: Low, Mid-Low, Low-Area, Mid-High and High for the 1:8 and 1:10 slope as defined in section 3.3.5 and Figure 23. The lower boundaries show more spreading of the results as depicted in Figure 33 (a) and (b). A reason for this could be that the wave energy left at the upper part is similar for each wave height. Higher waves reach the slope at a lower part the slope which means that breaking and wave energy dissipation starts at an earlier stage. The wave energy that is left when the wave reaches the upper damage locations synchronises for each wave. This results in a smaller standard deviation for the upper damage locations compared to the locations Low and Mid-Low.

Figure 33 (c) and (d) present the boxplots of the location where the maximum damage occurred based on the 2D and 3D damage parameters. The tests that are included in the boxplots are test series 1, 2, 3, 3N, 4 and 5 for the 1:8 slope and tests series 1, 2, 3, 4, 5 and 11 for the 1:10 slope. The reason that these test series are used is that within these test series the wave steepness is varied. The test for a thicker layer and ascending number of waves are not included since these might show slightly different and less comparable results. The individual results for all tests are added in Appendix I.

The results for the medians are schematised in Figure 34 to point out where erosion takes place and where rocks are entrained. Based on the medians, rocks are entrained between -2.7 H_s and 0.7 H_s for the 1:8 slope and -2.3 H_s and 0.5 H_s for the 1:10 slope. Most erosion and accretion occur between -1.1 and 0.6 H_s for the 1:8 slope and -1.2 and 0.4 H_s for the 1:10 slope considering the medians. This also illustrated in Figure 23. However, exploring the boxplots in Figure 33 (a) and (b) to increase certainty this value would be between -1.6 H_s (lowest value for the location Low-Area) and 0.9 H_s (highest value for Mid-High location) for the 1:8 slope. The 1:10 slope show slightly different results and are -2.0 H_s (lowest value for the location Low-Area) and 0.8 H_s (highest value for Mid-High location).

The maximum erosion differs per damage parameter. The outcomes reveal that the median of the maximum damage occurs at -0.2 H_s and -0.3 H_s below SWL based on the 2D damage parameters for both the 1:8 and 1:10 slope. The median values for the $E_{3D,m}$ damage parameters varies and are lower for both slopes compared to the 2D damage locations. This slight difference between the 3D and 2D parameters may require additional research. Overall there seem to be limited differences between the 1:8 and 1:10 slope.

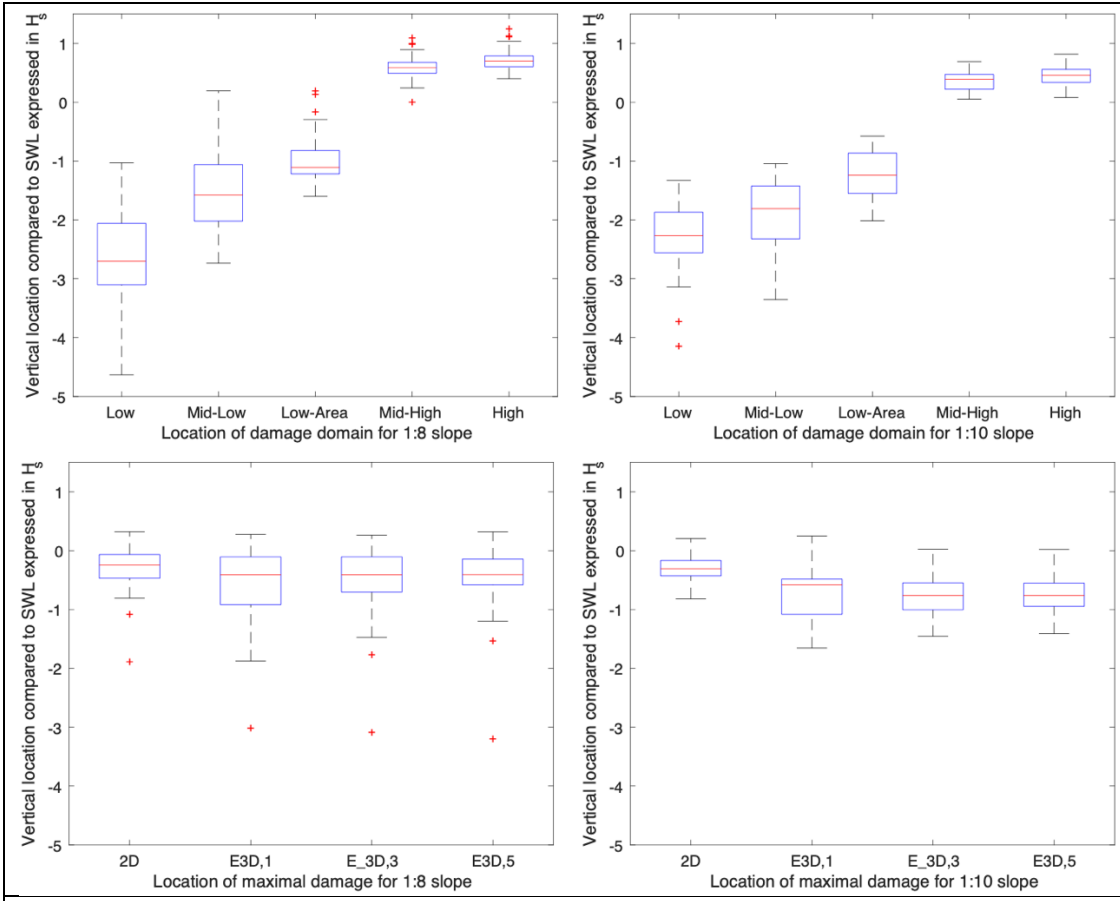

Figure 33: *(a) and (b) boxplot of the locations Low, Mid-Low, Mid-High and High for the 1:8 and 1:10 slope. (c) and (d) boxplots of the location of the maximum damage based on the 2D and 3D damage parameters expressed in significant wave height H_s compared to SWL. The crosses are outliers.*

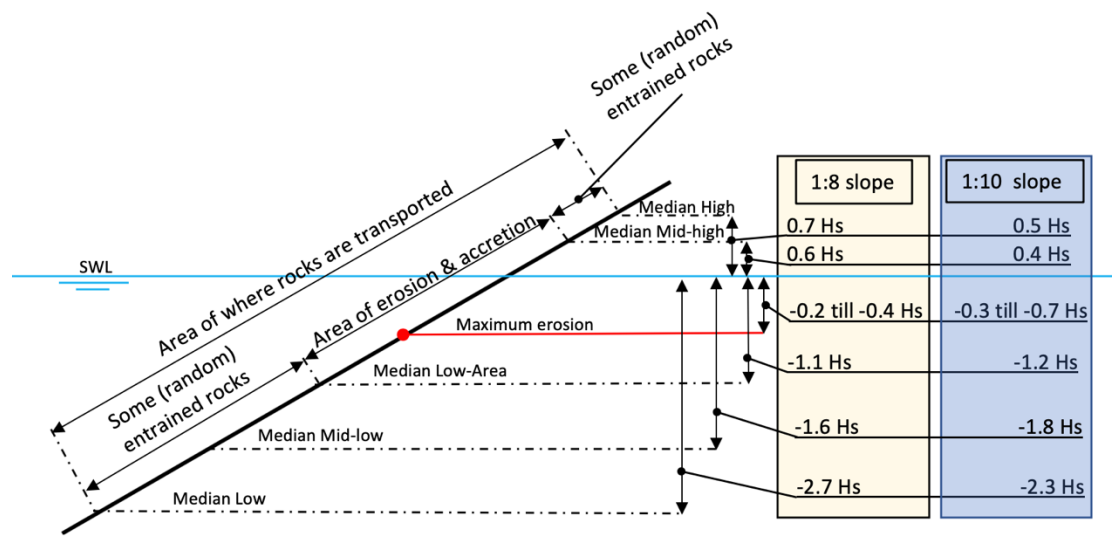

Figure 34: *Schematisation where rocks are entrained and where most and max erosion occurs on the 1:8 and 1:10 slope.*

4.4 Wave breaking types

The waves for six tests have been analysed to determine the distribution between plunging and spilling waves for the 1:8 slope. The approach was already described in section 3.4. For each wave

steepness $s_{o,p}$ (except for $s_{o,p}$=0.05) one test has been determined and the results are displayed in Table 17. For each wave steepness $s_{o,p}$, the test with the highest significant wave height H_s is determined. A high significant wave height H_s simplifies the distinction between a spilling and plunging. One additional test for a wave steepness $s_{o,p}$ of 0.05 is examined to investigate the variability of the distribution for a similar Iribarren number ξ_p and a different significant wave height H_s. A two percent difference is observed between test 5H and 5I as shown in in Table 17.

Figure 35 shows the percentage of plunging waves for each Iribarren number ξ_p for the 1:8 and 1:10 slope. The data for the 1:10 slope is based on Mossinkoff (2019). Based on these tests, it seems that the Iribarren number ξ_p can predict the distribution between plunging and spilling breaking waves. Even for a different slope, but a similar Iribarren number tξ_p he distribution seems to be approximately the same. Curve fitting is used to express the number of plunging waves by the Iribarren number ξ_p (% plunging wave = $\xi_p{}^{\alpha}$). This by minimizing the root mean squared error between the data pints ans the curve. According to results the best fit is % plunging wave = $\xi_p{}^{0.57}$. The number of tests analysed is limited and more research should confirm these preliminary conclusions.

Table 17: *The determined distribution between spilling and plunging waves for each wave steepness.*

Test Information			Test			Wave characteristics	
Series	Run	$s_{o,p}$	$H_{1/3}$	$\frac{Hs}{\Delta d_{n50}}$	ξ_p	Percentage of spilling waves [%]	Percentage of plunging waves [%]
1	H	0.009	0.081	2.82	1.25	0	100
2	I	0.019	0.110	3.83	0.88	4	96
3	I	0.030	0.145	5.05	0.72	10	90
4	F	0.020	0.174	6.06	0.63	22	78
5	H	0.050	0.171	5.94	0.56	32	68
	I	0.050	0.189	6.58	0.56	30	70

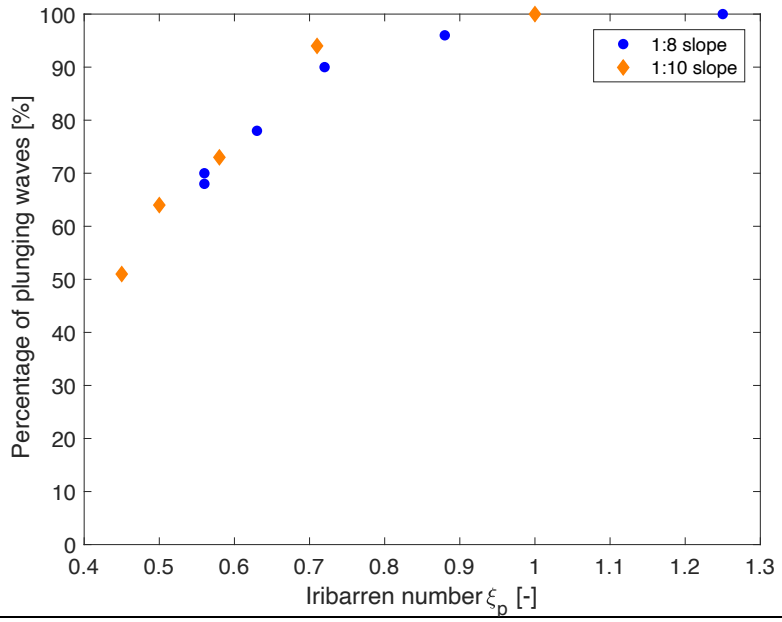

Figure 35: *The distribution between spilling and plunging waves for the 1:8 and 1:10 slope.*

4.5 Entrained and deposited individual coloured rocks

This section shows the outcomes of the rock counting method for coloured rocks in the strips. Section 3.5 already described the methodology in detail. Appendix J shows the results for the number of eroded, deposited and net transported stones per strip, the damage parameters N_{od} and S_{od} and the mobility parameter *MP*. Section 4.5.1 debates the damage parameter N_{od} and S_{od} and the influence of several hydraulic and structural parameters. The variability of the damage parameters is also discussed including the comparison between cumulative and non-cumulative tests. The mobility parameter *MP* and the nominal diameter of entrained rocks is analysed in section 4.5.2 followed by the transport direction of entrained and deposited rocks in section 4.5.3. The transport length is documented in section 4.5.4.

4.5.1 The damage parameters N_{od} and S_{od}

The damage parameters N_{od} and S_{od} are studied to analyse the influence of the significant wave height, wave steepness, slope angle, layer thickness and number of waves. Both damage parameters were defined in section 3.5. N_{od} is the net number of eroded rocks n_{net} times the nominal rock diameter d_{n50} divided by the width of the test *w*. The net number of eroded rocks n_{net} is based on the net transport of the coloured rocks between the different strips. The damage parameter N_{od} is transformed using the porosity to S_{od} which can be compared to the profile based damage parameter S_{all}.

Influence of hydraulic and structural parameters

Figure 36 shows graphs that reveal the correlations between the damage parameter N_{od} and the significant wave height H_s, wave steepness $s_{o,p}$, slope angle α, layer thickness *T* and number of waves *N*. These correlations have already been investigated in section 4.2 for the profile based damage parameters. The results in Figure 36 provide evidence and substantiates most of the outcomes observed for the profile based damage parameters. Table 18 shows the correlations for the damage parameter N_{od} and thus summarizes the outcomes of Figure 36. Section 4.2 already discussed the physics and the explanations for these results. For that reason, these explanations are not repeated in this section. The relationship found between the damage parameter N_{od} and the number of waves show some flattening (non-linear) for the higher number of waves. This deviates from the results for the profile based damage parameters studied in section 4.2. An explanation might be that for higher number of waves some transported stones are overlapping and will hide some coloured rocks.

Table 18: *The relationship between several hydraulic and structural parameters and the damage parameter N_{od}.*

Hydraulic or structural parameter	Correlation with damage parameter N_{od}
Significant wave height, H_s	Positive correlation
Wave steepness, s_{op}	Negative correlation
Slope angle, α	Positive correlation
Layer thickness, *T*	No correlation
Number of waves, *N*	Positive correlation

Variability of damage parameter N_{od}

Test series 9 for the 1:8 slope consists of repetition tests and provides insight on the standard deviation and variability of the damage parameters for identical test conditions as described in section 3.1. The test contained a significant wave height H_s of 0.12 m and wave steepness of 0.03. Table 19 shows the mean, standard deviations and the 90 percent confidence intervals for the damage parameter N_{od} based on the results of test series 9. A t-distribution is used to determine the 90 percent confidence intervals (90 % CI =$\mu \pm 2.132\ \sigma/\sqrt{5}$) assuming a normal distribution. The results show that the damage parameter N_{od} has a relative low variation compared to the variations of the profile based damage parameters discussed in section 4.2.5.

Cumulative and non-cumulative damage tests

Cumulative and non-cumulative damage results are compared to investigate whether there is a difference. The difference between cumulative and non-cumulative damage tests was discussed in section 4.2.4. Test 3NG is a cumulative damage test within test series 3 and the tests within test series 9 are non-cumulative tests. These tests have similar conditions and are therefore suitable to compare to each other (significant wave height H_s of 0.12 m and wave steepness $s_{o,p}$ of 0.03). The results of test 3NG are presented in Table 19. The value of the damage parameter N_{od} of test 3NG does not fit in the 90 percent confidence interval based on the damage values of N_{od} of test series 9. This suggests that test results of cumulative damage tests and non-cumulative damage tests differentiate from each other. This contradicts the evidence provided by the profile based damage parameters in section 4.2.5. These results indicated that cumulative damage tests and non-cumulative damage tests deliver similar results.

Table 19: *The mean, standard deviation and lower and upper boundary of a 90 percent confidence interval of test series 9 (non-cumulative damage). Results of Test 3N.G (cumulative damage) are also depicted to compare cumulative and non-cumulative damage results.*

Damage parameter	Mean μ	Standard deviation σ	Variation σ/μ	Lower boundary 90 percent CI	Upper boundary 90 percent CI	Test 3NG
N_{od}	1.04	0.08	0.08	0.97	1.12	1.47

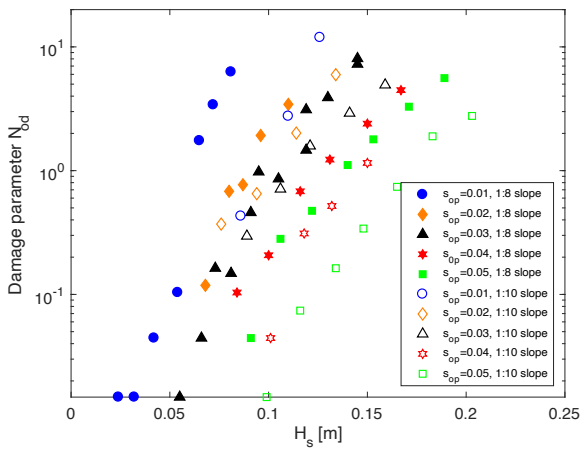

(a) Influence of wave height, wave steepness and slope angle

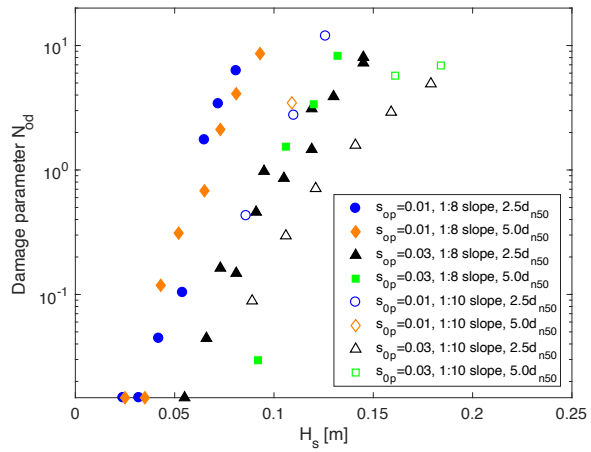

(b) Influence of layer thickness

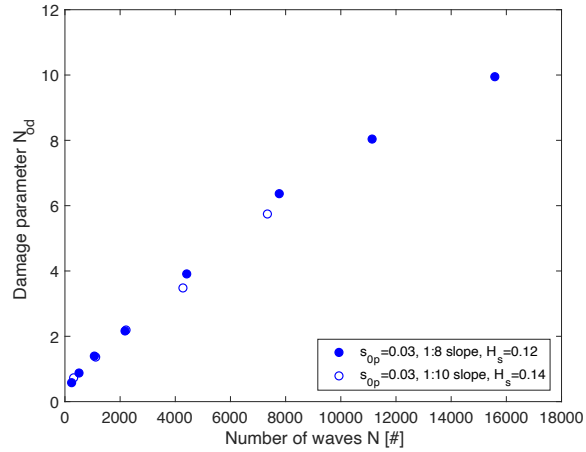

(c) Influence of number of waves

Figure 36: *The number of net eroded rocks to investigate the influence of wave height, wave steepness, slope angle, layer thickness and number of waves.*

Comparison between damage parameter S_{od} and profile based damage parameter S_{all}

S_{od} is an estimate of damage parameter S and is based on the damage parameter N_{od}. S_{od} is compared to the profile based damage parameter S_{all}. The comparison is made for tests where 100 rocks displaced from one strip to another to avoid outliers in in the test results. Boxplots are shown in Figure 37 and demonstrate that the median of the ratio between S_{all} and S_{od} for the 1:8 slope is equal to 1.35. For the 1:10 slope, this value is equal to 1.21. Higher values for the ratio between S_{all} and S_{od} seem to be associated with relative mild tests conditions containing a low significant wave height H_s. For these mild conditions relatively more coloured rocks transport within a coloured strip itself and less rocks end up in another coloured strip. This might explain the higher values for the ratio between S_{all} and S_{od}. Lower values for this ratio between S_{all} and S_{od} seem to be associated with severe test conditions with relatively high significant wave heights H_s. An explanation for this might be that relatively more rocks seem to be transported from one strip to another. Besides, S_{all} is based on the middle 80 cm and exclude the outer 10 cm close to the side walls and more damage is observed in these outer regions. S_{od} is based on the coloured rocks for the entire width of the flume of 1 m. This might explain the lower ratios found between S_{all} and S_{od}.

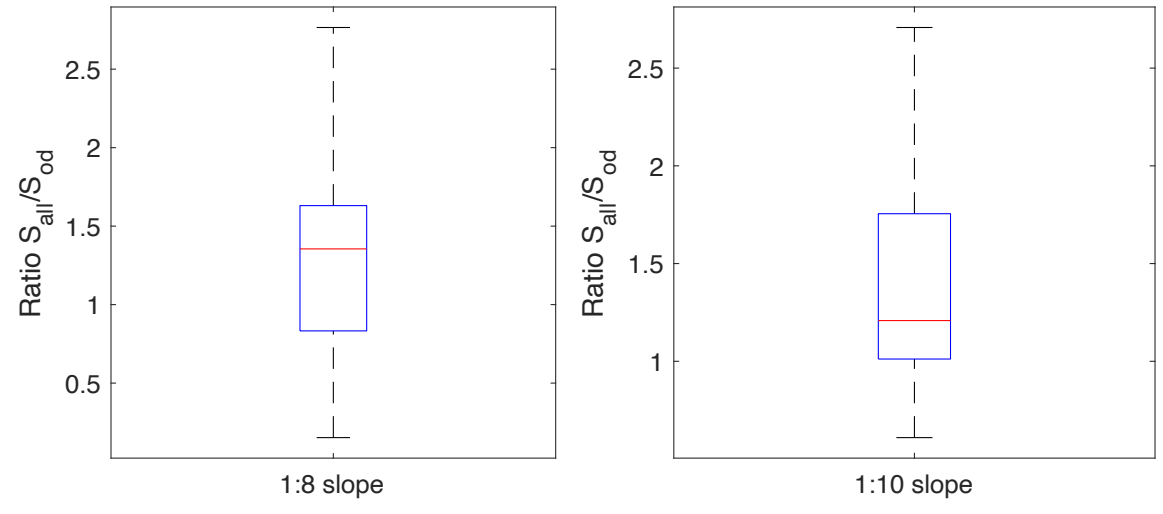

Figure 37: *The boxplots for the ratio's between the profile based damage parameter S_{oll} and the damage parameter S_{od}*

4.5.2 The mobility parameter *MP* and nominal diameter of entrained rocks

Mobility parameter MP

The mobility parameter *MP* is the gross number of transported rock n_{gross} divided by the net number of eroded rocks n_{net}. This was already explained in section 3.5. This parameter can give an indication of the mobility of the bed. Figure 38 shows the boxplots for the mobility parameter *MP* for the 1:8 and 1:10 slope. The median of the mobility parameter *MP* is 3.0 for the 1:8 slope and 2.9 for the 1:10 slope. This means that if approximately three rocks are displaced from one strip to another, only one transported rock causes erosion. This number is underestimated because rocks are also moving inside a coloured strip itself. For a steep slope with rather larger rocks one displaced rock can already generate severe damage. For that reason, the mobility parameter *MP* of steep slopes is close to 1.0 and deviates from the results found on mild slopes.

The nominal diameter d_{n50} of entrained rocks

The entrained rocks from repetition tests within test series 9 have been weighted. The nominal diameter d_{n50} of these entrained rocks has been determined to check whether it deviates from the nominal diameter d_{n50} of the batch of rocks (0.0148 m). For the five repetition tests the nominal diameter d_{n50} of the entrained rocks is 0.0157 m, 0.0158 m, 0.0156 m, 0.0157 m and 0.0157 m. This is larger compared to the nominal diameter of the rocks determined by Mossinkoff (2019). A plausible

explanation might be that larger stones are more exposed compared to the smaller stones and are therefore entrained more easily.

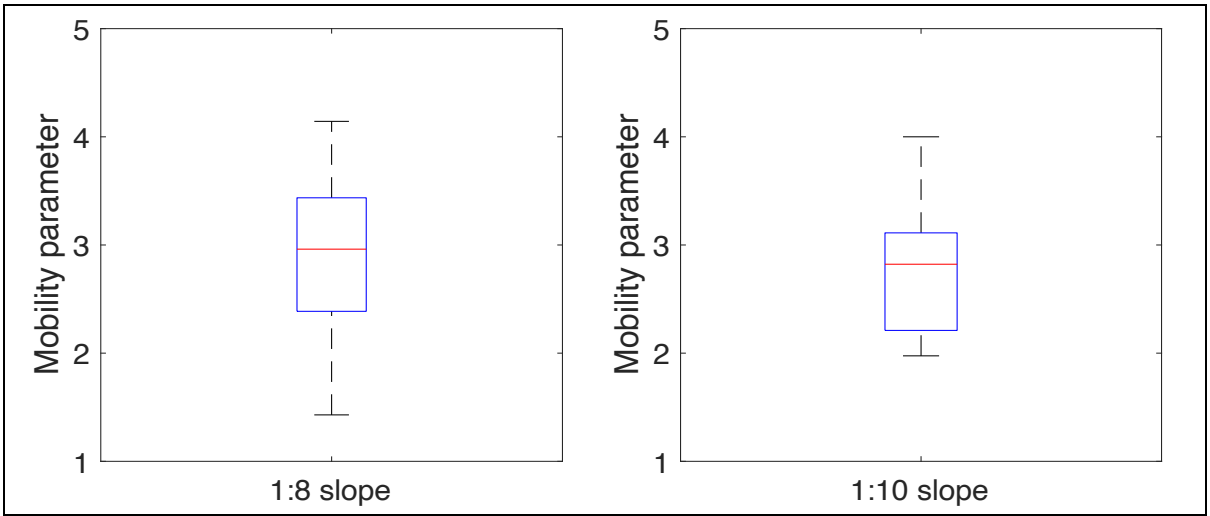

Figure 38: *The boxplots for the mobility parameters MP for the 1:8 and 1:10 slope.*

4.5.3 The transport direction of entrained and deposited coloured rocks

During a test the coloured rocks erode and will be deposited upslope or downslope. The transport direction is investigated for every wave steepness $s_{o,p}$ and slope angle α. In this study, the transport direction is only determined if a minimum of 100 eroded and deposited rocks is recorded. This threshold is used to reduce outliers in the distribution between upward and downward deposited rocks. Figure 39 (a) depicts the averaged percentage of eroded rocks deposited in an upslope coloured strip for each wave steepness $s_{o,p}$. For a wave steepness $s_{o,p}$ of 0.01, 92 percent of the rocks deposit upslope for the 1:10 slope. This number decreases to 82 percent for a wave steepness $s_{o,p}$ of 0.05. When analysing the 1:8 slope, the recorded results are lower. Only 82 percentage of the rocks deposit upslope for a wave steepness $s_{o,p}$ of 0.01 and this number reduces to 60 percent for a wave steepness $s_{o,p}$ of 0.05. For increasing wave steepnesses $s_{o,p}$ higher significant wave heights H_s were used in the tests. This might explain the lower percentages of eroded stones deposited upslope when wave steepness $s_{o,p}$ increases. This is also observed on beaches. In winter time, storms which high significant wave heights transport relatively more sediment downslope compared to calm summer times when the transport direction is more landward upslope (Quartel et al., 2008). The net transport rates of the coloured strips indicate that the wave steepness $s_{o,p}$ 0.01 shows more a berm profile and a wave steepness $s_{o,p}$ of 0.05 a combination of a berm profile and bar profile as illustrated in Figure 40. This is also seen the width average profile changes in Appendix F.

Figure 39 (b) shows the averaged percentages of rocks transported upslope for different Iribarren numbers ξ_p. The results of the 1:8 slope are lower compared to the 1:10 slope. The 1:8 slope is steeper compared to the 1:10 slope and the slope parallel component of the gravity force becomes more important on individual rocks. For this reason, it is plausible that the percentage of eroded rocks deposited upslope is lower for the 1:8 slope compared to the 1:10 slope.

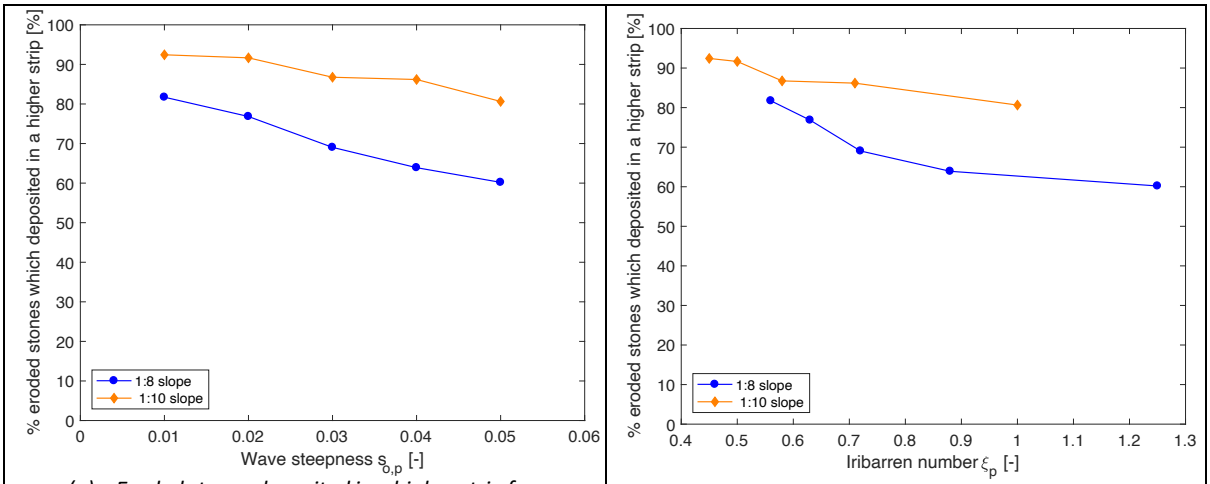

(a) Eroded stones deposited in a higher strip for every wave steepness

(b) Eroded stones deposited in a higher strip for every Iribarren number.

Figure 39: *The average percentage of eroded stone that are deposited in an higher strip to investigate the influence of wave steepness and Iribarren number for test where more than 100 transported rocks.*

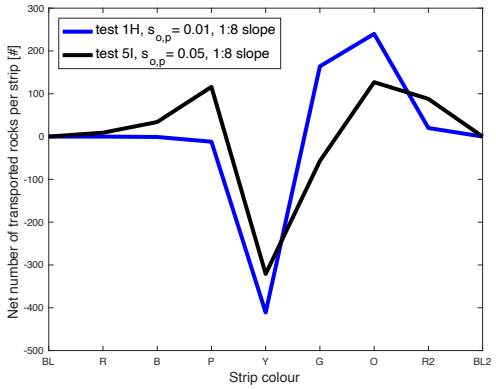

Figure 40: *Different profile development between a wave steepness $s_{o,p}$ equal to 0.01 and 0.05 for a 1:8 slope.*

4.5.4 The transport length of entrained and deposited coloured stones

Figure 41 (a) and (b) show the probability graphs of the final destination of the transported rocks for the 1:8 and 1:10 slope for a wave steepness $s_{o,p}$ of 0.03. Each strip has a strip length of 0.5 m. Based on these graphs, it can be concluded that all downward entrained rocks for the 1:8 and 1:10 slopes are deposited one strip downwards only. This is different for the upward transported rocks. Figure 41 (a) and (b) show that the majority of upward entrained rocks are deposited only one strip upslope. However, when the significant wave height H_s increases the fraction of rocks that travel two or three strips increases for all wave steepnesses $s_{o,p}$. The probability graphs for the other test series for the 1:8 and 1:10 slope are added in appendix L.

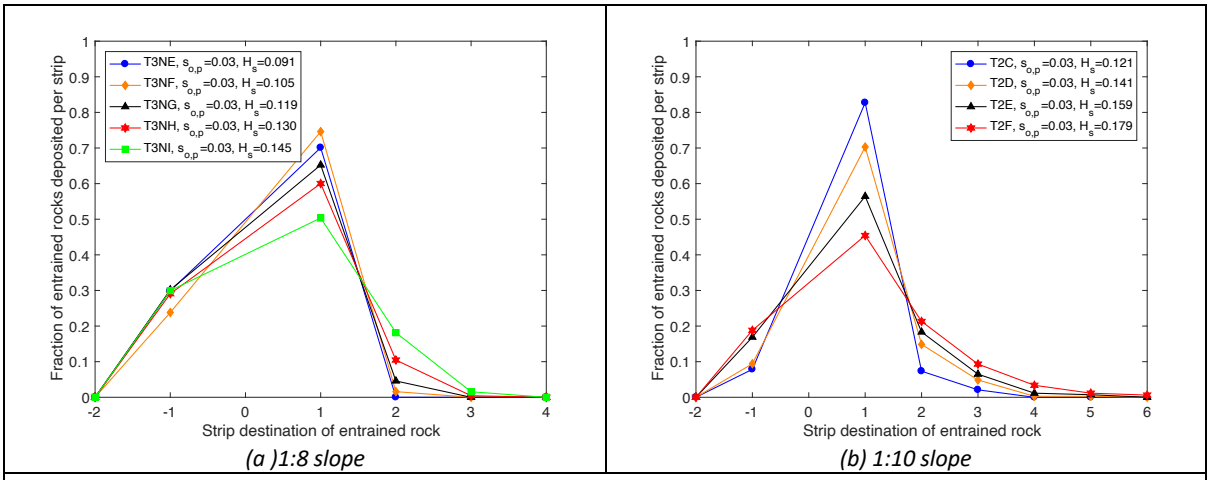

(a)1:8 slope *(b) 1:10 slope*

Figure 41: *the probability graphs of the final destination of the transported rocks for the 1:8 and 1:10 slope for a wave steepness of 0.03.*

4.6 Design formula for mild slopes

4.6.1 Damage limits

In the discussion of the results in section 4.7, the $E_{3D,3}$ damage parameter is considered to be used for the design formula for mild slopes. The damage limits available in the literature are discussed first and afterwards the damage limits are determined based on the performed physical model tests. The damage limits for the damage parameter $E_{3D,3}$ are determined by Mossinkoff (2019) for a layer thickness of 2.5 d_{n50} for a 1:10 slope. She concluded that the start of damage is around 0.5, intermediate damage is seen for values around 1.2 and failure occurs at a value of 2.3. Hofland et al. (2011) has also researched the damage limits for the $E_{3D,3}$ damage parameter for a 2 d_{n50} layer thickness on a 1:2 and 1:3 slope. He stated that start of damage occurs between 0.2 and 0.3. Intermediate damage happens for values between 0.5 and 0.6 and failure occurs between 1.5 and 1.6. Hofland et al. (2011) suggested that the failure limit of a thicker layer than 2 d_{n50} can be determined by the following relation: ((1.5-1.6) + (T-2)). The failure limit of a layer thickness of 2.5 d_{n50} would in this case be equal to a value between 2.0 and 2.1. This is lower compared to the failure damage limit observed by Mossinkoff (2019). When altering the layer thickness *T*, the beginning of damage (0.2-0.3) does not change since it is does not depend on the layer thickness *T*. Intermediate damage would occur between the beginning of damage and failure of the structure. Hofland et al. (2011) suggested that this intermediate limit should be adjusted as follows: (0.5-0.6)*(T/2). The result would be that intermediate damage would occur between 0.625 and 0.75 for a layer thickness of 2.5 d_{n50}.

In this study, the damage limits are determined for the damage parameter $E_{3D,3}$ based on top view photos and the test results of the damage parameters. This is similar to the approach of Mossinkoff (2019), but is executed with the re-analysed data for the 1:10 slope and the newly obtained data for the 1:8 slope. Initial damage occurs when the first rocks start to move randomly on the slope and this happens at a value of 0.3 for the damage parameter $E_{3D,3}$. Intermediate damage is observed when random displacements of individual rocks changes to transportations of groups of rocks that are eroded on the same position. This intermediate damage starts at a value of 0.6. Failure is observed for a value of 2.0 and this is defined as the moment where the impermeable core become visible. One remark needs to be made about damage limits. As shown in section 4.1 a restorative effect was recorded during testing. It might be that the slope made of rocks has temporary failed and healed again during testing. The result would be that the determined damage limits based on this approach does not capture this temporary failure. Temporary failure means that filter layers or the core are temporary exposed which needs to be prevented at all time. To avoid temporary failure a decrease of

the failure limit of 2.0 is proposed. Therefore, I suggest that the failure limit should be defined more conservatively to be more certain that the structure can be considered as stable. One way to do this is to restrict the damage parameter $E_{3D,3}$ to a value of 1.5. This ensures that 1 d_{n50} of the layer thickness T on the slope remains to be able to deal with the temporary failures. However, this decrease of 0.5 is still an initial number and needs further justification.

4.6.2 Design formula

Based on the analysis in this study, a design formula has been established and the formula is depicted in Eq. 4.1. The left part of the equation is equal to the stability number N_s. The right side contains the damage parameter $E_{3D,3}$, the Iribarren number ξ_p and the number of waves N. The layer thickness T has not been included into the relation since it does not seem to increase stability as described in section 4.2. Variations of the design formula are studied and are presented in Appendix K. One of the variations includes the distribution between plunging and spilling waves found in section 4.4.

$$\frac{H_s}{\Delta d_{n50}} = 7.55 * E_{3D,3}^{0.62} * \xi_p^{-1.10} * N^{-0.13} \qquad \text{Eq. 4.1}$$

This formula is verified for slopes between 1:8 and 1:10 and for a number of waves N of 15 000. The formula is validated for a layer thickness of 2.5 d_{n50} on an impermeable core and for Iribarren numbers ξ_p between 0.45 and 1.25. The design formula might also be used for a lower Iribarren number ξ_p than 0.45. This is because the number of spilling waves will increase and spilling waves have less impact compared to plunging waves. The damage limits were described in section 4.6.1 and are 0.3 for initial damage 0.6 for intermediate damage and 1.5 for failure for the damage parameter $E_{3D,3}$. This formula is based on the results for a characterization width of 27 d_{n50}. The length effect is not included is the design formula. This length effect is defined as the chance that damage exceeds a specified allowable damage level somewhere along the structure is larger when the width of the structure increases (Van Gent et al., 2019). Reference is made to Van Gent et al. (2019) to be able to deal with this length effect.

A root mean squared error (RMSE) as depicted in Eq. 4.2 is used to determine the coefficients on the right side of the Eq. 4.1. The lower the value of the RMSE, the better the curve fits. This RMSE presents the difference between the value of $E_{3D,3}$ derived from the physical model tests and $E_{3D,3}$ derived from the empirical design formula in Eq. 4.1. Minimizing the RMSE results in the coefficients presented in Eq. 4.1. When applying this formula RMSE is minimised and equal to 0.2.

$$RMSE = \sqrt{\sum_{i=1}^{n} \frac{(y_{formula} - y_{measured})^2}{n}} \qquad \text{Eq. 4.2}$$

The results of the physical model test and the design formula are depicted in Figure 42. Scatter seems to increase for larger values of the damage parameter $E_{3D,3}$. The observed scatter in general can be caused by:

- Measuring inaccuracy of the results
- The random character of turbulent flow and position of the bed (Hofland, 2005)
- The mobility of the rocks and the restoration effect observed during testing

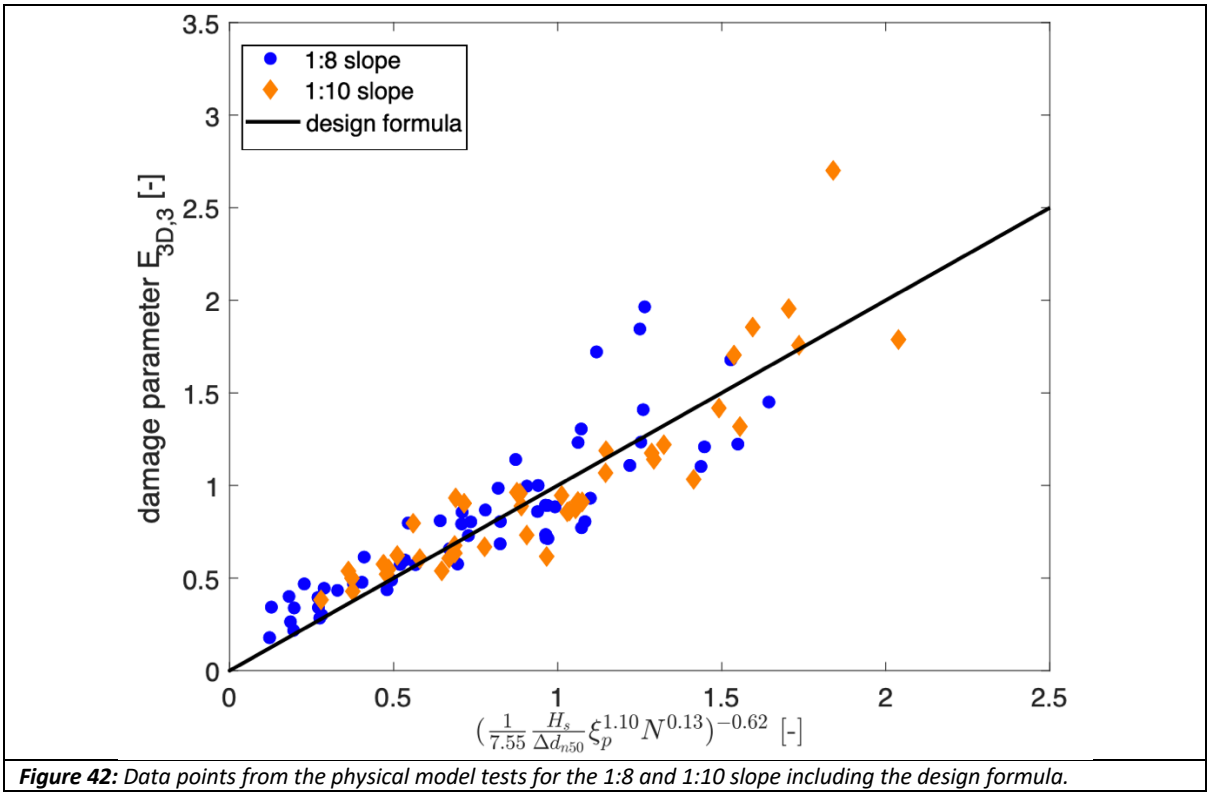

Figure 42: *Data points from the physical model tests for the 1:8 and 1:10 slope including the design formula.*

4.6.3 Comparison to an extrapolation of the Van der Meer (1988) formula

Van der Meer (1988) researched slopes until a 1:6 slope. As stated in chapter 1, an extrapolation of the Van der Meer (1988) formula for plunging waves is used for rock protection projects in the Netherlands. The design formula developed from the physical model tests for the 1:8 and 1:10 slope is compared with this extrapolation of the Van der Meer (1988) formula. Both design formulas are shown in Figure 43. Damage limits for start of damage (red), intermediate damage (blue) and failure damage (green) are illustrated in this figure for the design formula presented in this thesis. The Van der Meer (1988) formula (black) and an extrapolation of this formula (black dotted) are depicted in Figure 43 as well. According to Van der Meer (1988), the filter layer becomes visible for a damage level S value of 17 for a 1:4 and 1:6 slope. This *S* value is used in the extrapolation being the failure limit. It might be that this value of 17 is an underestimation for mild slopes than 1:6.

For failure of the structure, a value of 1.5 is allowed for the damage parameter $E_{3D,3}$ as discussed in section 4.6.1. Based on Figure 43 it can be concluded that the design formula presented in this thesis allows higher values of the stability number $N_s=H_s/(\Delta d_{n50})$ compared to the extrapolation of the Van der Meer (1988) formula. This is indicated by the green line representing the design formula from this study, which is above the dotted black line describing the extrapolated Van der Meer (1988) formula. For lower Iribarren numbers ξ_p relatively larger stability numbers N_s are allowed before failure occurs compared to the extrapolation of the Van der Meer (1988) formula. The first explanation might be the increasing share of spilling waves which have less impact on the structure compared to plunging waves. The second explanation can be the decreasing impact of the slope parallel component of the gravity force on rocks resulting in less rock movements downslope. The result is that structures allow larger stability numbers N_s before failure occurs. This thesis provides evidence and suggests that an extrapolation of the Van der Meer (1988) formula leads to conservative rock sizes. This is in line with the conclusion of Mossinkoff (2019). Comparing the stability number N_s values between the design formula in this thesis and the extrapolation of the Van der Meer (1988) formula in Figure 43, the

nominal rock diameter d_{n50} can be a few percent smaller for an Iribarren number ξ_p equal to 1.25. This percentage increases to 50 percent for a lower Iribarren number ξ_p equal to 0.45. This means that the nominal rock diameter d_{n50} can be half the size for this Iribarren number ξ_p comparing the design formula presented in this study to the extrapolation of Van der Meer (1988) formula.

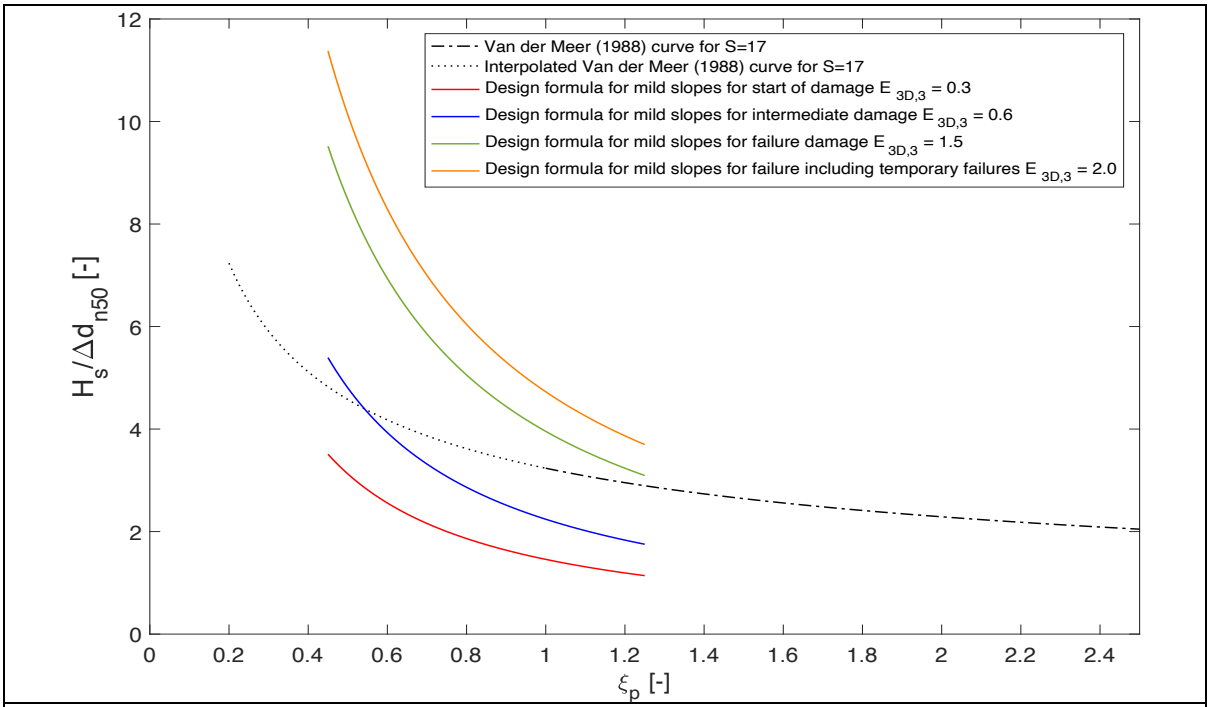

Figure 43: *The comparison of the design formula and the extrapolation of the Van der Meer (1988) formula for 1000 waves.*

4.7 Discussion of results

Damage parameters

The profile based damage parameters S, S_{all}, E_{2D}, $E_{3D,1}$, $E_{3D,3}$ and $E_{3D,5}$ and their correlations with hydraulic and structural parameters have been analysed. In this section insights are given into the suitability of the damage parameters for mild slopes. Each damage parameter is differently defined and has its own merits. The damage parameters S, S_{all} and E_{2D} are width average parameters and $E_{3D,m}$ is based on a spatial moving average which was also described in section 2.2 (De Almeida et al., 2019).

Damage parameters S and S_{all} give insights on the size of the erosion area and the number of eroded rocks. S focuses on the largest erosion area only and the S_{all} considers all the damage on the slope. As shown in Table 15, on average the parameter S does not include approximately 55 percent of the erosion areas A_e on the slope compared to damage parameter S_{all}. This demonstrates that multiple erosion areas are present on mild slopes. As discussed in section 2.2 the shape of the erosion area A_e is not taken into account for the determination of the damage parameters S and S_{all}. An erosion area A_e which is shallow and has a long erosion length can result in large values of S and S_{all} but without exposure to the filter layer or the core layer. It can also be vice versa. An erosion area A_e can be deep with a short erosion length L_e resulting in a low damage level S, but an exposed filter layer or core. This two-dimensional aspect of S and S_{all} makes these damage parameters less suitable to define failure of mild slopes. The damage parameter E_{2D} focuses on the maximum erosion depth averaged over the width of the flume as described in section 2.2. E_{2D} is not influenced by the two-dimensional aspect of the erosion area included in the S and S_{all}. For that reason, this damage parameter is more applicable to establish failure on (mild) slopes compared to the damage parameters S and S_{all}.

As described in section 4.3, most erosion and accretion occurs approximately between 1.1 H_s below SWL and 0.6 H_s above SWL for the 1:8 slope, which results in a large erosion length on mild slopes. Width averaged damage parameters have less ability to define the maximum damage on a slope. De Almeida (2017) concluded that width averaged damage parameters cannot detect hidden erosion. This means that the observed width averaged damage will decrease the magnitude of the maximum damage (De Almeida et al., 2019). For mild slopes damage is more spread over the slope due to a large erosion length. There is a possibility that the maximum erosion is hidden even more since areas of accretion and erosion are more distributed along the slope. Therefore, the 3D damage parameters are suggested to be more applicable for mild slopes.

The spatial moving averaged circle for the damage parameter $E_{3D,1}$ is rather small compared to the damage parameters $E_{3D,3}$ and $E_{3D,5}$, as described in section 2.2. For this reason, random variation that is not linked to the actual state of the bed can have a larger impact on the damage parameter $E_{3D,1}$. This can lead to relatively more bias and misleading results as shown in Table 14. Consequently, the damage parameters $E_{3D,3}$ and $E_{3D,5}$ are preferred to the damage parameter $E_{3D,1}$. Mossinkoff (2019) concludes that the damage parameter $E_{3D,1}$ is very sensitive for the removal of one individual rock. One entrained rock does not have large impact on the stability of a mild slope, but the damage parameter $E_{3D,1}$ will already increase in value. The same is concluded in this thesis. The damage parameters $E_{3D,3}$ and $E_{3D,5}$ are less sensitive for the removal of one rock. The variation for the damage parameter $E_{3D,3}$ is lower compared to $E_{3D,5}$ as shown in Table 15. For that reason, $E_{3D,3}$ is considered to be the best applicable profile based damage parameter for mild slopes and is used in the design formula of mild slopes.

Besides the profile based damage parameters also the damage parameter N_{od} is determined. This damage parameter is based on the coloured rocks in strips. As described in section 4.5.1, this damage parameter is probably underestimating the actual damage because rocks are also displaced within the coloured strips itself. This makes N_{od} less suitable to quantify failure of the bed.

Notional permeability of the structure

The notional permeability is determined using the method of Eldrup et al. (2019) for the 2.5 d_{n50} layer thickness and 5.0 d_{n50} layer. The latter has a notional permeability of 0.48 and the thinner 2.5 d_{n50} layer has a notional permeability of 0.12. More voids are present for the thicker layer and water flow can dissipate more easily into the thicker layer reducing destabilizing forces. Also during the run-down of the water within the armour layer a larger area is available reducing the forces on the outer stones of this armour layer. However, the results of the physical model tests show no evidence that an increase of the layer thickness T of the armour layer from 2.5 d_{n50} to 5.0 d_{n50} increases the stability of the structure. A plausible explanation could be that the reflection forces introduced by the impermeable core overrule the dissipating effect of doubling the layer thickness. This contradiction between the results of the physical model tests in this study and the method of Eldrup et al. (2019) should require more research.

Stability of bed for mild slopes

The approach of this thesis is orientated from a static perspective of the stability of bed by studying damage parameters and number of eroded rocks. However, the results give indications that rock on mild slope have their own damage characteristics and behaviour which deviate from statically stable structures. Dynamically stable structures are defined by deformation of a structure towards an equilibrium profile where transport of rocks is allowed (Wit, 2015). Statically stable structures are characterised by the allowance of none or limited displaced rocks of the structure (Van der Meer, 1988).

The first indication that rocks on mild slopes deviates from statically stable structures is the restorative effect observed during testing as described in section 4.1. Rocks seem to be transported into the gap of the failed bed causing a self-healing effect. Inspecting the photos in Figure 27 shows also that rocks displace over time. Currently, a conservative lower failure limit for damage is chosen such that the structure is considered to be statically stable. However, there is still a potential present to increase this failure limit which includes the temporary failures and which would result in more efficient designs. This potential is visualized in Figure 43. A failure limit equal to 2.0 allows higher values of the stability number N_s and includes the observed restorative effect and temporary failures. For example, geotextile could be used to protection the impermeable core during the temporary failures.

The second indication is recorded in the determination of the profile based damage parameters. As debated in section 4.1, relative more damage is observed close to the side walls of the flume. This effect is not representative for a real-life situation. For that reason, the outer 10 cm close to the side walls is not included when determining the damage parameters. However, some test results showed contrary outcomes for the 2D profile based damage parameters and 3D profile based damage parameter as mentioned in section 4.2.5. Some tests that were analysed included the outer 10 cm of the flume. The result is that the 2D damage parameters increased in value and this suggests that some longshore transport is present probably caused by the boundary effect. This is again an indication that the rock on mild slopes deviates statically stable structures.

The mobility parameters *MP* of rocks presented in section 4.5 describes the difference between the number of gross and net transported rocks based on displacements of coloured rocks. The median of this mobility parameter *MP* is 3.0 for the 1:8 slope and 2.9 for the 1:10 slope. This means that approximately three rocks seem moved where only one displaced rock is causing erosion. This value is based on the coloured rocks within other strips of 0.5 m. It is plausible that this number is underestimated since rocks will also move within a coloured strip itself.

Static stability is associated with a steep profile with rather large rocks. In such a design the rocks transport in downslope direction and every movement is considered as damage meaning that the entrained rocks do not remain in the area of wave attack. Dynamic stability relates to mild slopes with rather small rocks where rocks transport in both upslope and downslope direction and the structure is starting to deform towards an equilibrium profile. The physical model tests performed for this thesis seems to be somewhere between statically stable and dynamically stable structures. An equilibrium profile can never be reached within the executed physical model tests due to the limited number of rocks within the layer thickness of 2.5 d_{n50}. A beach of sand or pebbles has maybe a layer thickness of 100 to 10 000 d_{n50} where such an equilibrium can be pursued. Studying a relative thin layer thickness of 2.5 d_{n50} is therefore limited to a statically stable approach, where a limited number of displaced rocks within the structure is allowed. During the observed temporary failures and the restorative effect, the core or filter layers of a structure becomes visible which can be considered as failure of the structure. In such a situation, the core or filter layers will erode in a high pace such that it will affect the entire stability of the structure. Another approach of stability might be that a structure will fail when the filter layers or core becomes visible. From this perspective, the structure is not failing as long as the filter layer is protected. This is especially interesting for mild slopes where the nominal diameter of the rock is rather small and these rocks seem to be more mobile compared to steep slopes. It might be that the constructability of a layer thickness of 2.5 d_{n50} is impossible and that larger margins and thus thicker layers are needed. Based on all mentioned reasons, it might be more efficient to study the moment where the filter layer becomes visible instead of the static stability of rocks within the armour layer.

Feasibility and implementation in a real-life situation

In this thesis, stereophotogrammetry is used to monitor the progress of the profile-based damage parameters for different hydraulic loads. Stereophotogrammetry gives high resolutions. These higher resolutions might be hard to accomplish in a real-life situation. A recommendation is to start a pilot using stereophotogrammetry in a real-life situation. However, it will be difficult to measure profile changes because a large part of the slope will be under water. If tide is present this problem is smaller, because the construction will be party above the water level during ebb tide. Currently, monitoring of a real-life situation can be done by a (multi) beam or an excavator. Using these tools, it might be difficult to reach the same high resolutions as stereophotogrammetry, but the required accuracy in a real-life situation is lower compared to physical scale models. According to the report of Wilde et al. (2014) a precision of 6 cm can be achieved using a multi beam for material with a size between 2 and 135 mm. This precision decreases for finer materials. Using a lower resolution can lead to different values for the damage parameter $E_{3D,3}$. For that reason, a simplified grid is used to research the impact of a lower resolution of the grid on the damage parameter $E_{3D,3}$. The determination of this simplified grid and its impact on the damage parameter $E_{3D,3}$ are added to Appendix M. The result is that the damage parameter measured is on average 0.13 lower compared to a higher resolution scenario. If high resolution cannot be accomplished this effect should be taken into account.

Mild slopes are mainly present at pipeline landings on beaches and foreshore protections at sea defences, lakes and estuaries. Mild slopes have a relative long erosion length L_e compared to steep slopes. To optimize designs for mild slopes the locations where damage occurs need to be known. Section 4.3 presented the damage domain for mild slopes. If tide and flow conditions are not considered, damage is present between 2.0 H_s below SWL and 0.9 H_s above SWL. However, if the rock protection works is constructed on a sandy foreshore, extra protection is needed below and above the structure. A transition between the rock protection works and the sandy foreshore is needed such that erosion of sandy foreshore below the rock protection is prevented. Absence could otherwise lead to failure of the rock protection works used on mild slopes.

During the construction of a mild slope, it might be that a layer thickness of 2.5 d_{n50} is hard to construct due to rather small rock sizes. In such a situation the execution becomes leading instead of the design. Two options are available. An increase in the nominal diameter of the rocks or an increase of the layer thickness. Both increase the volume of used rocks. Assuming that the volume increase is equally, in general an increase in the nominal diameter of rock would incline costs relatively more. In such a situation a thicker layer is preferred. This thesis provides evidence that an increase in layer thickness does not necessarily leads to an increase in the stability of the rocks, but larger damage limits are allowed for these thicker layers.

5 Conclusion

This master thesis contributes to the understanding of the stability of rock on mild slopes. This chapter concludes and summarizes all the results gained to achieve the research objective of this thesis. This research objective was introduced in chapter 1 and states:

''Describe the stability of rock on mild slopes under wave attack for impermeable cores.''

The sub-research questions discussed in this thesis originate from the literature review and are used as an instrument to answer the main objective. Physical model tests have been executed on a 1:8 slope and the test results for the 1:10 slope executed by Mossinkoff (2019) have partly been re-analysed. During the re-analysis of the physical model tests of Mossinkoff (2019), I concluded that the outcomes contained biased results. After extensive research into what caused this problem, I found that the bias results were caused by the absence of Ground Control Points in the outer regions of the slope. It is important to use Ground Control Points over the entire part of the slope where photos are taken such that these photos are ''guided'' correctly in space to reduce bias. Therefore, this thesis contains improvements for the stereophotogrammetry procedure to provide more solid results. The sub-research questions are answered in the following paragraphs followed by concluding remarks on the research objective.

Influences of the hydraulic and structural parameters on damage
A positive correlation has been found between the significant wave height H_s and the damage parameters. This positive correlation might be explained by a positive quadratic relation between the significant wave height H_s and the wave energy. More wave energy results in higher damage. The wave steepness $s_{o,p}$ negatively influences the impact on the correlation between the significant wave height H_s and the damage parameters. A lower wave steepness $s_{o,p}$ increases the Iribarren number resulting in relatively more plunging waves. Plunging waves have more impact compared to spilling waves resulting in more damage. An increase in the slope angle α is correlated with higher values for the damage parameters for similar significant wave heights H_s. It is plausible that the slope parallel component of the gravity force on individual rocks becomes more important if the slope is steeper. An increase in the slope angle α from the 1:10 to a 1:8 slope leads also to a larger Iribarren number ξ_p which results in more plunging waves and thus causes more damage.

A linear increase is found between the number of waves *N* and the 2D damage parameters. Evidence is provided that even after 15000 waves damage still increases. A similar linear increase is found between the number of waves and the 3D damage parameters, but with an initial jump/offset. Results for the damage parameter N_{od}, based on the coloured rocks, show a non-linear increase and flattens for increasing number of waves. An explanation might be that for higher number of waves some transported stones are overlapping and will hide some displaced rocks. Based on the physical model tests, an increase in layer thickness *T* of 2.5 d_{n50} to 5.0 d_{n50} does not lead to an increase in stability of rocks. A plausible explanation could be that the reflection forces introduced by the impermeable core by far overrule the dissipating effect of doubling the layer thickness of the armour layer.

Damage parameters
For the 1:8 and 1:10 slopes, the profile based damage parameters *S*, S_{all}, E_{2D}, $E_{3D,1}$, $E_{3D,3}$ and $E_{3D,5}$ are studied and also the damage parameter N_{od} is determined. The damage parameter *S* focuses on the largest erosion area and the S_{all} considers all the erosion areas on the slope. Evidence is provided that on average the parameter S does not include approximately 55 percent of the erosion on the slope compared to damage parameter S_{all}. The latter is considered to give a better interpretation of the amount of rocks that are entrained and therefore S_{all} is preferred over *S*.

The variability of the damage parameters S and S_{all} based on the erosion areas is rather large compared to the damage parameters based on the erosion depth d_e. An erosion area which is shallow and has a long erosion length can result in large values of S and S_{all} but without exposure to the filter layer or core layer. It can also be vice versa. An erosion area A_e can be deep with a short erosion length L_e resulting in a low damage level S, but an exposed filter layer or core. This two-dimensional aspect of S and S_{all} makes these damage parameters less suitable to define failure of mild slopes. However, they do give an indication of the volume of stones eroded.

The erosion length L_e is rather large for mild slopes. Width averaged damage parameters (S, S_{all} and E_{2D}) have less ability to define the maximum damage on a slope and hidden erosion cannot be detected. Hidden erosion means that parts of accretion and erosion level each other out and the observed width averaged damage will decrease the magnitude of maximum erosion found by the 2D damage parameters. Damage is even more spread along the slope for mild slopes. There is a possibility that the maximum erosion is hidden even more since areas of accretion and erosion are more distributed along the slope (large erosion length). Therefore, the 3D damage parameters are suggested to be more applicable for mild slopes.

The spatial moving averaged circle for the damage parameter $E_{3D,1}$ is rather small compared to the damage parameters $E_{3D,3}$ and $E_{3D,5}$. For this reason, variations of the bed not linked to erosion of rocks can have larger impact on the damage parameter $E_{3D,1}$ and can lead to misleading results. $E_{3D,1}$ also indicates quite some damage if only one rock is entrained. However, one displaced rock does not necessary mean that the bed is already damaged. The variation for the $E_{3D,3}$ is lower compared to $E_{3D,5}$. For that reason, $E_{3D,3}$ is considered to be most suitable profile based damage parameter for mild slopes and is used in the further analysis of a design formula. Besides the profile based damage parameters also the damage parameter N_{od} is determined. This damage parameter is based on the coloured rocks in strips. Based on the results, this damage parameter probably underestimates damage, which makes N_{od} less suitable to quantify failure of the bed.

Distribution of plunging and spilling waves for mild slopes

The distribution between the plunging and spilling waves is determined for Iribarren numbers ξ_p between 0.56 and 1.25 on a 1:8 slope and these are compared to the results for a 1:10 slope analysed by Mossinkoff (2019). According to the results, the Iribarren number ξ_p is able to describe the distribution between plunging and spilling waves. The number of tests analysed is limited and more research should confirm these preliminary conclusions.

Direction of entrained deposited rocks and transportation length

The transportation direction of entrained and deposited rocks is determined for the 1:8 and 1:10 slope for all wave steepnesses $s_{o,p}$. For a wave steepness $s_{o,p}$ of 0.01, 92 percent of the rocks deposit upslope for the 1:10 slope This number decreases to 82 percent for a wave steepness $s_{o,p}$ of 0.05. The 1:8 slope showed lower results compared to the 1:10 slope. 82 percent of the rocks deposit upslope for a wave steepness $s_{o,p}$ of 0.01 and this reduces to 60 percent for a wave steepness $s_{o,p}$ of 0.05. The Iribarren number ξ_p does not seem to be able to describe the transport direction of entrained and deposited individual rocks on mild slopes. This might be caused by the larger slope parallel component of the gravity force for the 1:8 slope compared to the 1:10 slope. For that reason, it is considered that the Iribarren number ξ_p might not be enough to describe the direction of transported rocks which might lead a different damage development between the 1:8 and 1:10 slope. Based on the net transport rates of coloured rocks, the wave steepness $s_{o,p}$ equal to 0.01 shows a berm profile and a wave steepness $s_{o,p}$ of 0.05 is a combination of a berm profile and bar profile. Probability graphs are determined for the 1:8 and 1:10 slope. Downslope entrained rocks deposit one strip down only (strip width is 0.5 m). This is different for the upslope entrained rocks. A majority of the upward entrained

rocks are deposited only one strip upslope. However, when the significant wave height H_s increases the share of rocks that travel two or three strips increases for all wave steepnesses $s_{o,p}$.

Design formula for mild slopes
Based on this thesis, a design formula has been established for mild slopes and the formula is depicted below. The left part of the equation is equal to the stability number N_s. The right side contains the damage parameter $E_{3D,3}$, the Iribarren number ξ_p, the number of waves N.

$$\frac{H_s}{\Delta d_{n50}} = 7.55 * E_{3D,3}^{0.62} * \xi_p^{-1.10} * N^{-0.13}$$

The coefficients are determined based on the root mean squared error (RMSE) for damage parameter $E_{3D,3}$. To find the best curve fitting design formula, the RMSE is minimised. The minimal RMSE is equal to 0.20. The formula is valid for a layer thickness of 2.5 d_{n50} on an impermeable core and validated for Iribarren numbers ξ_p between 0.45 and 1.25. The design formula can probably be used for lower Iribarren number ξ_p, because the number of spilling waves will increase that leads to lower damage levels. The damage limits were described in section 4.6.1 and the values for the damage parameter $E_{3D,3}$ are 0.3 for initial damage, 0.6 for intermediate damage and 1.5 for failure of the structure. The failure limit is decreased to a more conservative value to deal with the observed temporary failures during testing. However, this decrease of 0.5 is still an initial number and needs further justification. Due to the conservative failure limit, the structure is considered to be handled as a stable structure. The results were compared with an extrapolation of Van der Meer (1988) formula. A damage level of 17, which is only verified for a 1:6 slope, was used for the Van der Meer formula (1988). This showed that failure occurs for higher values of the stability number N_s according to the design formula presented in this thesis. This means that an extrapolation of the Van der Meer (1988) formula leads to conservative rock sizes for mild slopes.

Concluding remarks on the stability of rock on mild slopes
The approach of this thesis is orientated from a static perspective of the stability of bed using profile based damage parameters and number of eroded rocks. However, the results give indications that rock on mild slope have their own damage characteristics and behaviour which deviate from statically stable structures. The first indication is the restorative effect observed during testing as rocks seem to be transported into the gap of a failed bed causing a self-healing effect. The second indication is seen when determining the profile based damage parameters. Relatively more damage is observed close to the side walls of the flume. This effect is not representative for a real-life situation. For that reason, the outer 10 cm close to the side walls is not included in the determination of the profile based damage parameter. However, some test results showed contrary results for the 2D profile based damage parameters and 3D profile based damage parameters. Some tests are analysed that include 7.5 of the 10 cm close to the side walls of the flume. The result is that the 2D damage parameters increased in value which might suggest that some longshore transport is present probably caused by the boundary effect. This is again an indication that bed is not completely statically stable. The mobility parameter is determined and is defined as the number of gross transported rocks divided by the net transported rocks. The median of this mobility parameter is 3.0 for the 1:8 slope and 2.9 for the 1:10 slope. This means that approximately three rocks seem to move where only one displaced rock is causing erosion. This value is based on the coloured rocks within strips of 0.5 m. It is plausible that this underestimates the mobility parameter *MP* since rocks will also move within a coloured strip itself. The direction of transport is mainly upslope directed for mild slopes, where for steep slopes this is mainly downward.

Static stability is associated with a steep profile with rather large rocks. In such a design the rocks transport in downslope direction and every movement is considered as damage and will not remain

within the profile. Dynamic stability relates to mild slopes with rather small rocks where rocks transport in both upslope and downslope direction and the structure is starting to deform towards an equilibrium profile. The physical model tests performed for this thesis seem to be somewhere between statically stable and dynamically stable structures. An equilibrium profile can never be reached within the executed physical model tests due to limited number of rocks within the layer thickness of 2.5 d_{n50}. A beach of sand or pebbles has a layer thickness of maybe 100 to 10 000 d_{n50} where such an equilibrium can be pursued. Studying a relative thin layer thickness of 2.5 d_{n50} is therefore limited to a statically stable approach, where a limited number of displaced rocks within the structure is allowed. During the observed temporary failures and the restorative effect, the core or filter layers of a structure becomes visible which can be considered as failure of the structure. In such a situation, the core or filter layers will erode in a high pace such that it will affect the entire stability of the structure. Another approach on stability might be that a structure will fail when the filter layers or core becomes visible. From this perspective, the structure is not failing as long as the filter layer is protected. This is especially interesting for mild slopes where the nominal diameter of the rock is rather small which seem to be more mobile compared to steep slopes. It might be that the constructability of a layer thickness of 2.5 d_{n50} is impossible and that larger margins and thus thicker layers are needed. Based on all mentioned reasons, it might be more efficient to study the moment when the filter layer or core becomes visible instead of the static stability of rocks within the armour layer itself.

6 Recommendations

The recommendations for future research are stated below:

- Rock on mild slopes seems to move relatively more compared to steeper slopes. For that reason, longshore transport caused by oblique incoming waves becomes more important. To understand the effect of oblique waves on rocks on mild slopes it would be recommended to perform physical model tests.
- Another recommendation would be to study the observed temporary failures and the self-healing effect of the bed during testing in more detail. Additional research must demonstrate whether more severe hydraulic loads are allowed. An example could be the application of geotextile, that prevent the erosion of underlayers or the core during a temporary failure.
- Limited data is available for mild slopes. Physical model tests have been performed for 1:8 and 1:10 slopes to understand the stability of rock on mild slopes. For these slopes plunging waves are still dominant compared to spilling waves. It might be interesting to research a milder slope where spilling waves start to dictate damage. On the other hand, the 1:8 slope revealed that the majority of entrained rocks is still upward directed. It would also be interesting to research whether damage on a steeper slope than 1:8 is still a combination of a bar and berm damage profile.
- Limited number of tests are analysed to determine the distribution between plunging and spilling waves. Video recordings are available for all tests and can be used to verify the preliminary conclusions found in this study.
- This study used stereophotogrammetry as a measuring method to determine profile changes and damage parameters. Van der Meer (1988) used a surface profiler to determine the profile change and calculated the damage parameter S for all his tests. This includes a 1:6 slope. Stereophotogrammetry gives opportunities to explore 3D damage parameters. It might be interesting to research for example a 1:6 slope to examine the 3D damage parameters.
- The variability of damage parameters has been investigated in this research. It might be interesting to study the variability for different stages of damage and analyse if this has an influence on the variability of the damage parameters. Variability is only researched for a wave steepness of 0.03. As indicated the transportation direction for entrained rocks vary for each wave steepness. For this reason, it might be interesting to research variability for different wave steepnesses. When more repetition tests are available an analysis of maximum damage can be performed on the 3D damage parameters to study the length effect for mild slopes. This analysis can be compared to the results of steep slopes researched by Van Gent et al. (2019).
- This study showed that an increase in layer thicknesses from 2.5 d_{n50} to 5.0 d_{n50} does not seem to influence the stability expressed by the damage parameters. Based on this observation, it might be interesting to research the effect of the core permeability for mild slopes. It might also be interesting to increase the layer thickness of the armour layer significantly to for example 10 d_{n50} or even 20 d_{n50}. As rocks for mild slopes are expected to be rather small, layer thicknesses of 2.5 d_{n50} might be hard to implement and the constructability might be low. Before studying thick armour layers of 10 d_{n50} or 20 d_{n50}, an analysis should indicate whether the constructability could indeed lead to thicker armour layers.

References

De Almeida, E. (2017). Damage assessment of coastal structures in climate change adaptation. Delft: Delft University of Technology.

De Almeida, E., Van Gent, M.R., & Hofland, B. (2019). *Damage characterization of rock slopes*. Journal of Marine Science and Engineering, 7(1), 10.

Battjes, J. A. (1974). *Surf similarity*, paper presented at 14th International Conference on Coastal Engineering. Am. Soc. of Civ. Eng., Copenhagen.
Battjes

Broderick, L.L., & Ahrens, J.P. (1982). *Riprap Stability Scale Effects* (No. CERC-TP-82-3). COASTAL ENGINEERING RESEARCH CENTER FORT BELVOIR VA.

Burcharth, H. F., Andersen, T. L. & Lara, J. L. (2014). *Upgrade of coastal defence structures against increased loadings caused by climate change: A first methodological approach*. Coastal Engineering 87, 112 - 121.

CIRIA, CUR & CETMEF (2007), The Rock Manual. *The use of rock in hydraulic engineering (2nd edition),* C883 CIRIA, London, United Kingdom.

CloudCompare Manual. (2020). *ICP.* Website: https://www.cloudcompare.org

Dai, Y. B., & Kamel, A. M. (1969). *Scale Effect Tests for Rubble-Mound Breakwaters: Hydraulic Model Investigation* (Vol. 69, No. 2). US Army Engineer Waterways Experiment Station.

Dessens, M. (2004). *The influence of flow acceleration on stone stability.* Delft: Delft University of Technology.

Eldrup, M. R., Lykke Andersen, T., & Burcharth, H. F. (2019). *Stability of rubble mound breakwaters—A study of the notional permeability factor, based on physical model tests.* Water, 11(5), 934.

Frostick, L. E., McLelland, S. J., & Mercer, T. G. (2011). *Users guide to physical modelling and experimentation: experience of the hydralab network* (Ser. Iahr design manual). CRC Press/Balkema Book.

Hofland, B. (2005). Rock and roll: Turbulence-induced damage to granular bed protections. Delft: Delft University of Technology.

Hofland, B., Van Gent, M. R. A., Raaijmakers, T., & Liefhebber, F. (2011). *Damage evaluation using the damage depth.* Coastal Structures 2011. Yokohama, Japan.

Holthuijsen, L. H. (2007). *Waves in oceanic and coastal waters*. Cambridge university press.

Huijsmans, M.A. (2006). *The influence of flow acceleration on the stability of stones.* Delft: Delft University of Technology.

Hudson, R. Y. (1952). *Wave forces on breakwaters*. In Proceedings of the American Society of Civil Engineers (Vol. 78, No. 1, pp. 1-22). ASCE.

Hughes, S. A. (1993). Physical models and laboratory techniques in coastal engineering (Vol. 7). World Scientific.

Iribarren, R. (1938). Una fórmula para el cálculo de los diques de escollera. Pasajes.

Izbash, S. V. (1935). Construction of dams by dumping stone in running water. Moscow, Leningrad.

Juul Jensen, O. and P. Klinting. 1983. "Evaluation of Scale Effects in Hydraulic Models by Analysis of Laminar and Turbulent Flows." *Coastal Engineering* 7(4):319–29.

Kramer, R. (2016). *The stability of rock on mild slops under wave attack.* Delft: Delft University of Technology.

Mossinkoff, L. (2019). *The stability of stones on mild slopes under wave attack.* Delft: Delft University of Technology.

Nielsen, P. (2006). *Sheet flow sediment transport under waves with acceleration skewness and boundary layer streaming*. Coastal Engineering, 53(9), 749-758.

Postma, M. G. (2016). *XBeach-G as a Design Tool for Rock on mild slopes under wave loading*. Delft: Delft University of Technology.

Quartel, S., Kroon, A., & Ruessink, B. G. (2008). *Seasonal accretion and erosion patterns of a microtidal sandy beach.* Marine Geology, *250*(1-2), 19-33.

Rees, W. G. (2013). *Physical principles of remote sensing*. Cambridge University Press.

Schiereck, G. J., Fontijn, H. L., Grote, W. V., & Sistermans, P. G. (1995). *Stability of rock on beaches.* In Coastal Engineering 1994 (pp. 1553-1567).

Schiereck, G. J., & Fontijn, H. L. (1996). *Pipeline protection in the surf zone*, 25th ICCE. Orlando, ASCE, New York.

Schiereck, G.J. and Verhagen, H.J. (2016). *Introduction to bed, bank and shore protection*. Delft Academic Press / VSSD

Sistermans, P.G.J. (1993). *Stability of Rock on Beaches.* Delft: TU Delft, Faculty of Civil Engineering and Geosciences, Hydraulic Engineering.

Sleath, J. F. (1978). Measurements of bed load in oscillatory flow. *Journal of the Waterway, Port, Coastal and Ocean Division*, *104*(3), 291-307.

Thompson, D. M., & Shuttler, R. M. (1975). *Riprap design for wind-wave attack, a laboratory study in random waves.* Wallingford report EX707 for CIRIA.

Tromp, M. (2004). Influences of fluid accelerations on the threshold of motion. Delft: Delft University of Technology.

Van der Meer, J.W. (1988). *Rock slopes and gravel beaches under wave attack.* (Vol. 396): Delft hydraulics.

Van Gent, M. R. A., Smale, A. J. & Kuiper, C. (2003). *Stability of rock slopes with shallow foreshores*. J. Melby, ed., Proc. 4th International Coastal Structures Conference Portland 2003, ASCE, Reston, VA, United States.

Van Gent, M. R., de Almeida, E., & Hofland, B. (2019). *Statistical Analysis of the Stability of Rock Slopes.* Journal of Marine Science and Engineering, 7(3), 60.

Van Rijn, L. C. (1984). Sediment transport, part II: suspended load transport. *Journal of hydraulic engineering*, *110*(11), 1613-1641

Van Rijn, L. C. (2007). Unified view of sediment transport by currents and waves. I: Initiation of motion, bed roughness, and bed-load transport. Journal of hydraulic engineering, 133(6), 649- 667.

Wit, E. M. (2015). *Stability of Gravel on Mild Slopes in Breaking Waves.* Delft: Delft University of Technology.

Wendt, E.A.F. (2017). *Stability of rock on mild slopes.* Delft: Delft University of Technology.

Wilde, D., Smith, G. & Roels, R., Lekkerkerk, H., Kant, G. & Blokland, T. & Visser, R. (2014). *Construction and Survey Accuracies for the execution of rockworks Best practices from the "Maasvlakte 2" Port Expansion Project.*

Ye, L. (1996). *Stability of Rock on Beaches.* Delft: TU Delft, Faculty of Civil Engineering and Geosciences, Hydraulic Engineering.

List of Figures

Figure 1: *The different types of wave breaking based on the Iribarren number on smooth slopes and regular waves (Battjes, 1974) & (CIRIA et al., 2007).* 6
Figure 2: *The different types of energy dissipation for spilling and plunging breakers and the plunging jet (Schriereck and Fontijn 1995 & 1996).* 7
Figure 3: *The notional permeability coefficient of various structures (Eldrup et al., 2019).* 8
Figure 4: *(a) A schematization to define the 2D damage parameter S and E_{2D}. (b) A schematization to define the 3D damage parameter $E_{3D,m}$.* 10
Figure 5: *Schematization of the average cross-section profiles found by Kramer (2016) the (a)1:5 slope and (b) 1:10 slope.* 12
Figure 6: *The stability of a homogeneous, permeable and impermeable structure researched by Van der Meer (1988) for a 1:2 slope and damage level S of 3.* 14
Figure 7: *(a)The influence of the number of waves N on the damage level S (Van der Meer, 1988). (b) The influence of the slope angle on the stability parameter $Hs/\Delta d_{n50}$ for slope angles between 1:2 and 1:6 for a damage level S of 3 (Van der Meer, 1988)* 15
Figure 8: *Results of Ye (1996) depicted in a (ξ, $H_s/\Delta d_{n50}$) diagram (Schiereck & Fontijn, 1996).* 16
Figure 9: *The influence of slope angle on the relation between the significant wave height Hs and the damage parameter $E_{3D,3}$ (Kramer, 2016). Estimates of for tolerable damage are used to determine the conditions for the tests. S_{VDM} is based on the work of Wit (2015) using an extrapolation of van der Meer (1998) compensation mild slopes. S_{norm} is based on van der Meer(1988) and S_{sf} is based on a extrapolation of Van der Meer (1998).* 18
Figure 10: *The effect of the wave steepness s_0p on the relationship between the significant wave height H_s and the damage parameter $E_{3D,3}$ (Mossinkoff, 2019).* 18
Figure 11: *(a) The influence of the number of waves N on the damage depth, E3D,3 for a slope of 1:10 of the structure with a layer thickness of 2.5 dn50 (Mossinkoff, 2019). (b) The influence of the wave steepness, the layer thickness and wave height on the damage depth (Mossinkoff, 2019).* 19
Figure 12: *The Van der Meer (1988) formula and the proposed design formula of Mossinkoff (2019) for 1000 waves and a layer thickness of 2.5 dn50 (Mossinkoff,2019).* 20
Figure 13: *The Pacific basin facility at Deltares during a test. The flume with the mild slope can be seen in the middle.* 21
Figure 14: *Sketch of test set-up of the flume for the 1:8 slope in the Pacific Basin.* 22
Figure 15: *Average profile plots from an undamaged profile where two tests contained the extra outer GCPs and one test were without the extra outer GCPs.* 25
Figure 16: *Sketch of the camera positions and the locations of the Ground Control Points including an example of a photo for the 1:8 slope tests.* 26
Figure 17: *Sketch of the test set-up of the flume for the 1:10 slope in the Pacific Basin (Mossinkoff, 2019)* 28
Figure 18: *Sketch of the camera positions and the locations of the Ground Control Points including an example of a photo for the 1:10 slope tests performed by Mossinkoff (2019).* 29
Figure 19: *Impressions of the resulting Point cloud containing approximately* 31
Figure 20: *Comparing two point clouds of the same profile before and after using the ICP tool.* 32
Figure 21: *Process of obtaining the 2D damage parameters* 34
Figure 22: *Process of obtaining the 3D damage parameters.* 36
Figure 23: *A top view of the profile change of the slope after test to determine the locations: Low, Mid-Low, Mid-High and High of the damage domain.* 37
Figure 24: *Determination of the distribution between plunging and spilling waves using the camera with the front view on the flume. The photos have irregular time steps and demonstrate the important steps during wave breaking.* 39
Figure 25: *Determination of erosion and mobility of coloured rocks.* 41
Figure 26: *The boundary effect visible close to the side walls. Example is test 1H of the 1:8 slope.* ... 42

Figure 27: *Restorative effect captured during test 4G for the 1:8 slope.* 43
Figure 28: *The damage parameters S, S_{all}, E_{2D}, $E_{3D,1}$, $E_{3D,3}$ and $E_{3D,5}$ related to the significant wave height H_s to investigate the influence of the significant wave height H_s, wave steepness $s_{o,p}$ and slope angle on damage for mild slopes after 1000 waves.* 45
Figure 29: *The damage parameters S, S_{all}, E_{2D}, $E_{3D,1}$, $E_{3D,3}$ and $E_{3D,5}$ related to the significant wave height H_s to investigate the influence of layer thickness on damage for mild slopes after 1000 waves.* 47
Figure 30: *Illustration of the size of the boundary effect for test 6.E compared to test 6.F which can cause the outlier for test 6.E.* 48
Figure 31: *The damage parameters S, S_{all}, E_{2D}, $E_{3D,1}$, $E_{3D,3}$ and $E_{3D,5}$ related to the significant wave height H_s to investigate the influence of number of waves on damage for mild slopes.* 49
Figure 32: *The observation that 2D damage parameters stagnated and 3D damage parameter still increased for tests series 2 of the 1:8 slope which are indicated by blue large circles.* 51
Figure 33: *(a) and (b) boxplot of the locations Low, Mid-Low, Mid-High and High for the 1:8 and 1:10 slope. (c) and (d) boxplots of the location of the maximum damage based on the 2D and 3D damage parameters expressed in significant wave height H_s compared to SWL. The crosses are outliers.* 53
Figure 34: *Schematisation where rocks are entrained and where most and max erosion occurs on the 1:8 and 1:10 slope.* 53
Figure 35: *The distribution between spilling and plunging waves for the 1:8 and 1:10 slope.* 54
Figure 36: *The number of net eroded rocks to investigate the influence of wave height, wave steepness, slope angle, layer thickness and number of waves.* 56
Figure 37: *The boxplots for the ratio's between the profile based damage parameter S_{oll} and the damage parameter S_{od}* 57
Figure 38: *The boxplots for the mobility parameters MP for the 1:8 and 1:10 slope.* 58
Figure 39: *The average percentage of eroded stone that are deposited in an higher strip to investigate the influence of wave steepness and Iribarren number for test where more than 100 transported rocks.* 59
Figure 40: *Different profile development between a wave steepness $s_{o,p}$ equal to 0.01 and 0.05 for a 1:8 slope.* 59
Figure 41: *the probability graphs of the final destination of the transported rocks for the 1:8 and 1:10 slope for a wave steepness of 0.03.* 60
Figure 42: *Data points from the physical model tests for the 1:8 and 1:10 slope including the design formula.* 62
Figure 43: *The comparison of the design formula and the extrapolation of the Van der Meer (1988) formula for 1000 waves.* 63
Figure 44: *Schematization of the gravity, friction, drag, lift and shear forces on a single stone (Huijsmans, 2006).* 81
Figure 45: *Schematization of the gravity, friction, drag, lift and shear forces on a single stone (Tromp, 2004).* 82
Figure 46: *The Shields diagram (Schiereck & Verhagen, 2016).* 83
Figure 47: *The adjusted Shields diagram for the research of Sleath (1978) (Schiereck & Verhagen, 2016).* 83
Figure 48: *The upward transported rocks per strip and deposited in another specific strip for 1:8 slope.* 149
Figure 49: *The downward transported rocks per strip and deposited in another specific strip for 1:8 slope.* 150
Figure 50: *The upward and downward transported rocks per strip and deposited in another specific strip for 1:8 slope.* 151
Figure 51: *Probability graphs of transported rocks for all wave steepnesses for the 1:8 slope.* 155
Figure 52: *Probability graphs of transported rocks for all wave steepnesses for the 1:10 slope.* 156

List of Tables

Table 1: *The hydraulic and structural parameters in this research.* 5
Table 2: *The distribution of plunging and spilling waves for different Iribarren numbers ξ_p under a constant slope of 1:10 (Mossinkoff, 2019).* 7
Table 3: *The initial damage, intermediate damage and failure damage limits for the damage level S, damage depth E_{2D} and $E_{3D,m}$ in different researches.* 10
Table 4: *Physical model tests performed by van der Meer (1988), PM is Pierson-Moskowitz spectrum.* 13
Table 5: *Physical scale tests performed by Ye (1996).* 15
Table 6: *Physical model tests performed by Kramer (2016).* 17
Table 7: *Physical model tests performed by Mossinkoff (2019).* 17
Table 8: *Main characteristics of the physical model tests for a 1:8 slope deduced from Mossinkoff (2019) to create similar circumstances to be able to make a comparison between the 1:8 and 1:10 slope.* 22
Table 9: *The XYZ coordinates of Ground Control Points for the two-layer thickness tested (2.5 d_{n50} and 5.0 d_{n50}) for the 1:8 slope.* 25
Table 10: *The executed test plan for the 1:8 slope.* 27
Table 11: *Main characteristics of the physical model tests for a 1:10 slope performed by Mossinkoff (2019).* 28
Table 12: *The XYZ coordinates of Ground Control Points for the two-layer thickness tested (2.5 d_{n50} and 5.0 d_{n50}) for the 1:10 slope performed by Mossinkoff (2019).* 29
Table 13: *The executed test plan for the 1:10 slope performed by Mossinkoff (2019)* 30
Table 14*: The effect of measuring accuracy on the damage parameters.* 35
Table 15: *The mean, standard deviation and lower and upper boundary of a 90 percent confidence interval of test series 9 (non-cumulative damage). Results of Section 1 and 2 of Test 3N.G (cumulative damage) are also depicted to compare cumulative and non-cumulative damage results.* 50
Table 16: *The determination of the 2D damage parameters S_{all}, S and E_{2D} for a width of 80 cm and 95 cm of the flume.* 51
Table 17: *The determined distribution between spilling and plunging waves for each wave steepness.* 54
Table 18: *The relationship between several hydraulic and structural parameters and the damage parameter N_{od}.* 55
Table 19: *The mean, standard deviation and lower and upper boundary of a 90 percent confidence interval of test series 9 (non-cumulative damage). Results of Test 3N.G (cumulative damage) are also depicted to compare cumulative and non-cumulative damage results.* 56
Table 20: *The extended version of test plan for the 1:8 slope.* 98
Table 21: *The most important settings in Metashape Agisoft.* 100
Table 22: *The most important settings for IPC tool in CloudCompare.* 100
Table 23: *The damage parameters for all test series for the 1:8 slope for a characterization width of 54 d_{n50}.* 142
Table 24: *The damage parameters for all test series for the 1:10 slope for a characterization width of 54 d_{n50}.* 143
Table 25: *The damage parameters for all test series for the 1:8 slope for a characterization width of 27 d_{n50}.* 144
Table 26: *The damage parameters for all test series for the 1:10 slope for a characterization width of 27 d_{n50}.* 145
Table 27: *The damage domain for the 1:8 for the locations Low, Mid-Low, Mid-High and High and the maximum damage location for the 2D and 3D damage parameters expressed in significant wave height H_s in vertical direction compared to SWL.* 146

Table 28: *the damage domain for the 1:10 for the locations Low, Mid-Low, Mid-High and High and the maximum damage location for the 2D and 3D damage parameters expressed in significant wave height H_s in vertical direction compared to SWL* 147
Table 29: *Overview of entrained, deposited and totally transported rocks per strip for 1:8 slope. Bl =Black strip 1 (<-2.5m), R =Red strip 1 (-2.5 - -2.0m) B =Blue strip (-2.0 - -1.5m), P =Purple strip (-1.5 – 1.0 -m), Y =Yellow strip (-1.0 - -0.5m) , G =Green strip (-0.5 – 0.0m), O =Orange strip (0.0 - 0.5m), R2 =Red strip 2 (0.5 - 1.0m), Bl2 =Black strip 2 (> 1.0m)*..... 148
Table 30: Overview of entrained, deposited and totally transported rocks per strip for 1:10 slope. Bl =Black strip 1 (<-2.5m), R =Red strip 1 (-2.5 - -2.0m) B =Blue strip (-2.0 - -1.5m), P =Purple strip (-1.5 – 1.0 -m), Y =Yellow strip (-1.0 - -0.5m) , G =Green strip (-0.5 – 0.0m), O =Orange strip (0.0 - 0.5m), R2 =Red strip 2 (0.5 - 1.0m), Bl2 =Black strip 2 (> 1.0m) 151
Table 31: *The results for the parameters n_{gross}, n_{net}, N_{od}, S_{od}, and the mobility parameter based on the entrained coloured rocks for the 1:10 slope.* 152
Table 32: *The results for the parameters n_{gross}, n_{net}, N_{od}, S_{od}, and the mobility parameter based on the entrained coloured rocks for the 1:10 slope.* 153
Table 33: *The results for a simplified grid to determine the damage parameters* 157

List of Symbols

Symbol	Unit	Description	Symbol	Unit	Description
A_e	m^2	Erosion area	H_s	m	Significant wave height
α	°	Slope angle	H_{sc}	m	Critical significant wave height
a ($\delta u/\delta t$)	m/s^2	Acceleration	H_{max}	m	Maximum wave height
A	m^2	Area of coloured strip	$H_{1/3}$	m	Significant wave height based on the highest one third waves
$C_{friction}$	-	Friction coefficient	$H_{1\%}$	m	Wave height exceeding 1%
C_{bulk}	-	Bulk coefficient	$H_{0,1\%}$	m	Wave height exceeding 0.1%
d_{50}	m	Mean diameter of grain	K_d	-	Dustbin factor
d_{n50}	m	Mean nominal diameter of rocks	L_e	m	Erosion length
d_{85}/d_{15}	-	Description for grading of rocks (=$(M_{85}/M_{15})^{1/3}$)	L	m	Wave length
d_e	m	Erosion depth	L_0	m	Wave length at deep water
Δ	-	Relative density	m	-	Diameter of spatial moving average
E_{2D}	-	Damage parameter	M	-	metres
$E_{3D,m}$	-	Damage parameter	M	Kg	Mass of stone
E_{wave}	J/m_2	Wave energy	M_{50}	Kg	Weight of grains where 50% of the sample is lighter
ξ	-	Iribarren number	M_{15}	Kg	Weight of grains where 15% of the sample is lighter
ξ_p	-	Iribarren number based on peak period	M_{85}	Kg	Weight of grains where 85% of the sample is lighter
ξ_m	-	Iribarren number based on mean period	MP	-	Mobility Parameter
f_p	1/s	Peak frequency	N	#	Number of waves
$F_{passive,gravity}$	N	Gravity force on stone	N_Δ	-	Erosion number used by Thompson and Shuttler (1975)
$F_{passive,friction}$	N	Friction force on stone	N_{od}	-	Damage parameter
$F_{active,bulk}$	N	Bulk force on stone	n_{strip}	#	Number of displaced stones in certain strip
g	m/s^2	Gravitational acceleration	n_{total}		Total number of displaced stones
h	m	Water depth	N_s	-	Stability number
H	m	Wave height	n_{net}	#	Net number of transported rocks

Symbol	Unit	Description
n_{gross}	#	Gross number of transported rocks
P	-	Notional Permeability coefficient
ψ_c	-	Shields stability parameter
ϕ	-	Angle of repose
Re		Reynolds number
ρ_s	Kg/m^3	Density of rock
ρ_w	Kg/m^3	Density of water
$s_{o,p}$	-	Wave steepness
S	-	Damage parameter
S_{all}	-	Damage parameter
S_{od}	-	Damage parameter
T	s	Wave period
T	m	Layer thickness
T_s	s	Significant wave period
T_p	s	Peak wave period
$T_{m-1,0}$	s	Spectral wave period
u_c	m/s	Critical velocity
u_{*c}	m/s	Critical bed shear stress
ν	m^2/s	Kinematic viscosity
V	m^3	Volume
w	m	Characterization width
W_{strip}	m	The width of the coloured strips in the physical model tests

Appendix A: Additional literature review

This Appendix presents the forces acting on an individual rock and initiation of motion. The second part of Appendix A is about the stability of rock on a horizontal bed.

Initiation of motion

Many different forces act on an individual rock. The passive forces ensure that the rock is kept in the same position. The active forces make it possible that the rock will start moving. The initial movement takes place when the momentum of the active forces is larger than the momentum of the passive forces around point A, as shown in Figure 44. The passive forces are the gravity force and the friction force. The gravity force and friction force are based on the density difference between the rock and water, $(\rho_s - \rho_w)$, the gravitational acceleration g and the volume of the rock V. The gravity force and the friction have a different vector direction. The friction force is represented by the friction coefficient $C_{friction}$ times the gravity force and is caused by the contact points between the individual rock and other particles. The gravity force and the friction force formulas are depicted in Eq. A.1 and A.2.

$$F_{passive,gravity} = ma = (\rho_s - \rho_w)gV \quad \text{Eq. A.1}$$

$$F_{passive,friction} = C_{friction}(\rho_s - \rho_w)gV = C_{friction}F_{passive,gravity} \quad \text{Eq. A.2}$$

The active forces are the drag force F_D, shear force F_S, lift force F_L and wave acceleration force F_{acc}. The active drag force F_D is caused by protrusion of stones into the flow causing pressure friction (Dessens, 2004). The lift force F_L is caused by the curvatures of the flow around the rock resulting in contracting flow lines (Dessens, 2004). The contraction causes flow increase and pressure differences which results in an upward force perpendicular to the flow direction (Dessens, 2004). The shear force F_s is caused by the interaction between the flow and the surface of the rock causing skin friction. These forces can be represented by the same equation and are all related to the density of the water ρ_w, the surface of the stone A_b that is exposed to the flow and the flow velocity near the bed u_b. Each active force has its own coefficient, but are gathered into one bulk coefficient C_{bulk} as shown in Eq. A.3. The stone will start to move when the momentum around point A caused by the active forces is larger than the momentum of the passive forces for a uniform flow situation.

$$F_{active,bulk} = \frac{1}{2}C_{bulk}\rho_w A_b u_b|u_b| \quad \text{Eq. A.3}$$

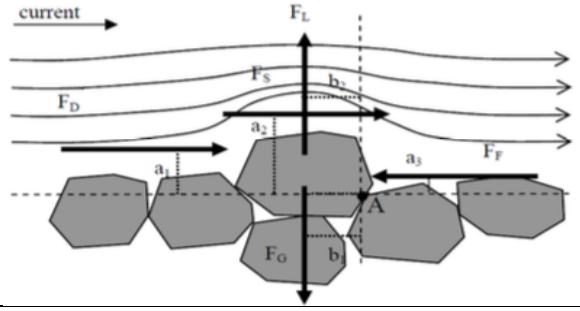

Figure 44: *Schematization of the gravity, friction, drag, lift and shear forces on a single stone (Huijsmans, 2006).*

All the forces which are discussed so far are valid for stationary flow. In this thesis however the stability of rocks is analysed under wave attack. Tromp (2004) and Dessens (2004) have studied the forces in a non-uniform flow. A wave causes flow differences and consequently pressures differences on a stone.

A formula is derived by Tromp (2004) for these effects and depends on the water density ρ_w, the horizontal acceleration $\frac{\delta u}{\delta t}$, the volume of the stone V, and a coefficient C_m.

$$F_{active,acc} = C_m \rho_w \frac{\delta u}{\delta t} V = C_m \rho_w a V \qquad \text{Eq. A.4}$$

Tromp (2004) has concluded that $F_{active,bulk}$ and $F_{active,acc}$ in Eq. A.4 and Eq. A.5 can be combined and the result is presented in Eq. A.6.

$$F_{active,combined} = \frac{1}{2} C_{bulk} \rho_w A_b u_b |u_b| + C_m \rho_w a V \qquad \text{Eq. A.5}$$

All the forces for a non-uniform flow are depicted in Figure 45. Stones move most easily under an angle between 30 and 45 degrees (Tromp, 2004). The active bulk force, the acceleration force and the gravity force are depicted and the momentum is determined around pivot A. The rock will start to move if the momentum caused by the bulk force and acceleration force are larger than the momentum caused by gravity force and this relation is depicted on Eq. A.6.

$$F_{active,Bulk} \cos(\varphi - \beta) + F_{active,acc} \cos\varphi > F_{passive,Gravity} \sin\varphi \qquad \text{Eq. A.6}$$

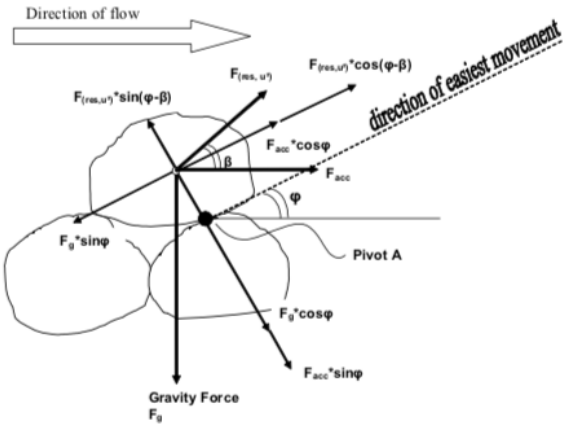

Figure 45: *Schematization of the gravity, friction, drag, lift and shear forces on a single stone (Tromp, 2004).*

Stability of rock on a horizontal bed

Izbash (1935)

Izbash (1935) studies the forces on an individual grain and the momentum of the passive and active forces. If the momentum of the active forces is larger compared to the momentum of the passive forces, the grain will start to move. The critical velocity u_c in the formula of Izbash (1935) shown in Eq. A.7 is causing the force needed for initial movement. The position where this critical velocity u_c is measured in the water column is however not defined. The exact definition of the diameter of the particles is also not known. Izbash (1935) has performed tests with rather large stones in shallow water and it is assumed that the nominal diameter d_n is used. The formula is suitable for non-uniform flow cases or in situations where the velocity does not depend on an equilibrium between the bed friction force and the flow force (Schiereck & Verhagen, 2016).

$$u_c = 1.2\sqrt{2\Delta g d} \quad or \quad \frac{u_c}{\sqrt{\Delta g d}} = 1.7 \quad or \quad \Delta d = \frac{{u_c}^2}{2g} \qquad \text{Eq. A.7}$$

Shields (1936)

Shields (1936) has studied the friction force caused by water flow on the bed. When this friction force is above a critical value the particles start to move and erosion occurs. The critical Shields parameter defines the critical value of this shear force (Schiereck & Verhagen, 2016). The particle Reynolds-number gives insight whether the grain protrudes into the turbulent boundary layer or is within the viscous sublayer (Schiereck & Verhagen, 2016). The Shields parameter gives a relation between the dimensionless shear stress and the particle Reynolds-number and is depicted in Eq. A.8.

$$\psi_c = \frac{\tau_c}{(\rho_s - \rho_w)gd} = \frac{u_{*c}^2}{\Delta g d} = f(Re_*) = f(\frac{u_{*c}\, d}{v}) \qquad \text{Eq. A.8}$$

$$where: u_{*c} = \sqrt{\frac{\tau_c}{\rho_w}} \qquad \text{Eq. A.9}$$

ψ_c is the Shields stability parameter, τ_c is the critical bed shear stress, u_{*c} is the critical bed shear velocity and v is the kinematic viscosity of water. The critical Shields stability parameter ψ_c is not constant for all particle Reynolds-numbers as shown in Figure 46. For higher particle Reynolds-numbers the critical shields parameter ψ_c becomes constant.

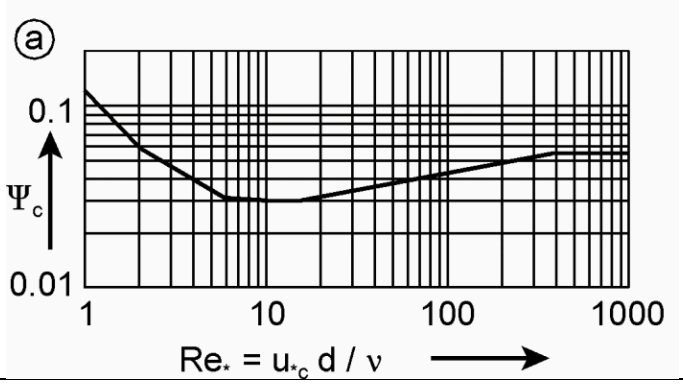

Figure 46: *The Shields diagram (Schiereck & Verhagen, 2016).*

Sleath (1978)

Sleath (1978) researches the stability of grains in oscillating flows caused by non-breaking waves. A bed shear stress for waves $\hat{\tau}_{c,w}$ is used based on Jonsson (1966). The results of Sleath (1978) are depicted in Figure 47. Sleath (1978) uses a dimensionless grain diameter which is also done by van Rijn (1984). For larger dimensionless diameters Sleath (1978) found a similar value for the critical Shields parameter.

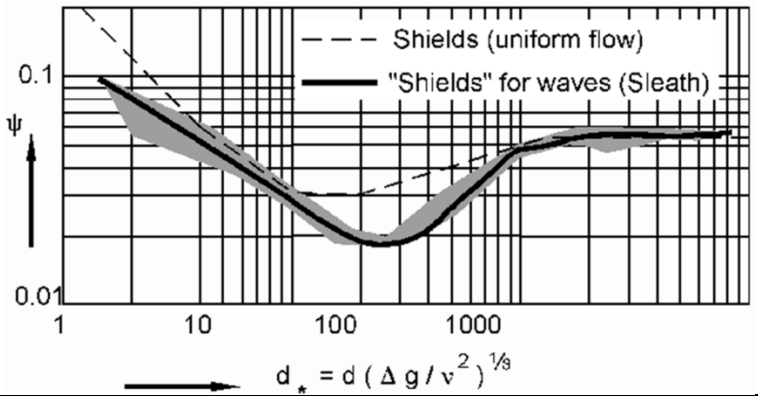

Figure 47: *The adjusted Shields diagram for the research of Sleath (1978) (Schiereck & Verhagen, 2016).*

Appendix B: Impressions of test set-up 1:8 slope


Eastern
Scheldt
Flume

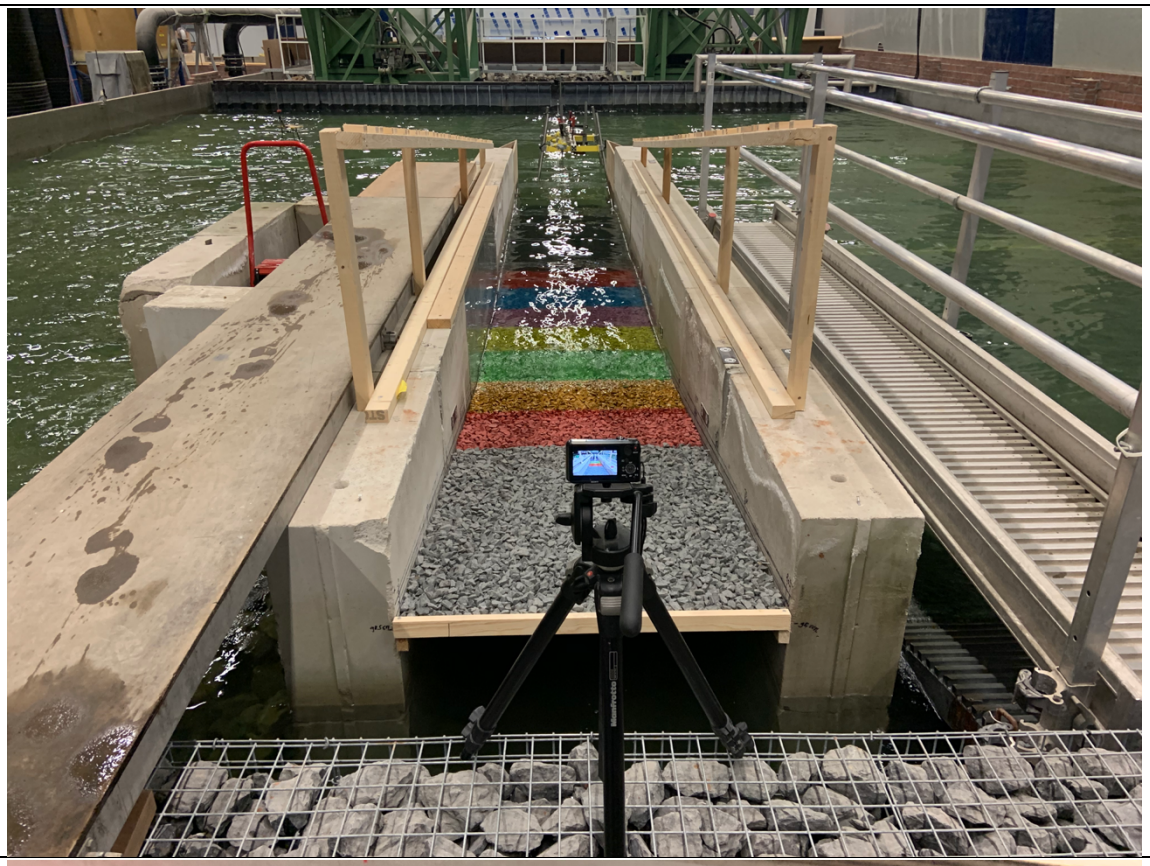

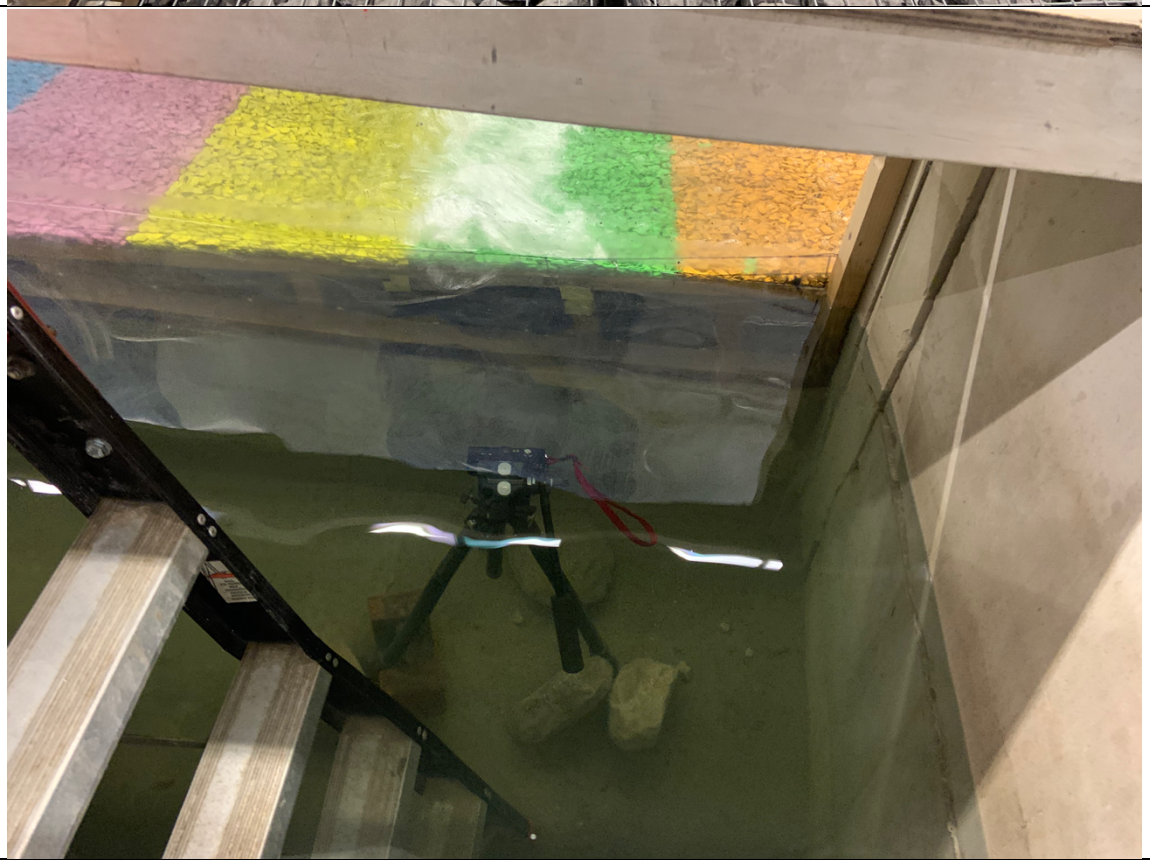

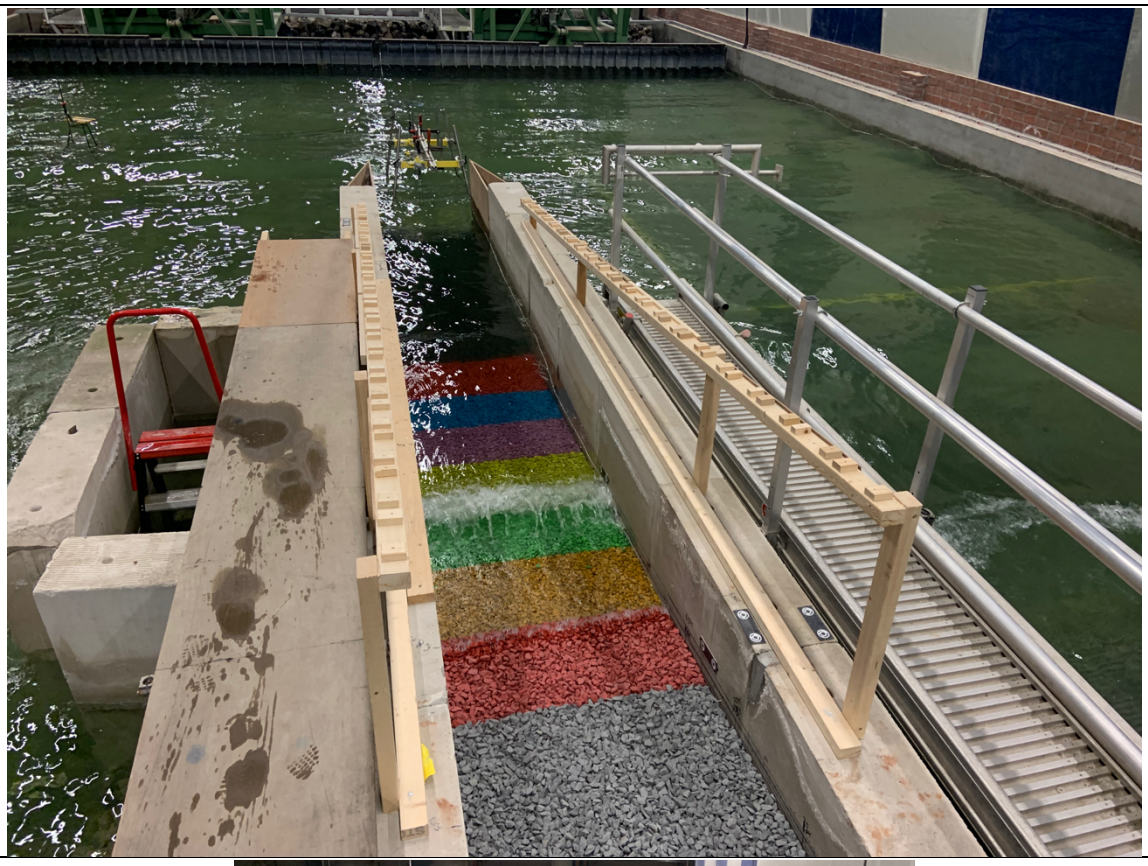

Appendix C: Distribution of significant wave heights during the tests

There are some graphs missing, since these plots can only be generated at Deltares. WHM1 is the first wave gauge (closest to the wave generators), WHM2 is the second wave gauge and WHM3 is the third wave gauge (closest to the structure).

1:8 slope:

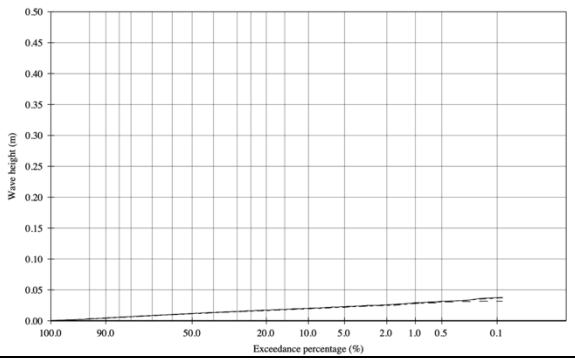

Test 1A

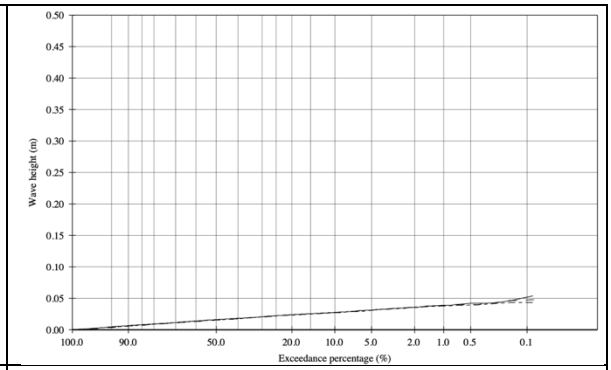

Test 1B

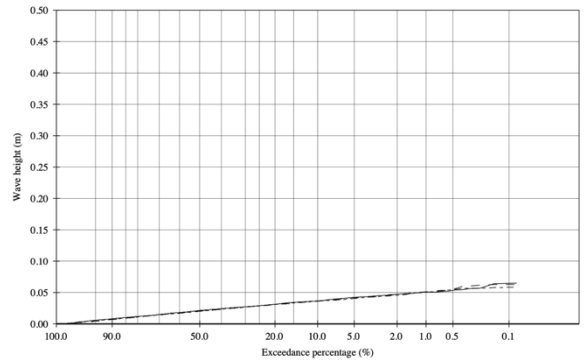

Test 1C

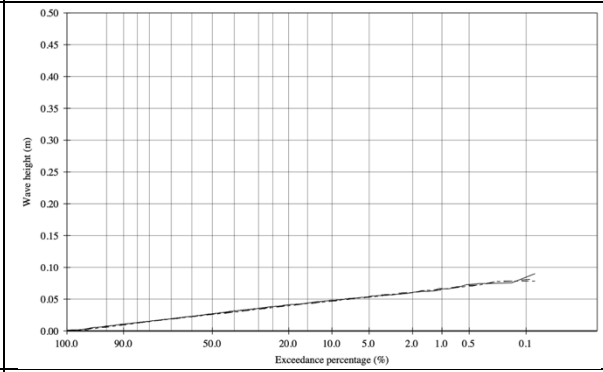

Test 1D

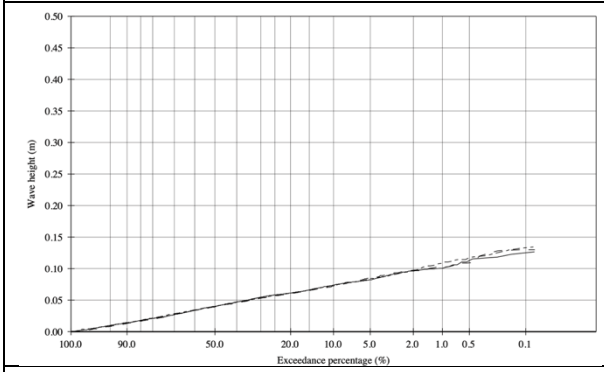

Test 1F

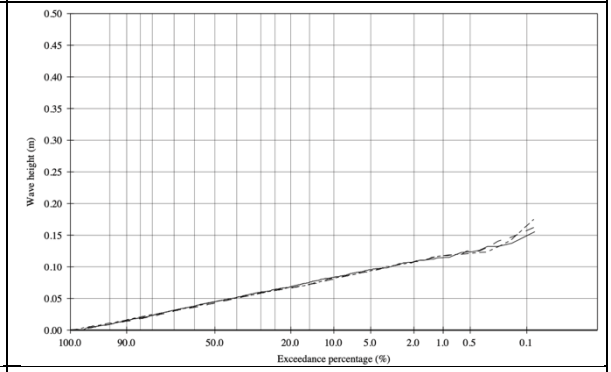

Test 1G

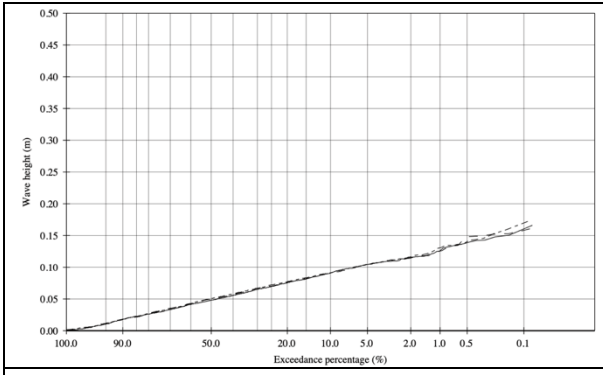

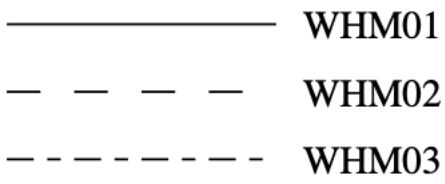

Test 1H

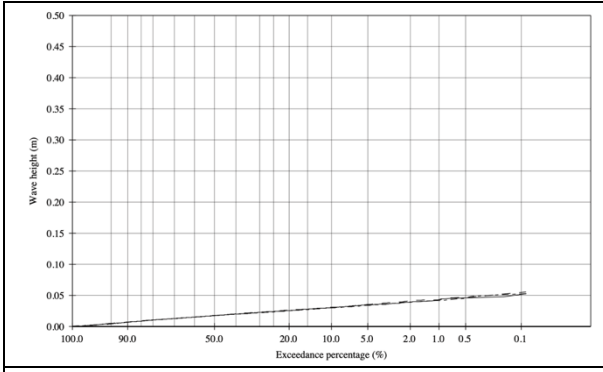

Test 2A

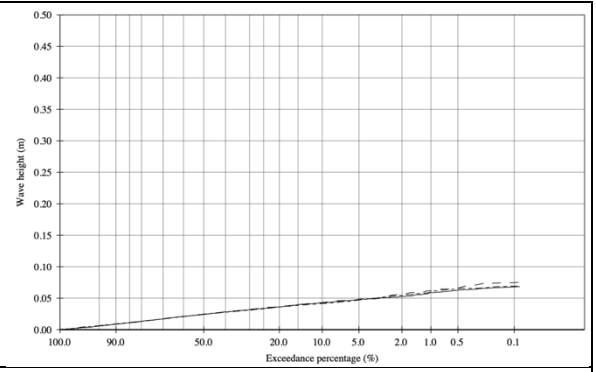

Test 2B

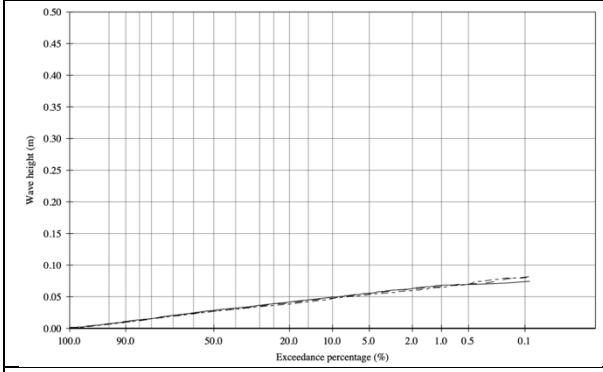

Test 2C

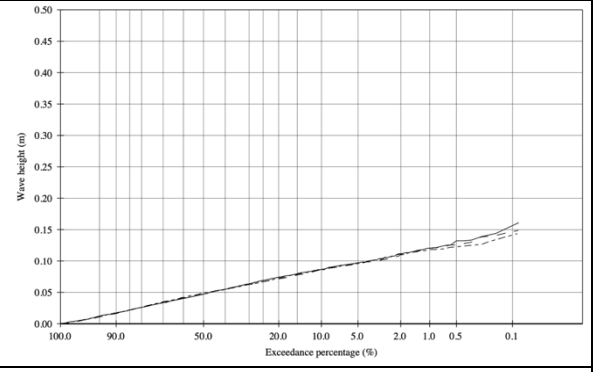

Test 2F

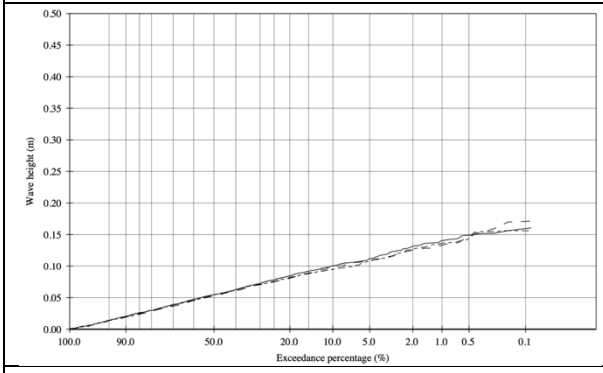

Test 2G

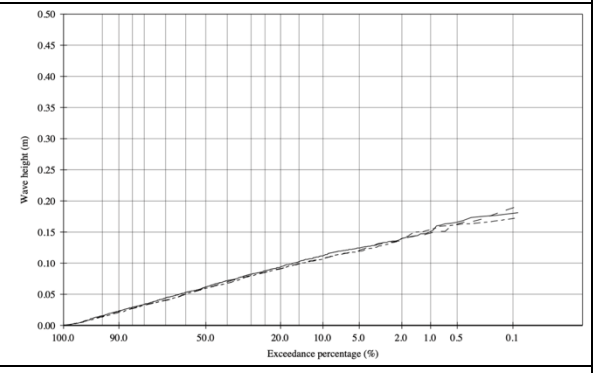

Test 2H

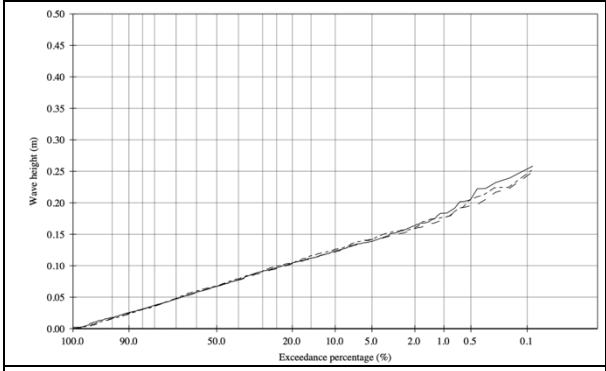

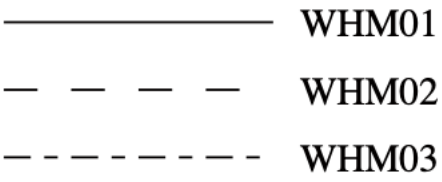

Test 2I

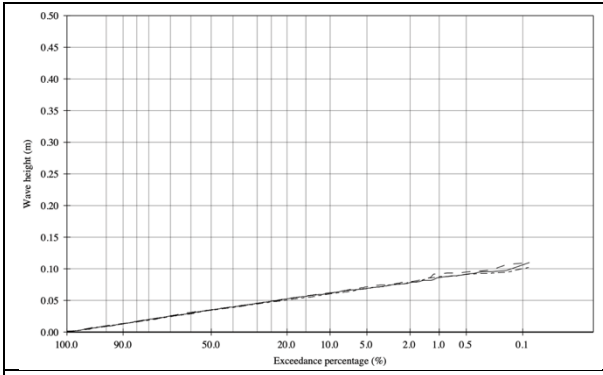

Test 3A

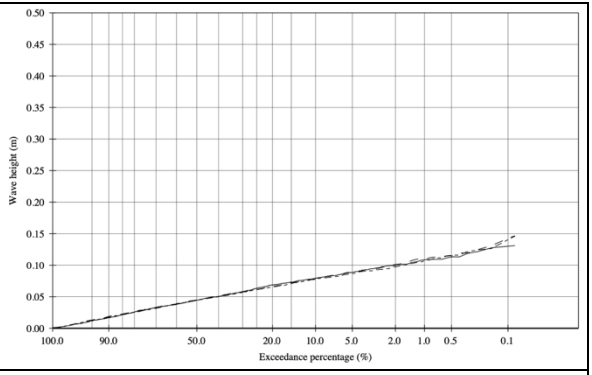

Test 3B

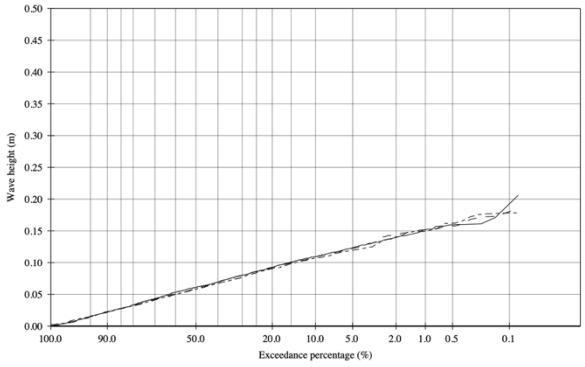

Test 3C

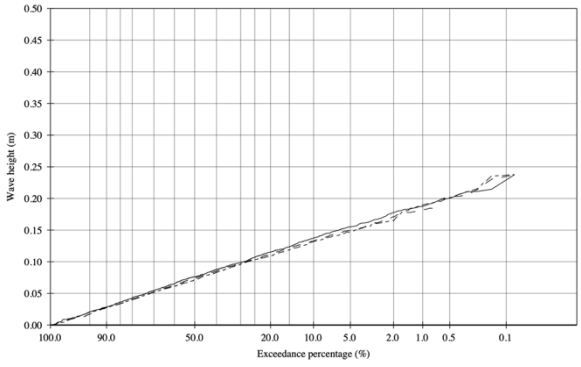

Test 3D

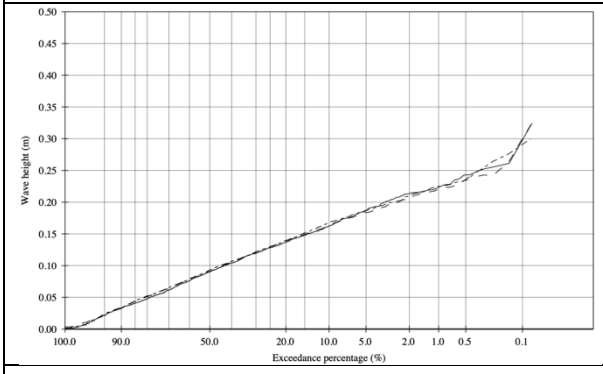

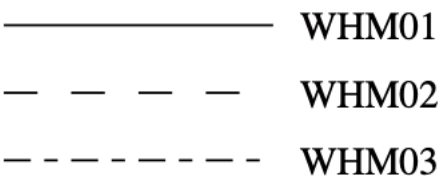

Test 3E

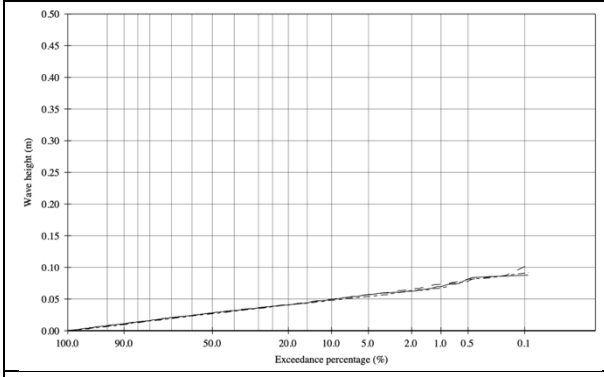

Test 3NA

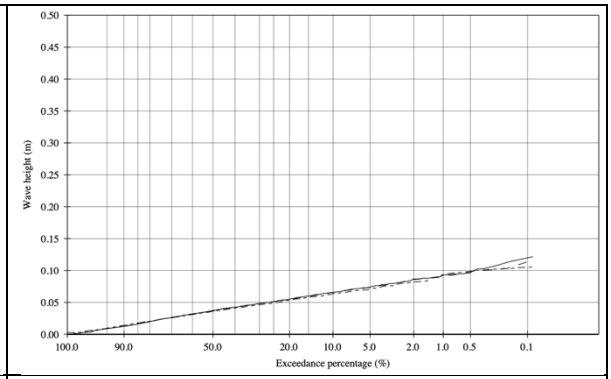

Test 3NB

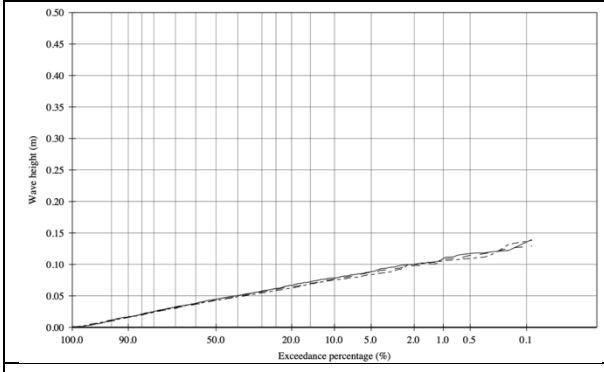

Test 3NC

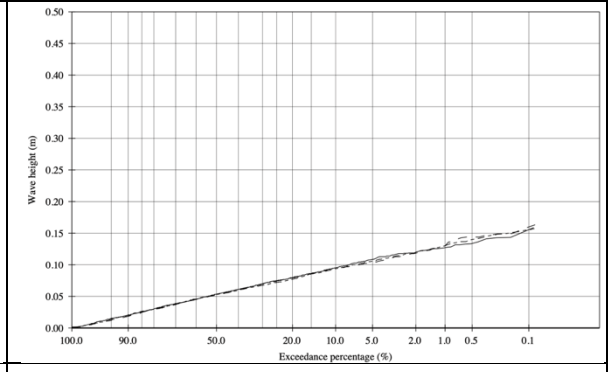

Test 3ND

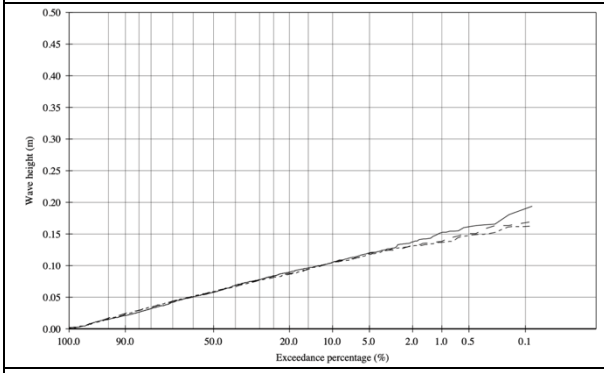

Test 3NE

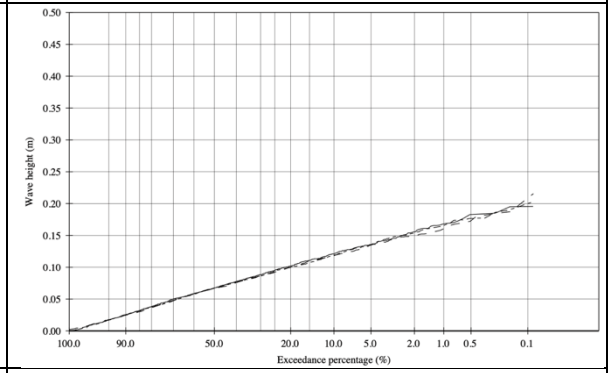

Test 3NF

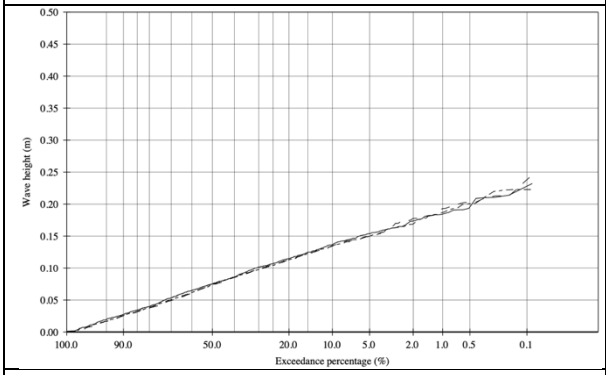

Test 3NG

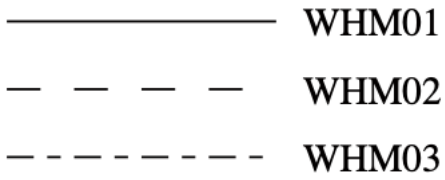

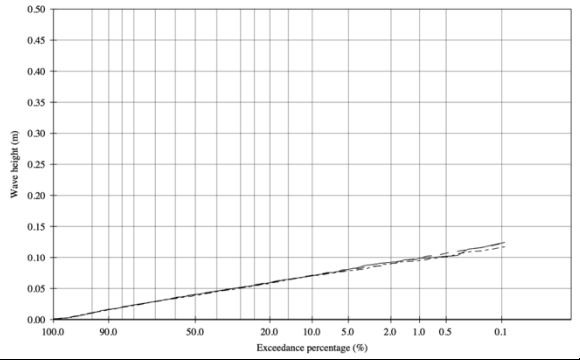

Test 5A

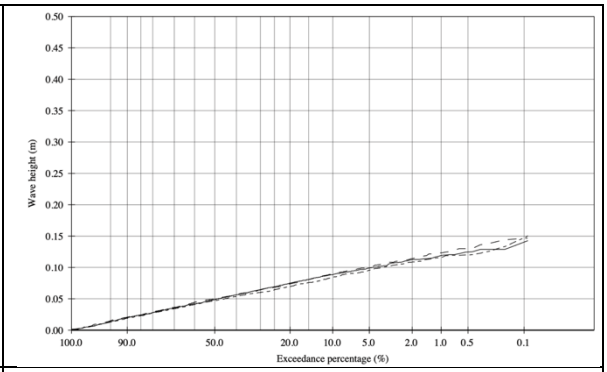

Test 5B

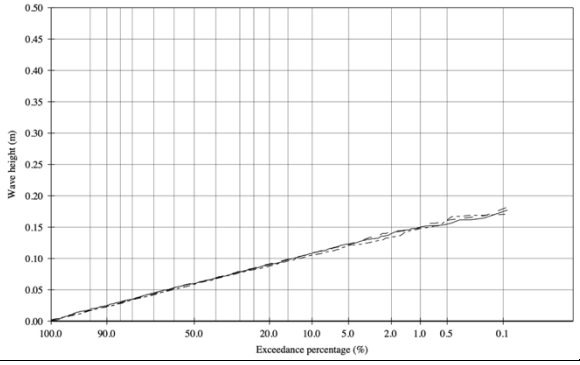

Test 5C

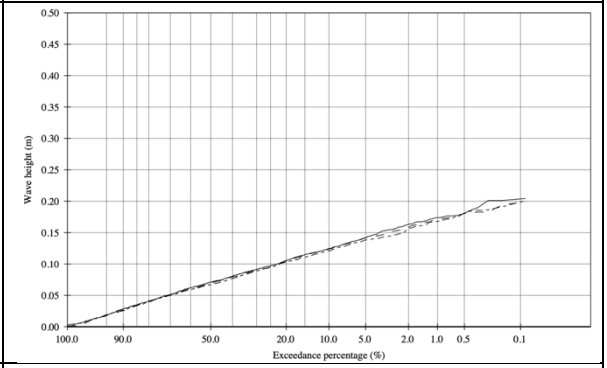

Test 5D

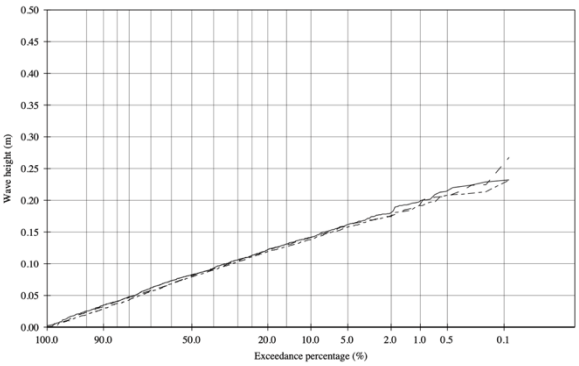

Test 5E

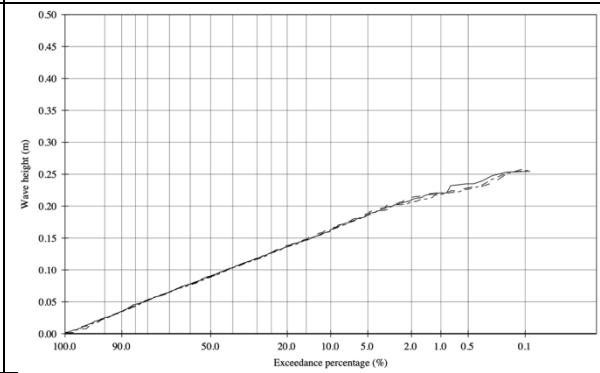

Test 5F

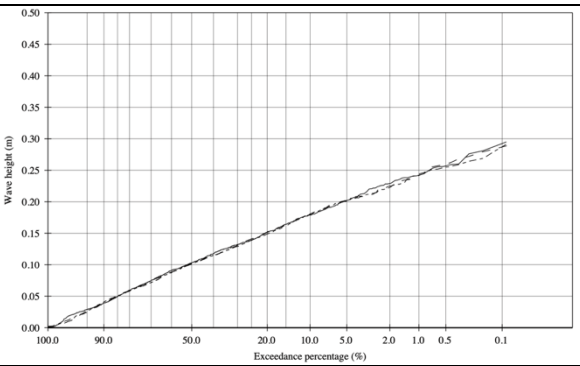

Test 5G

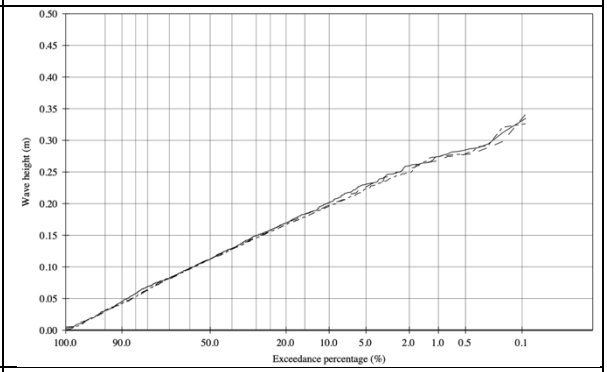

Test 5H

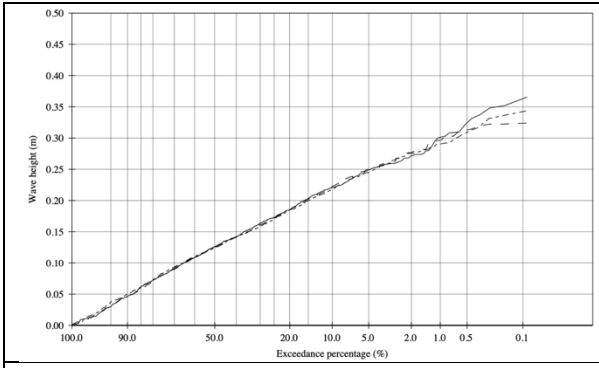

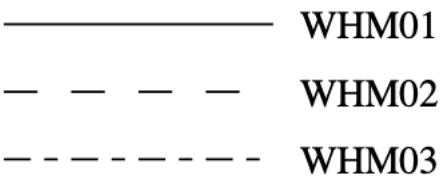

Test 5I

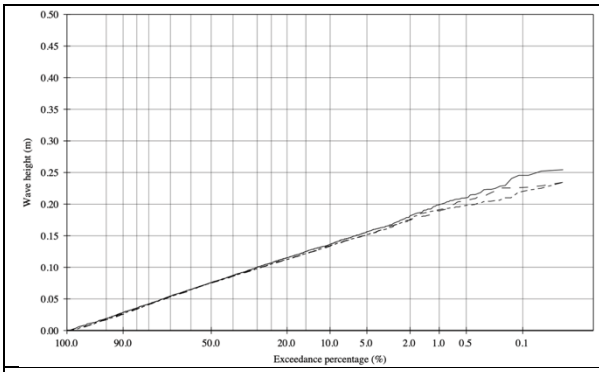

Test 6F

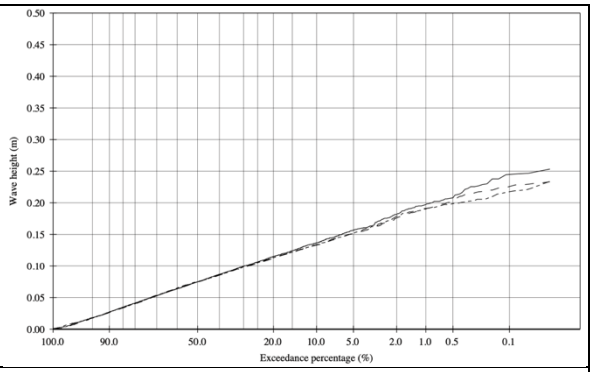

Test 6G

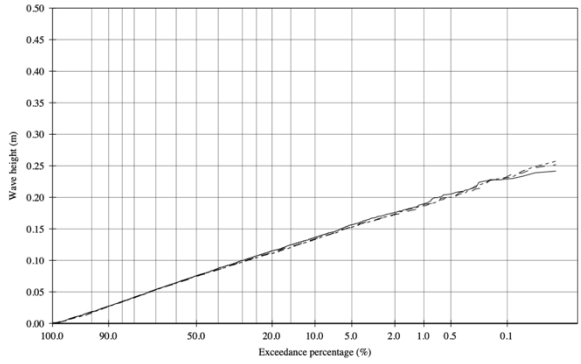

Test 6H

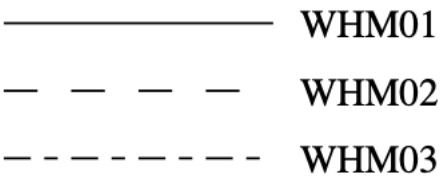

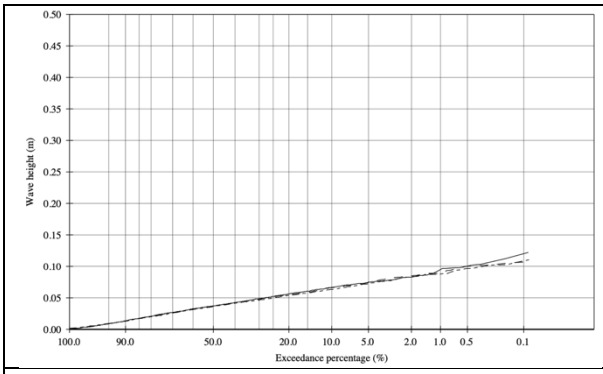

Test 7A

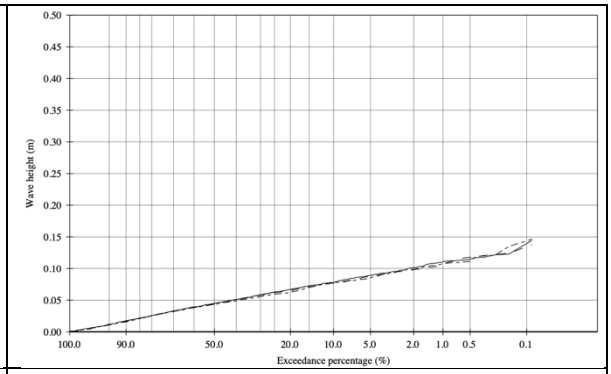

Test 7B

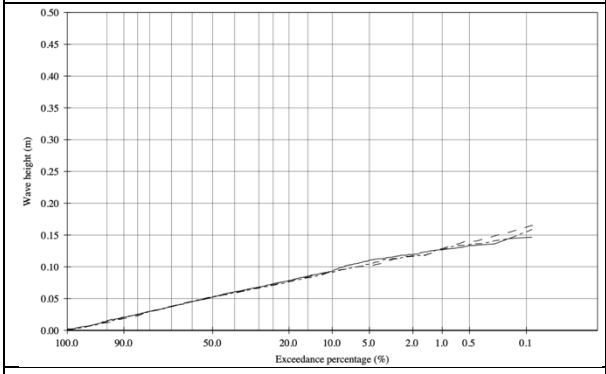

Test 7C

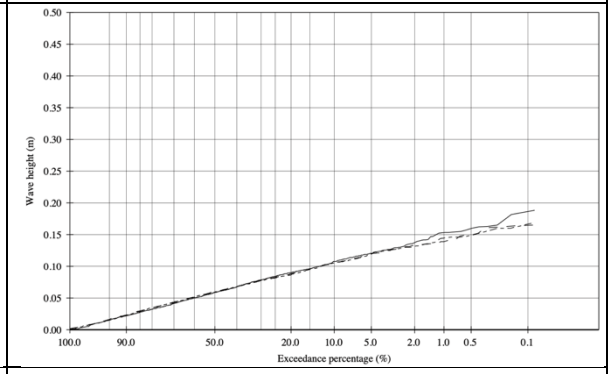

Test 7D

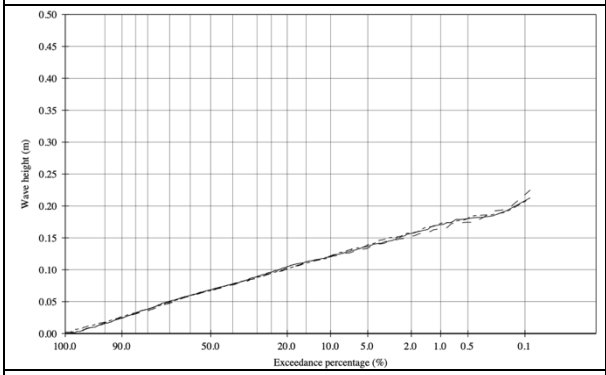

Test 7E

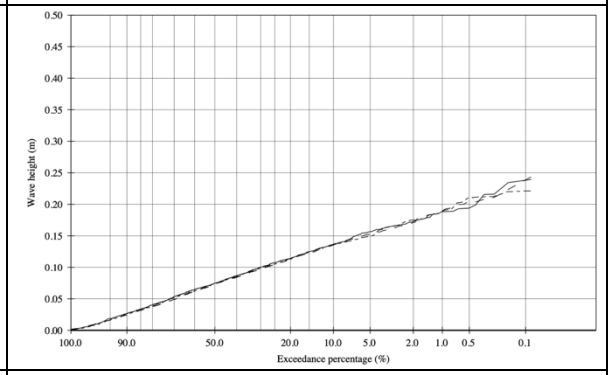

Test 7F

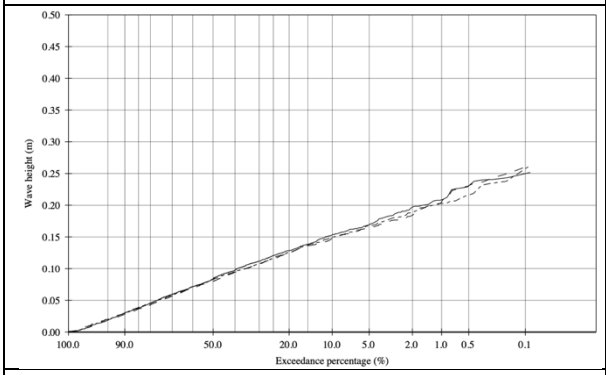

Test 7G

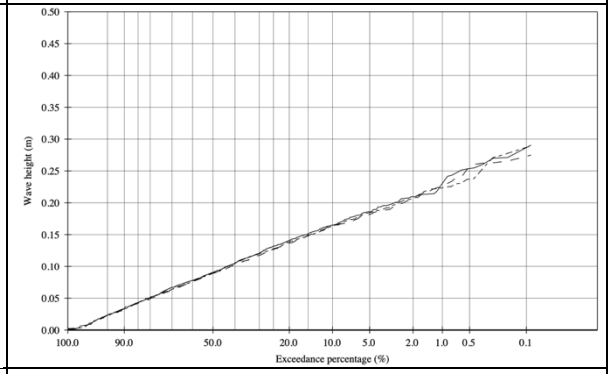

Test 7H

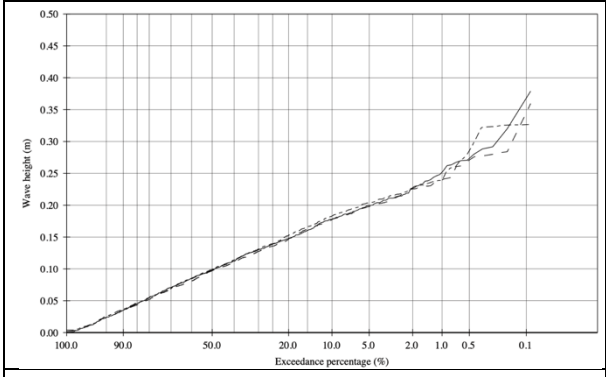

Test 7I

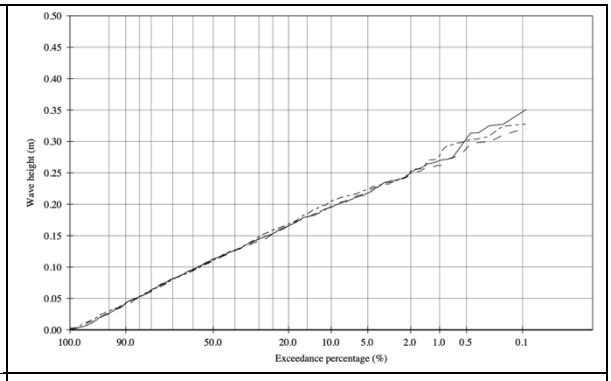

Test 7J

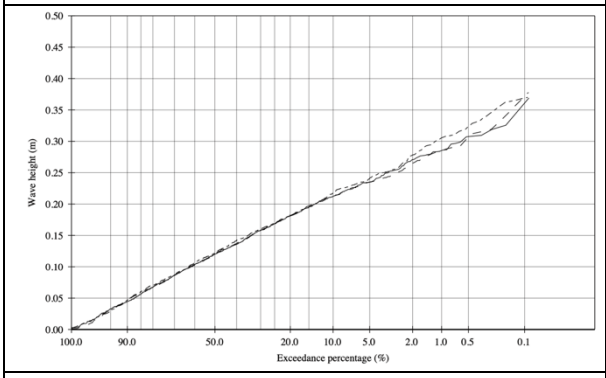

Test 7K

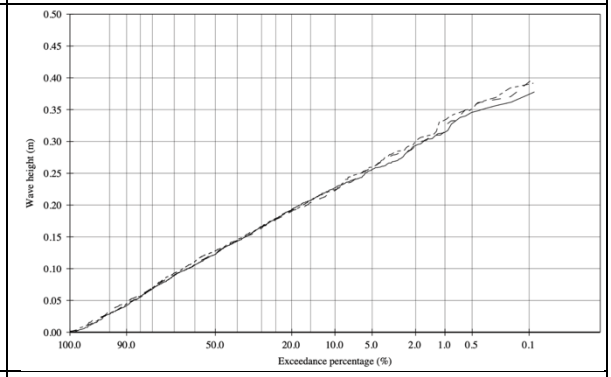

Test 7L

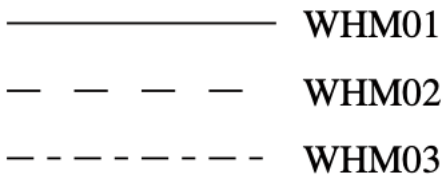

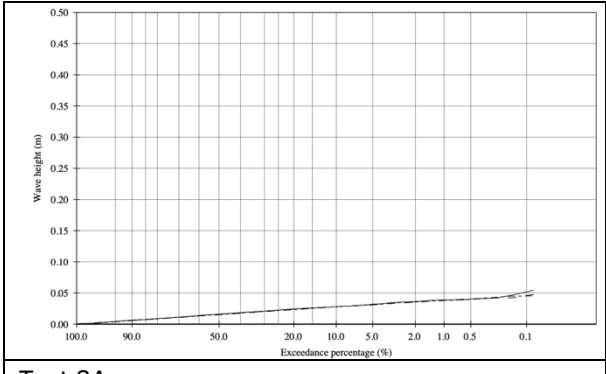

Test 8A

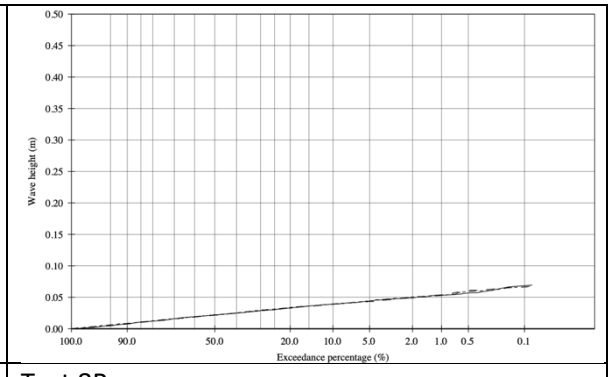

Test 8B

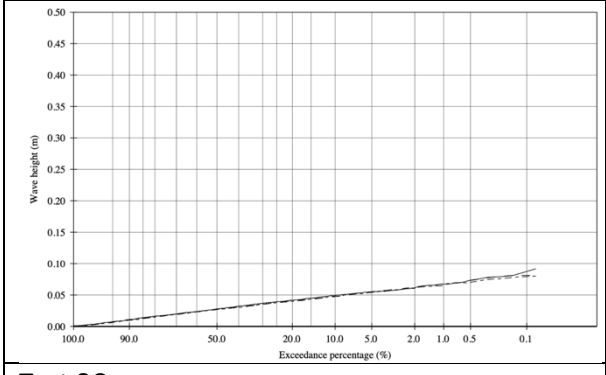

Test 8C

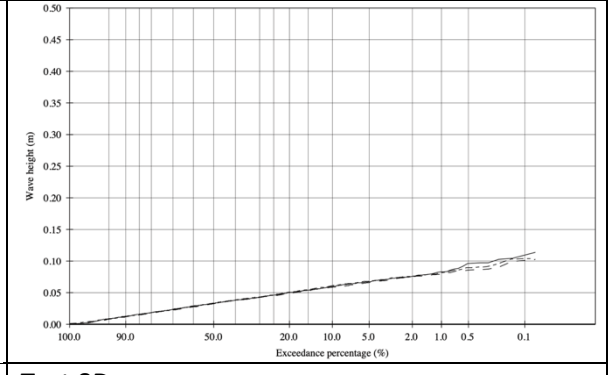

Test 8D

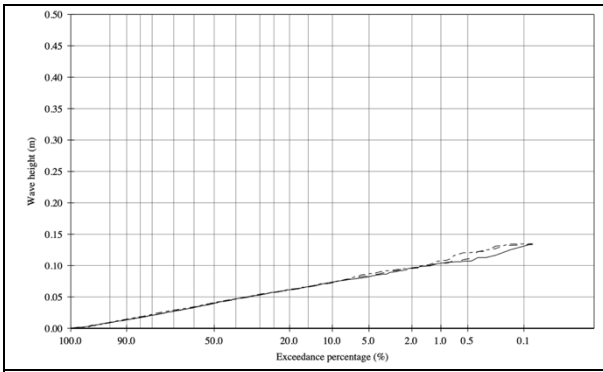

Test 8E

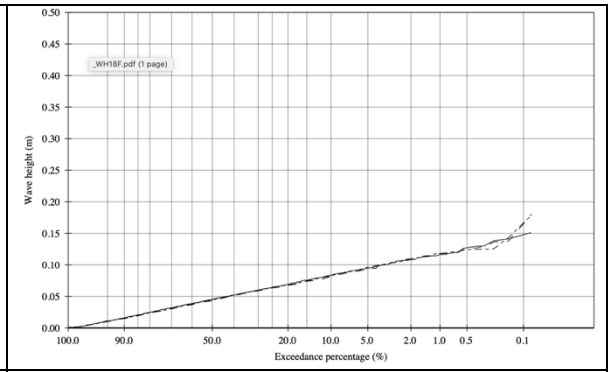

Test 8F

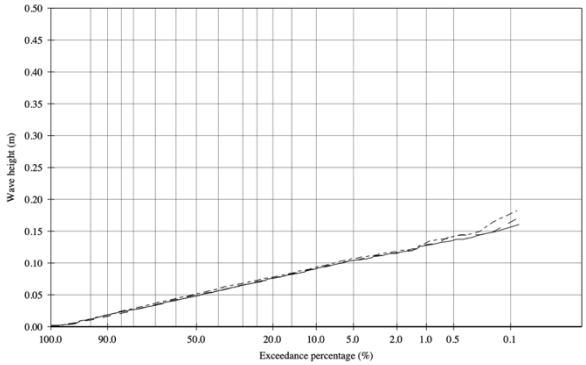

Test 8G

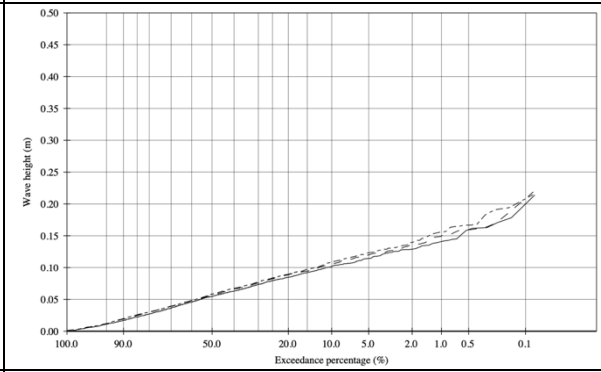

Test 8H

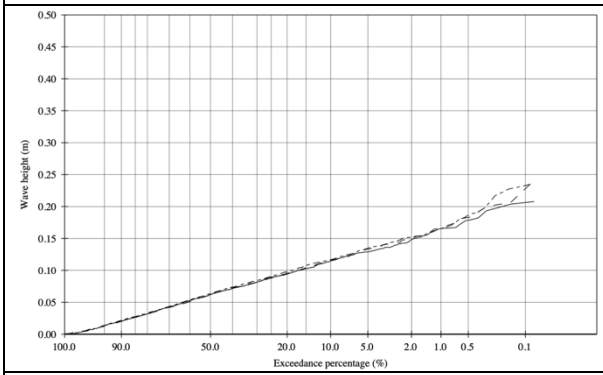

Test 8I

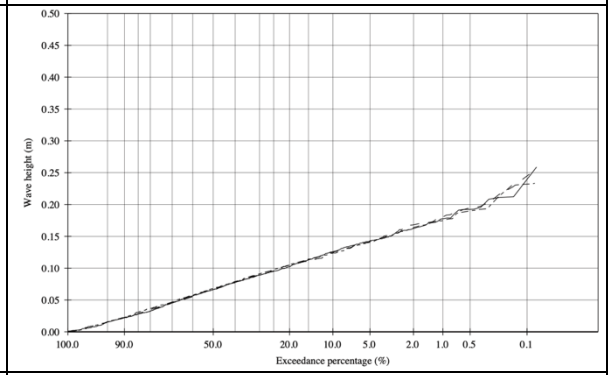

Test 8J

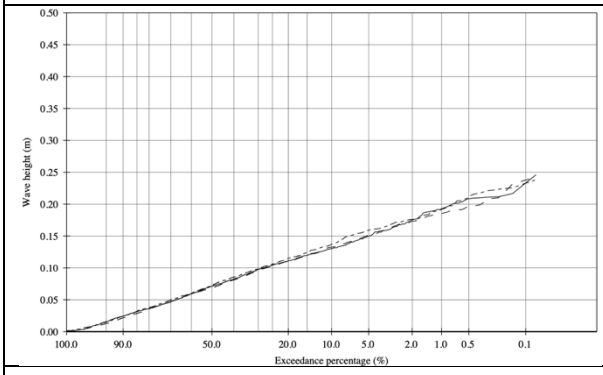

Test 8K

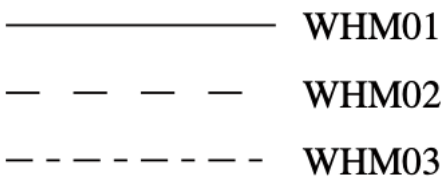

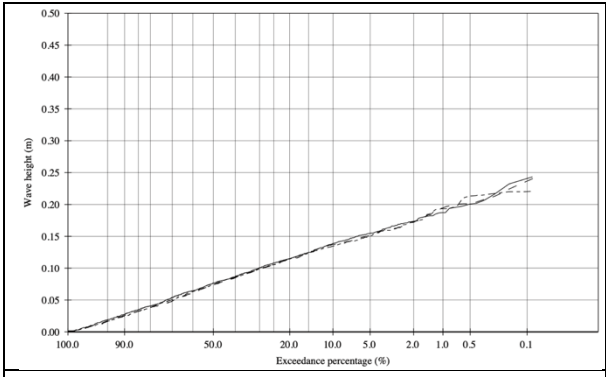

Test 9A

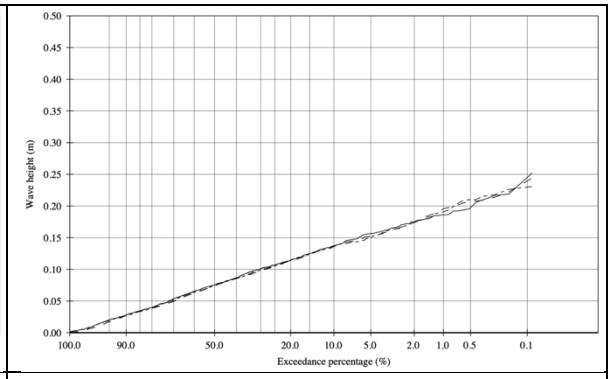

Test 9B

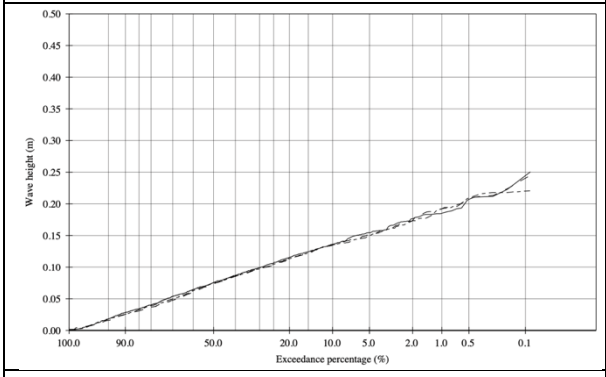

Test 9C

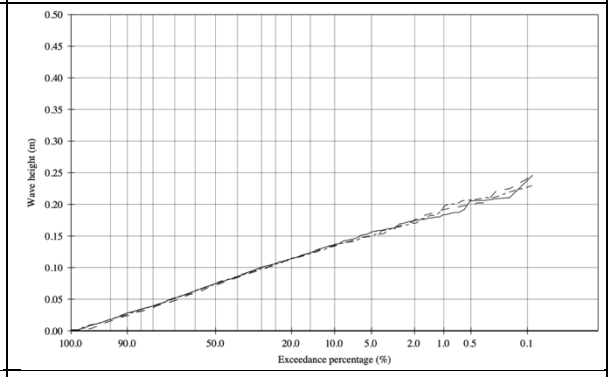

Test 9D

Appendix D: Complete test plan

Table 20: *The extended version of test plan for the 1:8 slope.*

Test series	Sub test	$s_{o,p}$	ξ_p	H_s	N	T	T_p
1	A	0.01	1.25	0.0200	1000	$2.5*d_{n50}$	1.132
	B	0.01	1.25	0.0300	1000	$2.5*d_{n50}$	1.36
	C	0.01	1.25	0.0400	1000	$2.5*d_{n50}$	1.53
	D	0.01	1.25	0.0501	1000	$2.5*d_{n50}$	1.68
	E	0.01	1.25	0.0603	1000	$2.5*d_{n50}$	1.83
	F	0.01	1.25	0.0705	1000	$2.5*d_{n50}$	2.05
	E	0.01	1.25	0.0779	1000	$2.5*d_{n50}$	2.15
	G	0.01	1.25	0.0881	1000	$2.5*d_{n50}$	2.29
2	A	0.02	0.88	0.0300	1000	$2.5*d_{n50}$	0.97
	B	0.02	0.88	0.0408	1000	$2.5*d_{n50}$	1.1
	C	0.02	0.88	0.0519	1000	$2.5*d_{n50}$	1.24
	D	0.02	0.88	0.0640	1000	$2.5*d_{n50}$	1.35
	E	0.02	0.88	0.0742	1000	$2.5*d_{n50}$	1.47
	F	0.02	0.88	0.0853	1000	$2.5*d_{n50}$	1.58
	E	0.02	0.88	0.0964	1000	$2.5*d_{n50}$	1.68
	G	0.02	0.88	0.1085	1000	$2.5*d_{n50}$	1.78
3	A	0.03	0.72	0.056	1000	$2.5*d_{n50}$	1.13
	B	0.03	0.72	0.074	1000	$2.5*d_{n50}$	1.3
	C	0.03	0.72	0.102	1000	$2.5*d_{n50}$	1.53
	D	0.03	0.72	0.130	1000	$2.5*d_{n50}$	1.72
	E	0.03	0.72	0.158	1000	$2.5*d_{n50}$	1.90
	NA	0.03	0.72	0.046	1000	$2.5*d_{n50}$	1.00
	NB	0.03	0.72	0.060	1000	$2.5*d_{n50}$	1.10
	NC	0.03	0.72	0.074	1000	$2.5*d_{n50}$	1.23
	ND	0.03	0.72	0.088	1000	$2.5*d_{n50}$	1.34
	NE	0.03	0.72	0.102	1000	$2.5*d_{n50}$	1.44
	NF	0.03	0.72	0.116	1000	$2.5*d_{n50}$	1.52
	NG	0.03	0.72	0.130	1000	$2.5*d_{n50}$	1.61
	NH	0.03	0.72	0.144	1000	$2.5*d_{n50}$	1.69
	NI	0.03	0.72	0.158	1000	$2.5*d_{n50}$	1.77
4	A	0.04	0.63	0.056	1000	$2.5*d_{n50}$	0.93
	B	0.04	0.63	0.074	1000	$2.5*d_{n50}$	1.06
	C	0.04	0.63	0.093	1000	$2.5*d_{n50}$	1.18
	D	0.04	0.63	0.111	1000	$2.5*d_{n50}$	1.3
	E	0.04	0.63	0.130	1000	$2.5*d_{n50}$	1.39
	F	0.04	0.63	0.148	1000	$2.5*d_{n50}$	1.47
	E	0.04	0.63	0.167	1000	$2.5*d_{n50}$	1.55
	G	0.04	0.63	0.185	1000	$2.5*d_{n50}$	1.63
5	A	0.05	0.56	0.060	1000	$2.5*d_{n50}$	0.877
	B	0.05	0.56	0.080	1000	$2.5*d_{n50}$	1.013
	C	0.05	0.56	0.100	1000	$2.5*d_{n50}$	1.132
	D	0.05	0.56	0.120	1000	$2.5*d_{n50}$	1.24
	E	0.05	0.56	0.140	1000	$2.5*d_{n50}$	1.34
	F	0.05	0.56	0.160	1000	$2.5*d_{n50}$	1.37
	E	0.05	0.56	0.180	1000	$2.5*d_{n50}$	1.41
	G	0.05	0.56	0.199	1000	$2.5*d_{n50}$	1.47
	H	0.05	0.56	0.218	1000	$2.5*d_{n50}$	1.54
6	A	0.03	0.72	0.130	250	$2.5*d_{n50}$	1.61
	B	0.03	0.72	0.130	500	$2.5*d_{n50}$	1.61
	C	0.03	0.72	0.130	1000	$2.5*d_{n50}$	1.61
	D	0.03	0.72	0.130	2000	$2.5*d_{n50}$	1.61
	E	0.03	0.72	0.130	4000	$2.5*d_{n50}$	1.61
	F	0.03	0.72	0.130	7000	$2.5*d_{n50}$	1.61
	G	0.03	0.72	0.130	10000	$2.5*d_{n50}$	1.61

Test series	Sub test	$s_{o,p}$	ξ_p	H_s	N	T	T_p
6	H	0.03	0.72	0.130	14000	$2.5*d_{n50}$	1.61
7	A	0.03	0.72	0.060	1000	$5*d_{n50}$	1.10
	B	0.03	0.72	0.074	1000	$5*d_{n50}$	1.23
	C	0.03	0.72	0.088	1000	$5*d_{n50}$	1.34
	D	0.03	0.72	0.102	1000	$5*d_{n50}$	1.44
	E	0.03	0.72	0.116	1000	$5*d_{n50}$	1.52
	F	0.03	0.72	0.130	1000	$5*d_{n50}$	1.61
	E	0.03	0.72	0.144	1000	$5*d_{n50}$	1.69
	G	0.03	0.72	0.158	1000	$5*d_{n50}$	1.77
	H	0.03	0.72	0.171	1000	$5*d_{n50}$	1.85
	I	0.03	0.72	0.185	1000	$5*d_{n50}$	1.92
	J	0.03	0.72	0.199	1000	$5*d_{n50}$	1.99
	K	0.03	0.72	0.213	1000	$5*d_{n50}$	2.06
8	A	0.05	0.56	0.0300	1000	$5*d_{n50}$	1.36
	B	0.05	0.56	0.0400	1000	$5*d_{n50}$	1.53
	C	0.05	0.56	0.0501	1000	$5*d_{n50}$	1.68
	D	0.05	0.56	0.0603	1000	$5*d_{n50}$	1.83
	E	0.05	0.56	0.0705	1000	$5*d_{n50}$	2.05
	F	0.05	0.56	0.0779	1000	$5*d_{n50}$	2.15
	E	0.05	0.56	0.0881	1000	$5*d_{n50}$	2.29
	G	0.05	0.56	0.0983	1000	$5*d_{n50}$	2.41
	H	0.05	0.56	0.1085	1000	$5*d_{n50}$	2.54
	I	0.05	0.56	0.1187	1000	$5*d_{n50}$	2.65
	J	0.05	0.56	0.1289	1000	$5*d_{n50}$	2.77
9	A	0.03	0.72	0.130	1000	$2.5*d_{n50}$	1.61
	B	0.03	0.72	0.130	1000	$2.5*d_{n50}$	1.61
	C	0.03	0.72	0.130	1000	$2.5*d_{n50}$	1.61
	D	0.03	0.72	0.130	1000	$2.5*d_{n50}$	1.61
	E	0.03	0.72	0.130	1000	$2.5*d_{n50}$	1.61
10	A	0.03	0.72	0.16	1000	$2.5*d_{n50}$	1.61

Appendix E: Software settings

The most important settings are shown in this appendix for the used software in this thesis. Table 21 shows the settings for Metashape Agisoft and the settings for the IPC tool in the CloudCompare software are displayed in Table 22.

Table 21: *The most important settings in Metashape Agisoft.*

Procedure	Parameter	Setting
Aligning photos	Accuracy	Highest
	Key point limit	40 000
	Tie point limit	4 000
Building dense cloud	Quality	Medium
	Depth filtering	Mild

Table 22: *The most important settings for IPC tool in CloudCompare.*

Procedure	Parameter	Setting
Parameters	RMS difference	1.0E-5
	Final overlap	60%
	Adjust scale	Disabled
Research	Random sampling limit	50 000
	Rotation	XYZ
	Translation	XYZ enabled
	Enable furthest point removal	disabled

Appendix F: Average profile change graphs

The average profile changes for the 1:8 slope:

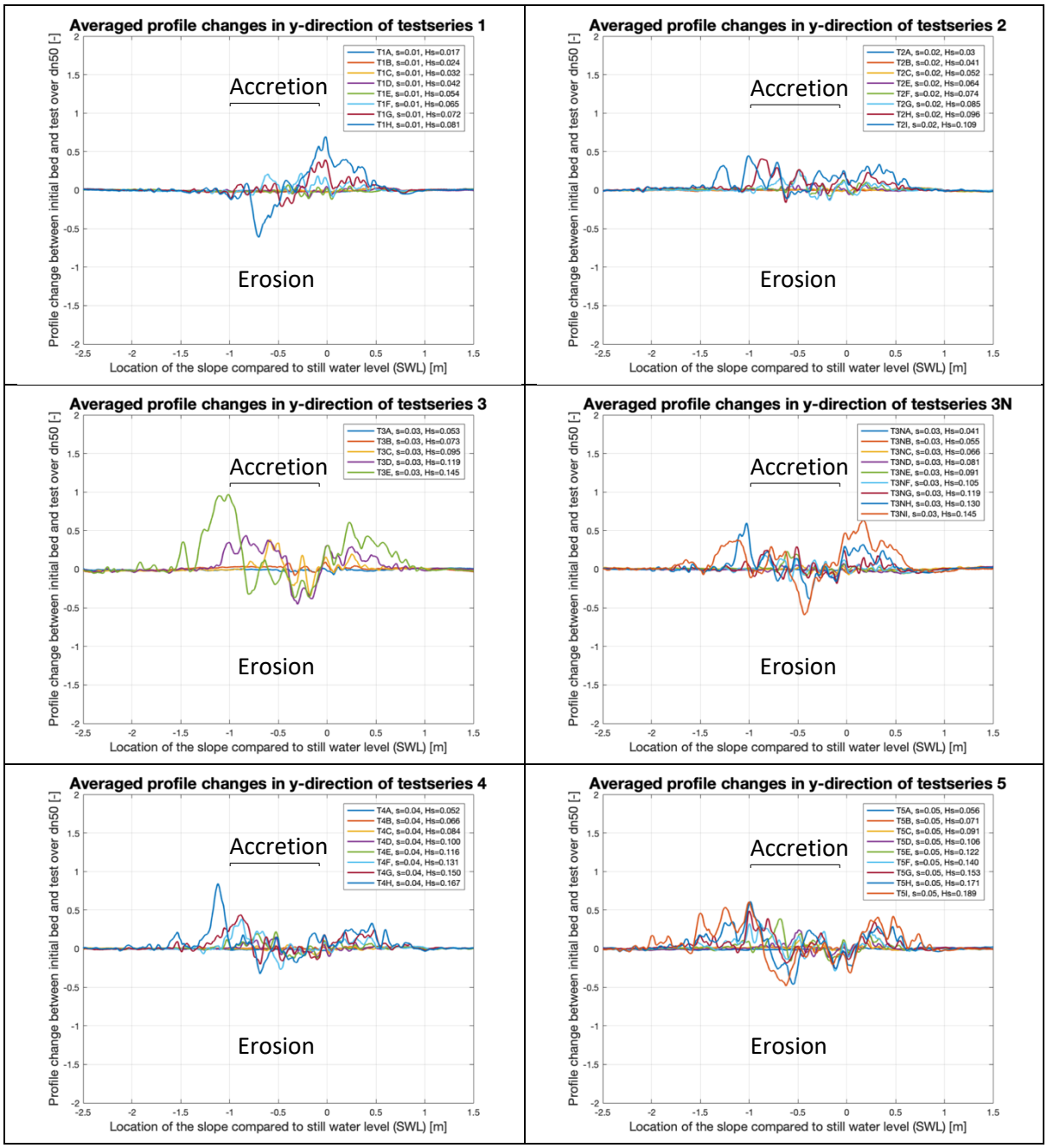

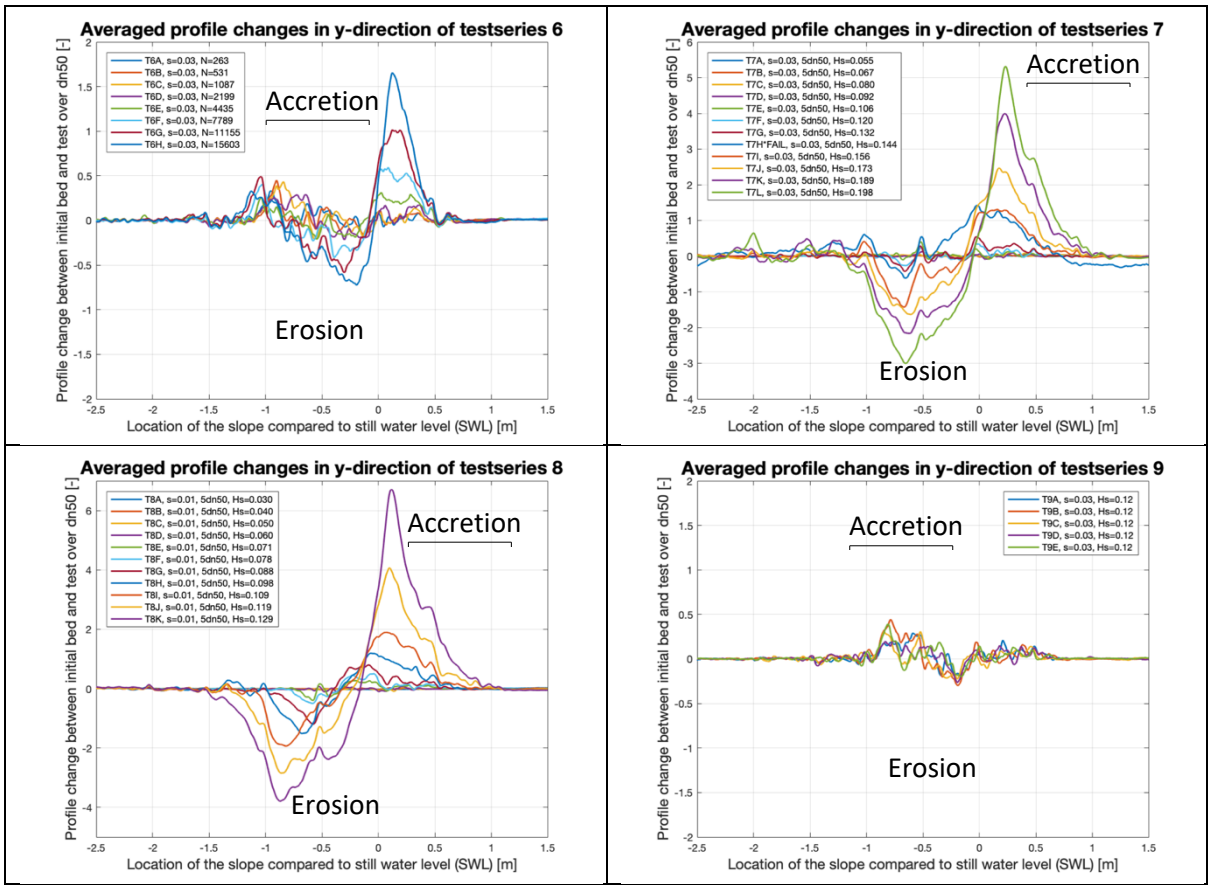
Averaged profile changes in y-direction of testseries 6
Profile change between initial bed and test over dn50 [-]
Location of the slope compared to still water level (SWL) [m]
T6A, s=0.03, N=263
T6B, s=0.03, N=531
T6C, s=0.03, N=1087
T6D, s=0.03, N=2199
T6E, s=0.03, N=4435
T6F, s=0.03, N=7789
T6G, s=0.03, N=11155
T6H, s=0.03, N=15603
Accretion
Erosion
Averaged profile changes in y-direction of testseries 7
Profile change between initial bed and test over dn50 [-]
Location of the slope compared to still water level (SWL) [m]
T7A, s=0.03, 5dn50, Hs=0.055
T7B, s=0.03, 5dn50, Hs=0.067
T7C, s=0.03, 5dn50, Hs=0.080
T7D, s=0.03, 5dn50, Hs=0.092
T7E, s=0.03, 5dn50, Hs=0.106
T7F, s=0.03, 5dn50, Hs=0.120
T7G, s=0.03, 5dn50, Hs=0.132
T7H*FAIL, s=0.03, 5dn50, Hs=0.144
T7I, s=0.03, 5dn50, Hs=0.156
T7J, s=0.03, 5dn50, Hs=0.173
T7K, s=0.03, 5dn50, Hs=0.189
T7L, s=0.03, 5dn50, Hs=0.198
Accretion
Erosion
Averaged profile changes in y-direction of testseries 8
Profile change between initial bed and test over dn50 [-]
Location of the slope compared to still water level (SWL) [m]
T8A, s=0.01, 5dn50, Hs=0.030
T8B, s=0.01, 5dn50, Hs=0.040
T8C, s=0.01, 5dn50, Hs=0.050
T8D, s=0.01, 5dn50, Hs=0.060
T8E, s=0.01, 5dn50, Hs=0.071
T8F, s=0.01, 5dn50, Hs=0.078
T8G, s=0.01, 5dn50, Hs=0.088
T8H, s=0.01, 5dn50, Hs=0.098
T8I, s=0.01, 5dn50, Hs=0.109
T8J, s=0.01, 5dn50, Hs=0.119
T8K, s=0.01, 5dn50, Hs=0.129
Accretion
Erosion
Averaged profile changes in y-direction of testseries 9
Profile change between initial bed and test over dn50 [-]
Location of the slope compared to still water level (SWL) [m]
T9A, s=0.03, Hs=0.12
T9B, s=0.03, Hs=0.12
T9C, s=0.03, Hs=0.12
T9D, s=0.03, Hs=0.12
T9E, s=0.03, Hs=0.12
Accretion
Erosion

The average profile changes for the 1:10 slope:

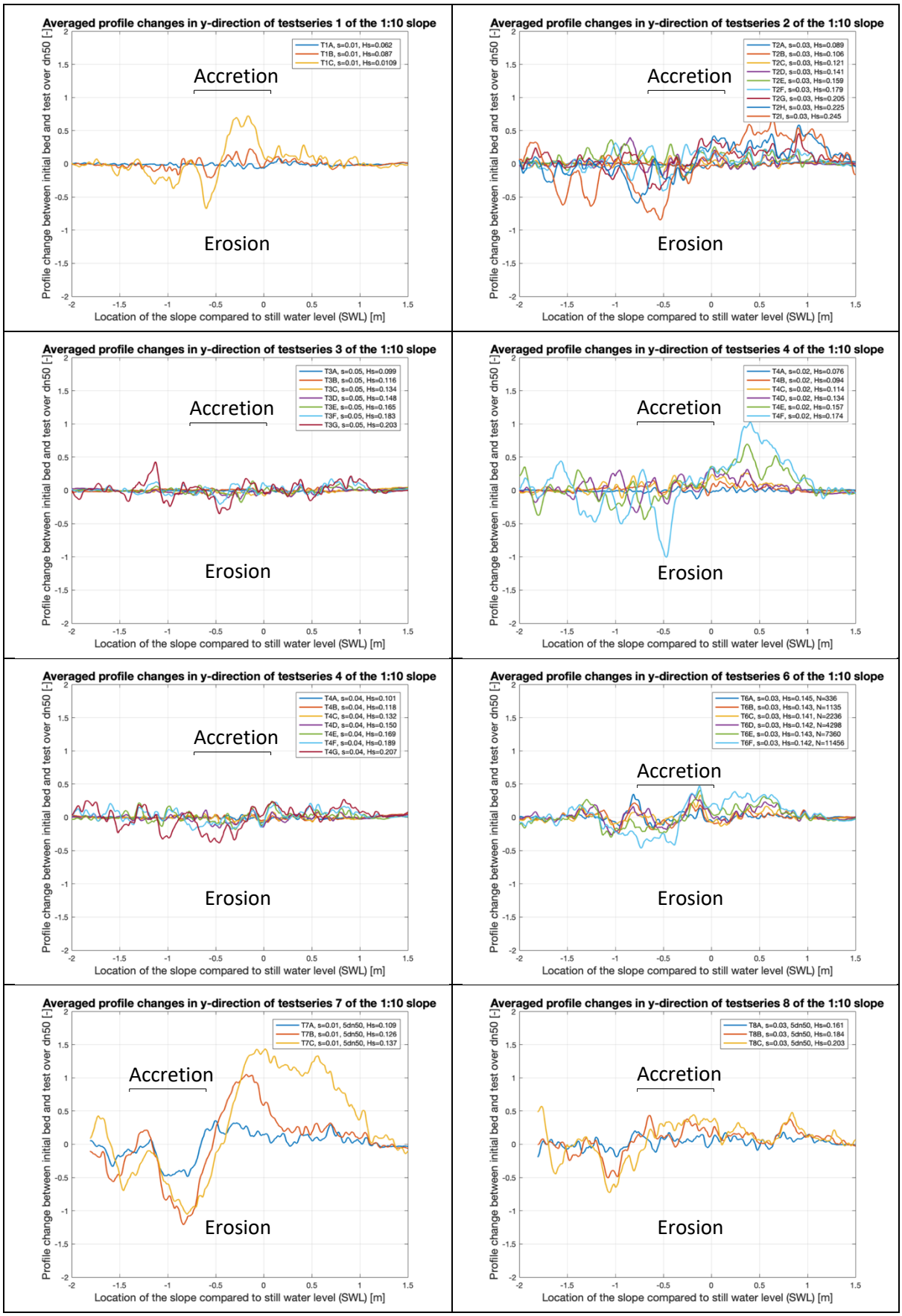

Appendix G: 3D profile change graphs

Results for 1:8 slope

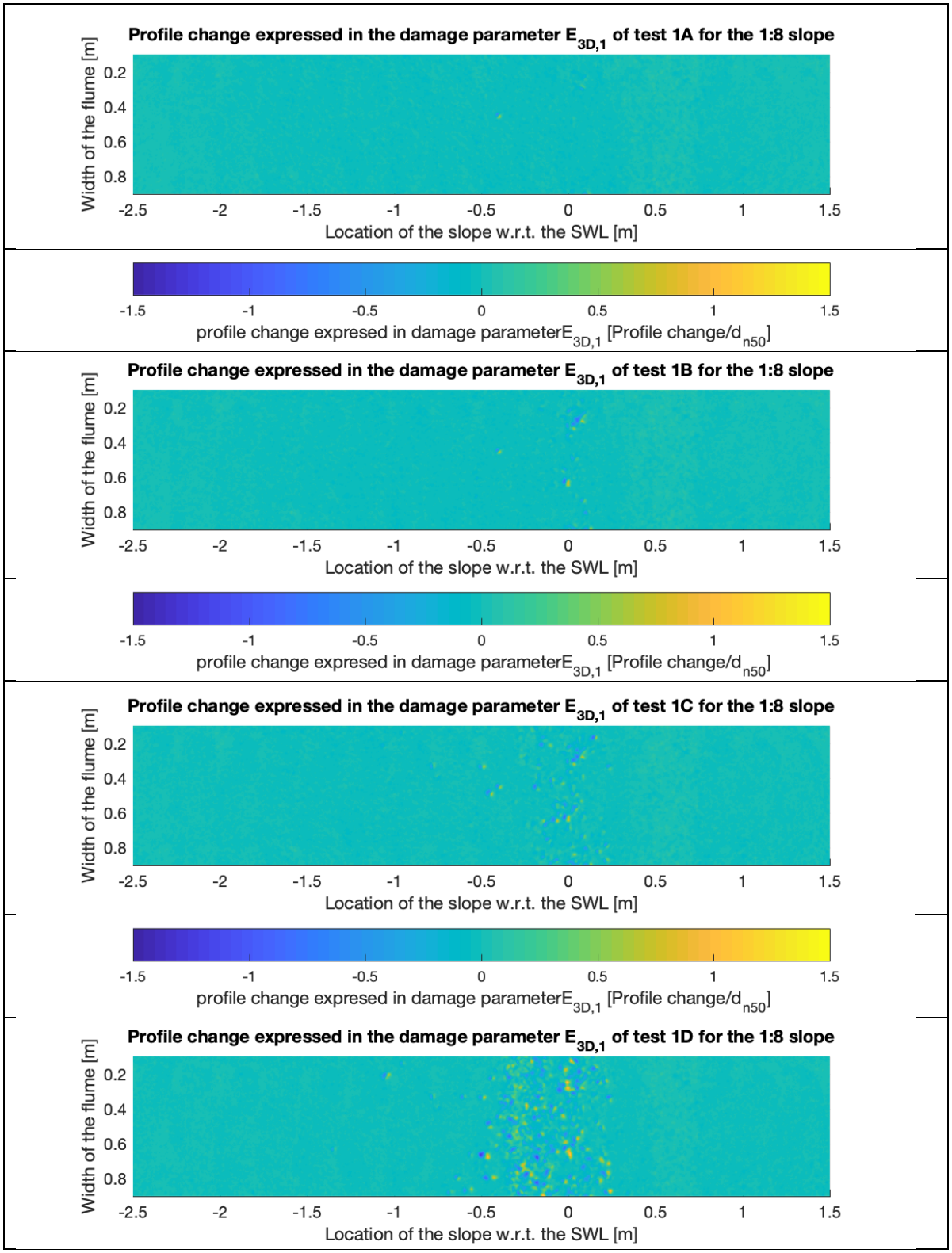

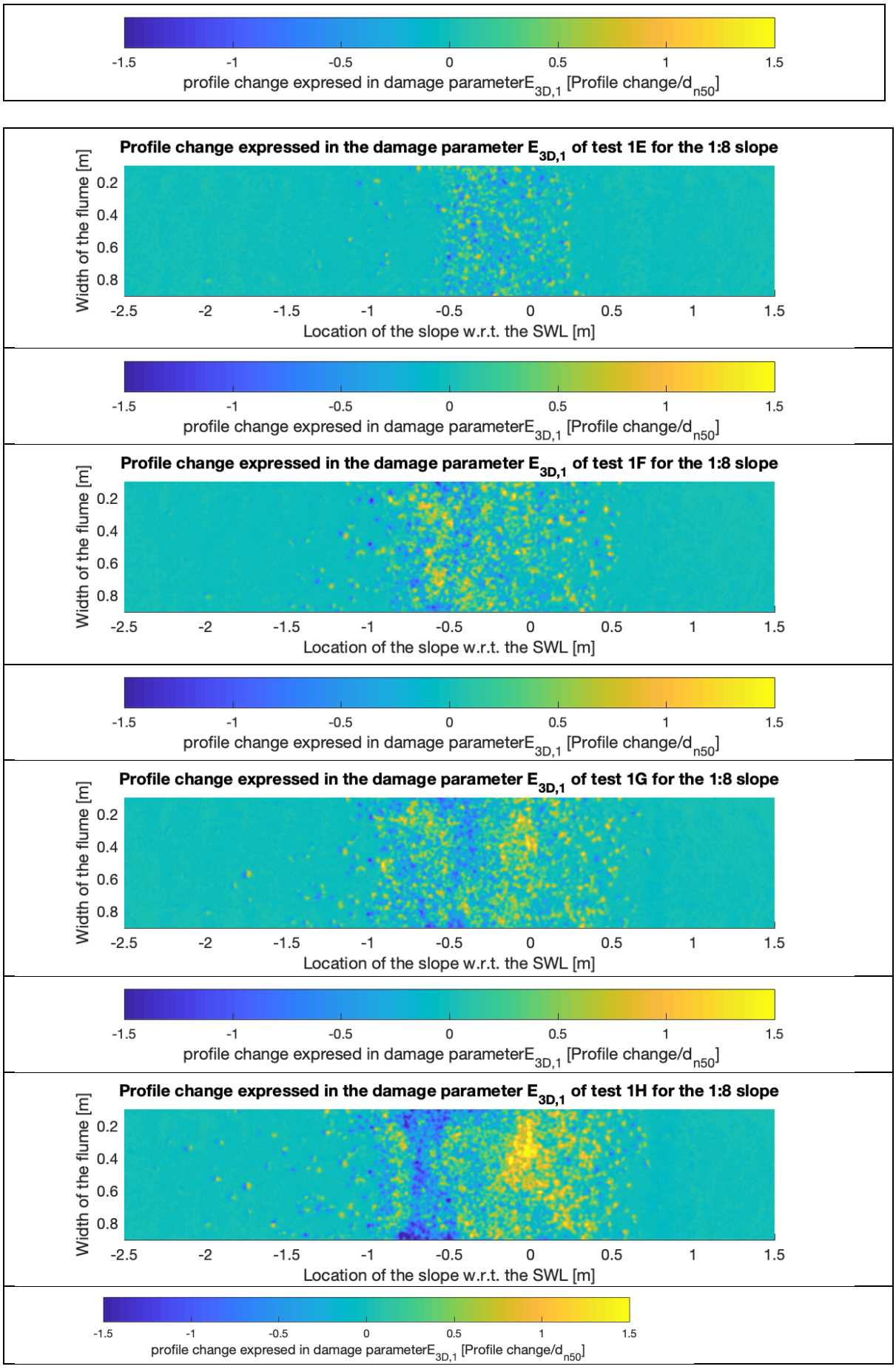
-1.5 -1 -0.5 0 0.5 1 1.5
profile change expresed in damage parameterE3D,1 [Profile change/dn50]
Profile change expressed in the damage parameter E3D,1 of test 1E for the 1:8 slope
Width of the flume [m]
0.2 0.4 0.6 0.8
-2.5 -2 -1.5 -1 -0.5 0 0.5 1 1.5
Location of the slope w.r.t. the SWL [m]
-1.5 -1 -0.5 0 0.5 1 1.5
profile change expresed in damage parameterE3D,1 [Profile change/dn50]
Profile change expressed in the damage parameter E3D,1 of test 1F for the 1:8 slope
Width of the flume [m]
0.2 0.4 0.6 0.8
-2.5 -2 -1.5 -1 -0.5 0 0.5 1 1.5
Location of the slope w.r.t. the SWL [m]
-1.5 -1 -0.5 0 0.5 1 1.5
profile change expresed in damage parameterE3D,1 [Profile change/dn50]
Profile change expressed in the damage parameter E3D,1 of test 1G for the 1:8 slope
Width of the flume [m]
0.2 0.4 0.6 0.8
-2.5 -2 -1.5 -1 -0.5 0 0.5 1 1.5
Location of the slope w.r.t. the SWL [m]
-1.5 -1 -0.5 0 0.5 1 1.5
profile change expresed in damage parameterE3D,1 [Profile change/dn50]
Profile change expressed in the damage parameter E3D,1 of test 1H for the 1:8 slope
Width of the flume [m]
0.2 0.4 0.6 0.8
-2.5 -2 -1.5 -1 -0.5 0 0.5 1 1.5
Location of the slope w.r.t. the SWL [m]
-1.5 -1 -0.5 0 0.5 1 1.5
profile change expresed in damage parameterE3D,1 [Profile change/dn50]

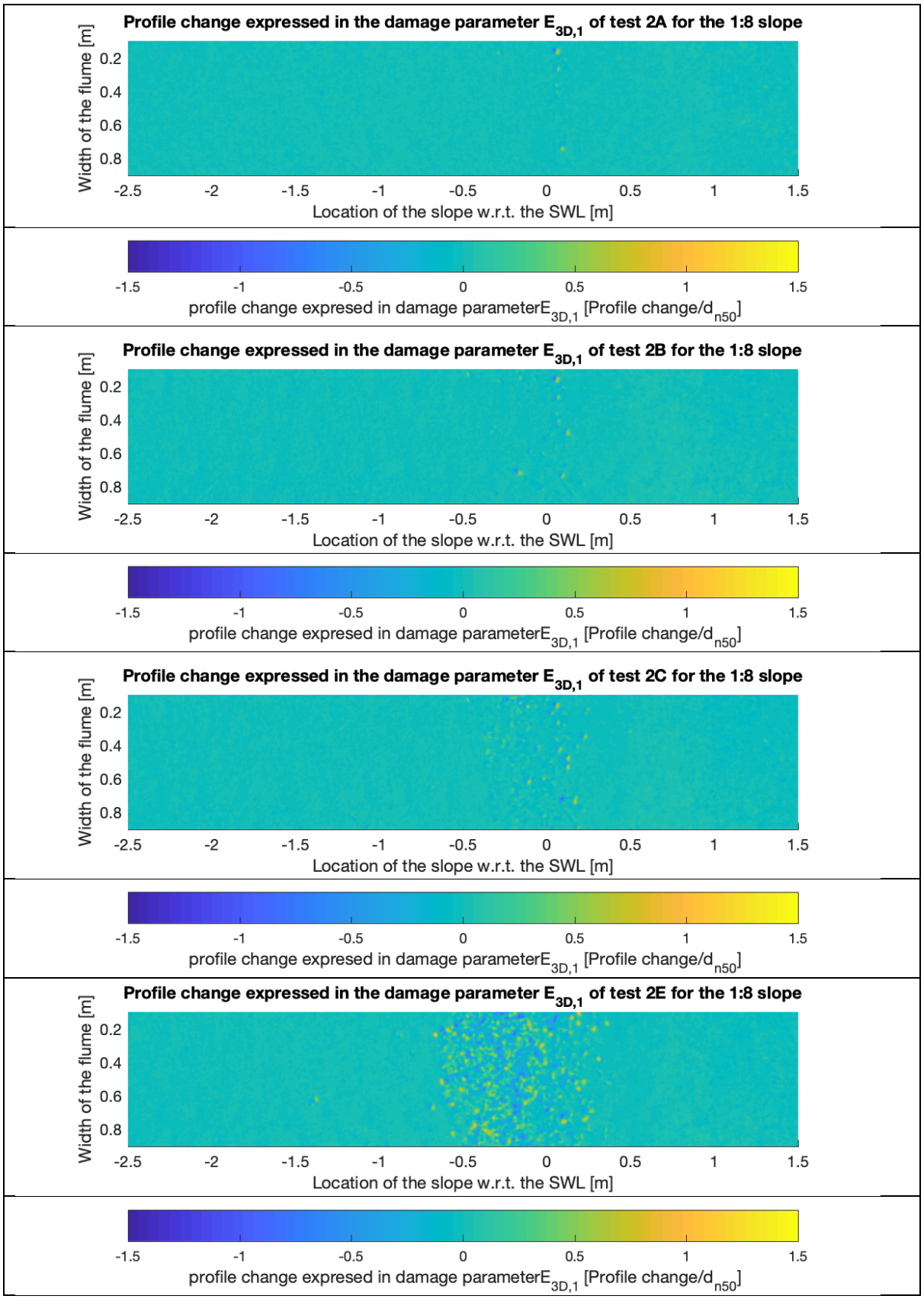
Profile change expressed in the damage parameter E3D,1 of test 2A for the 1:8 slope
Width of the flume [m]
0.2
0.4
0.6
0.8
-2.5
-2
-1.5
-1
-0.5
0
0.5
1
1.5
Location of the slope w.r.t. the SWL [m]
-1.5
-1
-0.5
0
0.5
1
1.5
profile change expresed in damage parameterE3D,1 [Profile change/dn50]
Profile change expressed in the damage parameter E3D,1 of test 2B for the 1:8 slope
Width of the flume [m]
0.2
0.4
0.6
0.8
-2.5
-2
-1.5
-1
-0.5
0
0.5
1
1.5
Location of the slope w.r.t. the SWL [m]
-1.5
-1
-0.5
0
0.5
1
1.5
profile change expresed in damage parameterE3D,1 [Profile change/dn50]
Profile change expressed in the damage parameter E3D,1 of test 2C for the 1:8 slope
Width of the flume [m]
0.2
0.4
0.6
0.8
-2.5
-2
-1.5
-1
-0.5
0
0.5
1
1.5
Location of the slope w.r.t. the SWL [m]
-1.5
-1
-0.5
0
0.5
1
1.5
profile change expresed in damage parameterE3D,1 [Profile change/dn50]
Profile change expressed in the damage parameter E3D,1 of test 2E for the 1:8 slope
Width of the flume [m]
0.2
0.4
0.6
0.8
-2.5
-2
-1.5
-1
-0.5
0
0.5
1
1.5
Location of the slope w.r.t. the SWL [m]
-1.5
-1
-0.5
0
0.5
1
1.5
profile change expresed in damage parameterE3D,1 [Profile change/dn50]

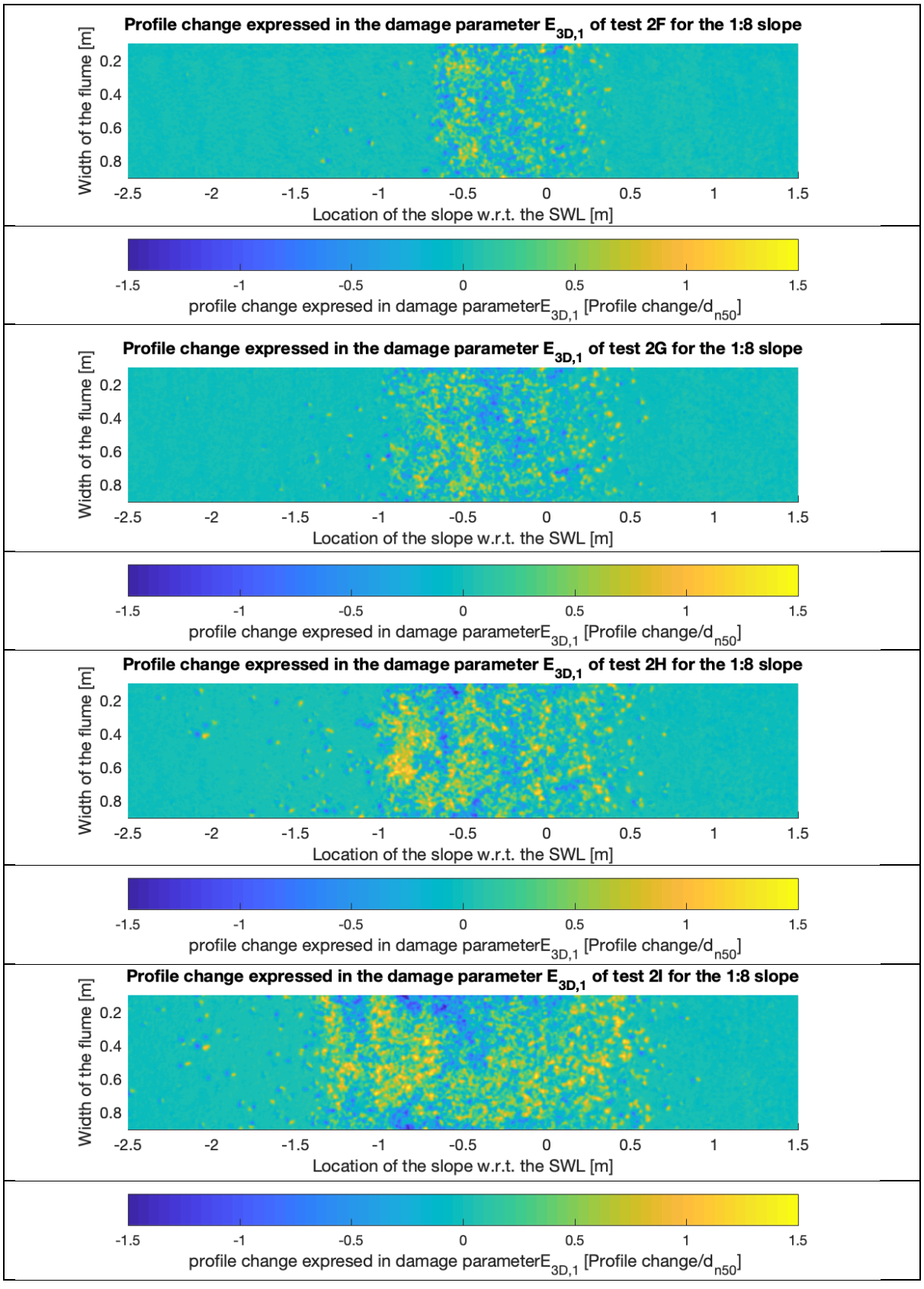
Profile change expressed in the damage parameter E3D,1 of test 2F for the 1:8 slope
Width of the flume [m]
0.2
0.4
0.6
0.8
-2.5
-2
-1.5
-1
-0.5
0
0.5
1
1.5
Location of the slope w.r.t. the SWL [m]
-1.5
-1
-0.5
0
0.5
1
1.5
profile change expresed in damage parameterE3D,1 [Profile change/dn50]
Profile change expressed in the damage parameter E3D,1 of test 2G for the 1:8 slope
Width of the flume [m]
0.2
0.4
0.6
0.8
-2.5
-2
-1.5
-1
-0.5
0
0.5
1
1.5
Location of the slope w.r.t. the SWL [m]
-1.5
-1
-0.5
0
0.5
1
1.5
profile change expresed in damage parameterE3D,1 [Profile change/dn50]
Profile change expressed in the damage parameter E3D,1 of test 2H for the 1:8 slope
Width of the flume [m]
0.2
0.4
0.6
0.8
-2.5
-2
-1.5
-1
-0.5
0
0.5
1
1.5
Location of the slope w.r.t. the SWL [m]
-1.5
-1
-0.5
0
0.5
1
1.5
profile change expresed in damage parameterE3D,1 [Profile change/dn50]
Profile change expressed in the damage parameter E3D,1 of test 2I for the 1:8 slope
Width of the flume [m]
0.2
0.4
0.6
0.8
-2.5
-2
-1.5
-1
-0.5
0
0.5
1
1.5
Location of the slope w.r.t. the SWL [m]
-1.5
-1
-0.5
0
0.5
1
1.5
profile change expresed in damage parameterE3D,1 [Profile change/dn50]

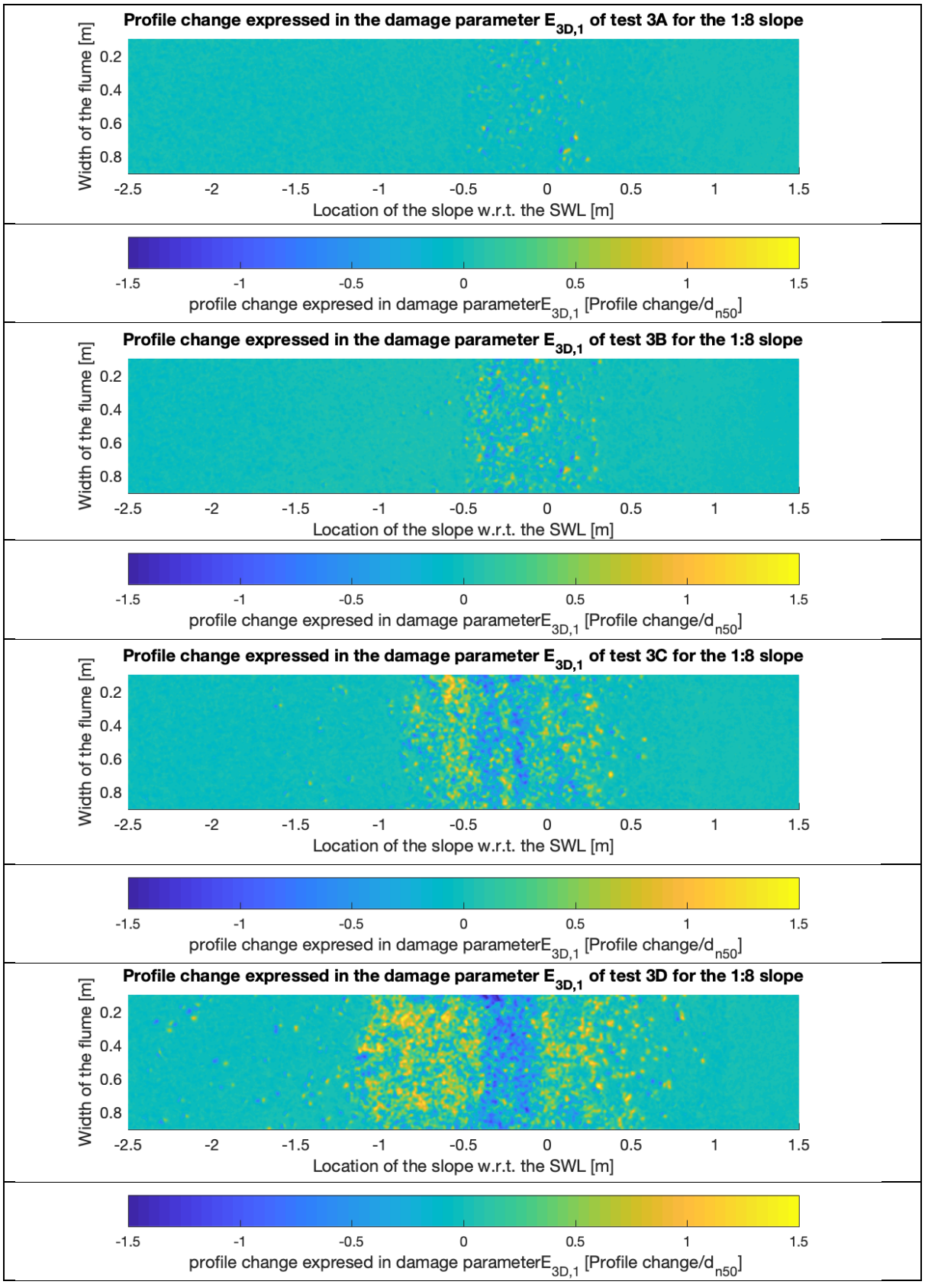
Profile change expressed in the damage parameter E3D,1 of test 3A for the 1:8 slope
Width of the flume [m]
0.2
0.4
0.6
0.8
-2.5
-2
-1.5
-1
-0.5
0
0.5
1
1.5
Location of the slope w.r.t. the SWL [m]
-1.5
-1
-0.5
0
0.5
1
1.5
profile change expresed in damage parameterE3D,1 [Profile change/dn50]
Profile change expressed in the damage parameter E3D,1 of test 3B for the 1:8 slope
Width of the flume [m]
0.2
0.4
0.6
0.8
-2.5
-2
-1.5
-1
-0.5
0
0.5
1
1.5
Location of the slope w.r.t. the SWL [m]
-1.5
-1
-0.5
0
0.5
1
1.5
profile change expresed in damage parameterE3D,1 [Profile change/dn50]
Profile change expressed in the damage parameter E3D,1 of test 3C for the 1:8 slope
Width of the flume [m]
0.2
0.4
0.6
0.8
-2.5
-2
-1.5
-1
-0.5
0
0.5
1
1.5
Location of the slope w.r.t. the SWL [m]
-1.5
-1
-0.5
0
0.5
1
1.5
profile change expresed in damage parameterE3D,1 [Profile change/dn50]
Profile change expressed in the damage parameter E3D,1 of test 3D for the 1:8 slope
Width of the flume [m]
0.2
0.4
0.6
0.8
-2.5
-2
-1.5
-1
-0.5
0
0.5
1
1.5
Location of the slope w.r.t. the SWL [m]
-1.5
-1
-0.5
0
0.5
1
1.5
profile change expresed in damage parameterE3D,1 [Profile change/dn50]

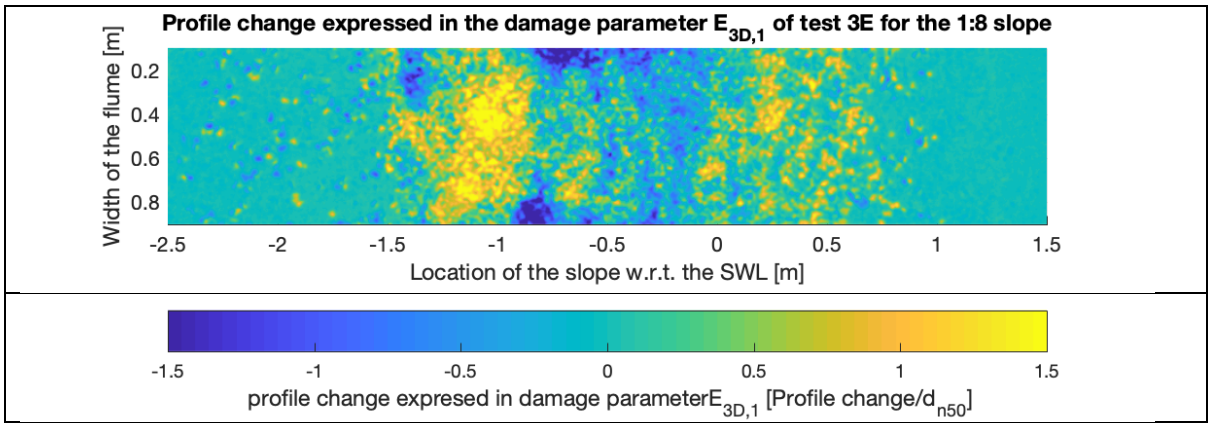
Profile change expressed in the damage parameter E3D,1 of test 3E for the 1:8 slope
Width of the flume [m]
0.2
0.4
0.6
0.8
-2.5
-2
-1.5
-1
-0.5
0
0.5
1
1.5
Location of the slope w.r.t. the SWL [m]
-1.5
-1
-0.5
0
0.5
1
1.5
profile change expresed in damage parameterE3D,1 [Profile change/dn50]

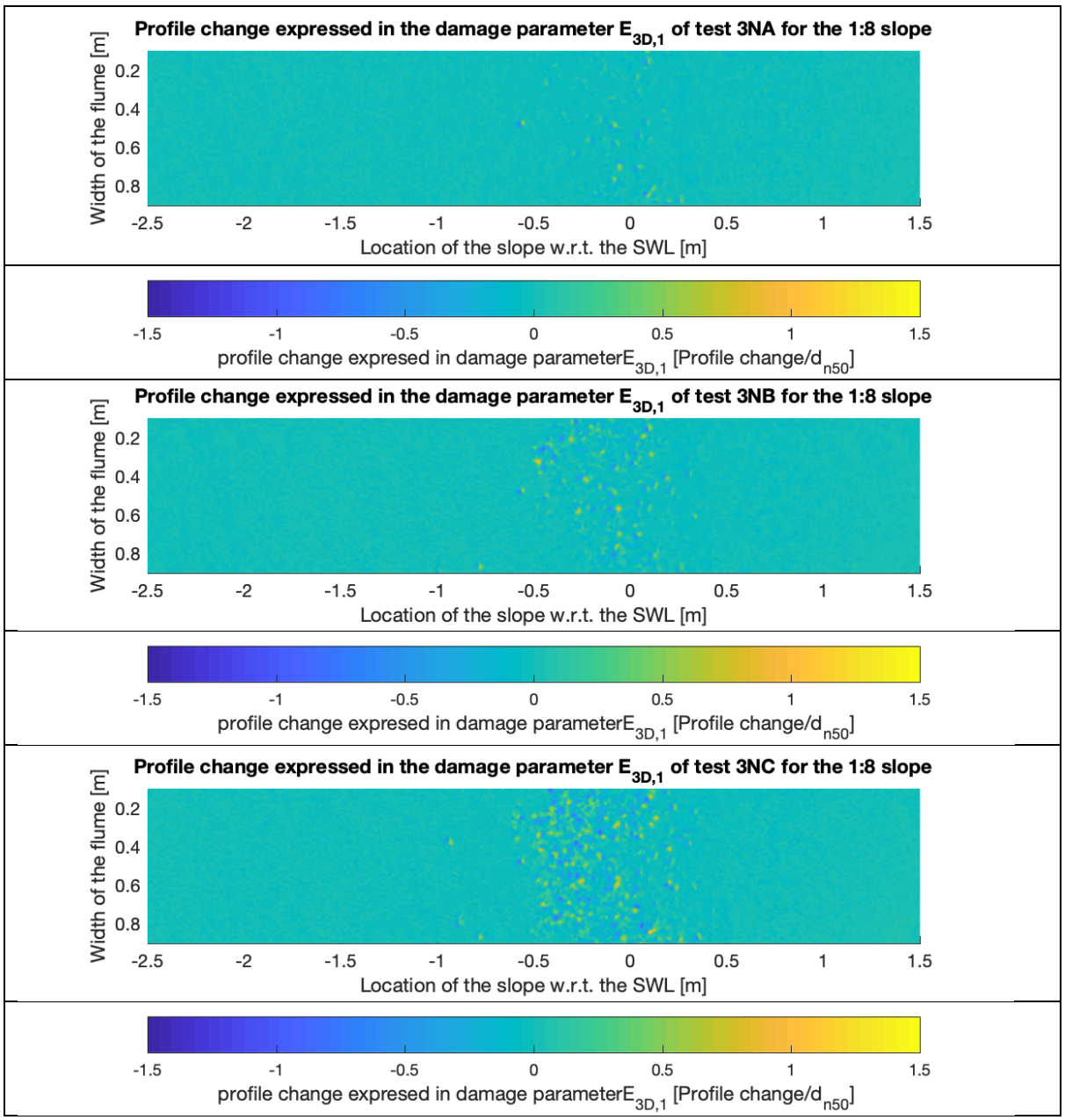
Profile change expressed in the damage parameter E3D,1 of test 3NA for the 1:8 slope
Width of the flume [m]
0.2
0.4
0.6
0.8
-2.5
-2
-1.5
-1
-0.5
0
0.5
1
1.5
Location of the slope w.r.t. the SWL [m]
-1.5
-1
-0.5
0
0.5
1
1.5
profile change expresed in damage parameterE3D,1 [Profile change/dn50]
Profile change expressed in the damage parameter E3D,1 of test 3NB for the 1:8 slope
Width of the flume [m]
0.2
0.4
0.6
0.8
-2.5
-2
-1.5
-1
-0.5
0
0.5
1
1.5
Location of the slope w.r.t. the SWL [m]
-1.5
-1
-0.5
0
0.5
1
1.5
profile change expresed in damage parameterE3D,1 [Profile change/dn50]
Profile change expressed in the damage parameter E3D,1 of test 3NC for the 1:8 slope
Width of the flume [m]
0.2
0.4
0.6
0.8
-2.5
-2
-1.5
-1
-0.5
0
0.5
1
1.5
Location of the slope w.r.t. the SWL [m]
-1.5
-1
-0.5
0
0.5
1
1.5
profile change expresed in damage parameterE3D,1 [Profile change/dn50]

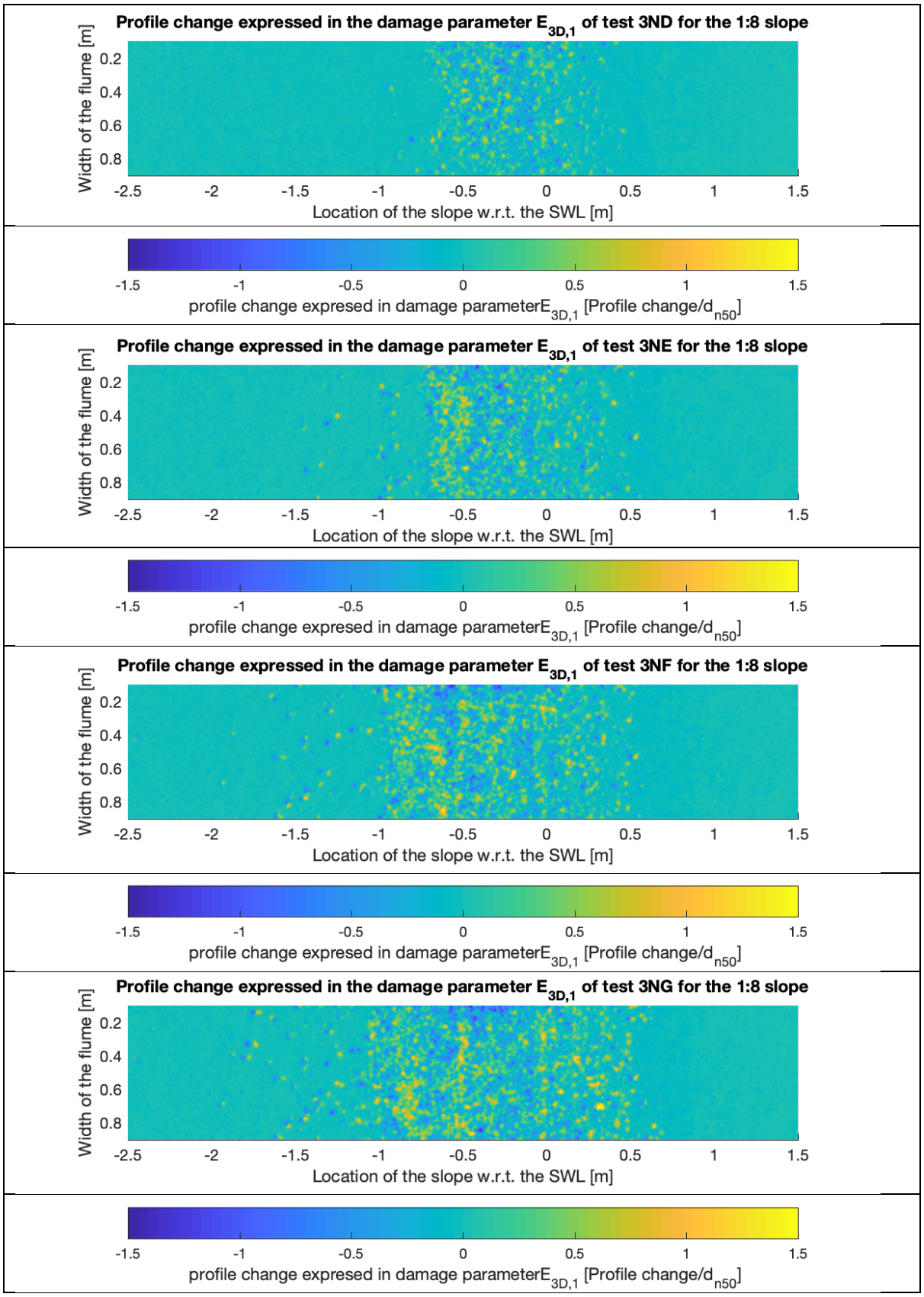
Profile change expressed in the damage parameter E3D,1 of test 3ND for the 1:8 slope
Width of the flume [m]
0.2
0.4
0.6
0.8
-2.5
-2
-1.5
-1
-0.5
0
0.5
1
1.5
Location of the slope w.r.t. the SWL [m]
-1.5
-1
-0.5
0
0.5
1
1.5
profile change expresed in damage parameterE3D,1 [Profile change/dn50]
Profile change expressed in the damage parameter E3D,1 of test 3NE for the 1:8 slope
Width of the flume [m]
0.2
0.4
0.6
0.8
-2.5
-2
-1.5
-1
-0.5
0
0.5
1
1.5
Location of the slope w.r.t. the SWL [m]
-1.5
-1
-0.5
0
0.5
1
1.5
profile change expresed in damage parameterE3D,1 [Profile change/dn50]
Profile change expressed in the damage parameter E3D,1 of test 3NF for the 1:8 slope
Width of the flume [m]
0.2
0.4
0.6
0.8
-2.5
-2
-1.5
-1
-0.5
0
0.5
1
1.5
Location of the slope w.r.t. the SWL [m]
-1.5
-1
-0.5
0
0.5
1
1.5
profile change expresed in damage parameterE3D,1 [Profile change/dn50]
Profile change expressed in the damage parameter E3D,1 of test 3NG for the 1:8 slope
Width of the flume [m]
0.2
0.4
0.6
0.8
-2.5
-2
-1.5
-1
-0.5
0
0.5
1
1.5
Location of the slope w.r.t. the SWL [m]
-1.5
-1
-0.5
0
0.5
1
1.5
profile change expresed in damage parameterE3D,1 [Profile change/dn50]

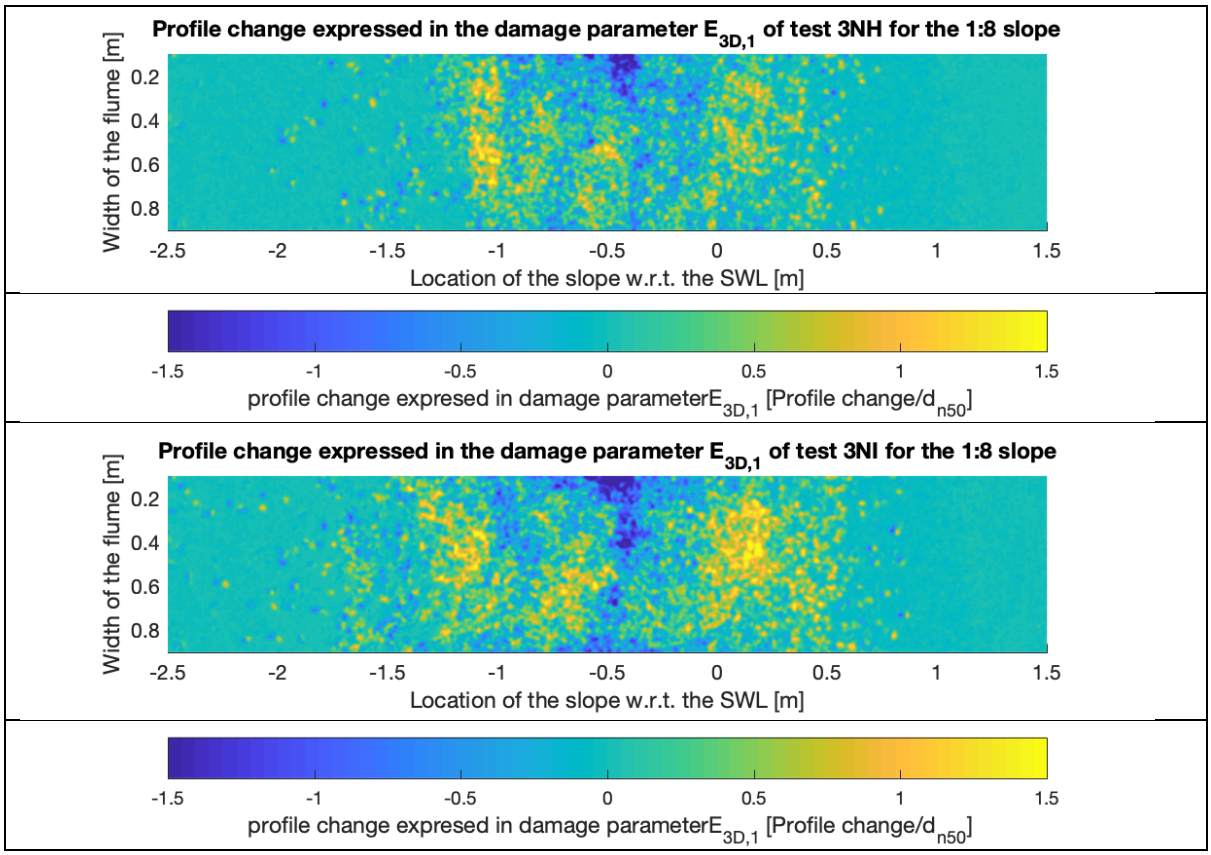
Profile change expressed in the damage parameter E3D,1 of test 3NH for the 1:8 slope
Width of the flume [m]
0.2
0.4
0.6
0.8
-2.5
-2
-1.5
-1
-0.5
0
0.5
1
1.5
Location of the slope w.r.t. the SWL [m]
-1.5
-1
-0.5
0
0.5
1
1.5
profile change expresed in damage parameterE3D,1 [Profile change/dn50]
Profile change expressed in the damage parameter E3D,1 of test 3NI for the 1:8 slope
Width of the flume [m]
0.2
0.4
0.6
0.8
-2.5
-2
-1.5
-1
-0.5
0
0.5
1
1.5
Location of the slope w.r.t. the SWL [m]
-1.5
-1
-0.5
0
0.5
1
1.5
profile change expresed in damage parameterE3D,1 [Profile change/dn50]

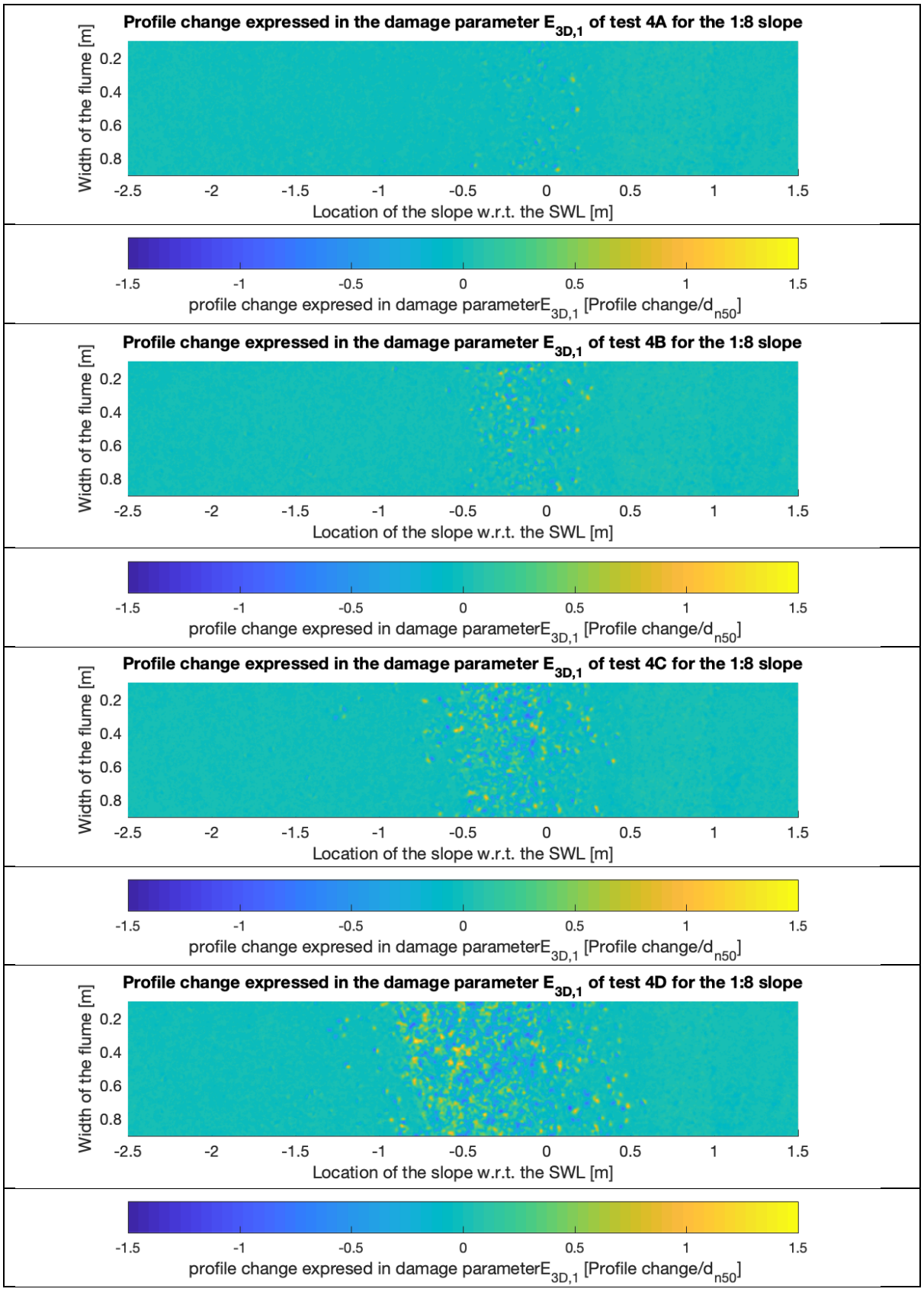
Profile change expressed in the damage parameter E3D,1 of test 4A for the 1:8 slope
Width of the flume [m]
0.2
0.4
0.6
0.8
-2.5
-2
-1.5
-1
-0.5
0
0.5
1
1.5
Location of the slope w.r.t. the SWL [m]
-1.5
-1
-0.5
0
0.5
1
1.5
profile change expresed in damage parameterE3D,1 [Profile change/dn50]
Profile change expressed in the damage parameter E3D,1 of test 4B for the 1:8 slope
Width of the flume [m]
0.2
0.4
0.6
0.8
-2.5
-2
-1.5
-1
-0.5
0
0.5
1
1.5
Location of the slope w.r.t. the SWL [m]
-1.5
-1
-0.5
0
0.5
1
1.5
profile change expresed in damage parameterE3D,1 [Profile change/dn50]
Profile change expressed in the damage parameter E3D,1 of test 4C for the 1:8 slope
Width of the flume [m]
0.2
0.4
0.6
0.8
-2.5
-2
-1.5
-1
-0.5
0
0.5
1
1.5
Location of the slope w.r.t. the SWL [m]
-1.5
-1
-0.5
0
0.5
1
1.5
profile change expresed in damage parameterE3D,1 [Profile change/dn50]
Profile change expressed in the damage parameter E3D,1 of test 4D for the 1:8 slope
Width of the flume [m]
0.2
0.4
0.6
0.8
-2.5
-2
-1.5
-1
-0.5
0
0.5
1
1.5
Location of the slope w.r.t. the SWL [m]
-1.5
-1
-0.5
0
0.5
1
1.5
profile change expresed in damage parameterE3D,1 [Profile change/dn50]

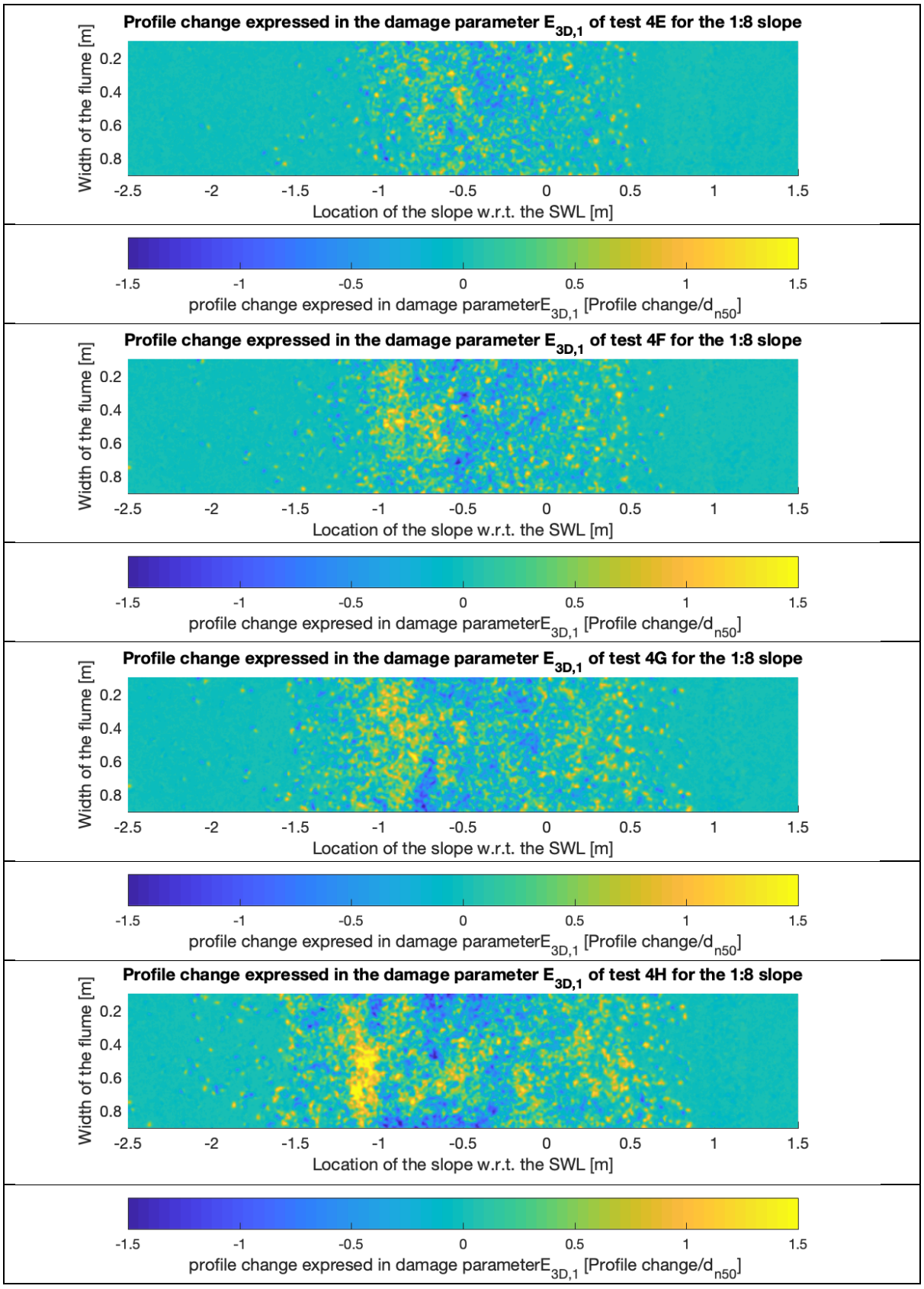
Profile change expressed in the damage parameter E3D,1 of test 4E for the 1:8 slope
Width of the flume [m]
0.2
0.4
0.6
0.8
-2.5
-2
-1.5
-1
-0.5
0
0.5
1
1.5
Location of the slope w.r.t. the SWL [m]
-1.5
-1
-0.5
0
0.5
1
1.5
profile change expresed in damage parameterE3D,1 [Profile change/dn50]
Profile change expressed in the damage parameter E3D,1 of test 4F for the 1:8 slope
Width of the flume [m]
0.2
0.4
0.6
0.8
-2.5
-2
-1.5
-1
-0.5
0
0.5
1
1.5
Location of the slope w.r.t. the SWL [m]
-1.5
-1
-0.5
0
0.5
1
1.5
profile change expresed in damage parameterE3D,1 [Profile change/dn50]
Profile change expressed in the damage parameter E3D,1 of test 4G for the 1:8 slope
Width of the flume [m]
0.2
0.4
0.6
0.8
-2.5
-2
-1.5
-1
-0.5
0
0.5
1
1.5
Location of the slope w.r.t. the SWL [m]
-1.5
-1
-0.5
0
0.5
1
1.5
profile change expresed in damage parameterE3D,1 [Profile change/dn50]
Profile change expressed in the damage parameter E3D,1 of test 4H for the 1:8 slope
Width of the flume [m]
0.2
0.4
0.6
0.8
-2.5
-2
-1.5
-1
-0.5
0
0.5
1
1.5
Location of the slope w.r.t. the SWL [m]
-1.5
-1
-0.5
0
0.5
1
1.5
profile change expresed in damage parameterE3D,1 [Profile change/dn50]

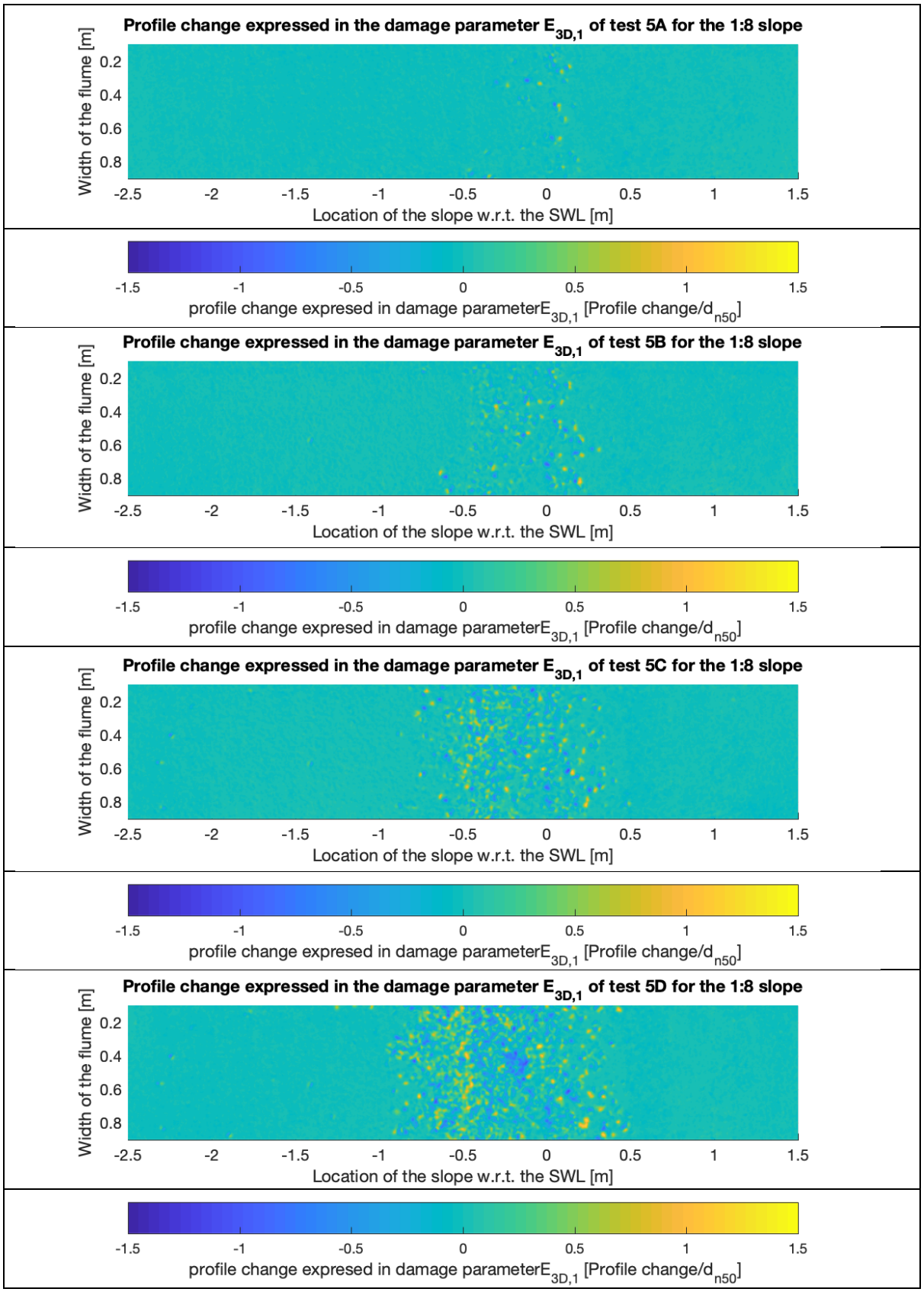
Profile change expressed in the damage parameter E3D,1 of test 5A for the 1:8 slope
Width of the flume [m]
0.2
0.4
0.6
0.8
-2.5
-2
-1.5
-1
-0.5
0
0.5
1
1.5
Location of the slope w.r.t. the SWL [m]
-1.5
-1
-0.5
0
0.5
1
1.5
profile change expresed in damage parameterE3D,1 [Profile change/dn50]
Profile change expressed in the damage parameter E3D,1 of test 5B for the 1:8 slope
Width of the flume [m]
0.2
0.4
0.6
0.8
-2.5
-2
-1.5
-1
-0.5
0
0.5
1
1.5
Location of the slope w.r.t. the SWL [m]
-1.5
-1
-0.5
0
0.5
1
1.5
profile change expresed in damage parameterE3D,1 [Profile change/dn50]
Profile change expressed in the damage parameter E3D,1 of test 5C for the 1:8 slope
Width of the flume [m]
0.2
0.4
0.6
0.8
-2.5
-2
-1.5
-1
-0.5
0
0.5
1
1.5
Location of the slope w.r.t. the SWL [m]
-1.5
-1
-0.5
0
0.5
1
1.5
profile change expresed in damage parameterE3D,1 [Profile change/dn50]
Profile change expressed in the damage parameter E3D,1 of test 5D for the 1:8 slope
Width of the flume [m]
0.2
0.4
0.6
0.8
-2.5
-2
-1.5
-1
-0.5
0
0.5
1
1.5
Location of the slope w.r.t. the SWL [m]
-1.5
-1
-0.5
0
0.5
1
1.5
profile change expresed in damage parameterE3D,1 [Profile change/dn50]

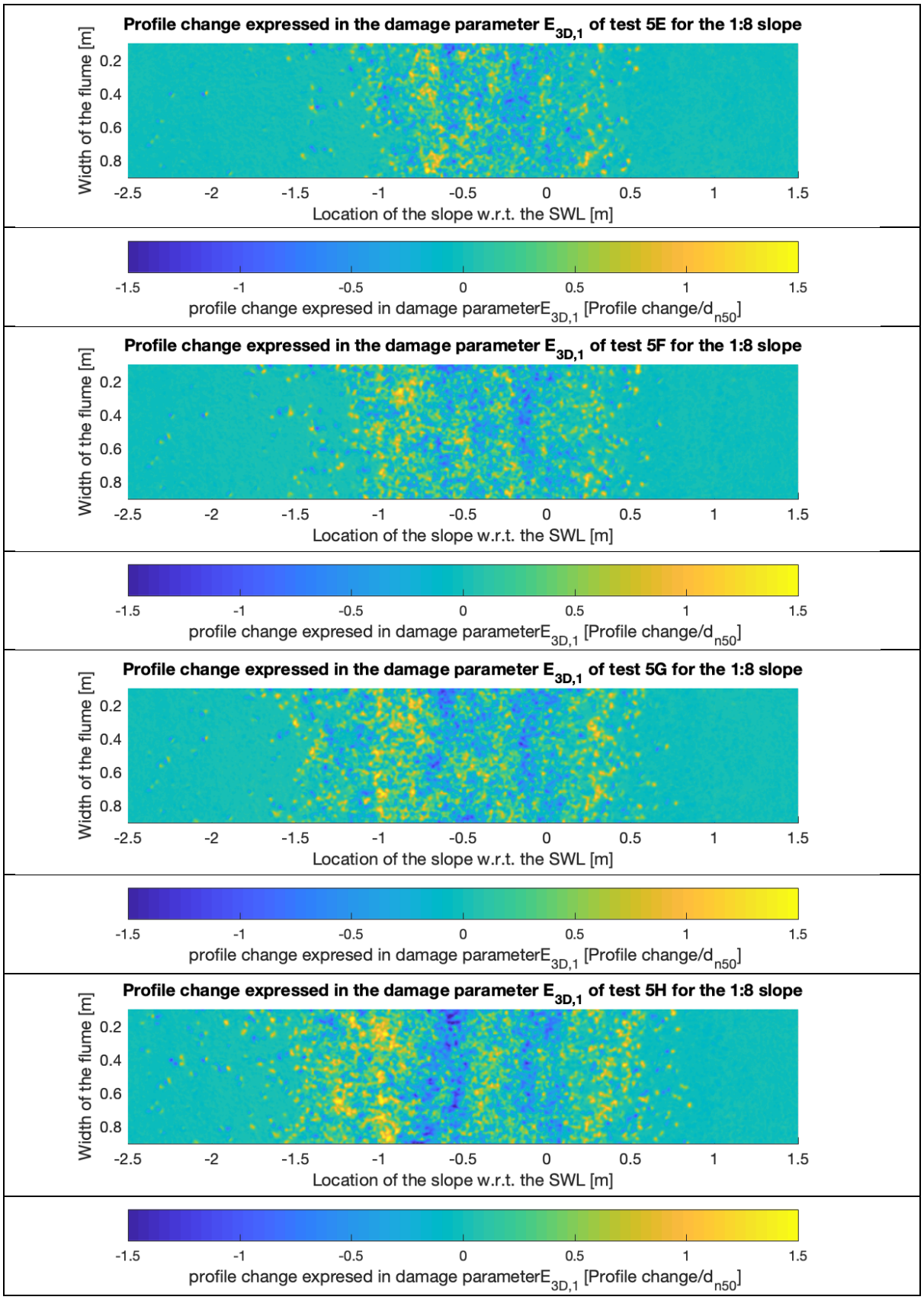
Profile change expressed in the damage parameter E3D,1 of test 5E for the 1:8 slope
Width of the flume [m]
0.2
0.4
0.6
0.8
-2.5
-2
-1.5
-1
-0.5
0
0.5
1
1.5
Location of the slope w.r.t. the SWL [m]
profile change expresed in damage parameterE3D,1 [Profile change/dn50]
Profile change expressed in the damage parameter E3D,1 of test 5F for the 1:8 slope
Width of the flume [m]
Location of the slope w.r.t. the SWL [m]
profile change expresed in damage parameterE3D,1 [Profile change/dn50]
Profile change expressed in the damage parameter E3D,1 of test 5G for the 1:8 slope
Width of the flume [m]
Location of the slope w.r.t. the SWL [m]
profile change expresed in damage parameterE3D,1 [Profile change/dn50]
Profile change expressed in the damage parameter E3D,1 of test 5H for the 1:8 slope
Width of the flume [m]
Location of the slope w.r.t. the SWL [m]
profile change expresed in damage parameterE3D,1 [Profile change/dn50]

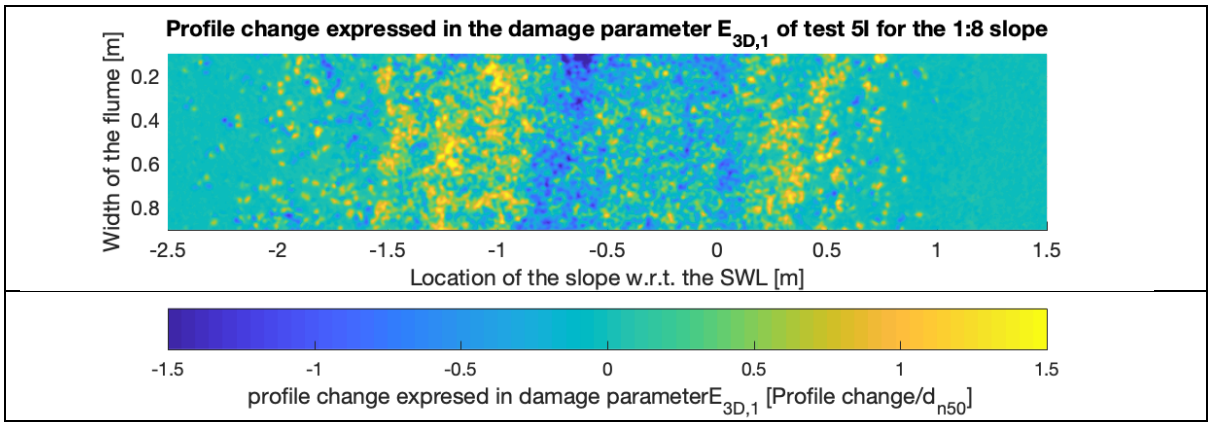
Profile change expressed in the damage parameter E3D,1 of test 5l for the 1:8 slope
Width of the flume [m]
0.2
0.4
0.6
0.8
-2.5
-2
-1.5
-1
-0.5
0
0.5
1
1.5
Location of the slope w.r.t. the SWL [m]
-1.5
-1
-0.5
0
0.5
1
1.5
profile change expresed in damage parameterE3D,1 [Profile change/dn50]

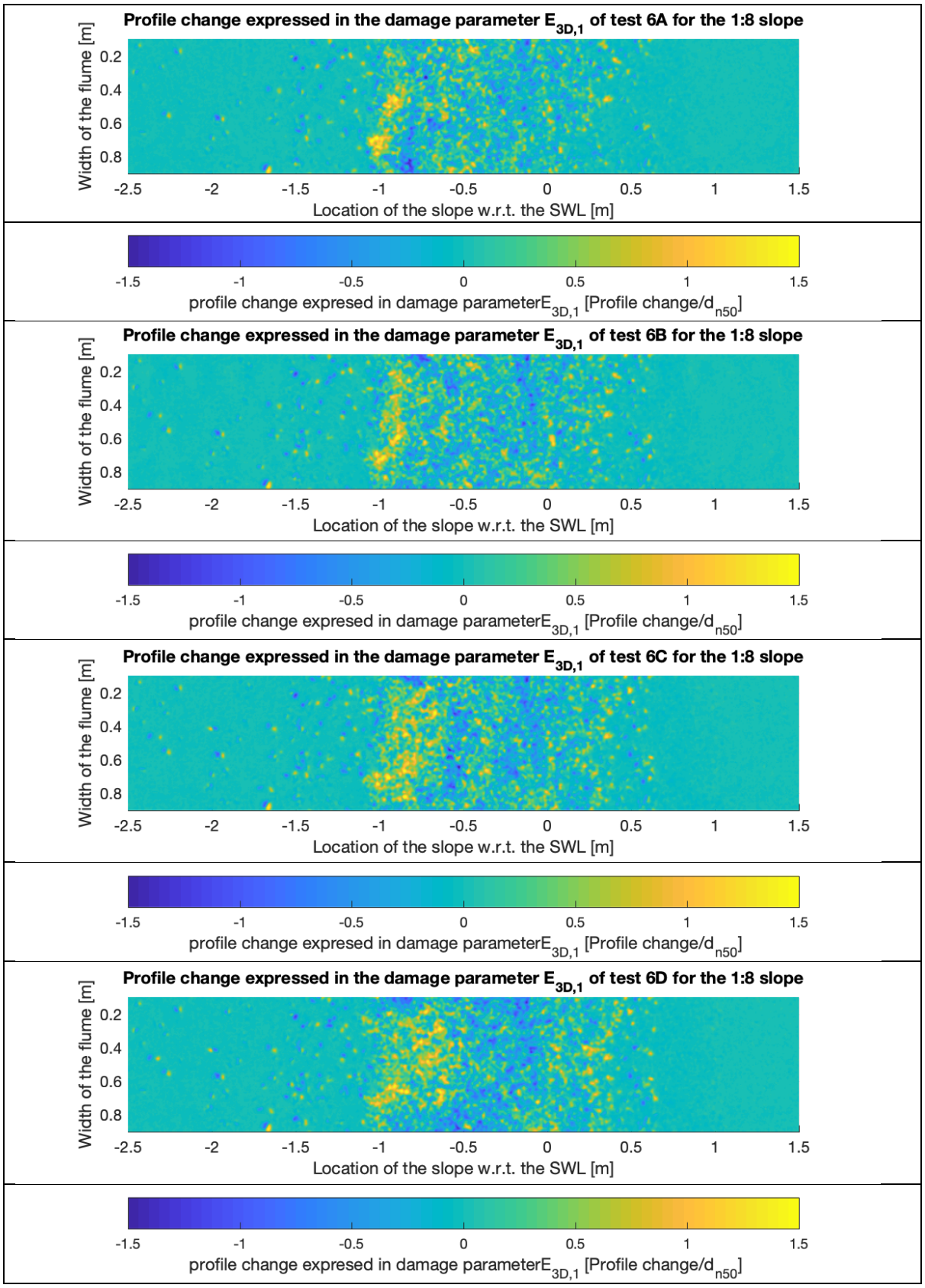
Profile change expressed in the damage parameter E3D,1 of test 6A for the 1:8 slope
Width of the flume [m]
0.2
0.4
0.6
0.8
-2.5
-2
-1.5
-1
-0.5
0
0.5
1
1.5
Location of the slope w.r.t. the SWL [m]
-1.5
-1
-0.5
0
0.5
1
1.5
profile change expresed in damage parameterE3D,1 [Profile change/dn50]
Profile change expressed in the damage parameter E3D,1 of test 6B for the 1:8 slope
Width of the flume [m]
0.2
0.4
0.6
0.8
-2.5
-2
-1.5
-1
-0.5
0
0.5
1
1.5
Location of the slope w.r.t. the SWL [m]
-1.5
-1
-0.5
0
0.5
1
1.5
profile change expresed in damage parameterE3D,1 [Profile change/dn50]
Profile change expressed in the damage parameter E3D,1 of test 6C for the 1:8 slope
Width of the flume [m]
0.2
0.4
0.6
0.8
-2.5
-2
-1.5
-1
-0.5
0
0.5
1
1.5
Location of the slope w.r.t. the SWL [m]
-1.5
-1
-0.5
0
0.5
1
1.5
profile change expresed in damage parameterE3D,1 [Profile change/dn50]
Profile change expressed in the damage parameter E3D,1 of test 6D for the 1:8 slope
Width of the flume [m]
0.2
0.4
0.6
0.8
-2.5
-2
-1.5
-1
-0.5
0
0.5
1
1.5
Location of the slope w.r.t. the SWL [m]
-1.5
-1
-0.5
0
0.5
1
1.5
profile change expresed in damage parameterE3D,1 [Profile change/dn50]

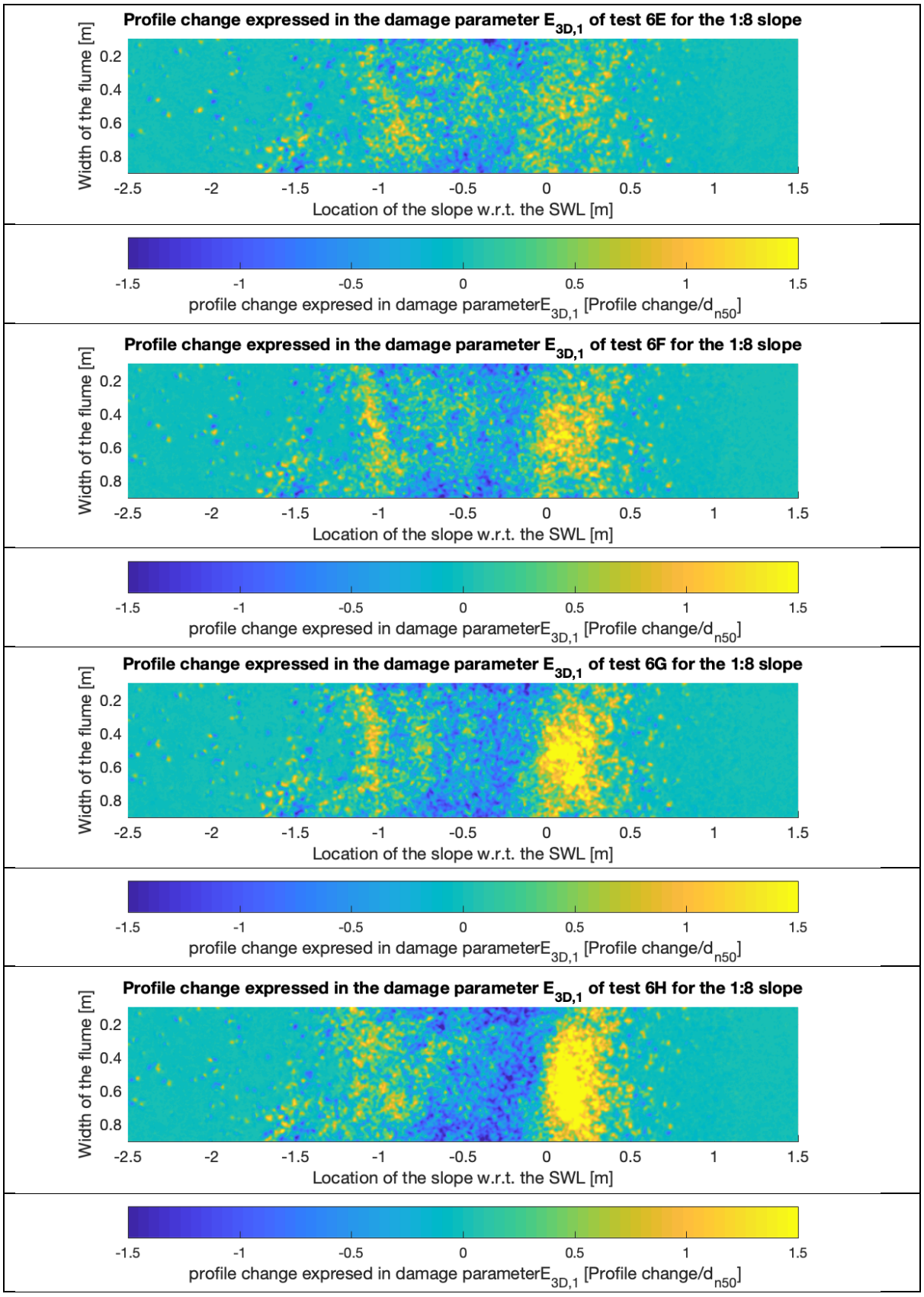
Profile change expressed in the damage parameter E3D,1 of test 6E for the 1:8 slope
Width of the flume [m]
0.2
0.4
0.6
0.8
-2.5
-2
-1.5
-1
-0.5
0
0.5
1
1.5
Location of the slope w.r.t. the SWL [m]
profile change expresed in damage parameterE3D,1 [Profile change/dn50]
Profile change expressed in the damage parameter E3D,1 of test 6F for the 1:8 slope
Width of the flume [m]
Location of the slope w.r.t. the SWL [m]
profile change expresed in damage parameterE3D,1 [Profile change/dn50]
Profile change expressed in the damage parameter E3D,1 of test 6G for the 1:8 slope
Width of the flume [m]
Location of the slope w.r.t. the SWL [m]
profile change expresed in damage parameterE3D,1 [Profile change/dn50]
Profile change expressed in the damage parameter E3D,1 of test 6H for the 1:8 slope
Width of the flume [m]
Location of the slope w.r.t. the SWL [m]
profile change expresed in damage parameterE3D,1 [Profile change/dn50]

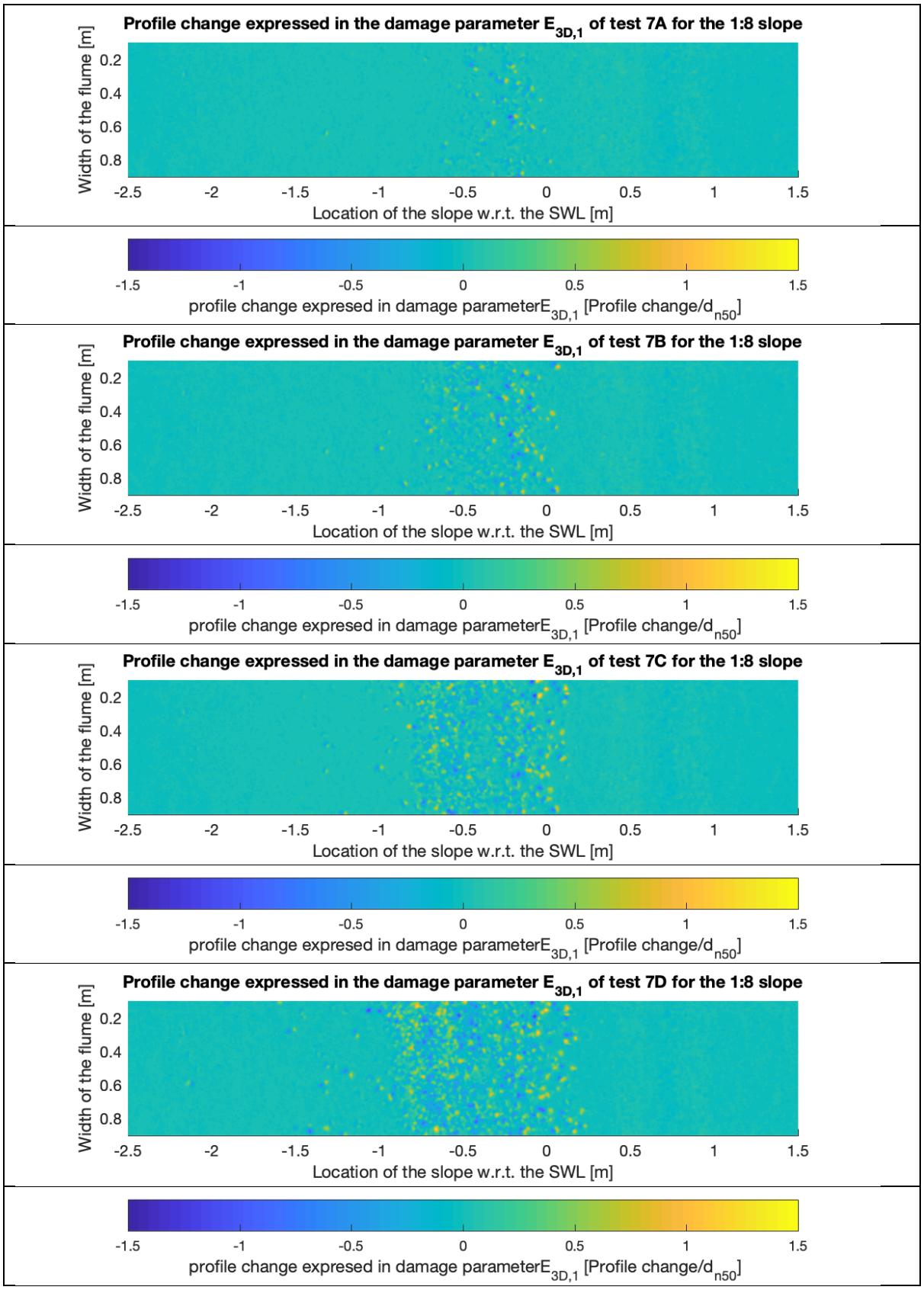
Profile change expressed in the damage parameter E3D,1 of test 7A for the 1:8 slope
Width of the flume [m]
0.2
0.4
0.6
0.8
-2.5
-2
-1.5
-1
-0.5
0
0.5
1
1.5
Location of the slope w.r.t. the SWL [m]
-1.5
-1
-0.5
0
0.5
1
1.5
profile change expresed in damage parameterE3D,1 [Profile change/dn50]
Profile change expressed in the damage parameter E3D,1 of test 7B for the 1:8 slope
Width of the flume [m]
0.2
0.4
0.6
0.8
-2.5
-2
-1.5
-1
-0.5
0
0.5
1
1.5
Location of the slope w.r.t. the SWL [m]
-1.5
-1
-0.5
0
0.5
1
1.5
profile change expresed in damage parameterE3D,1 [Profile change/dn50]
Profile change expressed in the damage parameter E3D,1 of test 7C for the 1:8 slope
Width of the flume [m]
0.2
0.4
0.6
0.8
-2.5
-2
-1.5
-1
-0.5
0
0.5
1
1.5
Location of the slope w.r.t. the SWL [m]
-1.5
-1
-0.5
0
0.5
1
1.5
profile change expresed in damage parameterE3D,1 [Profile change/dn50]
Profile change expressed in the damage parameter E3D,1 of test 7D for the 1:8 slope
Width of the flume [m]
0.2
0.4
0.6
0.8
-2.5
-2
-1.5
-1
-0.5
0
0.5
1
1.5
Location of the slope w.r.t. the SWL [m]
-1.5
-1
-0.5
0
0.5
1
1.5
profile change expresed in damage parameterE3D,1 [Profile change/dn50]

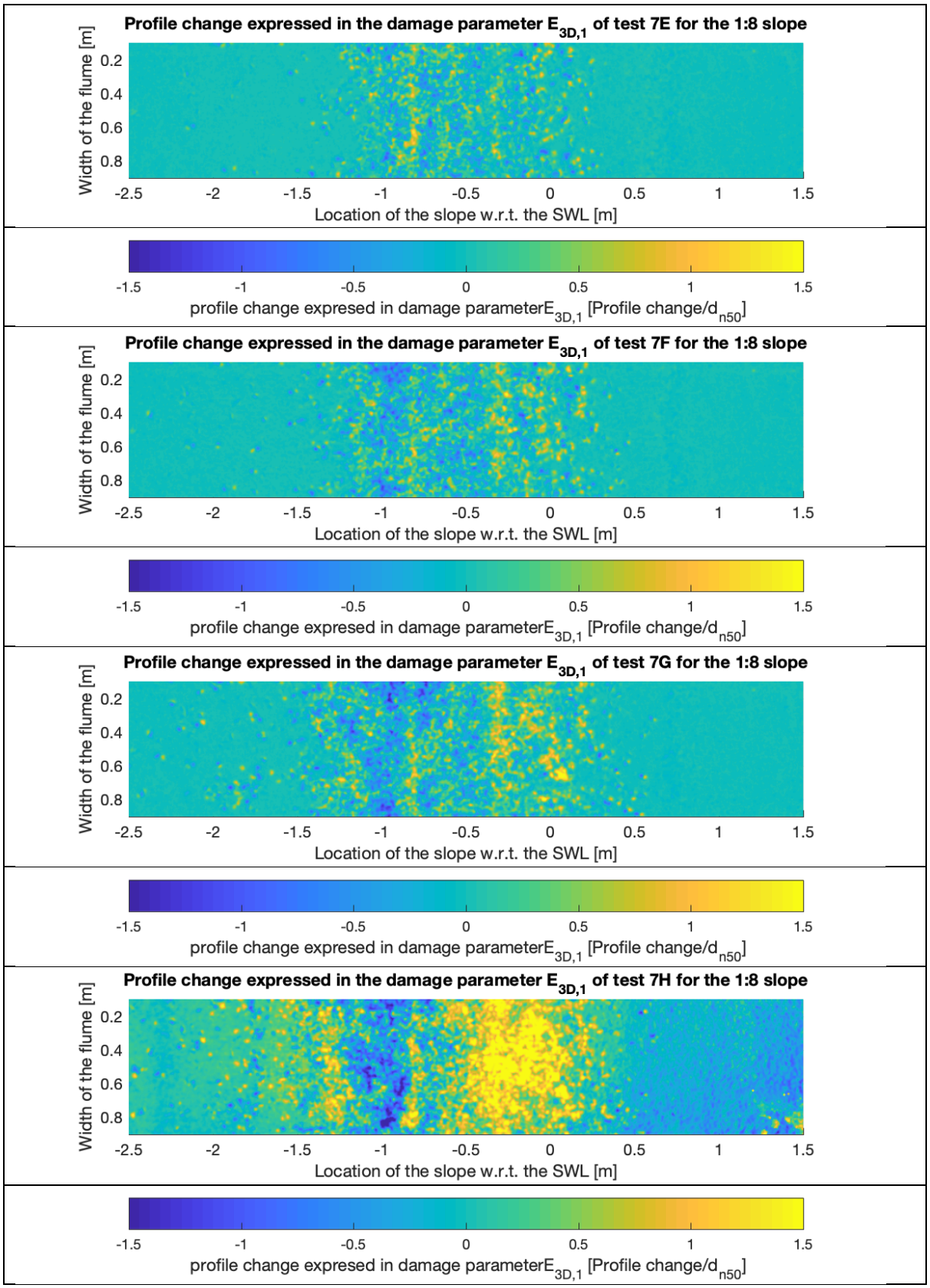
Profile change expressed in the damage parameter E3D,1 of test 7E for the 1:8 slope
Width of the flume [m]
0.2
0.4
0.6
0.8
-2.5
-2
-1.5
-1
-0.5
0
0.5
1
1.5
Location of the slope w.r.t. the SWL [m]
-1.5
-1
-0.5
0
0.5
1
1.5
profile change expresed in damage parameterE3D,1 [Profile change/dn50]
Profile change expressed in the damage parameter E3D,1 of test 7F for the 1:8 slope
Width of the flume [m]
0.2
0.4
0.6
0.8
-2.5
-2
-1.5
-1
-0.5
0
0.5
1
1.5
Location of the slope w.r.t. the SWL [m]
-1.5
-1
-0.5
0
0.5
1
1.5
profile change expresed in damage parameterE3D,1 [Profile change/dn50]
Profile change expressed in the damage parameter E3D,1 of test 7G for the 1:8 slope
Width of the flume [m]
0.2
0.4
0.6
0.8
-2.5
-2
-1.5
-1
-0.5
0
0.5
1
1.5
Location of the slope w.r.t. the SWL [m]
-1.5
-1
-0.5
0
0.5
1
1.5
profile change expresed in damage parameterE3D,1 [Profile change/dn50]
Profile change expressed in the damage parameter E3D,1 of test 7H for the 1:8 slope
Width of the flume [m]
0.2
0.4
0.6
0.8
-2.5
-2
-1.5
-1
-0.5
0
0.5
1
1.5
Location of the slope w.r.t. the SWL [m]
-1.5
-1
-0.5
0
0.5
1
1.5
profile change expresed in damage parameterE3D,1 [Profile change/dn50]

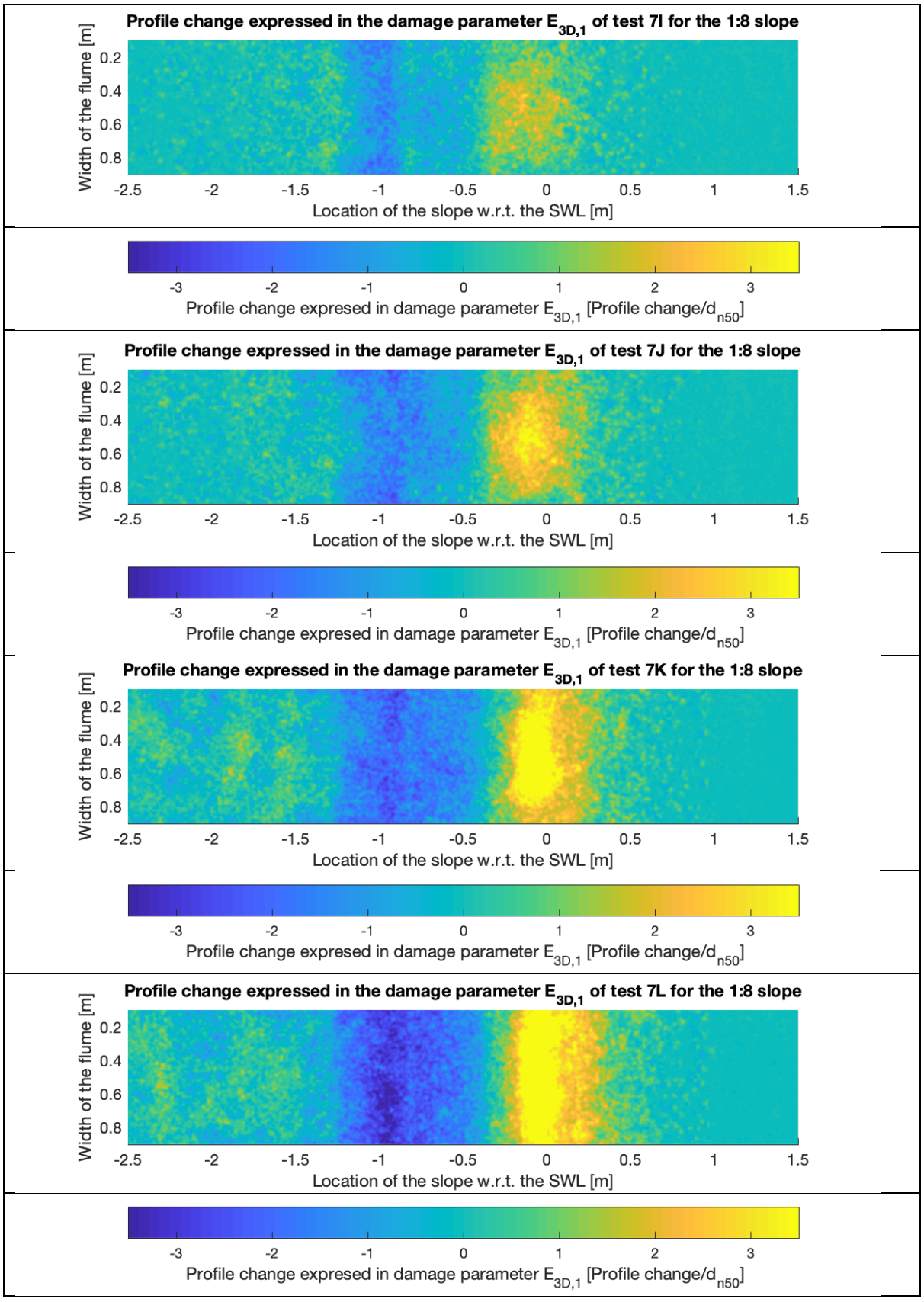
Profile change expressed in the damage parameter E3D,1 of test 7I for the 1:8 slope
Width of the flume [m]
0.2
0.4
0.6
0.8
-2.5
-2
-1.5
-1
-0.5
0
0.5
1
1.5
Location of the slope w.r.t. the SWL [m]
-3
-2
-1
0
1
2
3
Profile change expresed in damage parameter E3D,1 [Profile change/dn50]
Profile change expressed in the damage parameter E3D,1 of test 7J for the 1:8 slope
Width of the flume [m]
0.2
0.4
0.6
0.8
-2.5
-2
-1.5
-1
-0.5
0
0.5
1
1.5
Location of the slope w.r.t. the SWL [m]
-3
-2
-1
0
1
2
3
Profile change expresed in damage parameter E3D,1 [Profile change/dn50]
Profile change expressed in the damage parameter E3D,1 of test 7K for the 1:8 slope
Width of the flume [m]
0.2
0.4
0.6
0.8
-2.5
-2
-1.5
-1
-0.5
0
0.5
1
1.5
Location of the slope w.r.t. the SWL [m]
-3
-2
-1
0
1
2
3
Profile change expresed in damage parameter E3D,1 [Profile change/dn50]
Profile change expressed in the damage parameter E3D,1 of test 7L for the 1:8 slope
Width of the flume [m]
0.2
0.4
0.6
0.8
-2.5
-2
-1.5
-1
-0.5
0
0.5
1
1.5
Location of the slope w.r.t. the SWL [m]
-3
-2
-1
0
1
2
3
Profile change expresed in damage parameter E3D,1 [Profile change/dn50]

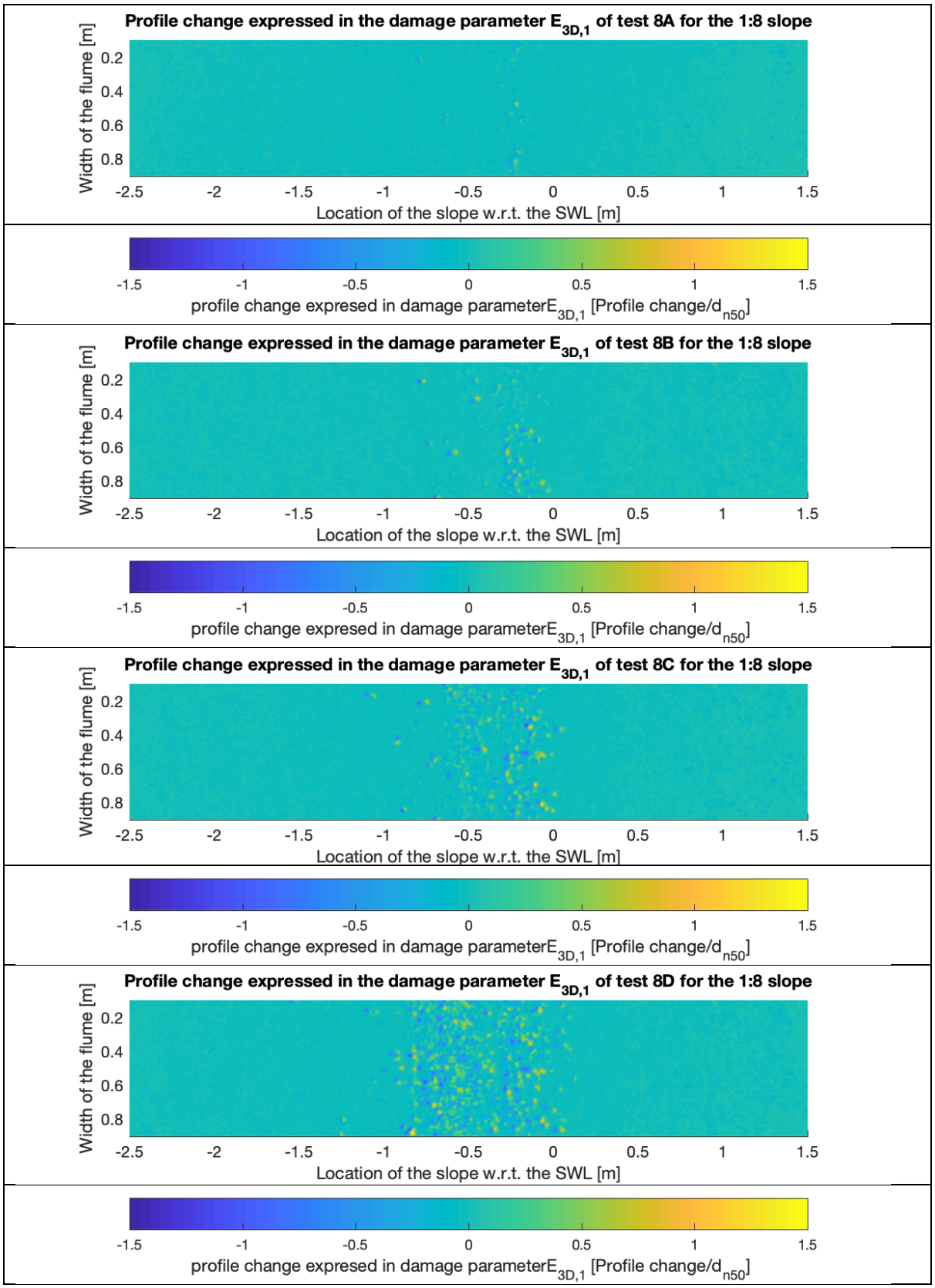
Profile change expressed in the damage parameter E3D,1 of test 8A for the 1:8 slope
Width of the flume [m]
0.2
0.4
0.6
0.8
-2.5
-2
-1.5
-1
-0.5
0
0.5
1
1.5
Location of the slope w.r.t. the SWL [m]
-1.5
-1
-0.5
0
0.5
1
1.5
profile change expresed in damage parameterE3D,1 [Profile change/dn50]
Profile change expressed in the damage parameter E3D,1 of test 8B for the 1:8 slope
Width of the flume [m]
0.2
0.4
0.6
0.8
-2.5
-2
-1.5
-1
-0.5
0
0.5
1
1.5
Location of the slope w.r.t. the SWL [m]
-1.5
-1
-0.5
0
0.5
1
1.5
profile change expresed in damage parameterE3D,1 [Profile change/dn50]
Profile change expressed in the damage parameter E3D,1 of test 8C for the 1:8 slope
Width of the flume [m]
0.2
0.4
0.6
0.8
-2.5
-2
-1.5
-1
-0.5
0
0.5
1
1.5
Location of the slope w.r.t. the SWL [m]
-1.5
-1
-0.5
0
0.5
1
1.5
profile change expresed in damage parameterE3D,1 [Profile change/dn50]
Profile change expressed in the damage parameter E3D,1 of test 8D for the 1:8 slope
Width of the flume [m]
0.2
0.4
0.6
0.8
-2.5
-2
-1.5
-1
-0.5
0
0.5
1
1.5
Location of the slope w.r.t. the SWL [m]
-1.5
-1
-0.5
0
0.5
1
1.5
profile change expresed in damage parameterE3D,1 [Profile change/dn50]

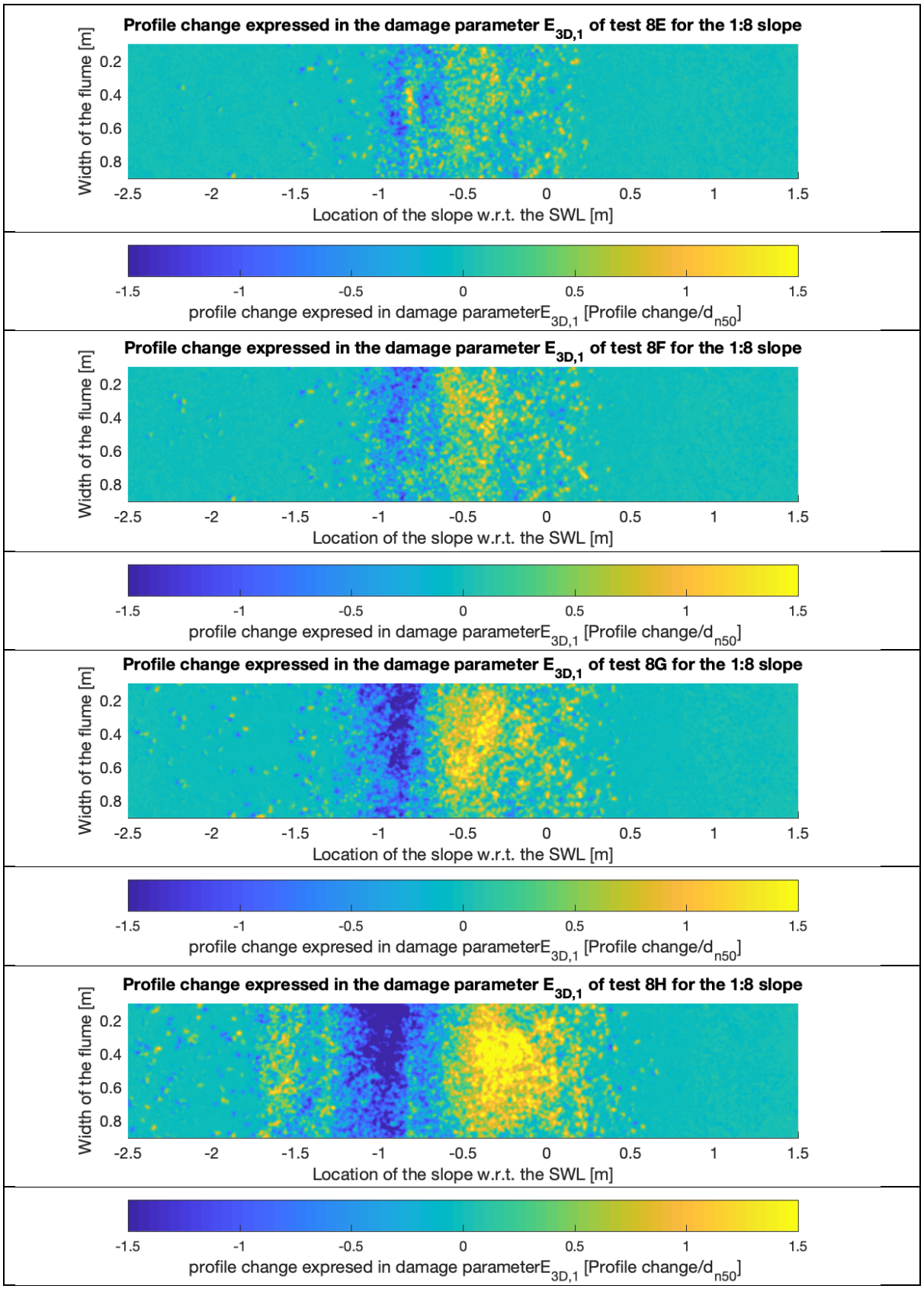
Profile change expressed in the damage parameter E3D,1 of test 8E for the 1:8 slope
Width of the flume [m]
0.2
0.4
0.6
0.8
-2.5
-2
-1.5
-1
-0.5
0
0.5
1
1.5
Location of the slope w.r.t. the SWL [m]
-1.5
-1
-0.5
0
0.5
1
1.5
profile change expresed in damage parameterE3D,1 [Profile change/dn50]
Profile change expressed in the damage parameter E3D,1 of test 8F for the 1:8 slope
Width of the flume [m]
0.2
0.4
0.6
0.8
-2.5
-2
-1.5
-1
-0.5
0
0.5
1
1.5
Location of the slope w.r.t. the SWL [m]
-1.5
-1
-0.5
0
0.5
1
1.5
profile change expresed in damage parameterE3D,1 [Profile change/dn50]
Profile change expressed in the damage parameter E3D,1 of test 8G for the 1:8 slope
Width of the flume [m]
0.2
0.4
0.6
0.8
-2.5
-2
-1.5
-1
-0.5
0
0.5
1
1.5
Location of the slope w.r.t. the SWL [m]
-1.5
-1
-0.5
0
0.5
1
1.5
profile change expresed in damage parameterE3D,1 [Profile change/dn50]
Profile change expressed in the damage parameter E3D,1 of test 8H for the 1:8 slope
Width of the flume [m]
0.2
0.4
0.6
0.8
-2.5
-2
-1.5
-1
-0.5
0
0.5
1
1.5
Location of the slope w.r.t. the SWL [m]
-1.5
-1
-0.5
0
0.5
1
1.5
profile change expresed in damage parameterE3D,1 [Profile change/dn50]

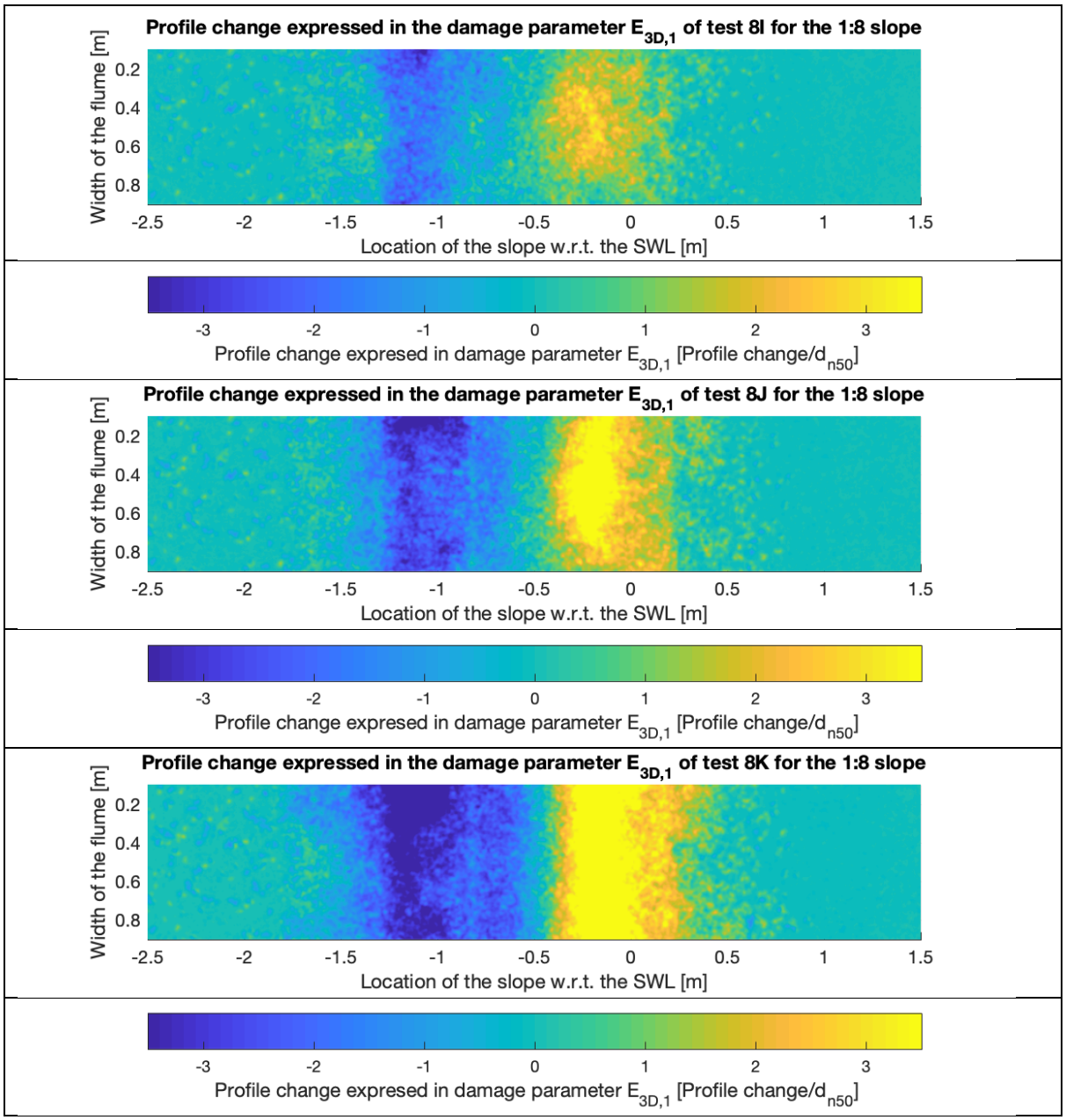
Profile change expressed in the damage parameter E3D,1 of test 8I for the 1:8 slope
Width of the flume [m]
0.2
0.4
0.6
0.8
-2.5
-2
-1.5
-1
-0.5
0
0.5
1
1.5
Location of the slope w.r.t. the SWL [m]
-3
-2
-1
0
1
2
3
Profile change expresed in damage parameter E3D,1 [Profile change/dn50]
Profile change expressed in the damage parameter E3D,1 of test 8J for the 1:8 slope
Width of the flume [m]
0.2
0.4
0.6
0.8
-2.5
-2
-1.5
-1
-0.5
0
0.5
1
1.5
Location of the slope w.r.t. the SWL [m]
-3
-2
-1
0
1
2
3
Profile change expresed in damage parameter E3D,1 [Profile change/dn50]
Profile change expressed in the damage parameter E3D,1 of test 8K for the 1:8 slope
Width of the flume [m]
0.2
0.4
0.6
0.8
-2.5
-2
-1.5
-1
-0.5
0
0.5
1
1.5
Location of the slope w.r.t. the SWL [m]
-3
-2
-1
0
1
2
3
Profile change expresed in damage parameter E3D,1 [Profile change/dn50]

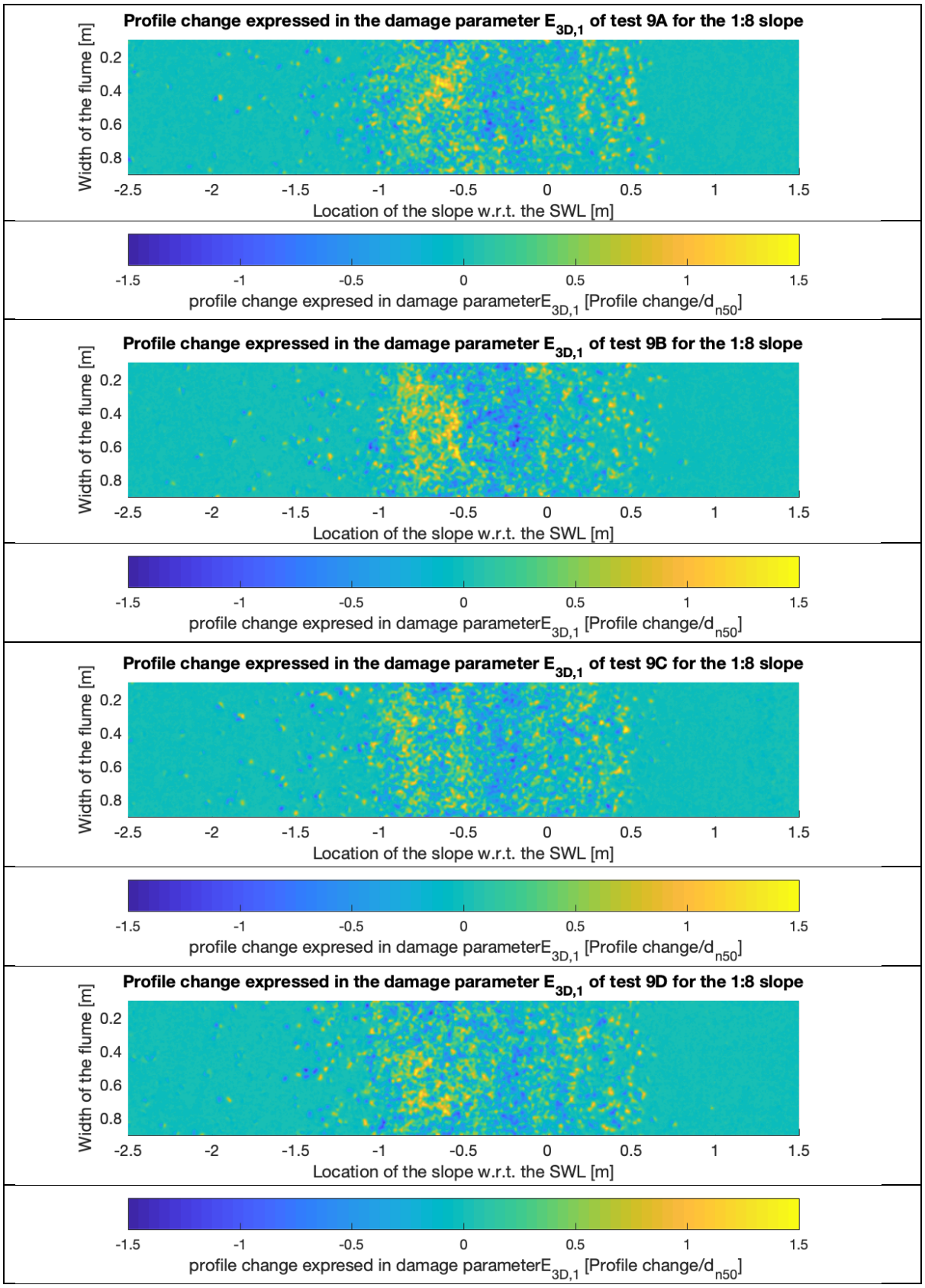
Profile change expressed in the damage parameter E3D,1 of test 9A for the 1:8 slope
Width of the flume [m]
0.2
0.4
0.6
0.8
-2.5
-2
-1.5
-1
-0.5
0
0.5
1
1.5
Location of the slope w.r.t. the SWL [m]
-1.5
-1
-0.5
0
0.5
1
1.5
profile change expresed in damage parameterE3D,1 [Profile change/dn50]
Profile change expressed in the damage parameter E3D,1 of test 9B for the 1:8 slope
Width of the flume [m]
0.2
0.4
0.6
0.8
-2.5
-2
-1.5
-1
-0.5
0
0.5
1
1.5
Location of the slope w.r.t. the SWL [m]
-1.5
-1
-0.5
0
0.5
1
1.5
profile change expresed in damage parameterE3D,1 [Profile change/dn50]
Profile change expressed in the damage parameter E3D,1 of test 9C for the 1:8 slope
Width of the flume [m]
0.2
0.4
0.6
0.8
-2.5
-2
-1.5
-1
-0.5
0
0.5
1
1.5
Location of the slope w.r.t. the SWL [m]
-1.5
-1
-0.5
0
0.5
1
1.5
profile change expresed in damage parameterE3D,1 [Profile change/dn50]
Profile change expressed in the damage parameter E3D,1 of test 9D for the 1:8 slope
Width of the flume [m]
0.2
0.4
0.6
0.8
-2.5
-2
-1.5
-1
-0.5
0
0.5
1
1.5
Location of the slope w.r.t. the SWL [m]
-1.5
-1
-0.5
0
0.5
1
1.5
profile change expresed in damage parameterE3D,1 [Profile change/dn50]

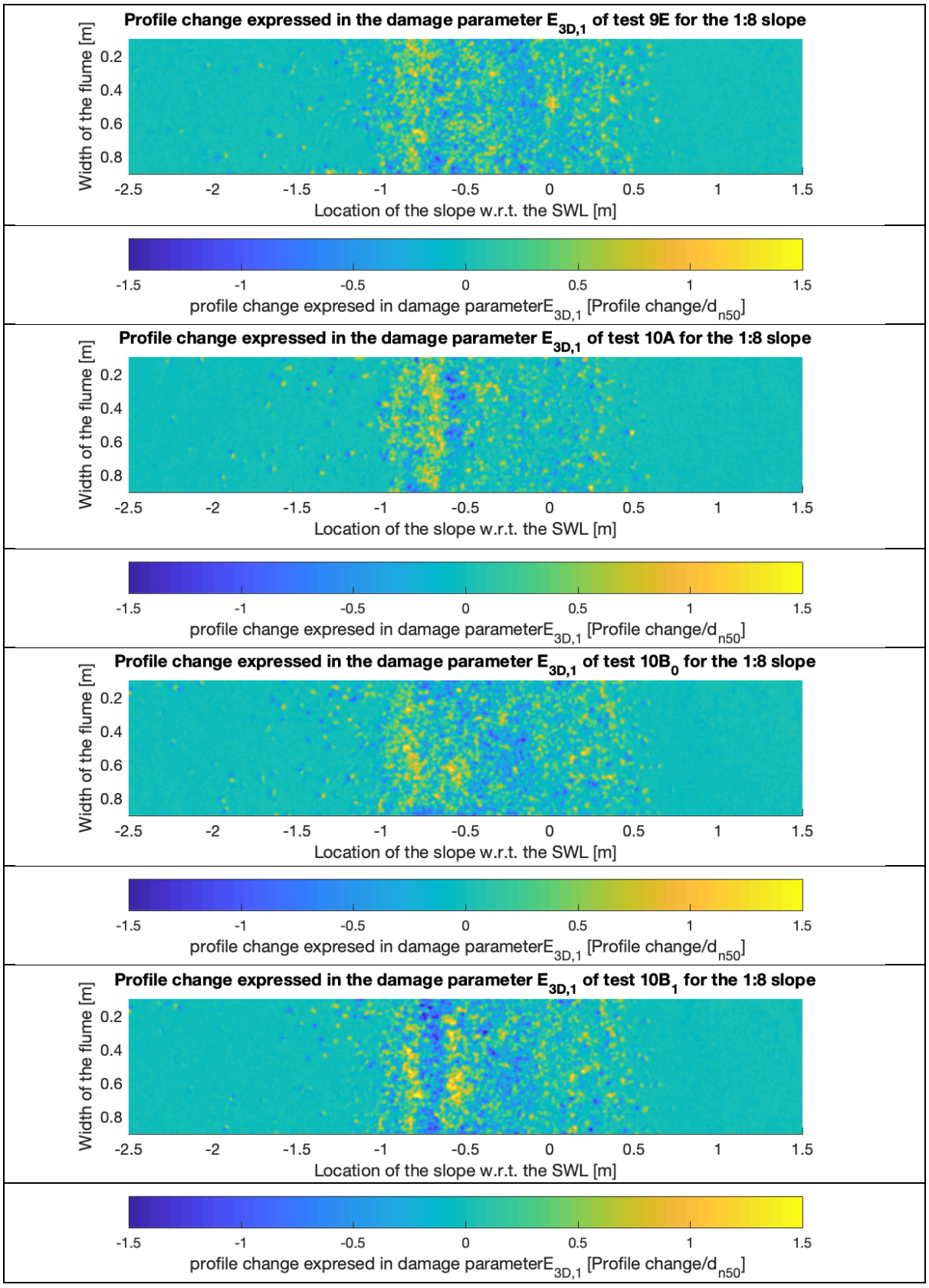
Profile change expressed in the damage parameter E3D,1 of test 9E for the 1:8 slope
Width of the flume [m]
0.2
0.4
0.6
0.8
-2.5
-2
-1.5
-1
-0.5
0
0.5
1
1.5
Location of the slope w.r.t. the SWL [m]
-1.5
-1
-0.5
0
0.5
1
1.5
profile change expresed in damage parameterE3D,1 [Profile change/dn50]
Profile change expressed in the damage parameter E3D,1 of test 10A for the 1:8 slope
Width of the flume [m]
0.2
0.4
0.6
0.8
-2.5
-2
-1.5
-1
-0.5
0
0.5
1
1.5
Location of the slope w.r.t. the SWL [m]
-1.5
-1
-0.5
0
0.5
1
1.5
profile change expresed in damage parameterE3D,1 [Profile change/dn50]
Profile change expressed in the damage parameter E3D,1 of test 10B0 for the 1:8 slope
Width of the flume [m]
0.2
0.4
0.6
0.8
-2.5
-2
-1.5
-1
-0.5
0
0.5
1
1.5
Location of the slope w.r.t. the SWL [m]
-1.5
-1
-0.5
0
0.5
1
1.5
profile change expresed in damage parameterE3D,1 [Profile change/dn50]
Profile change expressed in the damage parameter E3D,1 of test 10B1 for the 1:8 slope
Width of the flume [m]
0.2
0.4
0.6
0.8
-2.5
-2
-1.5
-1
-0.5
0
0.5
1
1.5
Location of the slope w.r.t. the SWL [m]
-1.5
-1
-0.5
0
0.5
1
1.5
profile change expresed in damage parameterE3D,1 [Profile change/dn50]

Results for 1:10 slope

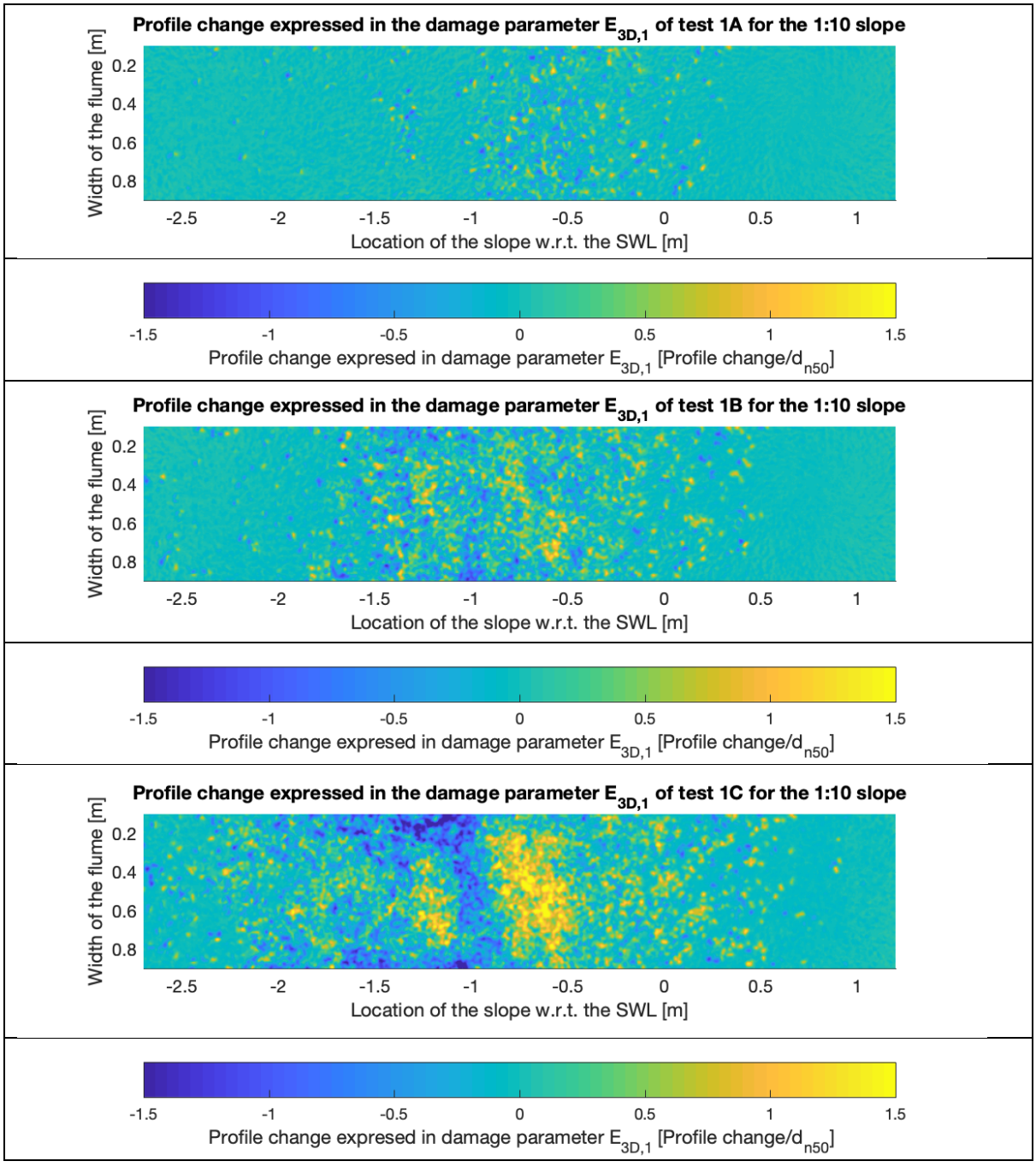

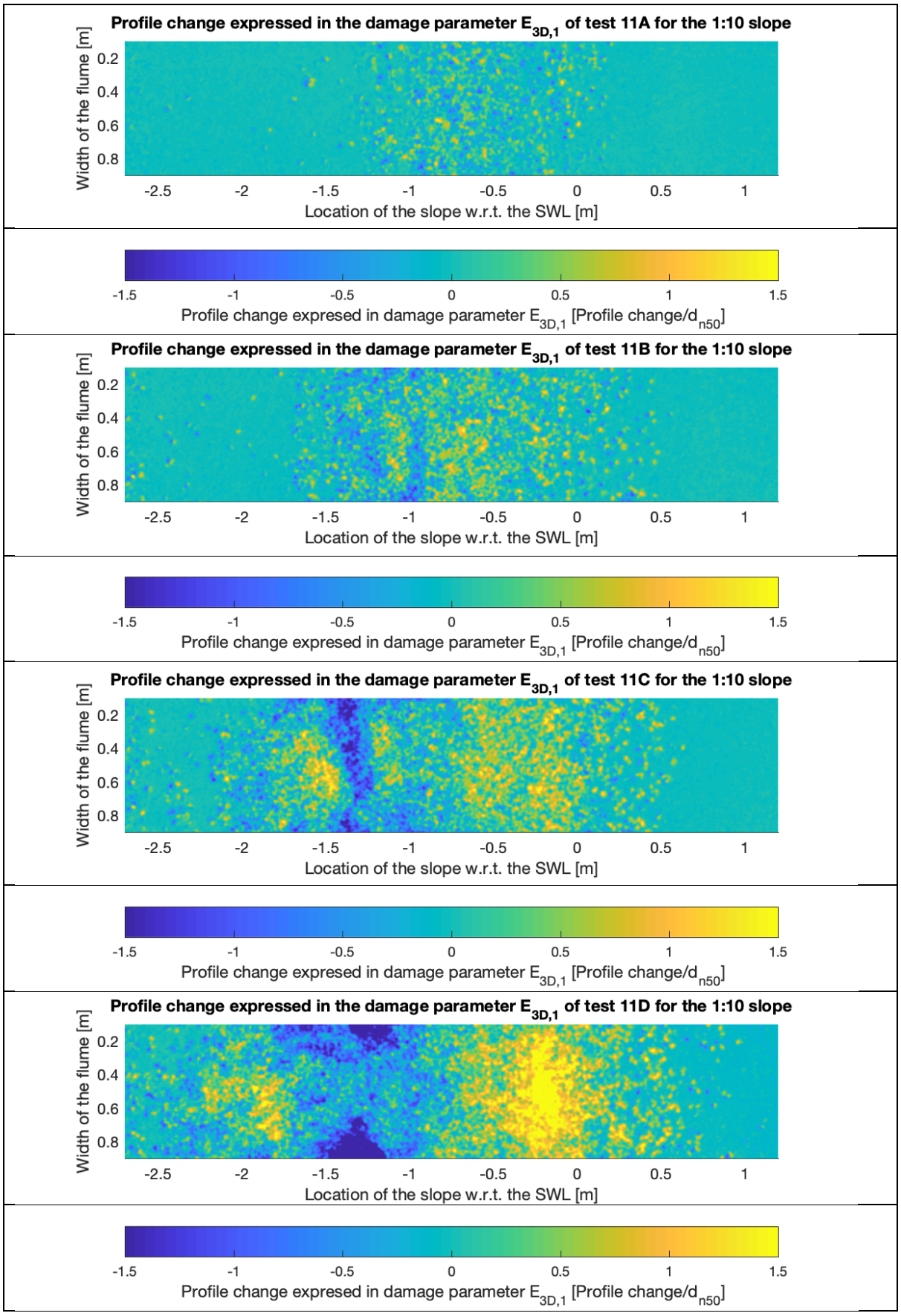
Profile change expressed in the damage parameter E3D,1 of test 11A for the 1:10 slope
Width of the flume [m]
0.2
0.4
0.6
0.8
-2.5
-2
-1.5
-1
-0.5
0
0.5
1
Location of the slope w.r.t. the SWL [m]
-1.5
-1
-0.5
0
0.5
1
1.5
Profile change expresed in damage parameter E3D,1 [Profile change/dn50]
Profile change expressed in the damage parameter E3D,1 of test 11B for the 1:10 slope
Width of the flume [m]
0.2
0.4
0.6
0.8
-2.5
-2
-1.5
-1
-0.5
0
0.5
1
Location of the slope w.r.t. the SWL [m]
-1.5
-1
-0.5
0
0.5
1
1.5
Profile change expresed in damage parameter E3D,1 [Profile change/dn50]
Profile change expressed in the damage parameter E3D,1 of test 11C for the 1:10 slope
Width of the flume [m]
0.2
0.4
0.6
0.8
-2.5
-2
-1.5
-1
-0.5
0
0.5
1
Location of the slope w.r.t. the SWL [m]
-1.5
-1
-0.5
0
0.5
1
1.5
Profile change expresed in damage parameter E3D,1 [Profile change/dn50]
Profile change expressed in the damage parameter E3D,1 of test 11D for the 1:10 slope
Width of the flume [m]
0.2
0.4
0.6
0.8
-2.5
-2
-1.5
-1
-0.5
0
0.5
1
Location of the slope w.r.t. the SWL [m]
-1.5
-1
-0.5
0
0.5
1
1.5
Profile change expresed in damage parameter E3D,1 [Profile change/dn50]

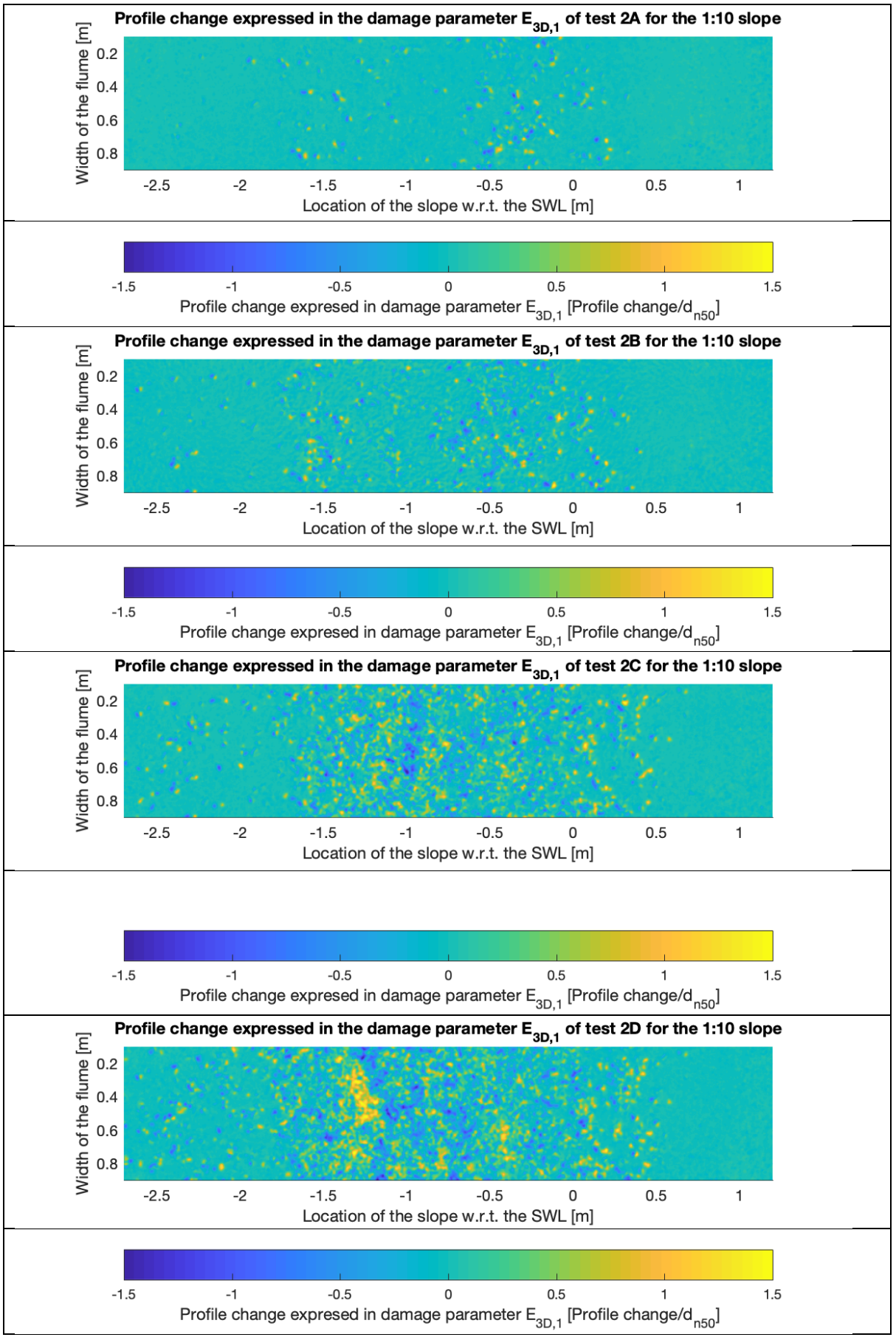
Profile change expressed in the damage parameter E3D,1 of test 2A for the 1:10 slope
Width of the flume [m]
0.2
0.4
0.6
0.8
-2.5
-2
-1.5
-1
-0.5
0
0.5
1
Location of the slope w.r.t. the SWL [m]
-1.5
-1
-0.5
0
0.5
1
1.5
Profile change expresed in damage parameter E3D,1 [Profile change/dn50]
Profile change expressed in the damage parameter E3D,1 of test 2B for the 1:10 slope
Width of the flume [m]
0.2
0.4
0.6
0.8
-2.5
-2
-1.5
-1
-0.5
0
0.5
1
Location of the slope w.r.t. the SWL [m]
-1.5
-1
-0.5
0
0.5
1
1.5
Profile change expresed in damage parameter E3D,1 [Profile change/dn50]
Profile change expressed in the damage parameter E3D,1 of test 2C for the 1:10 slope
Width of the flume [m]
0.2
0.4
0.6
0.8
-2.5
-2
-1.5
-1
-0.5
0
0.5
1
Location of the slope w.r.t. the SWL [m]
-1.5
-1
-0.5
0
0.5
1
1.5
Profile change expresed in damage parameter E3D,1 [Profile change/dn50]
Profile change expressed in the damage parameter E3D,1 of test 2D for the 1:10 slope
Width of the flume [m]
0.2
0.4
0.6
0.8
-2.5
-2
-1.5
-1
-0.5
0
0.5
1
Location of the slope w.r.t. the SWL [m]
-1.5
-1
-0.5
0
0.5
1
1.5
Profile change expresed in damage parameter E3D,1 [Profile change/dn50]

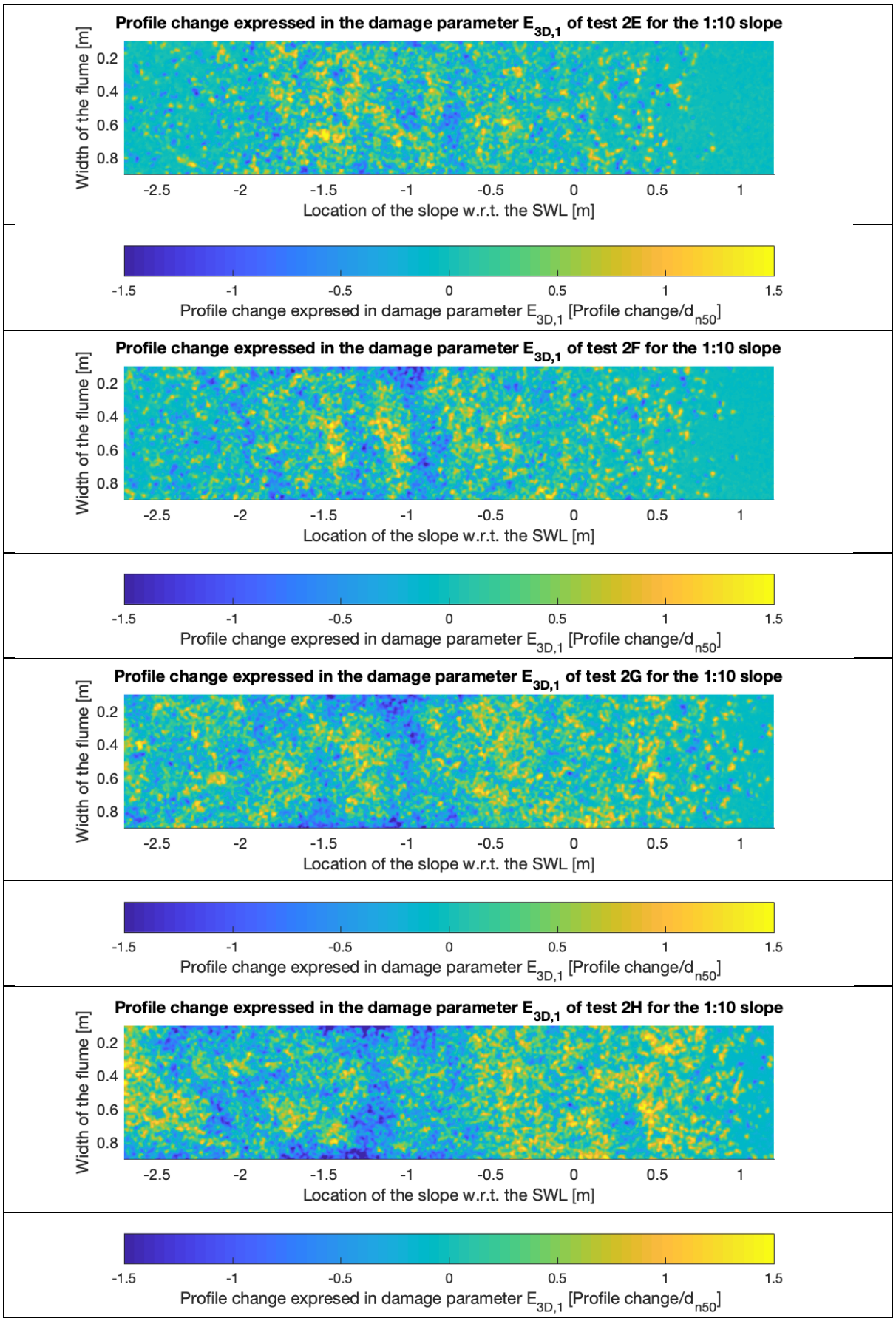
Profile change expressed in the damage parameter E3D,1 of test 2E for the 1:10 slope
Width of the flume [m]
0.2
0.4
0.6
0.8
-2.5
-2
-1.5
-1
-0.5
0
0.5
1
Location of the slope w.r.t. the SWL [m]
-1.5
-1
-0.5
0
0.5
1
1.5
Profile change expresed in damage parameter E3D,1 [Profile change/dn50]
Profile change expressed in the damage parameter E3D,1 of test 2F for the 1:10 slope
Width of the flume [m]
0.2
0.4
0.6
0.8
-2.5
-2
-1.5
-1
-0.5
0
0.5
1
Location of the slope w.r.t. the SWL [m]
-1.5
-1
-0.5
0
0.5
1
1.5
Profile change expresed in damage parameter E3D,1 [Profile change/dn50]
Profile change expressed in the damage parameter E3D,1 of test 2G for the 1:10 slope
Width of the flume [m]
0.2
0.4
0.6
0.8
-2.5
-2
-1.5
-1
-0.5
0
0.5
1
Location of the slope w.r.t. the SWL [m]
-1.5
-1
-0.5
0
0.5
1
1.5
Profile change expresed in damage parameter E3D,1 [Profile change/dn50]
Profile change expressed in the damage parameter E3D,1 of test 2H for the 1:10 slope
Width of the flume [m]
0.2
0.4
0.6
0.8
-2.5
-2
-1.5
-1
-0.5
0
0.5
1
Location of the slope w.r.t. the SWL [m]
-1.5
-1
-0.5
0
0.5
1
1.5
Profile change expresed in damage parameter E3D,1 [Profile change/dn50]

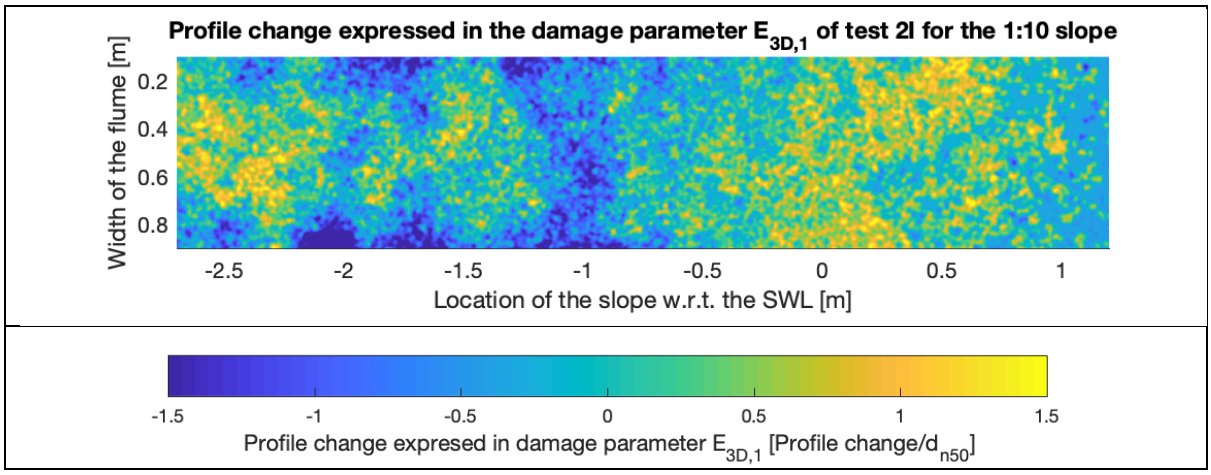
Profile change expressed in the damage parameter E3D,1 of test 2l for the 1:10 slope
Width of the flume [m]
0.2
0.4
0.6
0.8
-2.5
-2
-1.5
-1
-0.5
0
0.5
1
Location of the slope w.r.t. the SWL [m]
-1.5
-1
-0.5
0
0.5
1
1.5
Profile change expresed in damage parameter E3D,1 [Profile change/dn50]

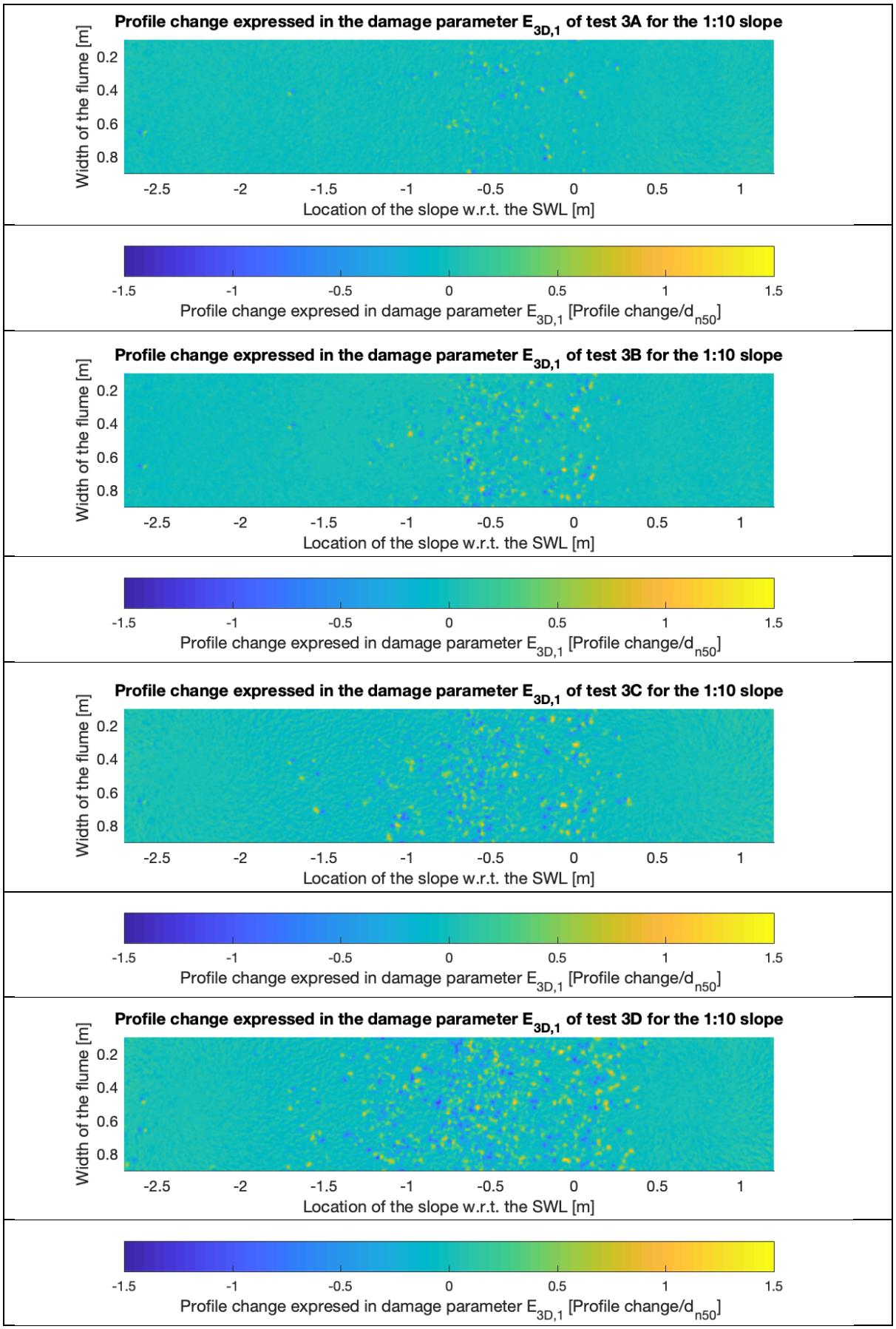
Profile change expressed in the damage parameter E3D,1 of test 3A for the 1:10 slope
Width of the flume [m]
0.2
0.4
0.6
0.8
-2.5
-2
-1.5
-1
-0.5
0
0.5
1
Location of the slope w.r.t. the SWL [m]
-1.5
-1
-0.5
0
0.5
1
1.5
Profile change expresed in damage parameter E3D,1 [Profile change/dn50]
Profile change expressed in the damage parameter E3D,1 of test 3B for the 1:10 slope
Width of the flume [m]
0.2
0.4
0.6
0.8
-2.5
-2
-1.5
-1
-0.5
0
0.5
1
Location of the slope w.r.t. the SWL [m]
-1.5
-1
-0.5
0
0.5
1
1.5
Profile change expresed in damage parameter E3D,1 [Profile change/dn50]
Profile change expressed in the damage parameter E3D,1 of test 3C for the 1:10 slope
Width of the flume [m]
0.2
0.4
0.6
0.8
-2.5
-2
-1.5
-1
-0.5
0
0.5
1
Location of the slope w.r.t. the SWL [m]
-1.5
-1
-0.5
0
0.5
1
1.5
Profile change expresed in damage parameter E3D,1 [Profile change/dn50]
Profile change expressed in the damage parameter E3D,1 of test 3D for the 1:10 slope
Width of the flume [m]
0.2
0.4
0.6
0.8
-2.5
-2
-1.5
-1
-0.5
0
0.5
1
Location of the slope w.r.t. the SWL [m]
-1.5
-1
-0.5
0
0.5
1
1.5
Profile change expresed in damage parameter E3D,1 [Profile change/dn50]

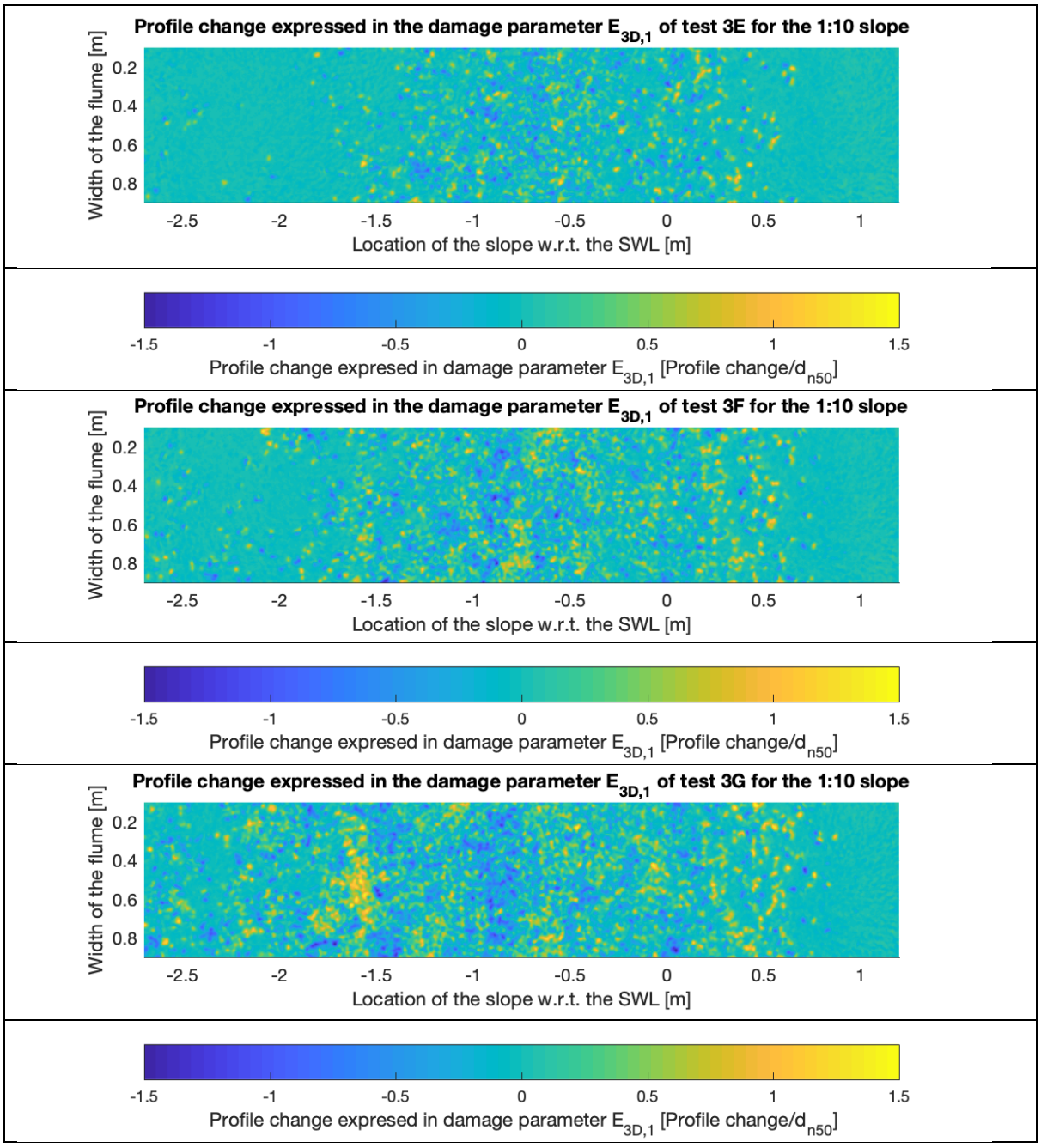
Profile change expressed in the damage parameter E3D,1 of test 3E for the 1:10 slope
Width of the flume [m]
0.2
0.4
0.6
0.8
-2.5
-2
-1.5
-1
-0.5
0
0.5
1
Location of the slope w.r.t. the SWL [m]
-1.5
-1
-0.5
0
0.5
1
1.5
Profile change expresed in damage parameter E3D,1 [Profile change/dn50]
Profile change expressed in the damage parameter E3D,1 of test 3F for the 1:10 slope
Width of the flume [m]
0.2
0.4
0.6
0.8
-2.5
-2
-1.5
-1
-0.5
0
0.5
1
Location of the slope w.r.t. the SWL [m]
-1.5
-1
-0.5
0
0.5
1
1.5
Profile change expresed in damage parameter E3D,1 [Profile change/dn50]
Profile change expressed in the damage parameter E3D,1 of test 3G for the 1:10 slope
Width of the flume [m]
0.2
0.4
0.6
0.8
-2.5
-2
-1.5
-1
-0.5
0
0.5
1
Location of the slope w.r.t. the SWL [m]
-1.5
-1
-0.5
0
0.5
1
1.5
Profile change expresed in damage parameter E3D,1 [Profile change/dn50]

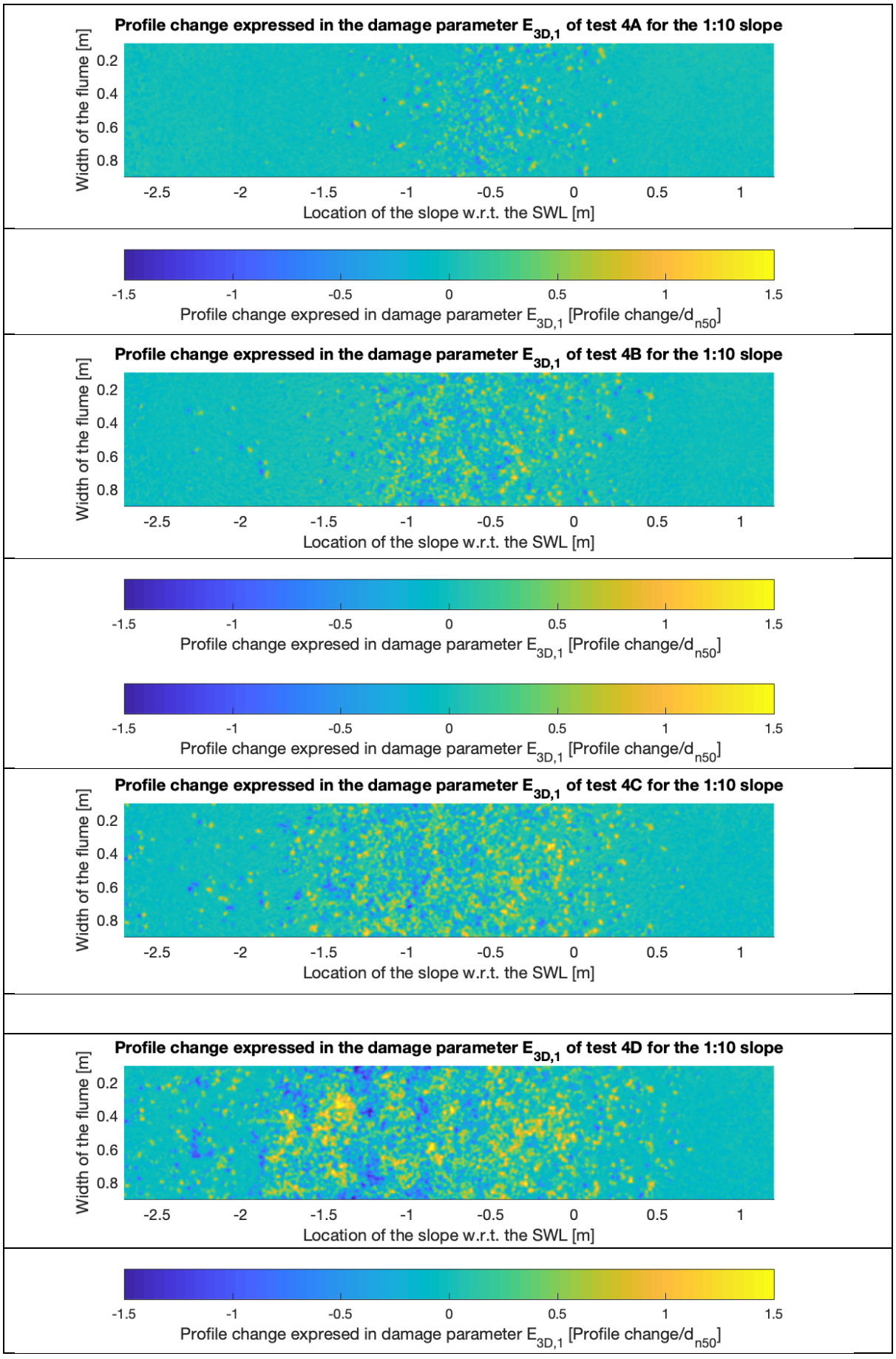
Profile change expressed in the damage parameter E3D,1 of test 4A for the 1:10 slope
Width of the flume [m]
0.2
0.4
0.6
0.8
-2.5
-2
-1.5
-1
-0.5
0
0.5
1
Location of the slope w.r.t. the SWL [m]
-1.5
-1
-0.5
0
0.5
1
1.5
Profile change expresed in damage parameter E3D,1 [Profile change/dn50]
Profile change expressed in the damage parameter E3D,1 of test 4B for the 1:10 slope
Width of the flume [m]
0.2
0.4
0.6
0.8
-2.5
-2
-1.5
-1
-0.5
0
0.5
1
Location of the slope w.r.t. the SWL [m]
-1.5
-1
-0.5
0
0.5
1
1.5
Profile change expresed in damage parameter E3D,1 [Profile change/dn50]
-1.5
-1
-0.5
0
0.5
1
1.5
Profile change expresed in damage parameter E3D,1 [Profile change/dn50]
Profile change expressed in the damage parameter E3D,1 of test 4C for the 1:10 slope
Width of the flume [m]
0.2
0.4
0.6
0.8
-2.5
-2
-1.5
-1
-0.5
0
0.5
1
Location of the slope w.r.t. the SWL [m]
Profile change expressed in the damage parameter E3D,1 of test 4D for the 1:10 slope
Width of the flume [m]
0.2
0.4
0.6
0.8
-2.5
-2
-1.5
-1
-0.5
0
0.5
1
Location of the slope w.r.t. the SWL [m]
-1.5
-1
-0.5
0
0.5
1
1.5
Profile change expresed in damage parameter E3D,1 [Profile change/dn50]

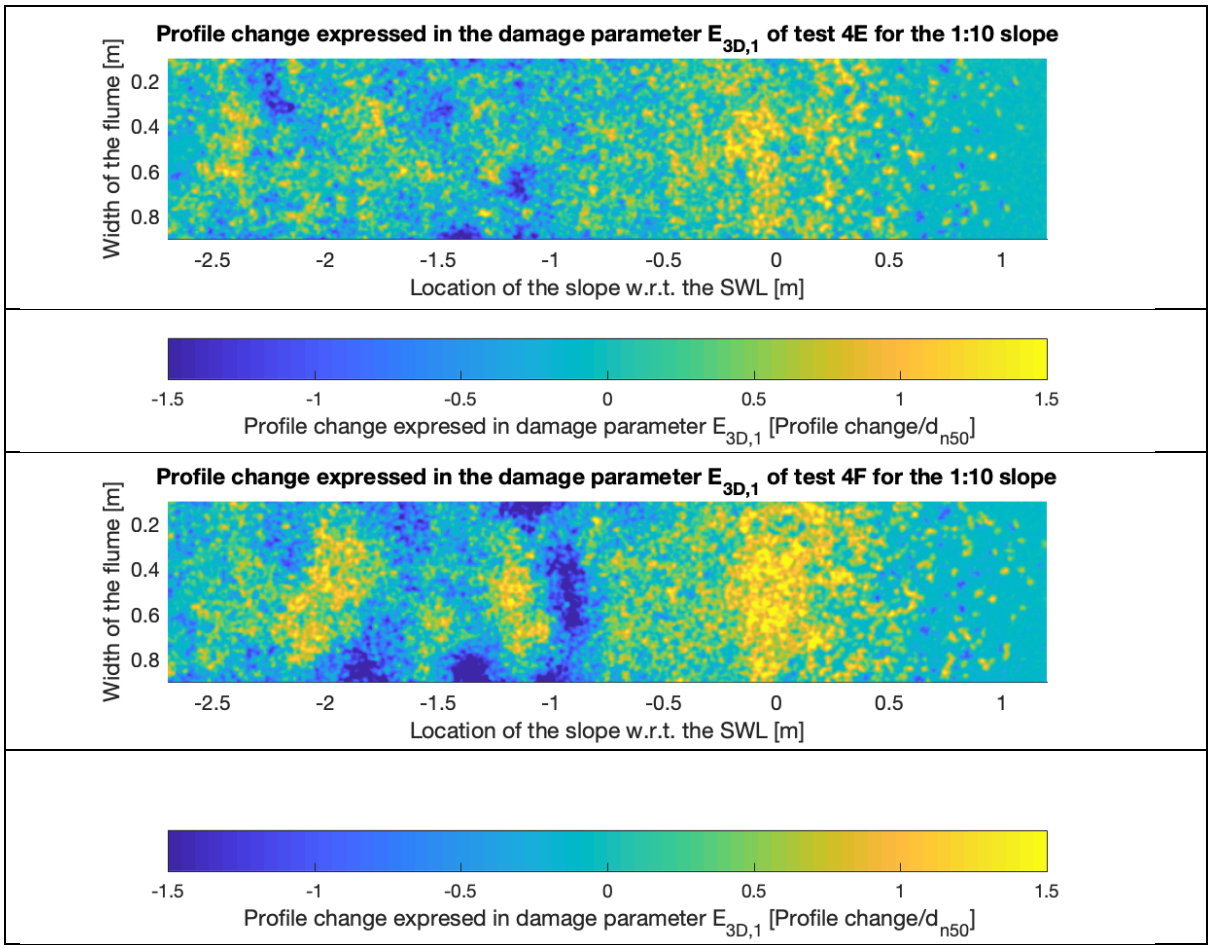
Profile change expressed in the damage parameter E3D,1 of test 4E for the 1:10 slope
Width of the flume [m]
0.2
0.4
0.6
0.8
-2.5
-2
-1.5
-1
-0.5
0
0.5
1
Location of the slope w.r.t. the SWL [m]
-1.5
-1
-0.5
0
0.5
1
1.5
Profile change expresed in damage parameter E3D,1 [Profile change/dn50]
Profile change expressed in the damage parameter E3D,1 of test 4F for the 1:10 slope
Width of the flume [m]
0.2
0.4
0.6
0.8
-2.5
-2
-1.5
-1
-0.5
0
0.5
1
Location of the slope w.r.t. the SWL [m]
-1.5
-1
-0.5
0
0.5
1
1.5
Profile change expresed in damage parameter E3D,1 [Profile change/dn50]

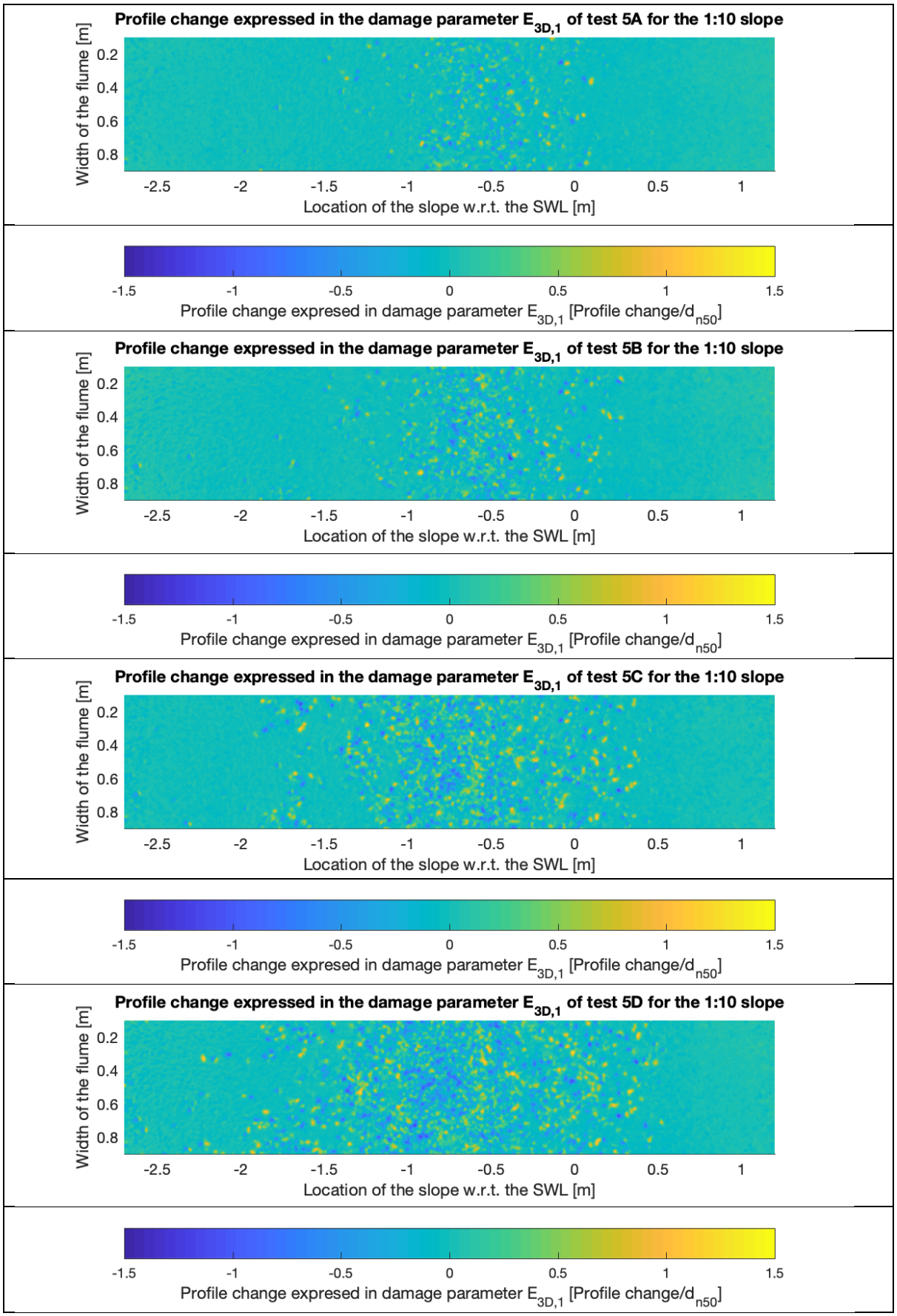
Profile change expressed in the damage parameter E3D,1 of test 5A for the 1:10 slope
Width of the flume [m]
0.2
0.4
0.6
0.8
-2.5
-2
-1.5
-1
-0.5
0
0.5
1
Location of the slope w.r.t. the SWL [m]
-1.5
-1
-0.5
0
0.5
1
1.5
Profile change expresed in damage parameter E3D,1 [Profile change/dn50]
Profile change expressed in the damage parameter E3D,1 of test 5B for the 1:10 slope
Width of the flume [m]
0.2
0.4
0.6
0.8
-2.5
-2
-1.5
-1
-0.5
0
0.5
1
Location of the slope w.r.t. the SWL [m]
-1.5
-1
-0.5
0
0.5
1
1.5
Profile change expresed in damage parameter E3D,1 [Profile change/dn50]
Profile change expressed in the damage parameter E3D,1 of test 5C for the 1:10 slope
Width of the flume [m]
0.2
0.4
0.6
0.8
-2.5
-2
-1.5
-1
-0.5
0
0.5
1
Location of the slope w.r.t. the SWL [m]
-1.5
-1
-0.5
0
0.5
1
1.5
Profile change expresed in damage parameter E3D,1 [Profile change/dn50]
Profile change expressed in the damage parameter E3D,1 of test 5D for the 1:10 slope
Width of the flume [m]
0.2
0.4
0.6
0.8
-2.5
-2
-1.5
-1
-0.5
0
0.5
1
Location of the slope w.r.t. the SWL [m]
-1.5
-1
-0.5
0
0.5
1
1.5
Profile change expresed in damage parameter E3D,1 [Profile change/dn50]

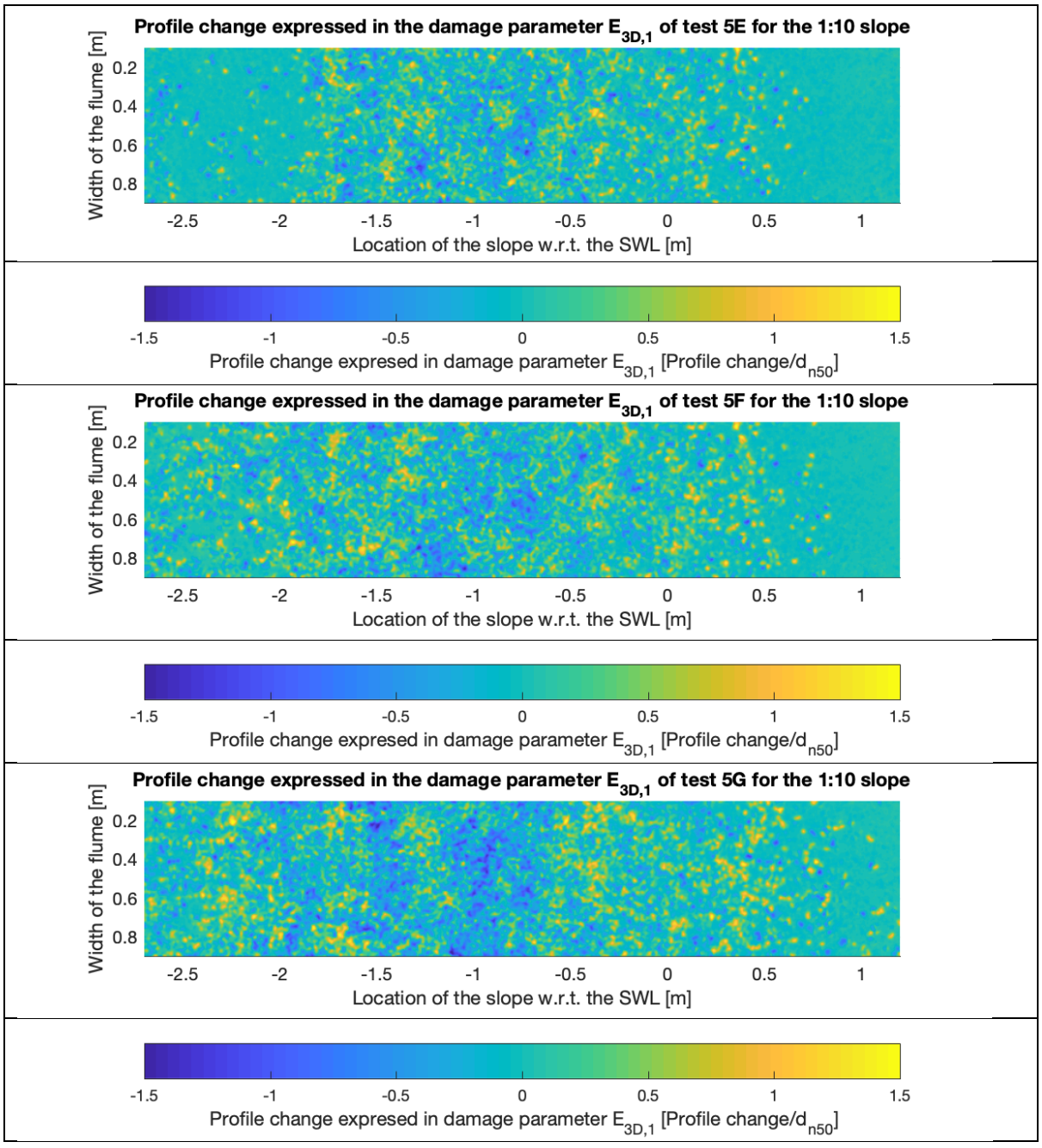
Profile change expressed in the damage parameter E3D,1 of test 5E for the 1:10 slope
Width of the flume [m]
0.2
0.4
0.6
0.8
-2.5
-2
-1.5
-1
-0.5
0
0.5
1
Location of the slope w.r.t. the SWL [m]
-1.5
-1
-0.5
0
0.5
1
1.5
Profile change expresed in damage parameter E3D,1 [Profile change/dn50]
Profile change expressed in the damage parameter E3D,1 of test 5F for the 1:10 slope
Width of the flume [m]
0.2
0.4
0.6
0.8
-2.5
-2
-1.5
-1
-0.5
0
0.5
1
Location of the slope w.r.t. the SWL [m]
-1.5
-1
-0.5
0
0.5
1
1.5
Profile change expresed in damage parameter E3D,1 [Profile change/dn50]
Profile change expressed in the damage parameter E3D,1 of test 5G for the 1:10 slope
Width of the flume [m]
0.2
0.4
0.6
0.8
-2.5
-2
-1.5
-1
-0.5
0
0.5
1
Location of the slope w.r.t. the SWL [m]
-1.5
-1
-0.5
0
0.5
1
1.5
Profile change expresed in damage parameter E3D,1 [Profile change/dn50]

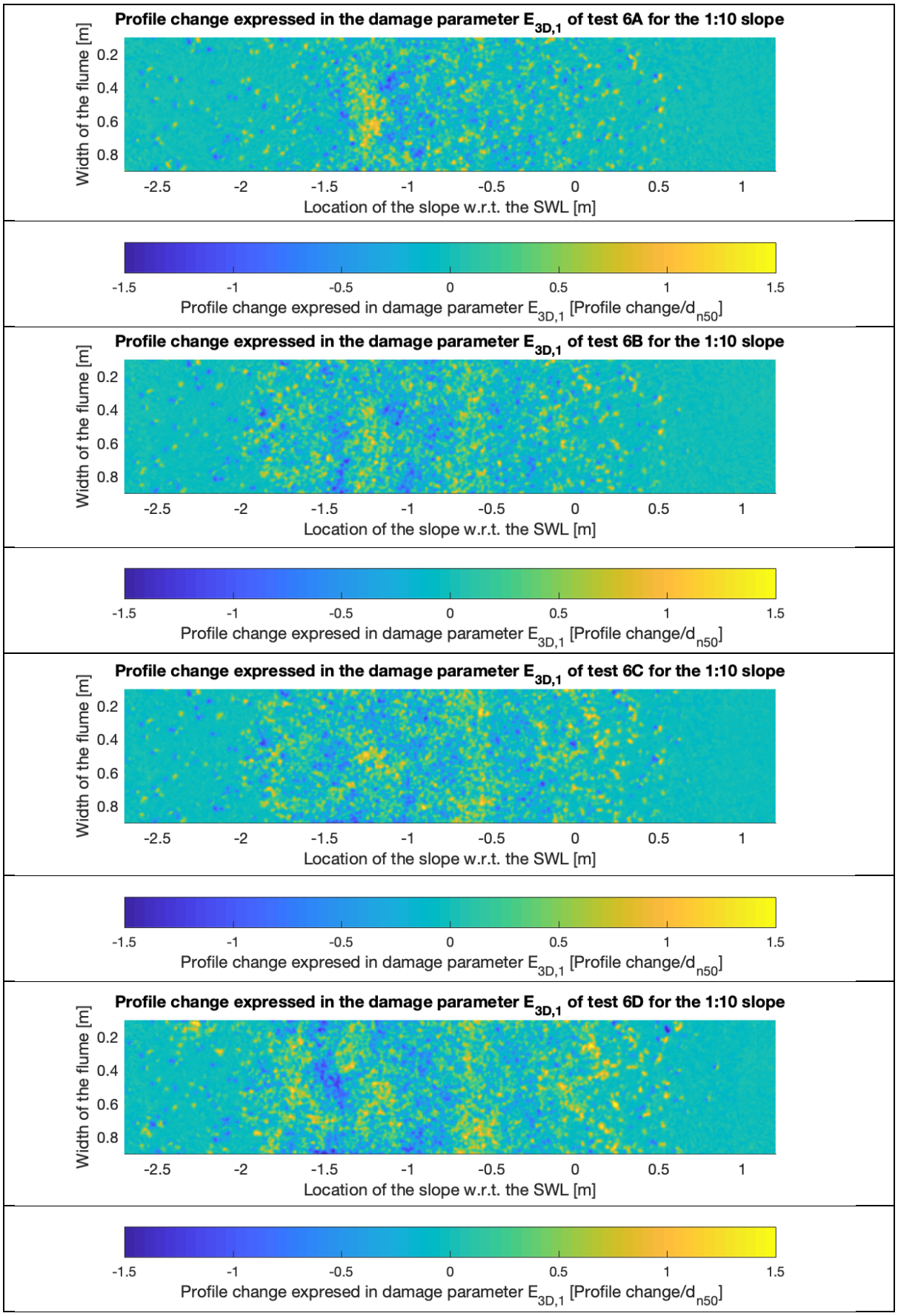
Profile change expressed in the damage parameter E3D,1 of test 6A for the 1:10 slope
Width of the flume [m]
0.2
0.4
0.6
0.8
-2.5
-2
-1.5
-1
-0.5
0
0.5
1
Location of the slope w.r.t. the SWL [m]
-1.5
-1
-0.5
0
0.5
1
1.5
Profile change expresed in damage parameter E3D,1 [Profile change/dn50]
Profile change expressed in the damage parameter E3D,1 of test 6B for the 1:10 slope
Width of the flume [m]
0.2
0.4
0.6
0.8
-2.5
-2
-1.5
-1
-0.5
0
0.5
1
Location of the slope w.r.t. the SWL [m]
-1.5
-1
-0.5
0
0.5
1
1.5
Profile change expresed in damage parameter E3D,1 [Profile change/dn50]
Profile change expressed in the damage parameter E3D,1 of test 6C for the 1:10 slope
Width of the flume [m]
0.2
0.4
0.6
0.8
-2.5
-2
-1.5
-1
-0.5
0
0.5
1
Location of the slope w.r.t. the SWL [m]
-1.5
-1
-0.5
0
0.5
1
1.5
Profile change expresed in damage parameter E3D,1 [Profile change/dn50]
Profile change expressed in the damage parameter E3D,1 of test 6D for the 1:10 slope
Width of the flume [m]
0.2
0.4
0.6
0.8
-2.5
-2
-1.5
-1
-0.5
0
0.5
1
Location of the slope w.r.t. the SWL [m]
-1.5
-1
-0.5
0
0.5
1
1.5
Profile change expresed in damage parameter E3D,1 [Profile change/dn50]

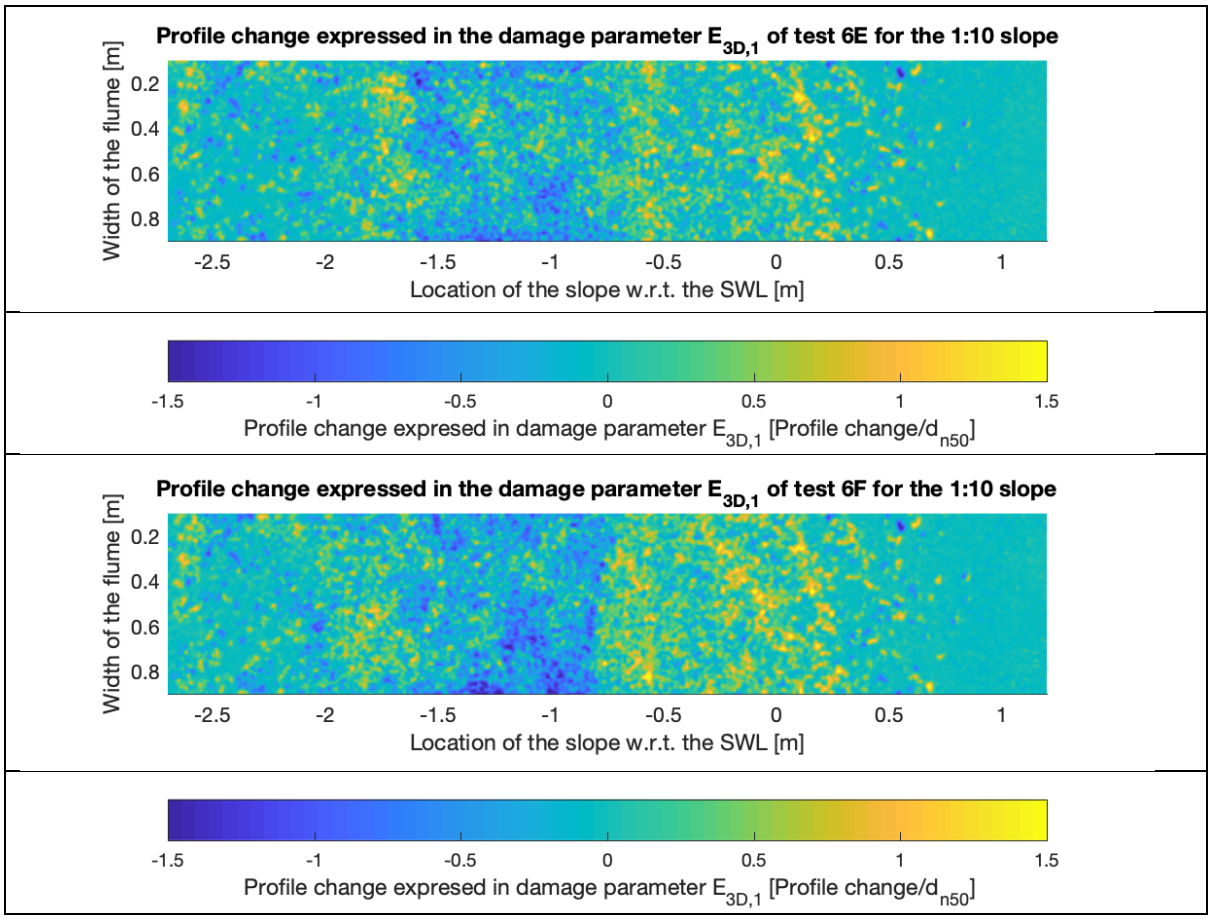
Profile change expressed in the damage parameter E3D,1 of test 6E for the 1:10 slope
Width of the flume [m]
0.2
0.4
0.6
0.8
-2.5
-2
-1.5
-1
-0.5
0
0.5
1
Location of the slope w.r.t. the SWL [m]
-1.5
-1
-0.5
0
0.5
1
1.5
Profile change expresed in damage parameter E3D,1 [Profile change/dn50]
Profile change expressed in the damage parameter E3D,1 of test 6F for the 1:10 slope
Width of the flume [m]
0.2
0.4
0.6
0.8
-2.5
-2
-1.5
-1
-0.5
0
0.5
1
Location of the slope w.r.t. the SWL [m]
-1.5
-1
-0.5
0
0.5
1
1.5
Profile change expresed in damage parameter E3D,1 [Profile change/dn50]

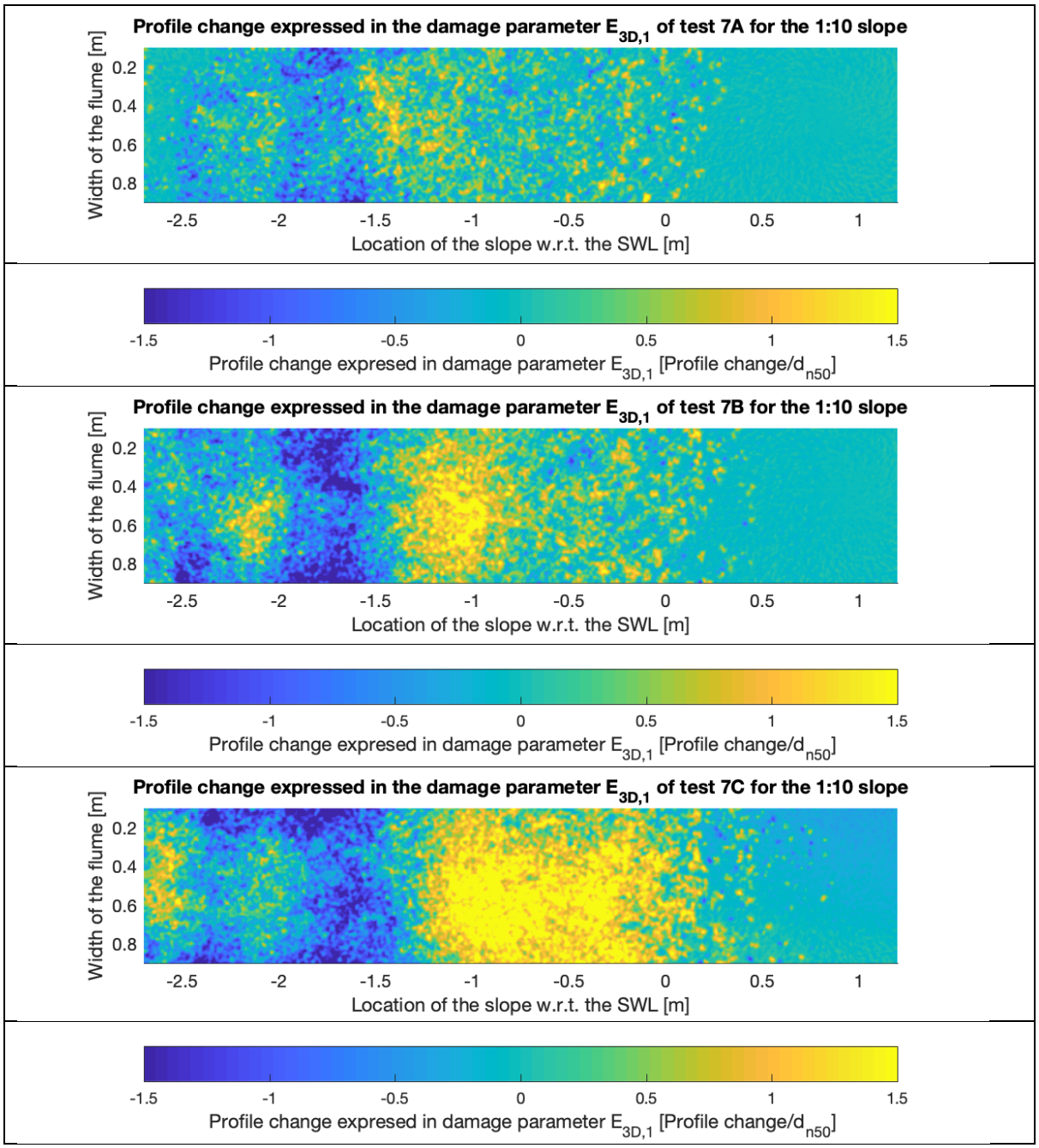
Profile change expressed in the damage parameter E3D,1 of test 7A for the 1:10 slope
Width of the flume [m]
0.2
0.4
0.6
0.8
-2.5
-2
-1.5
-1
-0.5
0
0.5
1
Location of the slope w.r.t. the SWL [m]
-1.5
-1
-0.5
0
0.5
1
1.5
Profile change expresed in damage parameter E3D,1 [Profile change/dn50]
Profile change expressed in the damage parameter E3D,1 of test 7B for the 1:10 slope
Width of the flume [m]
0.2
0.4
0.6
0.8
-2.5
-2
-1.5
-1
-0.5
0
0.5
1
Location of the slope w.r.t. the SWL [m]
-1.5
-1
-0.5
0
0.5
1
1.5
Profile change expresed in damage parameter E3D,1 [Profile change/dn50]
Profile change expressed in the damage parameter E3D,1 of test 7C for the 1:10 slope
Width of the flume [m]
0.2
0.4
0.6
0.8
-2.5
-2
-1.5
-1
-0.5
0
0.5
1
Location of the slope w.r.t. the SWL [m]
-1.5
-1
-0.5
0
0.5
1
1.5
Profile change expresed in damage parameter E3D,1 [Profile change/dn50]

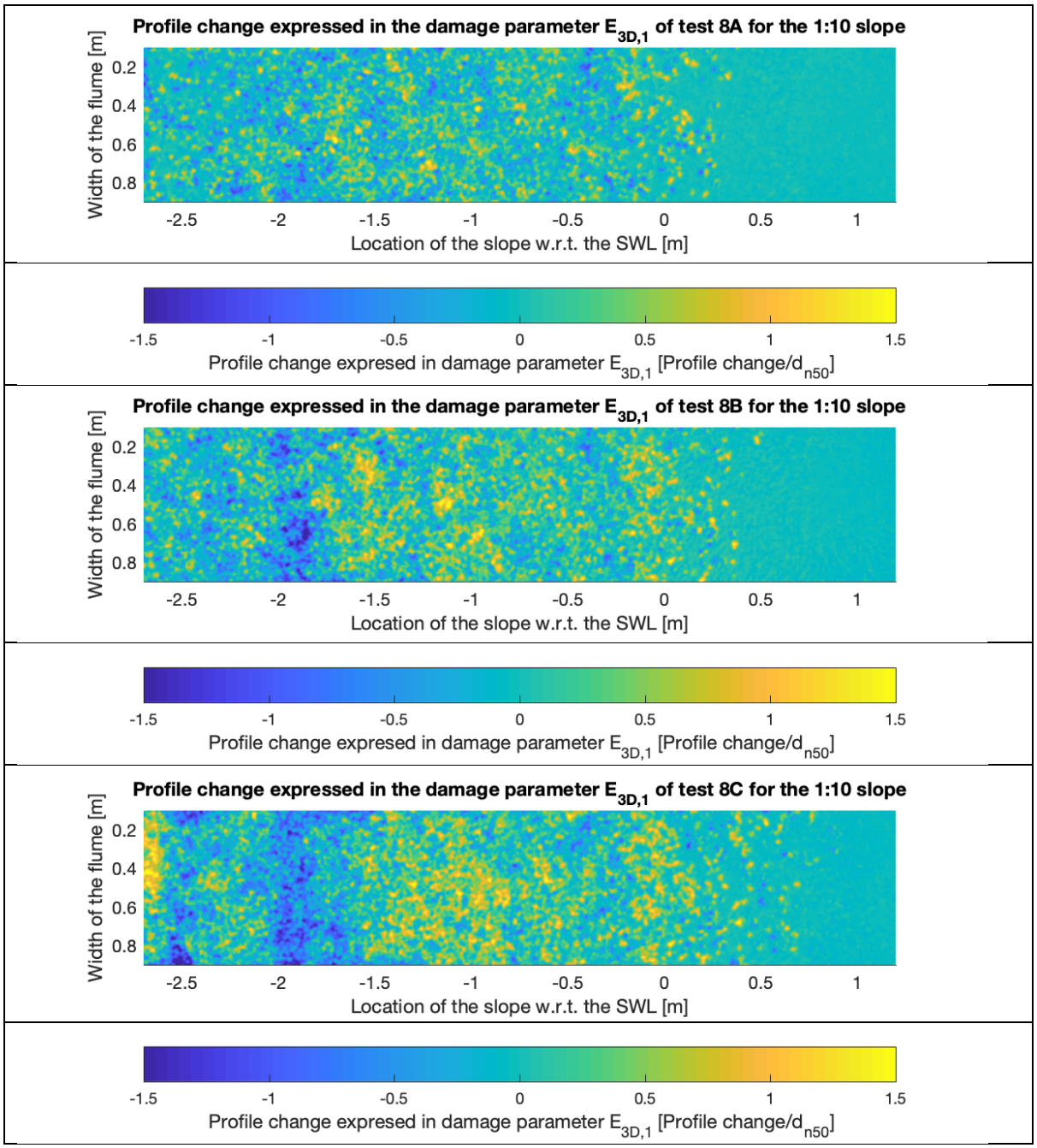
Profile change expressed in the damage parameter E3D,1 of test 8A for the 1:10 slope
Width of the flume [m]
0.2
0.4
0.6
0.8
-2.5
-2
-1.5
-1
-0.5
0
0.5
1
Location of the slope w.r.t. the SWL [m]
-1.5
-1
-0.5
0
0.5
1
1.5
Profile change expresed in damage parameter E3D,1 [Profile change/dn50]
Profile change expressed in the damage parameter E3D,1 of test 8B for the 1:10 slope
Width of the flume [m]
0.2
0.4
0.6
0.8
-2.5
-2
-1.5
-1
-0.5
0
0.5
1
Location of the slope w.r.t. the SWL [m]
-1.5
-1
-0.5
0
0.5
1
1.5
Profile change expresed in damage parameter E3D,1 [Profile change/dn50]
Profile change expressed in the damage parameter E3D,1 of test 8C for the 1:10 slope
Width of the flume [m]
0.2
0.4
0.6
0.8
-2.5
-2
-1.5
-1
-0.5
0
0.5
1
Location of the slope w.r.t. the SWL [m]
-1.5
-1
-0.5
0
0.5
1
1.5
Profile change expresed in damage parameter E3D,1 [Profile change/dn50]

Appendix H: Profile based damage parameters

Table 23: *The damage parameters for all test series for the 1:8 slope for a characterization width of 54 d_{n50}.*

Test Information		Test conditions						Damage parameters				
Series	**Run**	$s_{o,p}$	$H_{1/3}$	$H_{m,0}$	**N**	$\frac{Hs}{\Delta d_{n50}}$	**S**	S_{all}	E_{2D}	$E_{3D,1}$	$E_{3D,3}$	$E_{3D,5}$
1	A	0.009	0.017	0.018	1114	0.59	0.00	0.00	0.00	0.58	0.18	0.10
	B	0.008	0.024	0.025	1156	0.84	0.08	0.10	0.04	0.84	0.47	0.26
	C	0.009	0.032	0.034	1183	1.11	0.11	0.16	0.03	0.85	0.43	0.22
	D	0.009	0.042	0.045	1201	1.46	0.27	0.71	0.11	1.30	0.67	0.30
	E	0.011	0.054	0.056	1272	1.88	0.37	1.28	0.12	1.24	0.66	0.47
	F	0.010	0.065	0.068	1239	2.26	0.39	1.32	0.11	1.43	0.89	0.61
	G	0.010	0.072	0.074	1173	2.51	1.77	2.68	0.21	1.42	0.95	0.72
	H	0.009	0.081	0.084	1200	2.82	7.46	9.22	0.61	1.88	1.52	1.33
2	A	0.016	0.025	0.027	1083	0.87	0.00	0.00	0.00	0.87	0.34	0.14
	B	0.020	0.036	0.039	1086	1.25	0.00	0.00	0.00	0.85	0.34	0.15
	C	0.017	0.041	0.044	1110	1.43	0.04	0.11	0.04	0.91	0.39	0.16
	D*											
	E	0.020	0.068	0.071	1137	2.37	0.45	0.86	0.12	0.96	0.60	0.38
	F	0.020	0.08	0.075	1106	2.79	0.27	0.78	0.08	1.03	0.58	0.38
	G	0.020	0.087	0.091	1128	3.03	0.64	1.51	0.13	1.09	0.71	0.51
	H	0.020	0.096	0.101	1101	3.34	0.38	0.49	0.16	1.54	1.00	0.75
	I	0.019	0.110	0.114	1114	3.83	0.38	0.87	0.11	1.63	1.12	0.80
3	A	0.028	0.053	0.056	1180	1.85	0.19	0.41	0.07	1.01	0.48	0.25
	B	0.026	0.073	0.074	1181	2.54	0.22	0.70	0.08	0.98	0.46	0.31
	C	0.027	0.095	0.099	1227	3.31	1.51	3.10	0.35	1.16	0.88	0.66
	D	0.026	0.119	0.123	1164	4.14	6.60	7.24	0.45	1.61	1.31	0.91
	E	0.025	0.145	0.151	1231	5.05	5.22	9.44	0.37	2.23	1.97	1.76
3N	A	0.026	0.041	0.044	1037	1.43	0.00	0.00	0.03	0.74	0.26	0.14
	B	0.030	0.055	0.058	1094	1.92	0.16	0.34	0.06	0.89	0.40	0.23
	C	0.029	0.066	0.07	1131	2.30	0.34	0.88	0.07	0.94	0.47	0.29
	D	0.029	0.081	0.085	1109	2.82	0.79	1.82	0.11	1.06	0.57	0.45
	E	0.028	0.091	0.095	1154	3.17	0.41	1.61	0.15	1.27	0.81	0.53
	F	0.029	0.105	0.108	1117	3.66	0.71	2.39	0.16	1.37	0.87	0.61
	G	0.029	0.119	0.122	1125	4.14	0.71	3.20	0.19	1.40	0.89	0.68
	H	0.029	0.13	0.135	1097	4.53	2.72	5.08	0.39	2.23	1.72	1.57
	I	0.030	0.145	0.15	1097	5.05	6.52	7.49	0.59	2.21	1.96	1.68
4	A	0.038	0.052	0.056	1047	1.81	0.00	0.00	0.00	0.59	0.22	0.11
	B	0.038	0.066	0.072	1036	2.30	0.07	0.08	0.04	0.81	0.44	0.22
	C	0.040	0.084	0.088	1101	2.93	0.43	0.78	0.08	0.97	0.61	0.40
	D	0.038	0.1	0.105	1104	3.48	0.35	1.42	0.10	1.06	0.57	0.46
	E	0.038	0.116	0.121	1105	4.04	1.40	1.85	0.12	1.41	0.73	0.50
	F	0.038	0.131	0.136	1091	4.56	1.66	2.30	0.27	1.62	1.14	0.86
	G	0.039	0.15	0.153	1114	5.22	0.96	2.87	0.20	1.81	1.12	0.85
	H	0.040	0.167	0.173	1110	5.82	1.96	3.89	0.33	1.65	1.23	0.96
5	A	0.048	0.056	0.06	1079	1.95	0.00	0.00	0.00	0.85	0.40	0.18
	B	0.045	0.071	0.076	1060	2.47	0.13	0.14	0.06	0.92	0.49	0.21
	C	0.047	0.091	0.095	1107	3.17	0.14	0.19	0.07	1.09	0.58	0.28
	D	0.045	0.106	0.11	1127	3.69	0.61	1.26	0.11	1.11	0.80	0.57
	E	0.043	0.122	0.127	1132	4.25	1.23	2.14	0.16	1.33	0.86	0.72
	F	0.046	0.14	0.143	1108	4.88	1.57	3.02	0.29	1.13	0.81	0.74
	G	0.049	0.153	0.16	1088	5.33	2.23	3.96	0.25	1.33	1.00	0.84
	H	0.050	0.171	0.175	1113	5.96	5.32	8.27	0.46	1.67	1.23	1.06
	I	0.050	0.189	0.195	1122	6.58	6.95	10.94	0.48	2.27	1.85	1.43
6	A	0.028	0.117	0.124	263	4.07	0.86	2.59	0.23	1.68	1.08	0.82
	B	0.028	0.117	0.126	268	4.07	1.05	2.45	0.16	1.36	0.99	0.71
	C	0.029	0.118	0.122	556	4.11	1.75	3.25	0.21	1.56	0.91	0.65
	D	0.028	0.117	0.124	1112	4.07	4.32	5.00	0.22	1.38	0.93	0.67
	E	0.029	0.118	0.123	2236	4.11	2.62	4.99	0.21	1.83	1.41	0.99
	F	0.029	0.119	0.124	3354	4.14	10.61	11.78	0.42	1.84	1.22	0.96
	G	0.029	0.119	0.124	3366	4.14	14.67	15.22	0.58	1.71	1.22	0.98
	H	0.030	0.119	0.124	4448	4.14	22.92	23.45	0.73	2.13	1.46	1.25
7	A	0.030	0.055	0.058	1100	1.92	0.00	0.00	0.00	1.12	0.50	0.29
	B	0.029	0.067	0.071	1134	2.33	0.15	0.38	0.08	1.13	0.53	0.30
	C	0.028	0.08	0.084	1126	2.79	0.08	0.27	0.06	1.25	0.54	0.35
	D	0.029	0.092	0.096	1167	3.20	0.73	1.66	0.14	1.29	0.63	0.37
	E	0.030	0.106	0.109	1124	3.69	0.33	1.28	0.10	1.12	0.70	0.46
	F	0.029	0.12	0.123	1120	4.18	2.44	3.74	0.26	1.25	0.83	0.68
	G	0.029	0.132	0.136	1106	4.60	3.84	5.34	0.43	1.56	1.07	0.86
	H**	0.030	0.144	0.15	1084	5.02	7.16	20.79	0.62	2.07	1.76	1.36
	I	0.028	0.156	0.162	1073	5.43	34.50	35.34	1.43	2.43	2.01	1.78
	J	0.029	0.173	0.179	1031	6.03	57.24	60.23	1.64	2.82	2.51	2.29
	K	0.029	0.189	0.194	1093	6.58	91.92	95.23	2.17	3.23	2.81	2.54
	L	0.029	0.198	0.206	1124	6.90	127.04	131.26	3.00	4.07	3.71	3.50
8	A	0.008	0.025	0.026	1186	0.87	0.06	0.12	0.04	0.62	0.23	0.17
	B	0.010	0.035	0.036	1170	1.22	0.04	0.05	0.04	0.92	0.38	0.21
	C	0.010	0.043	0.046	1223	1.50	0.24	0.72	0.09	1.24	0.61	0.38
	D	0.010	0.052	0.056	1296	1.81	0.53	1.61	0.11	1.16	0.60	0.37
	E	0.010	0.065	0.068	1236	2.26	2.78	5.05	0.40	1.46	1.08	0.92
	F	0.010	0.073	0.075	1182	2.54	7.74	7.96	0.50	1.65	1.15	0.92
	G	0.009	0.081	0.084	1192	2.82	22.16	23.38	1.20	2.26	1.90	1.74
	H	0.010	0.093	0.096	1191	3.24	36.17	38.76	1.51	2.98	2.57	2.35
	I	0.011	0.101	0.104	1227	3.52	54.14	55.92	1.94	3.83	3.29	2.89
	J	0.011	0.11	0.114	1241	3.83	105.30	107.05	2.85	4.67	4.31	4.05
	K	0.010	0.118	0.122	1228	4.11	173.51	175.45	3.79	5.14	5.00	4.86
9	A	0.029	0.12	0.123	1133	4.18	1.59	2.58	0.19	1.27	0.78	0.60
	B	0.029	0.12	0.123	1120	4.18	3.22	4.57	0.30	1.46	0.89	0.69
9	C	0.029	0.119	0.122	1122	4.14	2.97	3.94	0.23	1.31	0.74	0.57
	D	0.029	0.119	0.122	1122	4.14	1.84	2.31	0.27	1.32	0.73	0.55
	E	0.029	0.119	0.121	1121	4.14	1.62	2.39	0.20	1.24	0.88	0.62
10	A	0.034	0.127	0.109	19	4.42	1.05	1.54	0.24	1.49	0.95	0.71
	Btov0	0.029	0.119	0.122	1122	4.14	1.36	2.64	0.19	1.37	0.89	0.65
	Btov1	0.029	0.119	0.018	1114	4.14	3.03	5.93	0.46	1.86	1.16	0.91

* Wave generators interrupted suddenly at this test and test is not completed. For that reason, this measurement/test is disregarded.

** 18 photos are missing at the upper slope. After consideration, it didn't affect the damage area and damage parameter significantly and for that reason is not disregarded.

Table 24: *The damage parameters for all test series for the 1:10 slope for a characterization width of 54 d_{n50}.*

Test Information					Test conditions			Damage parameters				
Series	Run	$s_{o,p}$	$H_{1/3}$	$H_{m,0}$	N	Hs Δd_{n50}	S	S_{all}	E_{2D}	$E_{3D,1}$	$E_{3D,3}$	$E_{3D,5}$
1	A	0.009	0.062	0.066	1361	2.16	0.58	1.30	0.08	1.12	0.61	0.40
	B	0.010	0.087	0.09	1332	3.03	1.58	4.72	0.21	1.44	0.99	0.81
	C	0.009	0.109	0.113	1381	3.80	6.58	15.61	0.68	2.29	1.86	1.50
11	A	0.009	0.066	0.069	1196	2.30	0.30	0.75	0.07	1.11	0.67	0.40
	B	0.010	0.086	0.089	1216	3.00	2.46	4.50	0.29	1.44	0.99	0.79
	C	0.010	0.11	0.112	1200	3.83	9.11	12.60	0.91	2.24	1.70	1.52
	D	0.010	0.126	0.127	1273	4.39	30.40	33.12	0.99	2.97	2.70	2.53
2	A	0.030	0.089	0.094	837	3.10	0.21	0.54	0.06	1.29	0.64	0.44
	B	0.031	0.106	0.112	1241	3.69	0.26	1.45	0.08	1.10	0.67	0.42
	C	0.027	0.121	0.127	1211	4.21	1.05	2.71	0.20	1.57	1.02	0.78
	D	0.029	0.141	0.146	1277	4.91	1.11	4.63	0.19	1.59	0.96	0.70
	E	0.028	0.159	0.166	1253	5.54	1.32	2.96	0.25	1.33	1.06	0.67
	F	0.028	0.179	0.185	1254	6.23	3.18	8.31	0.41	1.73	1.22	1.09
	G	0.030	0.205	0.21	1246	7.14	5.17	8.42	0.40	1.90	1.34	1.17
	H	0.031	0.225	0.23	1252	7.84	8.41	18.28	0.59	2.35	1.76	1.45
	I	0.029	0.245	0.249	1076	8.53	18.44	34.07	0.85	3.29	2.90	2.51
3	A	0.052	0.099	0.104	964	3.45	0.16	0.17	0.05	1.08	0.41	0.20
	B	0.052	0.116	0.122	1005	4.04	0.08	0.52	0.05	1.19	0.64	0.29
	C	0.051	0.134	0.138	1037	4.67	0.61	3.45	0.09	1.03	0.64	0.39
	D	0.050	0.148	0.159	1024	5.15	0.69	4.06	0.13	1.29	0.80	0.56
	E	0.048	0.165	0.172	1063	5.75	0.79	2.95	0.18	1.15	0.68	0.51
	F	0.044	0.183	0.189	1066	6.37	1.58	3.73	0.21	1.38	0.90	0.69
	G	0.045	0.203	0.211	1044	7.07	3.97	9.08	0.35	1.49	1.06	0.72
4	A	0.018	0.076	0.079	1152	2.65	0.51	0.85	0.13	1.13	0.55	0.37
	B	0.019	0.094	0.099	1164	3.27	0.17	0.89	0.08	1.10	0.63	0.44
	C	0.017	0.114	0.12	1140	3.97	0.43	2.38	0.12	1.31	0.78	0.51
	D	0.019	0.134	0.141	1212	4.67	2.54	7.24	0.34	1.57	1.19	0.86
	E	0.019	0.157	0.162	1139	5.47	1.24	12.23	0.44	2.03	1.57	1.33
	F	0.020	0.174	0.181	1188	6.06	11.04	24.54	1.00	2.57	2.18	2.08
5	A	0.038	0.101	0.105	928	3.52	0.58	0.81	0.09	0.96	0.44	0.25
	B	0.039	0.118	0.123	1103	4.11	0.40	1.71	0.11	1.32	0.62	0.37
	C	0.039	0.132	0.14	1063	4.60	0.47	2.17	0.11	1.26	0.61	0.44
	D	0.036	0.15	0.155	1093	5.22	1.76	4.31	0.16	1.25	0.76	0.51
	E	0.037	0.169	0.175	1076	5.89	1.04	3.96	0.18	1.39	1.05	0.79
	F	0.038	0.189	0.196	1053	6.58	3.01	5.81	0.20	1.41	0.92	0.70
	G	0.036	0.207	0.217	1048	7.21	8.74	14.23	0.39	1.70	1.17	0.88
6	A	0.029	0.145	0.153	336	5.05	0.90	3.52	0.15	1.35	0.93	0.72
	B	0.029	0.143	0.149	799	4.98	1.47	6.08	0.24	1.48	0.96	0.75
	C	0.028	0.141	0.149	1101	4.91	1.04	4.52	0.14	1.38	0.98	0.67
	D	0.029	0.142	0.15	2062	4.95	2.39	5.92	0.27	1.52	1.07	0.86
	E	0.029	0.143	0.149	3062	4.98	4.97	11.80	0.30	1.75	1.14	0.90
	F	0.029	0.142	0.148	4096	4.95	15.43	17.66	0.46	1.93	1.36	1.17
7	A	0.009	0.109	0.112	1194	3.80	11.92	16.55	0.49	2.08	1.62	1.17
	B	0.010	0.126	0.127	1292	4.39	29.43	40.21	1.21	2.38	1.99	1.78
	C	0.010	0.137	0.141	1315	4.77	40.67	42.80	1.05	2.34	2.34	1.82
8	A	0.028	0.161	0.168	1076	5.61	1.55	3.88	0.19	1.45	0.94	0.72
	B	0.028	0.184	0.191	1136	6.41	6.47	9.48	0.51	2.07	1.67	1.33
	C	0.029	0.203	0.21	1137	7.07	12.72	17.31	0.73	1.99	1.60	1.40

Table 25: *The damage parameters for all test series for the 1:8 slope for a characterization width of 27 d_{n50}.*

Test Information		Test conditions			Damage parameters											
Series	Run	$s_{o,p}$	$H_{1/3}$	$\frac{Hs}{\Delta d_{n50}}$	S		S_{all}		E_{2D}		$E_{3D,1}$		$E_{3D,3}$		$E_{3D,5}$	
					Part 1	Part 2	Part 1	Part 2	Part 1	Part 2	Part 1	Part 2	Part 1	Part 2	Part 1	Part 2
1	A	0.009	0.017	0.59	0.00	0.00	0.00	0.00	0.03	0.03	0.58	0.35	0.18	0.08	0.10	0.06
	B	0.008	0.024	0.84	0.25	0.08	0.25	0.15	0.06	0.05	0.79	0.84	0.47	0.30	0.26	0.15
	C	0.009	0.032	1.11	0.22	0.06	0.57	0.25	0.06	0.04	0.85	0.85	0.43	0.28	0.22	0.14
	D	0.009	0.042	1.46	0.31	0.25	0.91	0.85	0.12	0.11	0.83	1.30	0.49	0.67	0.27	0.30
	E	0.011	0.054	1.88	0.54	0.60	1.65	1.96	0.18	0.15	1.19	1.24	0.66	0.64	0.47	0.34
	F	0.010	0.065	2.26	1.10	1.10	2.92	2.22	0.26	0.15	1.43	1.28	0.89	0.81	0.59	0.61
	G	0.010	0.072	2.51	3.00	1.80	4.20	3.99	0.39	0.28	1.42	1.33	0.81	0.95	0.63	0.72
	H	0.009	0.081	2.82	6.46	8.87	8.82	11.13	0.56	0.68	1.55	1.88	1.21	1.52	0.97	1.33
2	A	0.016	0.025	0.87	0.05	0.06	0.06	0.00	0.04	0.01	0.87	0.37	0.34	0.12	0.14	0.07
	B	0.020	0.036	1.25	0.09	0.03	0.21	0.09	0.06	0.02	0.85	0.67	0.34	0.31	0.15	0.12
	C	0.017	0.041	1.43	0.12	0.05	0.51	0.13	0.07	0.04	0.83	0.91	0.34	0.39	0.14	0.16
	D*															
	E	0.020	0.068	2.37	0.39	0.48	1.62	0.79	0.14	0.15	0.96	0.91	0.60	0.49	0.34	0.38
	F	0.020	0.08	2.79	0.47	0.41	1.63	0.63	0.11	0.12	1.03	0.97	0.58	0.56	0.38	0.38
	G	0.020	0.087	3.03	1.90	0.76	3.04	1.26	0.25	0.15	1.06	1.09	0.69	0.71	0.51	0.46
	H	0.020	0.096	3.34	1.45	0.41	1.59	0.85	0.36	0.13	1.54	1.24	1.00	0.82	0.75	0.55
	I	0.019	0.110	3.83	3.94	0.16	4.78	0.88	0.31	0.03	1.63	1.46	1.11	1.12	0.80	0.67
3	A	0.028	0.053	1.85	0.17	0.30	0.38	0.58	0.06	0.11	0.68	1.01	0.28	0.48	0.14	0.25
	B	0.026	0.073	2.54	0.38	0.35	1.06	0.90	0.11	0.11	0.94	0.98	0.44	0.46	0.31	0.26
	C	0.027	0.095	3.31	1.88	1.39	3.82	3.45	0.31	0.39	1.12	1.16	0.80	0.88	0.66	0.61
	D	0.026	0.119	4.14	8.16	5.17	9.08	5.67	0.55	0.38	1.61	1.27	1.31	0.84	0.91	0.68
	E	0.025	0.145	5.05	14.25	3.62	16.58	8.40	0.46	0.49	2.14	2.23	1.68	1.97	1.61	1.76
3N	A	0.026	0.041	1.43	0.00	0.00	0.00	0.00	0.03	0.05	0.73	0.74	0.26	0.22	0.11	0.14
	B	0.030	0.055	1.92	0.18	0.16	0.70	0.49	0.07	0.07	0.89	0.70	0.40	0.31	0.23	0.18
	C	0.029	0.066	2.30	0.29	0.32	1.15	0.96	0.08	0.09	0.94	0.86	0.47	0.44	0.26	0.29
	D	0.029	0.081	2.82	1.19	1.01	2.61	2.12	0.17	0.16	1.06	1.03	0.57	0.51	0.45	0.36
	E	0.028	0.091	3.17	0.52	0.56	2.40	2.27	0.14	0.18	1.27	1.04	0.81	0.59	0.53	0.41
	F	0.029	0.105	3.66	1.68	0.54	4.25	2.82	0.32	0.16	1.37	1.06	0.87	0.71	0.61	0.46
	G	0.029	0.119	4.14	1.79	0.58	5.78	3.12	0.26	0.19	1.40	1.38	0.89	0.85	0.68	0.50
	H	0.029	0.13	4.53	8.69	1.09	12.60	2.65	0.62	0.30	2.23	1.31	1.72	0.88	1.57	0.62
	I	0.030	0.145	5.05	11.30	1.78	15.87	2.53	1.06	0.32	2.21	1.82	1.96	1.20	1.68	0.78
4	A	0.038	0.052	1.81	0.00	0.00	0.00	0.00	0.04	0.02	0.52	0.59	0.22	0.20	0.11	0.11
	B	0.038	0.066	2.30	0.00	0.20	0.00	0.21	0.03	0.08	0.81	0.77	0.44	0.28	0.22	0.16
	C	0.040	0.084	2.93	0.60	0.25	1.23	0.68	0.14	0.09	0.97	0.84	0.61	0.39	0.40	0.29
	D	0.038	0.1	3.48	1.22	0.49	2.14	1.87	0.17	0.19	1.00	1.06	0.57	0.53	0.46	0.42
	E	0.038	0.116	4.04	2.89	0.31	3.71	1.50	0.31	0.13	1.12	1.41	0.73	0.70	0.50	0.45
	F	0.038	0.131	4.56	1.28	2.38	3.55	2.73	0.26	0.28	1.45	1.62	1.14	1.13	0.86	0.76
	G	0.039	0.15	5.22	2.46	2.11	4.19	3.94	0.28	0.37	1.21	1.81	0.77	1.12	0.66	0.85
	H	0.040	0.167	5.82	4.00	2.27	7.00	4.10	0.54	0.31	1.59	1.65	1.23	1.14	0.96	0.84
5	A	0.048	0.056	1.95	0.05	0.00	0.05	0.00	0.04	0.02	0.85	0.65	0.40	0.27	0.18	0.13
	B	0.045	0.071	2.47	0.23	0.21	0.12	0.29	0.05	0.09	0.74	0.92	0.30	0.49	0.14	0.21
	C	0.047	0.091	3.17	0.46	0.26	0.66	0.61	0.08	0.10	1.01	1.09	0.48	0.58	0.27	0.28
	D	0.045	0.106	3.69	1.19	0.36	2.29	0.97	0.18	0.14	1.08	1.11	0.80	0.58	0.57	0.41
	E	0.043	0.122	4.25	2.08	0.44	4.03	1.45	0.29	0.15	1.33	1.13	0.86	0.62	0.72	0.40
	F	0.046	0.14	4.88	2.57	0.78	5.04	2.08	0.37	0.21	1.13	1.11	0.81	0.67	0.74	0.55
	G	0.049	0.153	5.33	2.95	1.78	6.86	2.34	0.36	0.22	1.33	1.25	1.00	0.86	0.84	0.72
	H	0.050	0.171	5.96	5.82	2.25	10.15	7.44	0.57	0.49	1.67	1.63	1.23	1.11	1.06	0.80
	I	0.050	0.189	6.58	7.05	7.10	14.15	10.37	0.73	0.50	2.27	1.46	1.85	0.95	1.43	0.75
6	A	0.028	0.117	4.07	1.32	2.20	3.52	3.34	0.26	0.09	1.68	1.46	0.79	1.08	0.49	0.82
	B	0.028	0.117	4.07	2.06	0.45	4.38	2.20	0.31	0.13	1.36	1.16	0.99	0.69	0.71	0.44
	C	0.029	0.118	4.11	2.72	1.60	4.62	4.24	0.35	0.32	1.41	1.56	0.86	0.91	0.65	0.64
	D	0.028	0.117	4.07	5.89	3.51	6.80	4.88	0.40	0.24	1.38	1.31	0.93	0.85	0.67	0.62
	E	0.029	0.118	4.11	3.52	5.69	6.96	6.77	0.25	0.32	1.83	1.48	1.41	1.05	0.99	0.80
	F	0.029	0.119	4.14	7.46	12.02	12.57	13.27	0.43	0.58	1.84	1.74	1.10	1.22	0.84	0.96
	G	0.029	0.119	4.14	13.93	15.06	15.87	16.35	0.58	0.60	1.71	1.51	1.22	1.09	0.98	0.92
	H	0.030	0.119	4.14	20.45	24.54	22.73	25.55	0.84	0.79	2.13	1.85	1.45	1.46	1.07	1.25
7	A	0.030	0.055	1.92	0.00	0.00	0.00	0.00	0.06	0.06	0.71	1.12	0.32	0.50	0.19	0.29
	B	0.029	0.067	2.33	0.23	0.17	0.14	0.45	0.09	0.13	0.92	1.13	0.50	0.53	0.26	0.30
	C	0.028	0.08	2.79	0.30	0.39	0.69	0.73	0.10	0.07	1.25	1.00	0.50	0.53	0.28	0.35
	D	0.029	0.092	3.20	1.07	0.68	2.55	1.46	0.19	0.11	1.29	0.98	0.63	0.60	0.37	0.32
	E	0.030	0.106	3.69	0.44	0.51	1.48	1.62	0.14	0.13	1.12	1.03	0.70	0.65	0.41	0.46
	F	0.029	0.12	4.18	3.60	1.65	5.73	3.49	0.37	0.21	1.17	1.25	0.80	0.83	0.68	0.68
	G	0.029	0.132	4.60	3.80	4.03	7.86	5.59	0.50	0.39	1.56	1.41	1.07	1.04	0.82	0.86
	H**	0.030	0.144	5.02	7.27	7.60	17.14	25.12	0.61	0.68	1.63	2.07	1.28	1.76	1.02	1.36
	I	0.028	0.156	5.43	34.60	34.56	35.72	36.14	1.45	1.48	2.13	2.43	1.77	2.01	1.69	1.78
	J	0.029	0.173	6.03	64.54	54.77	65.87	56.91	1.62	1.76	2.82	2.81	2.40	2.51	2.27	2.29
	K	0.029	0.189	6.58	90.39	93.59	95.47	96.59	2.29	2.26	3.23	3.05	2.81	2.67	2.54	2.50
	L	0.029	0.198	6.90	127.48	126.65	135.50	129.30	2.78	3.25	3.64	4.07	3.21	3.71	3.04	3.50
8	A	0.008	0.025	0.87	0.12	0.08	0.20	0.09	0.05	0.05	0.62	0.48	0.23	0.22	0.17	0.11
	B	0.010	0.035	1.22	0.08	0.13	0.14	0.25	0.04	0.07	0.92	0.83	0.38	0.35	0.21	0.15
	C	0.010	0.043	1.50	0.24	0.29	1.24	1.03	0.09	0.10	1.24	1.01	0.58	0.61	0.38	0.38
	D	0.010	0.052	1.81	0.41	0.62	1.87	1.98	0.16	0.15	1.16	1.06	0.58	0.60	0.37	0.34
	E	0.010	0.065	2.26	3.01	3.07	6.21	4.69	0.40	0.46	1.46	1.46	1.02	1.08	0.82	0.92
	F	0.010	0.073	2.54	10.98	3.94	11.17	5.64	0.66	0.36	1.65	1.46	1.15	0.92	0.92	0.68
	G	0.009	0.081	2.82	26.80	17.75	28.21	19.07	1.41	1.00	2.26	1.95	1.90	1.65	1.74	1.52
	H	0.010	0.093	3.24	44.71	27.93	48.02	30.95	1.88	1.23	2.98	2.08	2.57	1.73	2.35	1.62
	I	0.011	0.101	3.52	63.91	44.43	66.54	46.80	2.09	1.95	3.83	3.29	3.29	2.64	2.89	2.20
	J	0.011	0.11	3.83	115.88	95.43	118.70	96.79	3.07	2.65	4.67	3.72	4.31	3.30	4.05	3.05
	K	0.010	0.118	4.11	194.00	153.85	196.68	155.48	4.20	3.45	5.14	4.98	5.00	4.74	4.86	4.41
9	A	0.029	0.12	4.18	1.20	1.96	3.09	3.64	0.20	0.26	1.07	1.27	0.71	0.78	0.46	0.60
	B	0.029	0.12	4.18	5.95	3.02	6.27	4.11	0.39	0.26	1.35	1.46	0.89	0.88	0.69	0.66
	C	0.029	0.119	4.14	3.59	2.50	5.31	3.93	0.30	0.24	1.19	1.31	0.74	0.72	0.57	0.56
	D	0.029	0.119	4.14	1.26	2.56	2.81	4.14	0.24	0.28	1.30	1.32	0.73	0.71	0.52	0.55
	E	0.029	0.119	4.14	2.26	1.11	3.14	3.07	0.27	0.25	1.08	1.24	0.72	0.88	0.51	0.62
10	A	0.034	0.127	4.42	1.16	0.99	1.54	2.10	0.29	0.18	1.49	1.21	0.95	0.86	0.71	0.63
	Btov0	0.029	0.119	4.14	0.97	1.91	2.64	3.66	0.19	0.20	1.37	1.17	0.89	0.73	0.65	0.54
	Btov1	0.029	0.119	4.14	3.95	2.24	5.93	6.14	0.56	0.37	1.86	1.50	1.16	0.99	0.91	0.81

* Wave generators interrupted suddenly at this test and test is not completed. For that reason, this measurement/test is disregarded.

** 18 photos are missing at the upper slope. After consideration, it didn't affect the damage area and damage parameter significantly and for that reason is not disregarded.

Table 26: *The damage parameters for all test series for the 1:10 slope for a characterization width of 27 d_{n50}.*

Test Information			Test conditions		Damage parameters											
Series	Run	$s_{o,p}$	$H_{1/3}$	Hs Δd_{n50}	S		S_{all}		E_{2D}		$E_{3D,1}$		$E_{3D,3}$		$E_{3D,5}$	
					Part 1	Part 2	Part 1	Part 2	Part 1	Part 2	Part 1	Part 2	Part 1	Part 2	Part 1	Part 2
1	A	0.009	0.062	2.16	0.28	1.14	1.53	2.57	0.09	0.15	1.12	1.04	0.61	0.60	0.36	0.40
	B	0.010	0.087	3.03	2.03	2.22	6.45	7.27	0.30	0.33	1.43	1.44	0.87	0.99	0.62	0.81
	C	0.009	0.109	3.80	18.73	5.74	22.54	14.41	0.79	0.56	2.29	2.10	1.86	1.75	1.50	1.33
11	A	0.009	0.066	2.30	0.88	0.35	1.85	1.11	0.12	0.14	1.08	1.11	0.63	0.67	0.40	0.40
	B	0.010	0.086	3.00	1.10	2.41	4.08	6.21	0.25	0.46	1.44	1.43	0.86	0.99	0.60	0.79
	C	0.010	0.11	3.83	12.10	7.53	14.28	13.16	1.17	0.72	2.24	2.04	1.70	1.51	1.52	1.32
	D	0.010	0.126	4.39	31.13	31.48	34.06	34.30	0.96	1.21	2.89	2.97	2.70	2.67	2.36	2.53
2	A	0.030	0.089	3.10	0.32	0.33	1.48	0.77	0.09	0.09	1.29	1.11	0.50	0.64	0.23	0.44
	B	0.031	0.106	3.69	0.94	0.45	2.80	2.39	0.14	0.12	1.04	1.10	0.62	0.67	0.33	0.42
	C	0.027	0.121	4.21	1.63	1.16	4.88	3.84	0.33	0.21	1.34	1.57	0.90	1.02	0.75	0.78
	D	0.029	0.141	4.91	0.95	1.62	5.92	5.62	0.22	0.22	1.53	1.66	0.96	0.96	0.70	0.68
	E	0.028	0.159	5.54	0.60	2.11	3.72	5.30	0.19	0.36	1.33	1.29	0.91	1.06	0.50	0.67
	F	0.028	0.179	6.23	3.67	4.64	8.66	11.10	0.47	0.43	1.68	1.73	1.22	1.16	1.09	0.93
	G	0.030	0.205	7.14	6.78	3.84	10.25	9.85	0.53	0.38	1.86	1.90	1.32	1.34	1.00	1.17
	H	0.031	0.225	7.84	7.93	10.45	19.23	20.91	0.54	0.68	2.14	2.58	1.76	1.74	1.15	1.45
	I	0.029	0.245	8.53	17.35	19.72	34.13	40.02	0.72	1.10	2.41	3.29	1.79	2.90	1.56	2.51
3	A	0.052	0.099	3.45	0.25	0.09	0.30	0.32	0.06	0.04	0.80	1.08	0.38	0.41	0.18	0.20
	B	0.052	0.116	4.04	0.16	0.20	0.32	0.68	0.06	0.09	0.93	1.19	0.54	0.64	0.25	0.29
	C	0.051	0.134	4.67	0.54	0.73	3.24	4.40	0.11	0.13	0.96	1.03	0.58	0.64	0.30	0.39
	D	0.050	0.148	5.15	1.66	0.88	4.21	5.32	0.15	0.12	1.29	1.19	0.80	0.74	0.56	0.55
	E	0.048	0.165	5.75	1.39	0.62	3.46	4.20	0.20	0.16	1.13	1.15	0.68	0.60	0.51	0.51
	F	0.044	0.183	6.37	2.78	1.11	5.37	6.09	0.26	0.22	1.38	1.37	0.89	0.90	0.69	0.59
	G	0.045	0.203	7.07	4.06	3.30	9.30	11.13	0.33	0.40	1.29	1.49	0.86	1.06	0.63	0.72
4	A	0.018	0.076	2.65	0.50	0.56	1.60	1.11	0.12	0.15	1.13	0.97	0.52	0.55	0.29	0.37
	B	0.019	0.094	3.27	0.38	0.40	0.83	1.40	0.10	0.13	1.02	1.10	0.54	0.63	0.33	0.44
	C	0.017	0.114	3.97	0.69	0.43	2.76	2.89	0.16	0.11	1.13	1.31	0.62	0.78	0.39	0.51
	D	0.019	0.134	4.67	2.38	2.95	8.53	7.94	0.39	0.35	1.57	1.54	1.19	0.99	0.86	0.85
	E	0.019	0.157	5.47	5.77	5.97	15.20	12.42	0.63	0.66	2.03	1.84	1.42	1.57	1.21	1.33
	F	0.020	0.174	6.06	11.61	11.48	23.91	31.68	0.92	1.10	2.41	2.57	1.95	2.18	1.68	2.08
5	A	0.038	0.101	3.52	0.24	0.97	1.28	1.44	0.07	0.10	0.96	0.95	0.43	0.44	0.21	0.25
	B	0.039	0.118	4.11	1.16	0.87	2.01	2.66	0.14	0.12	0.96	1.32	0.55	0.62	0.37	0.35
	C	0.039	0.132	4.60	0.44	2.30	2.53	3.83	0.15	0.18	1.26	1.22	0.61	0.61	0.42	0.44
	D	0.036	0.15	5.22	3.18	1.47	5.61	5.18	0.23	0.20	1.25	1.24	0.67	0.76	0.47	0.51
	E	0.037	0.169	5.89	1.62	1.48	5.79	6.29	0.24	0.25	1.30	1.39	0.73	1.05	0.60	0.79
	F	0.038	0.189	6.58	1.60	4.60	7.52	7.30	0.24	0.32	1.26	1.41	0.91	0.92	0.65	0.70
	G	0.036	0.207	7.21	9.70	6.01	16.44	14.71	0.44	0.42	1.52	1.70	1.17	1.17	0.88	0.87
6	A	0.029	0.145	5.05	2.08	0.97	4.30	5.22	0.26	0.21	1.35	1.16	0.93	0.87	0.72	0.62
	B	0.029	0.143	4.98	2.05	2.42	6.36	7.61	0.28	0.44	1.48	1.33	0.96	0.86	0.65	0.75
	C	0.028	0.141	4.91	1.13	1.64	5.84	6.20	0.16	0.21	1.38	1.30	0.95	0.98	0.62	0.67
	D	0.029	0.142	4.95	3.35	3.20	7.18	7.86	0.44	0.35	1.52	1.50	1.07	0.96	0.86	0.79
	E	0.029	0.143	4.98	4.89	11.01	12.01	13.77	0.44	0.39	1.75	1.46	1.14	1.02	0.90	0.81
	F	0.029	0.142	4.95	11.86	19.40	14.25	22.29	0.36	0.64	1.51	1.93	1.03	1.36	0.72	1.17
7	A	0.009	0.109	3.80	12.14	12.53	15.73	19.22	0.59	0.58	1.94	2.19	1.29	1.62	1.11	1.17
	B	0.010	0.126	4.39	29.18	29.68	37.64	44.25	1.25	1.21	2.21	2.62	1.87	1.99	1.69	1.78
	C	0.010	0.137	4.77	41.29	32.96	45.16	41.96	0.95	1.19	2.34	2.15	2.34	1.78	1.82	1.55
8	A	0.028	0.161	5.61	0.23	2.51	6.89	4.66	0.26	0.29	1.21	1.45	0.88	0.94	0.57	0.72
	B	0.028	0.184	6.41	3.95	9.43	7.82	12.75	0.52	0.78	1.63	2.07	1.25	1.67	0.98	1.33
	C	0.029	0.203	7.07	11.24	14.57	15.08	20.81	0.62	0.86	1.86	1.99	1.17	1.60	0.96	1.40

Appendix I: Damage domain and damage location

Table 27: *The damage domain for the 1:8 for the locations Low, Mid-Low, Mid-High and High and the maximum damage location for the 2D and 3D damage parameters expressed in significant wave height H_s in vertical direction compared to SWL.*

Test Information		Test conditions			Damage domain				Max damage location			
Series	Run	$s_{o,p}$	$H_{1/3}$	$\frac{Hs}{\Delta d_{n50}}$	Low	Mid-Low	Mid-High	High	2D max	$E_{3D,1}$ max	$E_{3D,3}$ max	$E_{3D,5}$ max
1	A	0.009	0.017	0.59	-3.03	0.00	0.00	0.72	-	-3.01	-3.09	-3.20
	B	0.008	0.024	0.84	-2.14	-0.17	0.67	1.03	0.18	-0.13	0.26	0.18
	C	0.009	0.032	1.11	-3.09	-0.67	0.89	0.97	0.13	-0.10	0.14	0.14
	D	0.009	0.042	1.46	-4.02	-1.82	0.68	0.74	-0.55	-1.50	-1.47	-1.53
	E	0.011	0.054	1.88	-4.63	-2.11	0.55	0.78	0.11	-1.17	-0.82	-0.42
	F	0.010	0.065	2.26	-3.85	-2.70	1.00	1.11	-1.89	-1.88	-1.10	-1.07
	G	0.010	0.072	2.51	-3.48	-2.54	1.09	1.25	-0.80	-1.72	-1.09	-1.08
	H	0.009	0.081	2.82	-4.57	-2.70	0.99	1.12	-1.08	-1.18	-1.17	-1.20
2	A	0.016	0.025	0.87	-1.31	0.19	0.24	0.54	-	0.23	0.18	0.10
	B	0.020	0.036	1.25	-1.60	0.13	0.31	0.72	-	0.16	0.12	0.10
	C	0.017	0.041	1.43	-1.41	-1.13	0.64	0.64	0.09	0.27	0.26	0.32
	D*											
	E	0.020	0.068	2.37	-2.60	-1.18	0.49	0.64	-0.33	-0.27	-0.28	-0.33
	F	0.020	0.08	2.79	-3.38	-1.11	0.54	0.58	-0.26	-0.24	0.12	0.12
	G	0.020	0.087	3.03	-3.11	-2.03	0.80	0.92	-0.25	-1.36	0.15	-0.45
	H	0.020	0.096	3.34	-3.04	-2.74	0.73	0.92	-0.81	-0.70	-0.72	-0.74
	I	0.019	0.110	3.83	-3.07	-2.50	0.82	1.00	-0.70	-0.96	-0.96	-0.98
3	A	0.028	0.053	1.85	-1.89	-1.11	0.37	0.54	0.16	0.19	0.18	0.17
	B	0.026	0.073	2.54	-2.30	-0.88	0.55	0.55	-0.57	0.14	-0.52	-0.50
	C	0.027	0.095	3.31	-3.57	-2.08	0.60	0.73	-0.23	-0.22	-0.23	-0.26
	D	0.026	0.119	4.14	-3.34	-2.48	0.88	0.99	-0.32	-0.39	-0.39	-0.32
	E	0.025	0.145	5.05	-2.74	-2.04	0.81	0.82	-0.29	-0.75	-0.72	-0.72
3N	A	0.026	0.041	1.43	-1.77	-0.34	0.27	0.79	-	0.24	-1.77	0.03
	B	0.030	0.055	1.92	-1.84	-1.05	0.59	0.75	0.32	-1.02	-1.05	-1.00
	C	0.029	0.066	2.30	-1.82	-1.73	0.62	0.79	0.05	-0.79	-0.77	0.14
	D	0.029	0.081	2.82	-1.48	-1.41	0.55	0.71	-0.24	-0.41	-0.41	-0.28
	E	0.028	0.091	3.17	-2.01	-1.99	0.59	0.75	-0.14	-0.57	-0.39	-0.38
	F	0.029	0.105	3.66	-3.06	-1.93	0.64	0.66	-0.69	-0.67	-0.67	-0.35
	G	0.029	0.119	4.14	-2.70	-1.89	0.68	0.69	-0.11	-0.48	-0.48	-0.32
	H	0.029	0.13	4.53	-3.06	-1.92	0.64	0.77	-0.37	-0.40	-0.39	-0.43
	I	0.030	0.145	5.05	-2.74	-2.23	0.72	0.73	-0.37	-0.42	-0.42	-0.42
4	A	0.038	0.052	1.81	-1.11	-0.56	0.43	0.57	-	0.12	0.24	-0.02
	B	0.038	0.066	2.30	-3.37	-0.87	0.41	0.49	0.04	-0.21	-0.15	-0.15
	C	0.040	0.084	2.93	-2.65	-1.24	0.56	0.64	-0.17	-0.45	-0.16	-0.14
	D	0.038	0.1	3.48	-2.08	-1.56	0.57	0.74	-0.13	0.18	-0.62	-0.63
	E	0.038	0.116	4.04	-3.36	-1.58	0.63	0.64	-0.36	-1.03	-0.11	-0.44
	F	0.038	0.131	4.56	-2.98	-2.00	0.64	0.69	-0.45	-0.51	-0.47	-0.47
	G	0.039	0.15	5.22	-2.60	-2.19	0.66	0.70	-0.57	-0.61	-0.61	-0.62
	H	0.040	0.167	5.82	-2.40	-1.97	0.62	0.63	-0.51	-0.58	-0.51	-0.52
5	A	0.048	0.056	1.95	-1.03	-0.29	0.33	0.40	-	-0.27	-0.27	-0.23
	B	0.045	0.071	2.47	-2.49	-0.80	0.35	0.51	0.03	-0.30	0.00	0.02
	C	0.047	0.091	3.17	-3.20	-1.24	0.53	0.64	0.01	0.18	0.16	-0.19
	D	0.045	0.106	3.69	-2.75	-1.10	0.47	0.55	-0.22	0.15	-0.16	-0.17
	E	0.043	0.122	4.25	-3.02	-1.46	0.49	0.51	-0.17	-1.44	-0.58	-0.59
	F	0.046	0.14	4.88	-2.64	-1.43	0.59	0.61	-0.11	0.02	-0.10	-0.55
	G	0.049	0.153	5.33	-2.46	-1.68	0.46	0.60	-0.09	-1.15	-0.51	-0.51
	H	0.050	0.171	5.96	-2.20	-1.92	0.53	0.60	-0.40	-0.41	-0.57	-0.42
	I	0.050	0.189	6.58	-2.05	-1.75	0.55	0.65	-0.41	-0.40	-0.41	-0.41
6	A	0.028	0.117	4.07	-2.79	-1.80	0.66	0.68	-0.87	-0.77	-0.88	-0.87
	B	0.028	0.117	4.07	-2.79	-1.80	0.65	-0.40	-0.14	-0.13	-0.80	-0.80
	C	0.029	0.118	4.11	-2.77	-2.11	0.64	0.65	-0.61	-0.56	-0.60	-0.87
	D	0.028	0.117	4.07	-2.79	-2.13	0.65	0.66	-0.32	-0.13	-0.10	-0.90
	E	0.029	0.118	4.11	-3.35	-3.13	0.70	0.86	-0.58	-0.38	-0.37	-0.36
	F	0.029	0.119	4.14	-3.35	-3.10	0.70	0.82	-0.41	-0.13	-0.66	-0.65
	G	0.029	0.119	4.14	-3.35	-3.10	0.77	0.87	-0.32	-0.12	-0.12	-0.37
	H	0.030	0.119	4.14	-3.35	-3.10	0.77	0.90	-0.20	-0.66	-0.24	-0.38
7	A	0.030	0.055	1.92	-4.21	-0.76	0.47	0.70	-	-0.50	-0.50	-0.50
	B	0.029	0.067	2.33	-3.46	-0.86	0.61	0.65	0.14	-0.41	-0.41	-0.34
	C	0.028	0.08	2.79	-2.90	-0.93	0.60	0.65	-0.25	-0.12	-0.34	-0.28
	D	0.029	0.092	3.20	-2.52	-2.50	0.61	0.69	-0.55	-0.10	-0.10	-0.96
	E	0.030	0.106	3.69	-2.32	-2.19	0.66	0.76	-0.80	-0.20	-0.21	-1.13
	F	0.029	0.12	4.18	-2.78	-1.93	0.73	0.79	-0.68	-1.04	-1.03	-0.98
	G	0.029	0.132	4.60	-2.71	-1.84	0.80	0.86	-0.63	-0.90	-0.90	-0.92
	H**	0.030	0.144	5.02	-2.49	-1.70	0.76	0.80	-0.57	-0.82	-0.85	-0.84
	I	0.028	0.156	5.43	-2.29	-2.15	0.83	0.90	-0.53	-0.84	-0.84	-0.81
	J	0.029	0.173	6.03	-2.07	-1.96	0.75	0.84	-0.44	-0.68	-0.68	-0.67
	K	0.029	0.189	6.58	-1.91	-1.89	0.82	0.82	-0.41	-0.59	-0.60	-0.59
	L	0.029	0.198	6.90	-1.82	-1.81	0.78	0.78	-0.41	-0.60	-0.59	-0.59
8	A	0.008	0.025	0.87	-2.52	-1.77	0.38	0.63	0.23	-3.98	-4.05	-4.13
	B	0.010	0.035	1.22	-1.80	-0.69	0.56	0.70	0.00	-2.82	-2.86	-2.89
	C	0.010	0.043	1.50	-2.34	-1.99	0.69	0.95	0.41	-0.47	-0.48	-0.48
	D	0.010	0.052	1.81	-2.36	-2.32	0.81	1.00	-0.89	-2.04	-0.40	-0.40
	E	0.010	0.065	2.26	-3.68	-2.37	0.82	0.97	-1.12	-1.77	-1.77	-1.67
	F	0.010	0.073	2.54	-3.58	-3.24	0.95	1.16	-1.00	-1.36	-1.57	-1.42
	G	0.009	0.081	2.82	-3.83	-3.20	1.18	1.20	-0.89	-1.41	-1.39	-1.38
	H	0.010	0.093	3.24	-3.61	-3.54	1.10	1.26	-0.91	-1.34	-1.33	-1.28
	I	0.011	0.101	3.52	-3.33	-3.26	1.17	1.28	-1.01	-1.32	-1.33	-1.34
	J	0.011	0.11	3.83	-3.23	-2.99	1.19	1.26	-0.98	-1.33	-1.31	-1.31
	K	0.010	0.118	4.11	-3.01	-2.79	1.10	1.17	-0.92	-1.17	-1.18	-1.22
9	A	0.029	0.12	4.18	-2.72	-2.62	0.69	0.70	-0.23	-0.36	-0.35	-0.35
	B	0.029	0.12	4.18	-3.31	-2.25	0.64	0.84	-0.20	-0.19	-0.25	-0.27
	C	0.029	0.119	4.14	-2.84	-2.31	0.67	0.81	-0.21	-0.22	-0.41	-0.73
	D	0.029	0.119	4.14	-2.83	-2.52	0.66	0.78	-0.21	-1.51	-0.65	-0.63
	E	0.029	0.119	4.14	-3.24	-1.98	0.65	0.75	-0.17	0.40	-0.70	-0.59

* Wave generators interrupted suddenly at this test and test is not completed. For that reason, this measurement/test is disregarded.
** 18 photos are missing at the upper slope. After consideration, it didn't affect the damage area and damage parameter significantly and for that reason is not disregarded.

Table 28: *the damage domain for the 1:10 for the locations Low, Mid-Low, Mid-High and High and the maximum damage location for the 2D and 3D damage parameters expressed in significant wave height H_s in vertical direction compared to SWL*

Test Information		Test conditions			Damage domain				Max damage location			
Series	Run	$s_{o,p}$	$H_{1/3}$	Hs Δd_{n50}	Low	Mid-Low	Mid-High	High	2D max	$E_{3D,1}$ max	$E_{3D,3}$ max	$E_{3D,5}$ max
	A	0.009	0.062	2.16	-4.15	-3.35	0.44	0.50	-0.34	-1.10	-1.10	-0.71
1	B	0.010	0.087	3.03	-3.10	-3.00	0.47	0.59	-0.63	-1.66	-1.16	-1.16
	C	0.009	0.109	3.80	-2.48*	-2.47	0.53	0.82	-0.55	-1.04	-1.04	-1.03
	A	0.009	0.066	2.30	-3.73	-2.48	0.23	0.29	0.17	-1.41	-1.42	-1.41
11	B	0.010	0.086	3.00	-3.14	-3.13	0.49	0.63	-0.61	0.08	-1.19	-1.20
	C	0.010	0.11	3.83	-2.45	-2.45	0.38	0.49	-0.82	-1.24	-1.24	-1.25
	D	0.010	0.126	4.39	-2.14*	-2.14	0.69	0.71	-0.64	-1.12	-1.12	-1.10
	A	0.030	0.089	3.10	-2.19	-1.85	0.19	0.36	-0.09	-0.40	-0.56	-0.57
	B	0.031	0.106	3.69	-2.48	-2.28	0.17	0.47	-0.03	-0.16	-0.16	-0.48
	C	0.027	0.121	4.21	-2.23	-2.17	0.40	0.54	-0.44	-0.82	-0.83	-0.81
	D	0.029	0.141	4.91	-1.91*	-1.87	0.35	0.45	-0.36	-0.83	-0.83	-0.82
2	E	0.028	0.159	5.54	-1.70*	-1.70*	0.49	0.50	-0.18	-1.42	-1.02	-0.80
	F	0.028	0.179	6.23	-1.51*	-1.51*	0.44	0.53	-0.32	-0.49	-0.53	-0.53
	G	0.030	0.205	7.14	-1.32*	-1.32*	0.56	0.56	-0.26	-0.51	-0.71	-0.79
	H	0.031	0.225	7.84	-1.20*	-1.20*	0.50	0.51	-0.34	-0.58	-0.56	-0.56
	I	0.029	0.245	8.53	-1.10*	-1.10*	0.46*	0.47*	-0.22	-0.83	-0.84	-0.84
	A	0.052	0.099	3.45	-2.64	-1.70	0.05	0.31	0.00	-0.18	-0.18	-0.18
	B	0.052	0.116	4.04	-2.25	-1.04	0.10	0.27	-0.06	-0.54	-0.55	-0.44
	C	0.051	0.134	4.67	-1.95	-1.14	0.19	0.23	0.21	-0.55	-0.76	-0.75
3	D	0.050	0.148	5.15	-1.79	-1.76	0.19	0.34	-0.17	-0.55	-0.55	-0.55
	E	0.048	0.165	5.75	-1.61	-1.58	0.38	0.39	-0.14	-0.57	-0.54	-0.76
	F	0.044	0.183	6.37	-1.45	-1.42	0.39	0.42	-0.25	-0.48	-0.79	-0.79
	G	0.045	0.203	7.07	-1.33	-1.33	0.40	0.41	-0.23	-0.84	0.02	0.02
	A	0.018	0.076	2.65	-1.96	-1.76	0.25	0.29	-0.20	-1.49	-0.76	-0.76
	B	0.019	0.094	3.27	-2.48	-2.01	0.43	0.46	-0.04	-0.48	-0.97	-0.96
4	C	0.017	0.114	3.97	-2.37	-2.36	0.39	0.57	-0.82	-0.87	-1.46	-1.29
	D	0.019	0.134	4.67	-2.01*	-2.01	0.46	0.56	-0.58	-0.97	-0.97	-0.97
	E	0.019	0.157	5.47	-1.72*	-1.72*	0.57	0.67	-0.50	-1.37	-0.89	-0.89
	F	0.020	0.174	6.06	-1.55*	-1.55*	0.51	0.67	-0.40	-0.78	-0.76	-0.78
	A	0.038	0.101	3.52	-1.78	-1.31	0.07	0.08	-0.31	-0.08	-0.37	-0.37
	B	0.039	0.118	4.11	-2.29	-1.20	0.22	0.24	-0.24	-0.33	-0.31	-0.62
	C	0.039	0.132	4.60	-2.05*	-1.36	0.22	0.33	-0.33	-1.24	-0.28	-0.55
5	D	0.036	0.15	5.22	-1.80*	-1.77	0.31	0.35	-0.31	0.25	-0.61	-0.61
	E	0.037	0.169	5.89	-1.60*	-1.60	0.41	0.41	-0.17	-0.43	-0.75	-0.75
	F	0.038	0.189	6.58	-1.43*	-1.43	0.41	0.42	-0.39	-0.55	-0.56	-0.41
	G	0.036	0.207	7.21	-1.30*	-1.30	0.57	0.57	-0.23	-0.54	-0.73	-0.53
	A	0.029	0.145	5.05	-1.83	-1.79	0.34	0.46	-0.42	-0.77	-0.77	-0.77
	B	0.029	0.143	4.98	-1.89*	-1.82	0.34	0.46	-0.68	-0.74	-1.30	-0.99
6	C	0.028	0.141	4.91	-1.91*	-1.84	0.35	0.47	0.07	-0.63	-0.93	-0.94
	D	0.029	0.142	4.95	-1.90*	-1.87	0.46	0.58	-0.73	0.39	-1.06	-1.04
	E	0.029	0.143	4.98	-1.89*	-1.85	0.46	0.58	-0.73	-1.11	-0.91	-0.91
	F	0.029	0.142	4.95	-1.90*	-1.87	0.46	0.58	-0.52	-0.87	-0.87	-0.93
	A	0.009	0.109	3.80	-2.12*	-2.12*	0.51	0.72	-0.73	-1.46	-1.47	-1.46
7	B	0.010	0.126	4.39	-1.83*	-1.83*	0.56	0.63	-0.66	-1.26	-1.27	-1.36
	C	0.010	0.137	4.77	-1.69*	-1.69*	0.82	0.90	-0.58	-1.34	-1.28	-1.25
	A	0.028	0.161	5.61	-1.43*	-1.43*	0.41	0.43	-0.69	-1.76	-1.38	-1.38
8	B	0.028	0.184	6.41	-1.26*	-1.26*	0.36	0.41	-0.59	-1.01	-1.01	-1.01
	C	0.029	0.203	7.07	-1.14*	-1.14*	0.48	0.63	-0.52	-1.25	-1.24	-1.24
				Average values	-2.4	-1.9	0.4	0.5	-0.4	-0.8	-0.8	-0.8

* These tests are considered to be unreliable, because the damage location is expected to be outside the measured area.

Appendix J: Results of entrained and deposited coloured rocks

Table 29: *Overview of entrained, deposited and totally transported rocks per strip for 1:8 slope. Bl =Black strip 1 (<-2.5m), R =Red strip 1 (-2.5 - -2.0m) B =Blue strip (-2.0 - -1.5m), P =Purple strip (-1.5 – 1.0 -m), Y =Yellow strip (-1.0 - -0.5m) , G =Green strip (-0.5 – 0.0m), O =Orange strip (0.0 - 0.5m), R2 =Red strip 2 (0.5 - 1.0m), Bl2 =Black strip 2 (> 1.0m)*

Eroded stones per strip

Test	Bl	R	B	P	Y	G	O	R2	Bl2
1a	0	0	0	0	0	0	0	0	0
1b	0	0	0	0	0	1	0	0	0
1c	0	0	0	0	0	1	0	0	0
1d	0	0	0	0	0	3	0	0	0
1e	0	0	0	0	5	9	1	0	0
1f	0	0	0	3	155	73	4	0	0
1g	0	0	0	4	315	151	6	0	0
1h	0	0	1	13	614	320	13	0	0
2a	0	0	0	0	0	0	0	0	0
2b	0	0	0	0	0	0	0	0	0
2c	0	0	0	0	0	0	0	0	0
2d									
2e	0	0	0	0	5	8	0	0	0
2f	0	0	0	0	48	20	0	0	0
2g	0	0	0	1	98	88	3	0	0
2h	0	1	1	7	212	157	8	1	0
2i	0	3	3	31	380	278	20	3	0
3a	0	0	0	0	0	0	0	0	0
3b	0	0	0	0	1	12	1	0	0
3c	0	0	0	0	33	96	3	0	0
3d	0	0	2	21	208	344	17	0	0
3e	0	5	17	117	599	624	53	5	0
3Na	0	0	0	0	0	0	0	0	0
3NB	0	0	0	0	0	1	0	0	0
3NC	0	0	0	0	0	3	0	0	0
3ND	0	0	0	0	13	17	2	0	0
3NE	0	0	0	1	42	60	4	0	0
3NF	0	0	0	1	100	85	3	0	0
3NG	0	0	0	1	184	176	10	0	0
3NH	0	0	3	27	353	290	15	0	0
3NI	0	2	5	67	710	478	27	2	0
4A	0	0	0	0	0	0	0	0	0
4B	0	0	0	0	0	0	0	0	0
4C	0	0	0	0	0	7	0	0	0
4D	0	0	0	0	12	25	0	0	0
4E	0	0	0	3	39	72	2	0	0
4F	0	0	0	12	121	157	6	0	0
4G	0	0	1	33	243	220	19	0	0
4H	0	1	6	82	494	312	29	1	0
5A	0	0	0	0	0	0	0	0	0
5B	0	0	0	0	0	0	0	0	0
5C	0	0	0	0	0	4	2	0	0
5D	0	0	0	0	10	29	2	0	0
5E	0	0	0	3	53	55	5	0	0
5F	0	0	0	12	105	102	10	0	0
5G	0	0	2	24	186	163	17	0	0
5H	0	1	4	42	330	232	44	1	0
5I	0	4	17	69	496	342	69	4	0
6A	0	0	0	14	55	54	4	0	0
6B	0	0	1	20	79	79	4	0	0
6C	0	0	2	21	160	144	8	0	0
6D	0	0	3	19	222	243	9	0	0
6E	0	0	9	29	424	374	12	0	0
6F	0	0	6	29	561	444	16	0	0
6G	0	0	6	45	637	591	22	0	0
6H	0	0	6	74	755	738	56	0	0
7A	0	0	0	0	0	1	0	0	0
7B	0	0	0	0	0	2	1	0	0
7C	0	0	0	0	0	9	1	0	0
7D	0	0	0	0	8	27	3	0	0
7E	0	0	0	2	59	50	6	0	0
7F	0	0	0	10	163	143	15	0	0
7G	0	2	0	27	301	258	17	2	0
7H	0	2	6	66	624	339	22	3	0
7I	0	0	0	0	0	0	0	0	0
7J	0	0	0	0	0	0	0	0	0
7K	0	0	0	0	0	0	0	0	0
7L	0	0	0	0	0	0	0	0	0
8A	0	0	0	0	0	0	0	0	0
8B	0	0	0	0	0	0	0	0	0
8C	0	0	0	0	1	1	0	0	0
8D	0	0	0	0	1	5	2	0	0
8E	0	0	0	4	109	61	7	0	0
8F	0	0	0	5	243	102	8	0	0
8G	0	0	1	14	587	177	20	0	0
8H	0	0	0	0	0	0	0	0	0
8I	0	0	0	0	0	0	0	0	0
8J	0	0	0	0	0	0	0	0	0
8K	0	0	0	0	0	0	0	0	0
9A	0	0	3	19	119	133	15	0	0
9B	0	1	3	6	97	168	24	1	0
9C	0	0	2	4	93	109	7	0	0
9D	0	0	2	5	116	94	5	0	0
9E	0	0	1	10	124	122	9	0	0
10A	0	0	1	5	37	5	2	0	0
10B	0	0	1	7	111	138	4	0	0

Deposited stones per strip

Test	Bl	R	B	P	Y	G	O	R2	Bl2
1a	0	0	0	0	0	0	0	0	0
1b	0	0	0	0	0	0	1	0	0
1c	0	0	0	0	0	0	1	0	0
1d	0	0	0	0	0	0	3	0	0
1e	0	0	0	0	1	6	8	0	0
1f	0	0	0	0	40	155	38	2	0
1g	0	0	0	0	89	286	94	7	0
1h	0	0	0	1	203	484	253	20	0
2a	0	0	0	0	0	0	0	0	0
2b	0	0	0	0	0	0	0	0	0
2c	0	0	0	0	0	0	0	0	0
2d	0								
2e	0	0	0	0	0	5	8	0	0
2f	0	0	0	0	2	48	18	0	0
2g	0	0	0	0	47	98	42	3	0
2h	0	0	1	1	89	200	86	9	0
2i	1	0	2	15	168	309	193	28	0
3a	0	0	0	0	0	0	0	0	0
3b	0	0	0	0	0	2	12	0	0
3c	0	0	0	0	43	30	57	2	0
3d	0	0	0	37	193	151	185	26	0
3e	0	0	9	195	385	361	344	121	0
3Na	0	0	0	0	0	0	0	0	0
3NB	0	0	0	0	0	0	1	0	0
3NC	0	0	0	0	0	0	3	0	0
3ND	0	0	0	0	5	15	12	0	0
3NE	0	0	0	2	28	43	33	1	0
3NF	0	0	0	2	42	97	47	1	0
3NG	0	0	0	11	99	162	89	10	0
3NH	0	1	3	67	152	228	210	27	0
3NI	0	0	14	139	283	363	426	64	0
4A	0	0	0	0	0	0	0	0	0
4B	0	0	0	0	0	0	0	0	0
4C	0	0	0	0	2	0	5	0	0
4D	0	0	0	1	16	11	9	0	0
4E	0	0	0	11	39	26	37	3	0
4F	0	0	0	20	98	97	76	5	0
4G	0	0	5	52	135	166	132	26	0
4H	0	2	28	143	197	307	196	51	0
5A	0	0	0	0	0	0	0	0	0
5B	0	0	0	0	0	0	0	0	0
5C	0	0	0	0	2	1	2	1	0
5D	0	0	0	1	18	10	11	1	0
5E	0	0	3	11	35	41	21	5	0
5F	0	0	6	28	56	76	52	11	0
5G	0	0	15	46	91	137	84	19	0
5H	0	0	24	116	133	208	127	45	0
5I	0	13	51	185	175	285	196	92	0
6A	0	0	0	15	31	40	37	4	0
6B	0	0	0	20	43	58	57	5	0
6C	0	1	1	23	80	132	89	9	0
6D	0	1	1	29	146	176	133	10	0
6E	0	5	4	45	227	313	240	14	0
6F	0	3	2	59	238	342	391	21	0
6G	0	3	7	72	326	360	507	26	0
6H	0	3	7	112	423	399	652	33	0
7A	0	0	0	0	0	0	1	0	0
7B	0	0	0	0	0	1	2	0	0
7C	0	0	0	0	1	1	8	0	0
7D	0	0	0	0	5	9	22	2	0
7E	0	0	0	0	15	60	37	5	0
7F	0	0	0	0	30	145	140	16	0
7G	0	0	5	9	67	235	269	20	0
7H	0	0	13	30	80	403	483	51	0
7I	0	0	0	0	0	0	0	0	0
7J	0	0	0	0	0	0	0	0	0
7K	0	0	0	0	0	0	0	0	0
7L	0	0	0	0	0	0	0	0	0
8A	0	0	0	0	0	0	0	0	0
8B	0	0	0	0	0	0	0	0	0
8C	0	0	0	0	0	1	1	0	0
8D	0	0	0	0	3	3	2	0	0
8E	0	0	0	0	9	109	60	3	0
8F	0	0	0	0	20	222	103	13	0
8G	0	0	0	1	42	480	246	30	0
8H	0	0	0	0	0	0	0	0	0
8I	0	0	0	0	0	0	0	0	0
8J	0	0	0	0	0	0	0	0	0
8K	0	0	0	0	0	0	0	0	0
9A	0	0	0	11	84	105	73	16	0
9B	0	0	2	6	109	94	68	20	0
9C	0	0	0	9	52	82	65	7	0
9D	0	0	0	12	56	94	53	7	0
9E	0	0	0	6	69	112	69	10	0
10A	0	0	0	7	5	32	5	1	0
10B	0	0	0	1	7	100	63	4	0

Total transported stones per strip

Test	Bl	R	B	P	Y	G	O	R2	Bl2
1a	0	0	0	0	0	0	0	0	0
1b	0	0	0	0	0	-1	1	0	0
1c	0	0	0	0	0	-1	1	0	0
1d	0	0	0	0	0	-3	3	0	0
1e	0	0	0	0	-4	-3	7	0	0
1f	0	0	0	-3	-115	82	34	2	0
1g	0	0	0	-4	-226	135	88	7	0
1h	0	0	-1	-12	-411	164	240	20	0
2a	0	0	0	0	0	0	0	0	0
2b	0	0	0	0	0	0	0	0	0
2c	0	0	0	0	0	0	0	0	0
2d									
2e	0	0	0	0	-5	-3	8	0	0
2f	0	0	0	0	-46	28	18	0	0
2g	0	0	0	-1	-51	10	39	3	0
2h	0	-1	0	-6	-123	43	78	8	0
2i	1	-3	-1	-16	-212	31	173	25	0
3a	0	0	0	0	0	0	0	0	0
3b	0	0	0	0	-1	-10	11	0	0
3c	0	0	0	0	10	-66	54	2	0
3d	0	0	-2	16	-15	-193	168	26	0
3e	0	-5	-8	78	-214	-263	291	116	0
3Na	0	0	0	0	0	0	0	0	0
3NB	0	0	0	0	0	-1	1	0	0
3NC	0	0	0	0	0	-3	3	0	0
3ND	0	0	0	0	-8	-2	10	0	0
3NE	0	0	0	1	-14	-17	29	1	0
3NF	0	0	0	1	-58	12	44	1	0
3NG	0	0	0	10	-85	-14	79	10	0
3NH	0	1	0	40	-201	-62	195	27	0
3NI	0	-2	9	72	-427	-115	399	62	0
4A	0	0	0	0	0	0	0	0	0
4B	0	0	0	0	0	0	0	0	0
4C	0	0	0	0	2	-7	5	0	0
4D	0	0	0	1	4	-14	9	0	0
4E	0	0	0	8	0	-46	35	3	0
4F	0	0	0	8	-23	-60	70	5	0
4G	0	0	4	19	-108	-54	113	26	0
4H	0	1	22	61	-297	-5	167	50	0
5A	0	0	0	0	0	0	0	0	0
5B	0	0	0	0	0	0	0	0	0
5C	0	0	0	0	2	-3	0	1	0
5D	0	0	0	1	8	-19	9	1	0
5E	0	0	3	8	-18	-14	16	5	0
5F	0	0	6	16	-49	-26	42	11	0
5G	0	0	13	22	-95	-26	67	19	0
5H	0	-1	20	74	-197	-24	83	44	0
5I	0	9	34	116	-321	-57	127	88	0
6A	0	0	0	1	-24	-14	33	4	0
6B	0	0	-1	0	-36	-21	53	5	0
6C	0	1	-1	2	-80	-12	81	9	0
6D	0	1	-2	10	-76	-67	124	10	0
6E	0	5	-5	16	-197	-61	228	14	0
6F	0	3	-4	30	-323	-102	375	21	0
6G	0	3	1	27	-311	-231	485	26	0
6H	0	3	1	38	-332	-339	596	33	0
7A	0	0	0	0	0	-1	1	0	0
7B	0	0	0	0	0	-1	1	0	0
7C	0	0	0	0	1	-8	7	0	0
7D	0	0	0	0	-3	-18	19	2	0
7E	0	0	0	-2	-44	10	31	5	0
7F	0	0	0	-10	-133	2	125	16	0
7G	0	-2	5	-18	-234	-23	252	18	0
7H	0	-2	7	-36	-544	64	461	48	0
7I	0	0	0	0	0	0	0	0	0
7J	0	0	0	0	0	0	0	0	0
7K	0	0	0	0	0	0	0	0	0
7L	0	0	0	0	0	0	0	0	0
8A	0	0	0	0	0	0	0	0	0
8B	0	0	0	0	0	0	0	0	0
8C	0	0	0	0	0	0	0	0	0
8D	0	0	0	0	2	-2	0	0	0
8E	0	0	0	-4	-100	48	53	3	0
8F	0	0	0	-5	-223	120	95	13	0
8G	0	0	-1	-13	-545	303	226	30	0
8H	0	0	0	0	0	0	0	0	0
8I	0	0	0	0	0	0	0	0	0
8J	0	0	0	0	0	0	0	0	0
8K	0	0	0	0	0	0	0	0	0
9A	0	0	-3	-8	-35	-28	58	16	0
9B	0	-1	-1	0	12	-74	44	19	0
9C	0	0	-2	5	-41	-27	58	7	0
9D	0	0	-2	7	-60	0	48	7	0
9E	0	0	-1	-4	-55	-10	60	10	0
10A	0	0	-1	2	-32	27	3	1	0
10B	0	0	-1	-6	-104	-38	59	4	0

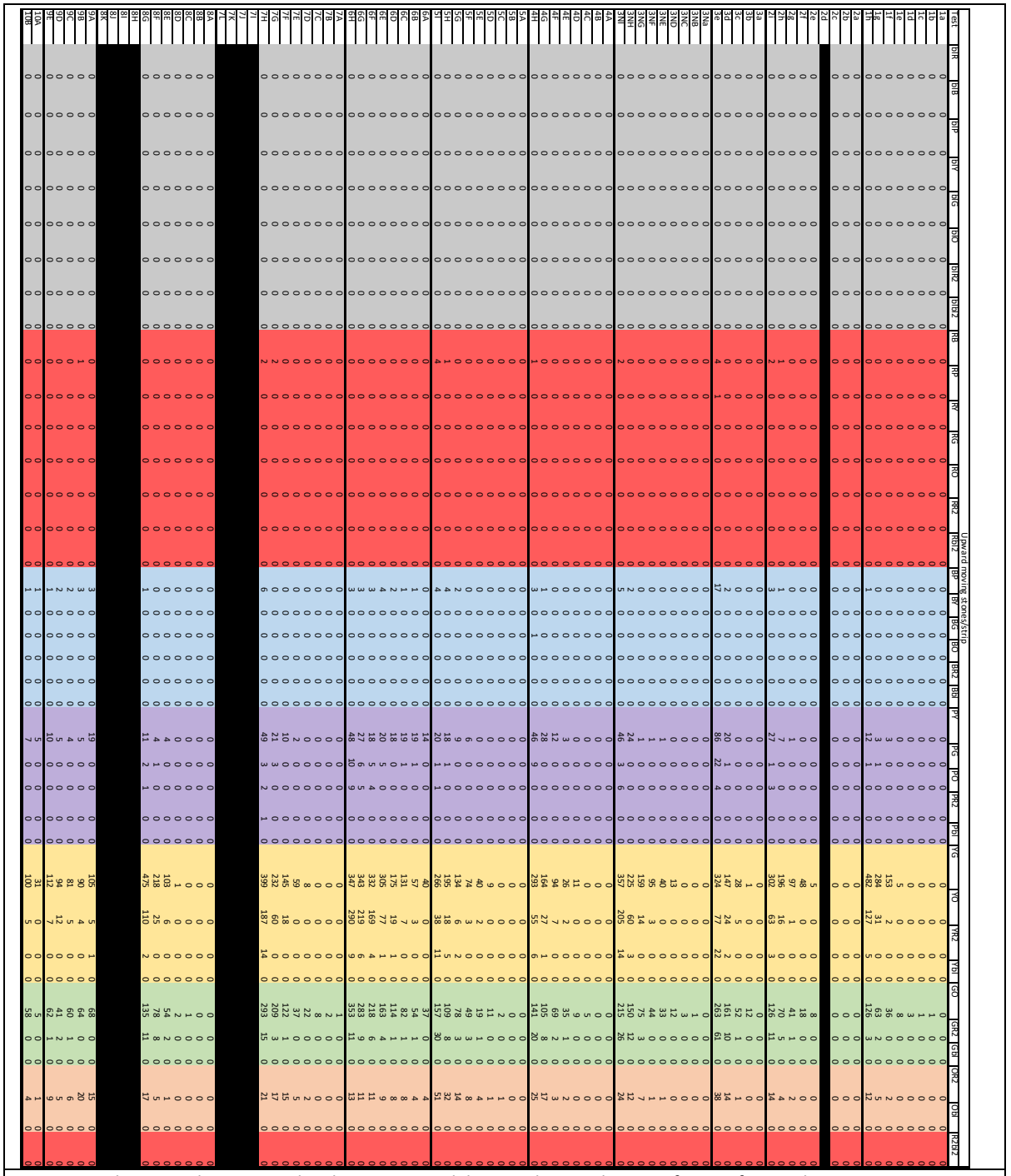

Figure 48: *The upward transported rocks per strip and deposited in another specific strip for 1:8 slope.*

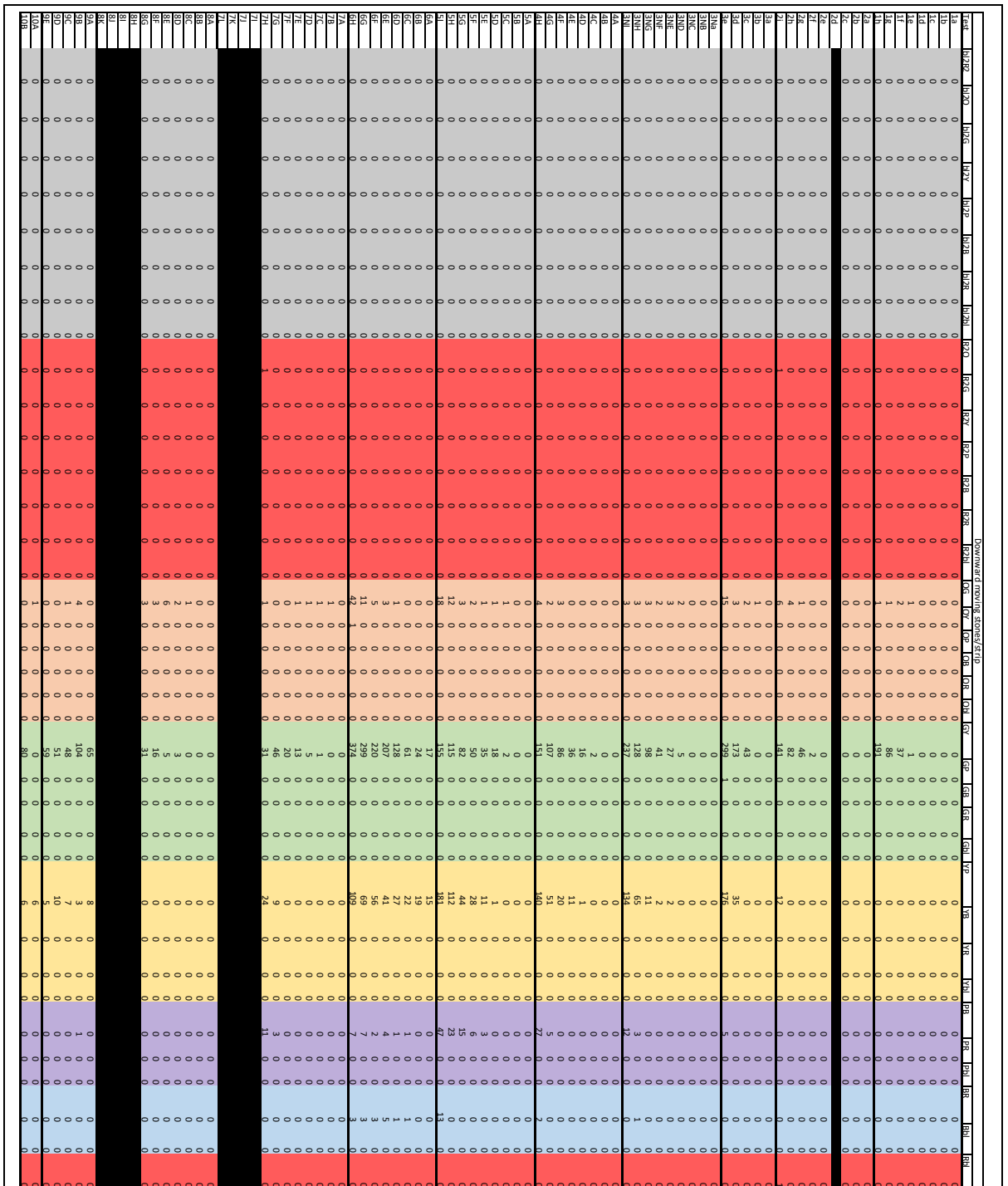

Figure 49: *The downward transported rocks per strip and deposited in another specific strip for 1:8 slope.*

Table 30: *Overview of entrained, deposited and totally transported rocks per strip* for 1:10 slope. *Bl =Black strip 1 (<-2.5m), R =Red strip 1 (-2.5 - -2.0m) B =Blue strip (-2.0 - -1.5m), P =Purple strip (-1.5 – 1.0 -m), Y =Yellow strip (-1.0 - -0.5m) , G =Green strip (-0.5 – 0.0m), O =Orange strip (0.0 - 0.5m), R2 =Red strip 2 (0.5 - 1.0m), Bl2 =Black strip 2 (> 1.0m)*

Eroded stones per strip							
Test	Bl	R	B	P	Y	G	O
1.2a	0	0	0	6	31	9	0
1.2b	0	2	7	214	207	32	5
1.2c	6	23	213	870	420	44	14
2a	0	1	3	3	0	3	0
2b	3	2	11	13	1	7	0
2c	22	60	48	27	22	12	1
2d	54	107	100	43	28	18	3
2e	162	224	167	67	48	25	13
2f	339	379	216	93	63	37	22
3a	0	0	0	0	1	1	0
3b	0	0	0	0	2	6	0
3c	0	0	0	1	9	10	0
3d	0	0	2	4	24	22	0
3e	0	0	2	14	51	36	7
3f	0	0	27	79	131	68	23
3g	0	7	74	170	186	97	37
4a	0	0	0	3	25	5	0
4b	0	1	0	15	45	17	0
4c	1	5	17	87	151	38	3
4d	6	19	55	412	313	50	13
5a	0	0	0	0	3	1	0
5b	0	0	0	0	22	3	0
5c	0	0	1	0	40	19	0
5d	0	0	7	18	89	38	3
6a	0	11	8	55	50	17	9
6b	0	11	22	104	92	46	7
6c	0	13	31	174	134	85	8
6d	0	15	57	271	229	109	13
6e	0	31	86	399	333	131	12
7a	6	92	456	244	137	30	0
8a	5	37	123	141	50	34	0
8b	19	102	328	265	112	52	0

Deposited stones per strip								
Test	Bl	R	B	P	Y	G	O	Bl
1.2a	0	0	0	2	6	29	9	0
1.2b	0	0	3	34	215	180	29	6
1.2c	0	8	70	229	645	494	127	17
2a	0	0	1	3	3	0	3	0
2b	0	3	2	11	13	1	7	0
2c	0	34	56	38	23	25	14	2
2d	11	64	79	87	44	36	27	5
2e	70	148	138	149	75	63	40	23
2f	131	254	243	186	119	92	67	57
3a	0	0	0	0	0	1	1	0
3b	0	0	0	0	1	2	5	0
3c	0	0	1	1	1	7	10	0
3d	0	0	2	5	4	19	22	0
3e	0	0	5	6	9	45	38	7
3f	0	8	37	29	53	107	65	29
3g	0	34	78	61	108	141	97	52
4a	0	0	0	0	3	25	5	0
4b	0	0	1	0	17	45	15	0
4c	0	3	8	27	87	136	37	4
4d	0	8	38	93	263	376	72	18
5a	0	0	0	0	0	3	1	0
5b	0	0	0	0	1	22	2	0
5c	0	0	0	5	6	35	14	0
5d	0	4	2	14	20	73	39	3
6a	0	0	13	18	53	39	18	9
6b	0	3	34	35	78	75	50	7
6c	0	3	35	37	142	116	104	8
6d	0	3	42	65	228	196	144	16
6e	0	15	62	89	296	304	207	19
7a	0	8	79	390	270	179	39	0
8a	0	14	41	108	127	64	36	0
8b	0	52	96	266	227	152	83	2

Total transported stones per strip								
Test	Bl	R	B	P	Y	G	O	Bl
1.2a	0	0	0	-4	-25	20	9	0
1.2b	0	-2	-4	-180	8	148	24	6
1.2c	-6	-15	-143	-641	225	450	113	17
2a	0	-1	-2	0	3	-3	3	0
2b	-3	1	-9	-2	12	-6	7	0
2c	-22	-26	8	11	1	13	13	2
2d	-43	-43	-21	44	16	18	24	5
2e	-92	-76	-29	82	27	38	27	23
2f	-208	-125	27	93	56	55	45	57
3a	0	0	0	0	-1	0	1	0
3b	0	0	0	0	-1	-4	5	0
3c	0	0	1	0	-8	-3	10	0
3d	0	0	0	1	-20	-3	22	0
3e	0	0	3	-8	-42	9	31	7
3f	0	8	10	-50	-78	39	42	29
3g	0	27	4	-109	-78	44	60	52
4a	0	0	0	-3	-22	20	5	0
4b	0	-1	1	-15	-28	28	15	0
4c	-1	-2	-9	-60	-64	98	34	4
4d	-6	-11	-17	-319	-50	326	59	18
5a	0	0	0	0	-3	2	1	0
5b	0	0	0	0	-21	19	2	0
5c	0	0	-1	5	-34	16	14	0
5d	0	4	-5	-4	-69	35	36	3
6a	0	-11	5	-37	3	22	9	9
6b	0	-8	12	-69	-14	29	43	7
6c	0	-10	4	-137	8	31	96	8
6d	0	-12	-15	-206	-1	87	131	16
6e	0	-16	-24	-310	-37	173	195	19
7a	0	-6	-84	-377	146	133	149	39
8a	0	-5	-23	-82	-33	77	30	36
8b	0	-19	-50	-232	1	115	100	83

Eroded stones per strip							
Test	Bl	R	B	P	Y	G	O
1.2a	0	0	0	6	31	9	0
1.2b	0	2	7	214	207	32	5
1.2c	6	23	213	870	420	44	14
2a	0	1	3	3	0	3	0
2b	3	2	11	13	1	7	0
2c	22	60	48	27	22	12	1
2d	54	107	100	43	28	18	3
2e	162	224	167	67	48	25	13
2f	339	379	216	93	63	37	22
3a	0	0	0	0	1	1	0
3b	0	0	0	0	2	6	0
3c	0	0	0	1	9	10	0
3d	0	0	2	4	24	22	0
3e	0	0	2	14	51	36	7
3f	0	0	27	79	131	68	23
3g	0	7	74	170	186	97	37
4a	0	0	0	3	25	5	0
4b	0	1	0	15	45	17	0
4c	1	5	17	87	151	38	3
4d	6	19	55	412	313	50	13
5a	0	0	0	0	3	1	0
5b	0	0	0	0	22	3	0
5c	0	0	1	0	40	19	0
5d	0	0	7	18	89	38	3
6a	0	11	8	55	50	17	9
6b	0	11	22	104	92	46	7
6c	0	13	31	174	134	85	8
6d	0	15	57	271	229	109	13
6e	0	31	86	399	333	131	12
7a	6	92	456	244	137	30	0
8a	5	37	123	141	50	34	0
8b	19	102	328	265	112	52	0

Deposited stones per strip								
Test	Bl	R	B	P	Y	G	O	Bl
1.2a	0	0	0	2	6	29	9	0
1.2b	0	0	3	34	215	180	29	6
1.2c	0	8	70	229	645	494	127	17
2a	0	0	1	3	3	0	3	0
2b	0	3	2	11	13	1	7	0
2c	0	34	56	38	23	25	14	2
2d	11	64	79	87	44	36	27	5
2e	70	148	138	149	75	63	40	23
2f	131	254	243	186	119	92	67	57
3a	0	0	0	0	0	1	1	0
3b	0	0	0	0	1	2	5	0
3c	0	0	1	1	1	7	10	0
3d	0	0	2	5	4	19	22	0
3e	0	0	5	6	9	45	38	7
3f	0	8	37	29	53	107	65	29
3g	0	34	78	61	108	141	97	52
4a	0	0	0	0	3	25	5	0
4b	0	0	1	0	17	45	15	0
4c	0	3	8	27	87	136	37	4
4d	0	8	38	93	263	376	72	18
5a	0	0	0	0	0	3	1	0
5b	0	0	0	0	1	22	2	0
5c	0	0	0	5	6	35	14	0
5d	0	4	2	14	20	73	39	3
6a	0	0	13	18	53	39	18	9
6b	0	3	34	35	78	75	50	7
6c	0	3	35	37	142	116	104	8
6d	0	3	42	65	228	196	144	16
6e	0	15	62	89	296	304	207	19
7a	0	8	79	390	270	179	39	0
8a	0	14	41	108	127	64	36	0
8b	0	52	96	266	227	152	83	2

Total transported stones per strip								
Test	Bl	R	B	P	Y	G	O	Bl
1.2a	0	0	0	-4	-25	20	9	0
1.2b	0	-2	-4	-180	8	148	24	6
1.2c	-6	-15	-143	-641	225	450	113	17
2a	0	-1	-2	0	3	-3	3	0
2b	-3	1	-9	-2	12	-6	7	0
2c	-22	-26	8	11	1	13	13	2
2d	-43	-43	-21	44	16	18	24	5
2e	-92	-76	-29	82	27	38	27	23
2f	-208	-125	27	93	56	55	45	57
3a	0	0	0	0	-1	0	1	0
3b	0	0	0	0	-1	-4	5	0
3c	0	0	1	0	-8	-3	10	0
3d	0	0	0	1	-20	-3	22	0
3e	0	0	3	-8	-42	9	31	7
3f	0	8	10	-50	-78	39	42	29
3g	0	27	4	-109	-78	44	60	52
4a	0	0	0	-3	-22	20	5	0
4b	0	-1	1	-15	-28	28	15	0
4c	-1	-2	-9	-60	-64	98	34	4
4d	-6	-11	-17	-319	-50	326	59	18
5a	0	0	0	0	-3	2	1	0
5b	0	0	0	0	-21	19	2	0
5c	0	0	-1	5	-34	16	14	0
5d	0	4	-5	-4	-69	35	36	3
6a	0	-11	5	-37	3	22	9	9
6b	0	-8	12	-69	-14	29	43	7
6c	0	-10	4	-137	8	31	96	8
6d	0	-12	-15	-206	-1	87	131	16
6e	0	-16	-24	-310	-37	173	195	19
7a	0	-6	-84	-377	146	133	149	39
8a	0	-5	-23	-82	-33	77	30	36
8b	0	-19	-50	-232	1	115	100	83

Figure 50: *The upward and downward transported rocks per strip and deposited in another specific strip for 1:8 slope.*

Table 31: *The results for the parameters n_{gross}, n_{net}, N_{od}, S_{od}, and the mobility parameter based on the entrained coloured rocks for the 1:10 slope.*

Test Information		Test conditions			Parameters				
Series	Run	$s_{o,p}$	$H_{1/3}$	$\frac{Hs}{\Delta d_{n50}}$	n_{gross}	n_{net}	N_{od}	S_{od}	Mobility parameter
	A	0.009	0.017	0.59	0	0	0.0	0.0	
	B	0.008	0.024	0.84	1	-1	0.0	0.0	
	C	0.009	0.032	1.11	1	-1	0.0	0.0	
	D	0.009	0.042	1.46	3	-3	0.0	0.0	
1	E	0.011	0.054	1.88	15	-7	0.1	0.0	
	F	0.010	0.065	2.26	235	-118	1.7	0.7	2.0
	G	0.010	0.072	2.51	476	-230	3.4	1.4	2.1
	H	0.009	0.081	2.82	961	-424	6.3	2.6	2.3
	A	0.016	0.025	0.87	0	0	0.0	0.0	
	B	0.020	0.036	1.25	0	0	0.0	0.0	
	C	0.017	0.041	1.43	0	0	0.0	0.0	
	D*								
2	E	0.020	0.068	2.37	13	-8	0.1	0.0	
	F	0.020	0.08	2.79	68	-46	0.7	0.3	
	G	0.020	0.087	3.03	190	-52	0.8	0.3	3.7
	H	0.020	0.096	3.34	387	-130	1.9	0.8	3.0
	I	0.019	0.110	3.83	718	-232	3.4	1.4	3.1
	A	0.028	0.053	1.85	0	0	0.0	0.0	
	B	0.026	0.073	2.54	14	-11	0.2	0.1	
3	C	0.027	0.095	3.31	132	-66	1.0	0.4	2.0
	D	0.026	0.119	4.14	592	-210	3.1	1.3	2.8
	E	0.025	0.145	5.05	1420	-490	7.3	3.0	2.9
	A	0.026	0.041	1.43	0	0	0.0	0.0	
	B	0.030	0.055	1.92	1	-1	0.0	0.0	
	C	0.029	0.066	2.30	3	-3	0.0	0.0	
	D	0.029	0.081	2.82	32	-10	0.1	0.1	
3N	E	0.028	0.091	3.17	107	-31	0.5	0.2	3.5
	F	0.029	0.105	3.66	189	-58	0.9	0.4	3.3
	G	0.029	0.119	4.14	371	-99	1.5	0.6	3.7
	H	0.029	0.13	4.53	688	-263	3.9	1.6	2.6
	I	0.030	0.145	5.05	1291	-544	8.1	3.4	2.4
	A	0.038	0.052	1.81	0	0	0.0	0.0	
	B	0.038	0.066	2.30	0	0	0.0	0.0	
	C	0.040	0.084	2.93	7	-7	0.1	0.0	
4	D	0.038	0.1	3.48	37	-14	0.2	0.1	
	E	0.038	0.116	4.04	116	-46	0.7	0.3	2.5
	F	0.038	0.131	4.56	296	-83	1.2	0.5	3.6
	G	0.039	0.15	5.22	516	-162	2.4	1.0	3.2
	H	0.040	0.167	5.82	925	-302	4.5	1.9	3.1
	A	0.048	0.056	1.95	0	0	0.0	0.0	
	B	0.045	0.071	2.47	0	0	0.0	0.0	
	C	0.047	0.091	3.17	6	-3	0.0	0.0	
	D	0.045	0.106	3.69	41	-19	0.3	0.1	
5	E	0.043	0.122	4.25	116	-32	0.5	0.2	3.6
	F	0.046	0.14	4.88	229	-75	1.1	0.5	3.1
	G	0.049	0.153	5.33	392	-121	1.8	0.7	3.2
	H	0.050	0.171	5.96	654	-222	3.3	1.4	2.9
	I	0.050	0.189	6.58	1001	-378	5.6	2.3	2.6
	A	0.028	0.117	4.07	127	-38	0.6	0.2	3.3
	B	0.028	0.117	4.07	183	-58	0.9	0.4	3.2
	C	0.029	0.118	4.11	335	-93	1.4	0.6	3.6
	D	0.028	0.117	4.07	496	-145	2.1	0.9	3.4
6	E	0.029	0.118	4.11	848	-263	3.9	1.6	3.2
	F	0.029	0.119	4.14	1056	-429	6.3	2.6	2.5
	G	0.029	0.119	4.14	1301	-542	8.0	3.3	2.4
	H	0.030	0.119	4.14	1629	-671	9.9	4.1	2.4
	A	0.030	0.055	1.92	1	-1	0.0	0.0	
	B	0.029	0.067	2.33	3	-1	0.0	0.0	
	C	0.028	0.08	2.79	10	-8	0.1	0.0	
	D	0.029	0.092	3.20	38	-21	0.3	0.1	
	E	0.030	0.106	3.69	117	-46	0.7	0.3	2.5
7	F	0.029	0.12	4.18	331	-143	2.1	0.9	2.3
	G	0.029	0.132	4.60	607	-277	4.1	1.7	2.2
	H	0.030	0.144	5.02	1062	-582	8.6	3.6	1.8
	I	0.028	0.156	5.43					
	J	0.029	0.173	6.03					
	K	0.029	0.189	6.58					
	L	0.029	0.198	6.90					
	A	0.008	0.025	0.87	0	0	0.0	0.0	
	B	0.010	0.035	1.22	0	0	0.0	0.0	
	C	0.010	0.043	1.50	2	0	0.0	0.0	
	D	0.010	0.052	1.81	8	-2	0.0	0.0	
	E	0.010	0.065	2.26	181	-104	1.5	0.6	1.7
8	F	0.010	0.073	2.54	358	-228	3.4	1.4	1.6
	G	0.009	0.081	2.82	799	-559	8.3	3.4	1.4
	H	0.010	0.093	3.24					
	I	0.011	0.101	3.52					
	J	0.011	0.11	3.83					
	K	0.010	0.118	4.11					
	A	0.029	0.12	4.18	289	-74	1.1	0.5	3.9
	B	0.029	0.12	4.18	300	-76	1.1	0.5	3.9
9	C	0.029	0.119	4.14	215	-70	1.0	0.4	3.1
	D	0.029	0.119	4.14	222	-62	0.9	0.4	3.6
	E	0.029	0.119	4.14	266	-70	1.0	0.4	3.8

Table 32: *The results for the parameters n_{gross}, n_{net}, N_{od}, S_{od}, and the mobility parameter based on the entrained coloured rocks for the 1:10 slope.*

Test Information		Test conditions			Parameters				
Series	**Run**	**$s_{o,p}$**	**$H_{1/3}$**	**Hs Δd_{n50}**	**n_{gross}**	**n_{net}**	**N_{od}**	**S_{od}**	**Mobility parameter**
	A	0.009	0.062	2.16	46	-29	0.4	0.1	
1	B	0.010	0.087	3.03	467	-186	2.8	0.7	2.5
	C	0.009	0.109	3.80	1590	-805	11.9	3.0	2.0
	A	0.009	0.066	2.30					
11	B	0.010	0.086	3.00					
	C	0.010	0.11	3.83					
	D	0.010	0.126	4.39					
	A	0.030	0.089	3.10	10	-6	0.1	0.0	
	B	0.031	0.106	3.69	37	-20	0.3	0.1	
	C	0.027	0.121	4.21	192	-48	0.7	0.2	4.0
	D	0.029	0.141	4.91	353	-107	1.6	0.4	3.3
2	E	0.028	0.159	5.54	706	-197	2.9	0.7	3.6
	F	0.028	0.179	6.23	1149	-333	4.9	1.2	3.5
	G	0.030	0.205	7.14					
	H	0.031	0.225	7.84					
	I	0.029	0.245	8.53					
	A	0.052	0.099	3.45	2	-1	0.0	0.0	
	B	0.052	0.116	4.04	8	-5	0.1	0.0	
	C	0.051	0.134	4.67	20	-11	0.2	0.0	
3	D	0.050	0.148	5.15	52	-23	0.3	0.1	
	E	0.048	0.165	5.75	110	-50	0.7	0.2	2.2
	F	0.044	0.183	6.37	328	-128	1.9	0.5	2.6
	G	0.045	0.203	7.07	571	-187	2.8	0.7	3.1
	A	0.018	0.076	2.65	33	-25	0.4	0.1	
	B	0.019	0.094	3.27	78	-44	0.7	0.2	
4	C	0.017	0.114	3.97	302	-136	2.0	0.5	2.2
	D	0.019	0.134	4.67	868	-403	6.0	1.5	2.2
	E	0.019	0.157	5.47					
	F	0.020	0.174	6.06					
	A	0.038	0.101	3.52	4	-3	0.0	0.0	
	B	0.039	0.118	4.11	25	-21	0.3	0.1	
	C	0.039	0.132	4.60	60	-35	0.5	0.1	
5	D	0.036	0.15	5.22	155	-78	1.2	0.3	2.0
	E	0.037	0.169	5.89					
	F	0.038	0.189	6.58					
	G	0.036	0.207	7.21					
	A	0.029	0.145	5.05	150	-48	0.7	0.2	3.1
	B	0.029	0.143	4.98	282	-91	1.3	0.3	3.1
6	C	0.028	0.141	4.91	445	-147	2.2	0.5	3.0
	D	0.029	0.142	4.95	694	-234	3.5	0.9	3.0
	E	0.029	0.143	4.98	992	-387	5.7	1.4	2.6
	F	0.029	0.142	4.95					
	A	0.009	0.109	3.80	965	-467	6.9	1.7	2.1
7	B	0.010	0.126	4.39					
	C	0.010	0.137	4.77					
	A	0.028	0.161	5.61	390	-143	2.1	0.5	2.7
8	B	0.028	0.184	6.41	878	-301	4.5	1.1	2.9
	C	0.029	0.203	7.07					

Appendix K: Determining the design formula

Several variations of the design formula are explored to determine the best fit. First a design formula has been established for the determined for the 1:8 and 1:10 slope separately. This determined based on minimizing the RMSE as depicted in Eq. 4.2 in chapter 4 for damage parameter $E_{3D,3}$. The RMSE and the best fit are depicted in Eq. K.1 and K.2. Data from both slopes are used to determine the best fit which is presented in Eq. K.3. Another variation includes the number of plunging waves N_p. The number of plunging waves is based on the distribution between plunging and spilling waves. Adding this factor results in a slight reduce in the RMSE as depicted in Eq. K.4, but this improvement is very small. For that reason, this more complex formula is not added in the main report. Other variations could be studied to analyse if a better curve fitting can be reached.

Info for 1:8 slope with RMSE ($E_{3D,3}$) = 0.18156

$$\frac{H_s}{\Delta d_{n50}} = 8.04 * E_{3D,3}^{0.74} * \xi_p^{-0.95} * N^{-0.13} \qquad \text{Eq. K.1}$$

Info for 1:10 slope with RMSE ($E_{3D,3}$) = 0.21224

$$\frac{H_s}{\Delta d_{n50}} = 7.09 * E_{3D,3}^{0.59} * \xi_p^{-1.23} * N^{-0.13} \qquad \text{Eq. K.2}$$

All info with RMSE ($E_{3D,3}$) = 0.204822

$$\frac{H_s}{\Delta d_{n50}} = 7.55 * E_{3D,3}^{0.62} * \xi_p^{-1.10} * N^{-0.13} \qquad \text{Eq. K.3}$$

All info with additional term with RMSE ($E_{3D,3}$) = 0.20424

$$\frac{H_s}{\Delta d_{n50}} = 7.39 * E_{3D,3}^{0.62} * \xi_p^{-1.07} * (N_p)^{-0.13} \qquad \text{Eq. K.4}$$

$$N_p = \xi_p^{0.57} N \qquad for\ \xi_p < 1$$

$$N_p = N \qquad for\ \xi_p > 1$$

Appendix L: Probability graphs of entrained rocks

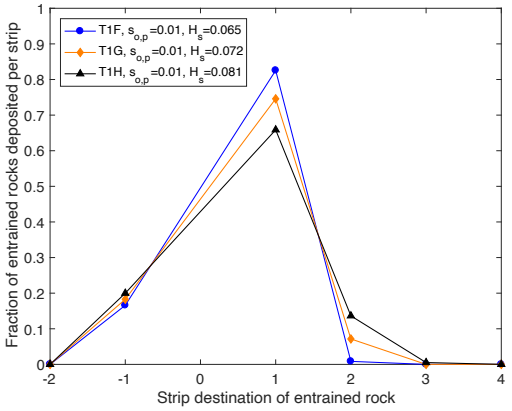

1. *Wave steepness $s_{o,p}$=0.01*

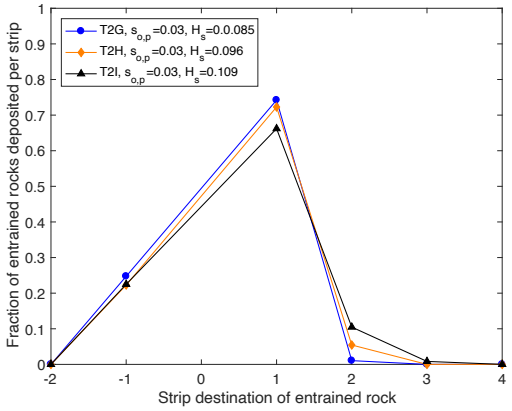

2. *Wave steepness $s_{o,p}$=0.02*

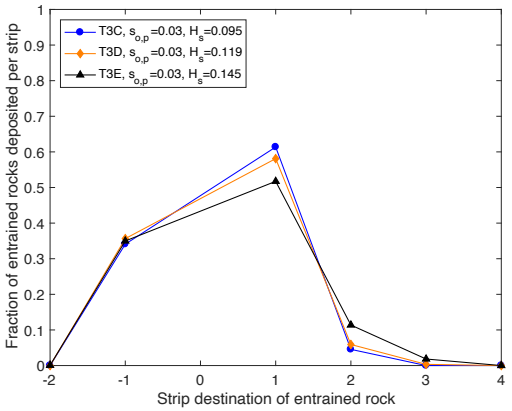

3. *Wave steepness $s_{o,p}$=0.03 of Test series 3*

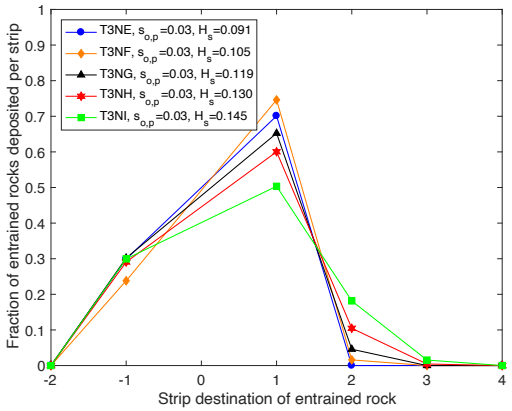

4. *Wave steepness $s_{o,p}$=0.03 of test series 3N*

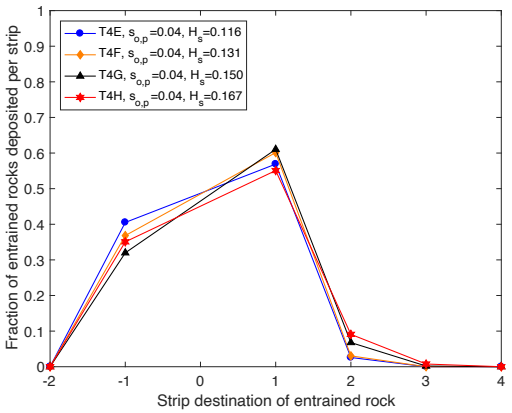

5. *Wave steepness $s_{o,p}$=0.04*

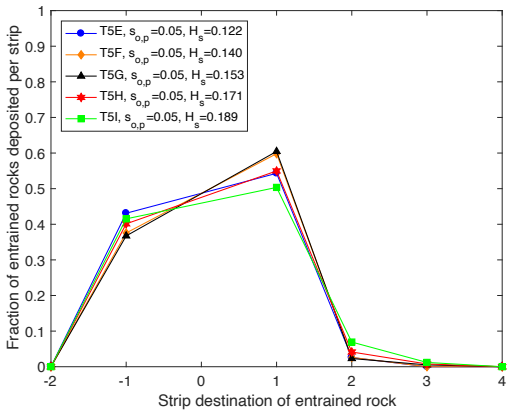

6. *Wave steepness $s_{o,p}$=0.05*

Figure 51: *Probability graphs of transported rocks for all wave steepnesses for the 1:8 slope.*

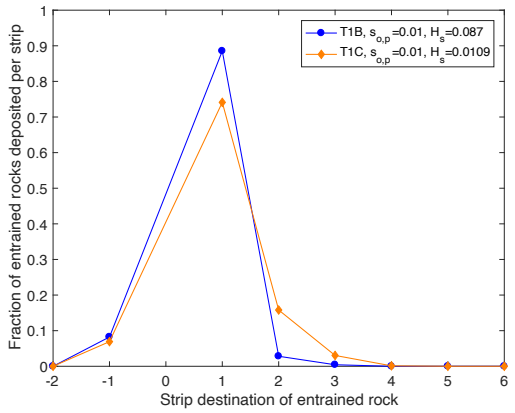

1. *Wave steepness $s_{o,p}$=0.01*

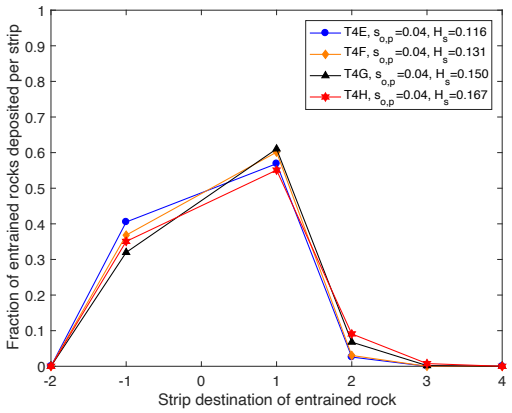

2. *Wave steepness $s_{o,p}$=0.02*

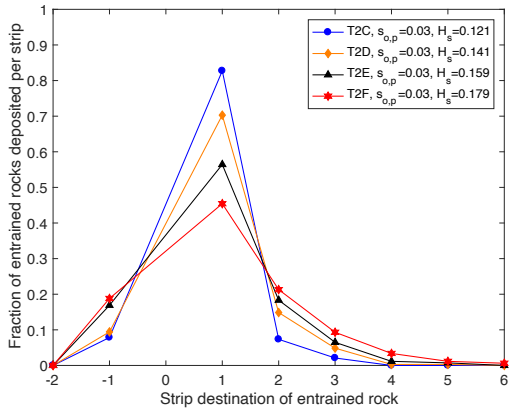

3. *Wave steepness $s_{o,p}$=0.03*

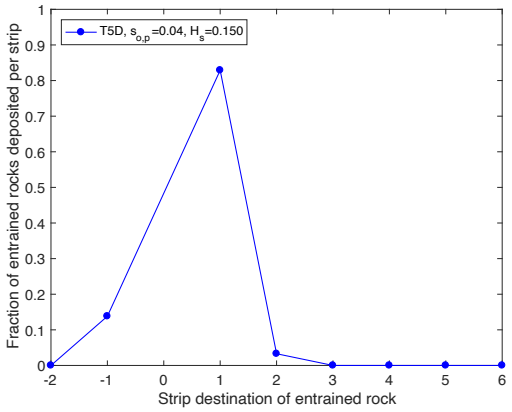

4. *Wave steepness $s_{o,p}$=0.04*

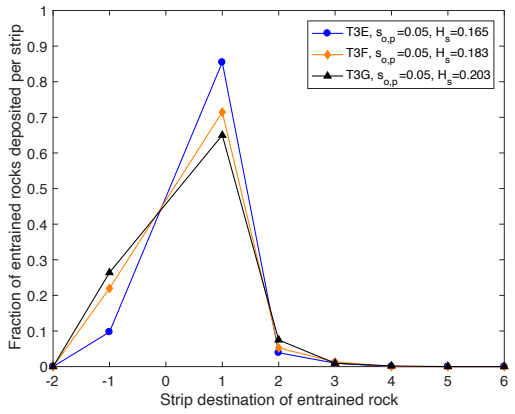

5. *Wave steepness $s_{o,p}$=0.05*

Figure 52: *Probability graphs of transported rocks for all wave steepnesses for the 1:10 slope.*

Appendix M: Simplified approach to determine $E_{3D,3}$

Simplified grid fields are used to determine $E_{3D,1}$, $E_{3D,3}$ and $E_{3D,5}$. A 2.0 by 2.0 cm grid field is used for the damage parameter $E_{3D,1}$, a 4.0 by 4.0 cm grid field is used for the damage parameter $E_{3D,3}$ and a 8.0 by 8.0 cm grid field is used for the damage parameter $E_{3D,5}$. The profile changes are determined for these grids without using a spatial moving average. Test series 1 is researched to investigate the impact of a simplified grids on the damage parameters. The results for the damage parameters are shown in Table 33 and examples of the 3D top view plots are depicted in the figures for test 1G. On average $E_{3D,1}$ is 0.31 lower, $E_{3D,3}$ is 0.13 lower and $E_{3D,5}$ is 0.16 lower. If in practice during monitoring the high resolution of stereophotogrammetry cannot be reached a simplified grid can be used and The difference should be taken into account.

Table 33: *The results for a simplified grid to determine the damage parameters*

Test Information					Test conditions		Damage parameters			Damage parameters simple		
Series	Run	$s_{o,p}$	$H_{1/3}$	$H_{m,0}$	N	$\frac{Hs}{\Delta d_{n50}}$	$E_{3D,1}$	$E_{3D,3}$	$E_{3D,5}$	$E_{3D,1}$	$E_{3D,3}$	$E_{3D,5}$
1	A	0.009	0.017	0.018	1114	0.59	0.58	0.18	0.10	0.23	0.07	0.05
	B	0.008	0.024	0.025	1156	0.84	0.84	0.47	0.26	0.72	0.43	0.14
	C	0.009	0.032	0.034	1183	1.11	0.85	0.43	0.22	0.52	0.38	0.11
	D	0.009	0.042	0.045	1201	1.46	1.30	0.67	0.30	0.83	0.40	0.14
	E	0.011	0.054	0.056	1272	1.88	1.24	0.66	0.47	0.86	0.45	0.22
	F	0.010	0.065	0.068	1239	2.26	1.43	0.89	0.61	1.19	0.75	0.40
	G	0.010	0.072	0.074	1173	2.51	1.42	0.95	0.72	1.09	0.79	0.64
	H	0.009	0.081	0.084	1200	2.82	1.88	1.52	1.33	1.67	1.45	1.02

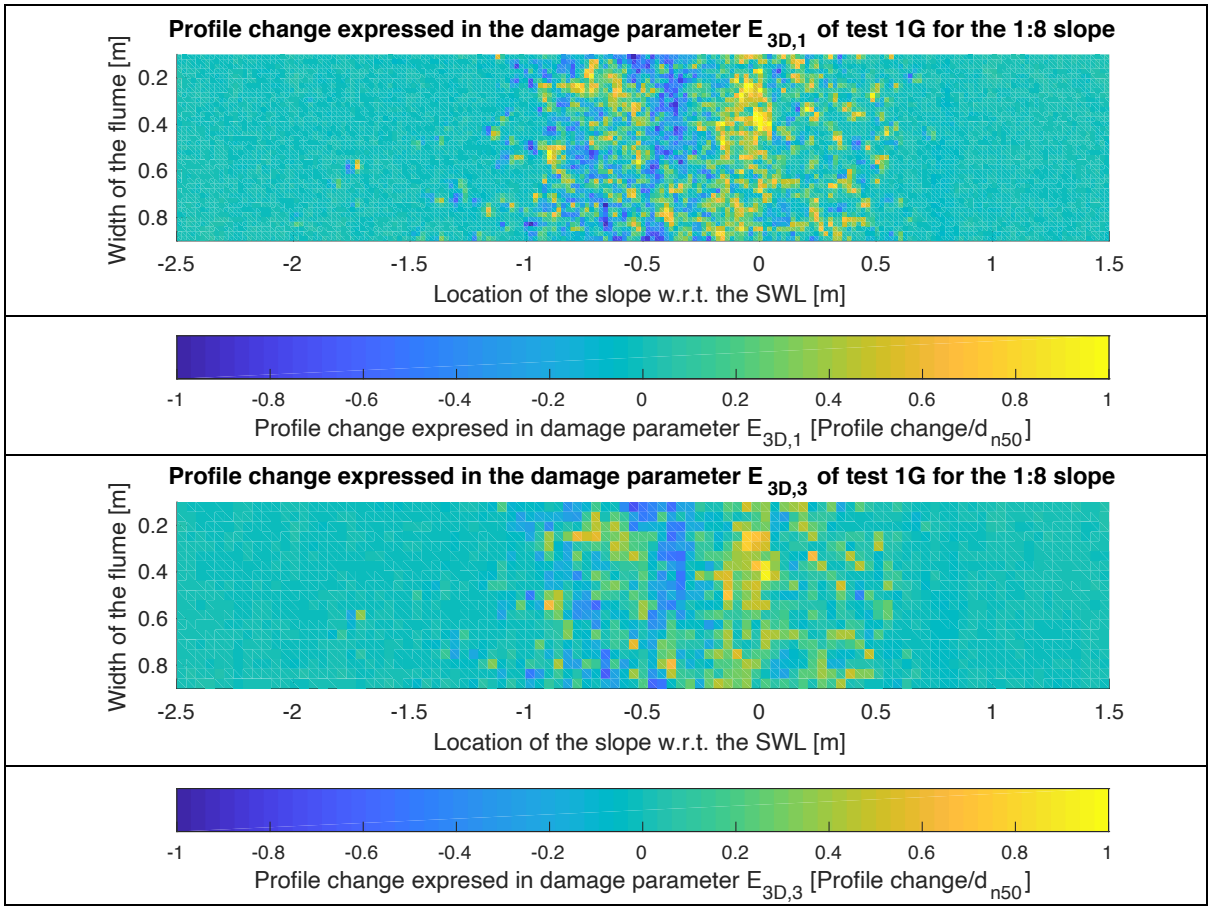

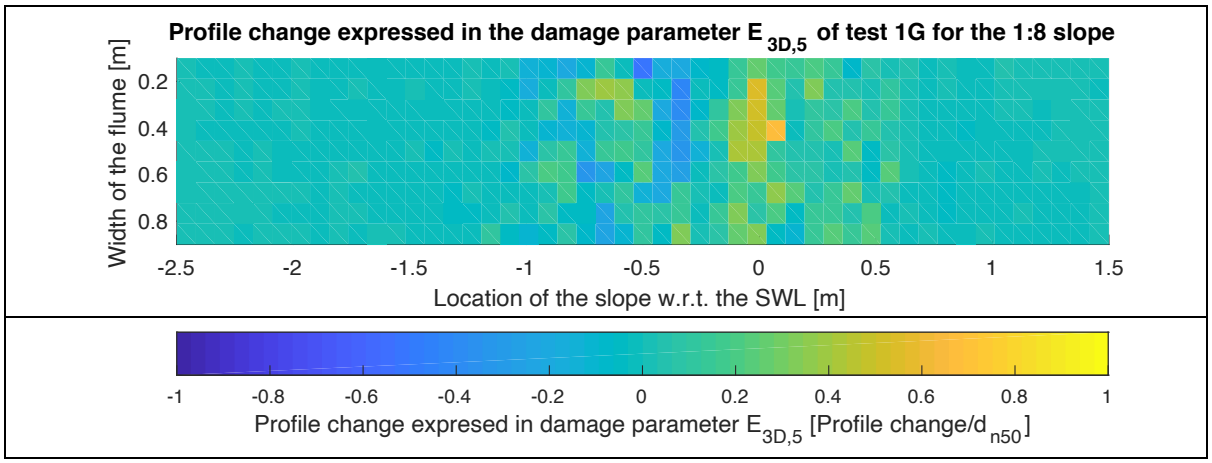
Profile change expressed in the damage parameter E 3D,5 of test 1G for the 1:8 slope
Width of the flume [m]
0.2
0.4
0.6
0.8
-2.5
-2
-1.5
-1
-0.5
0
0.5
1
1.5
Location of the slope w.r.t. the SWL [m]
-1
-0.8
-0.6
-0.4
-0.2
0
0.2
0.4
0.6
0.8
1
Profile change expresed in damage parameter E3D,5 [Profile change/dn50]